



Development and Mechanistic Understanding of Photochemical Reactions

Ana Bahamonde Jiménez

ADVERTIMENT. L'accés als continguts d'aquesta tesi doctoral i la seva utilització ha de respectar els drets de la persona autora. Pot ser utilitzada per a consulta o estudi personal, així com en activitats o materials d'investigació i docència en els termes establerts a l'art. 32 del Text Refós de la Llei de Propietat Intel·lectual (RDL 1/1996). Per altres utilitzacions es requereix l'autorització prèvia i expressa de la persona autora. En qualsevol cas, en la utilització dels seus continguts caldrà indicar de forma clara el nom i cognoms de la persona autora i el títol de la tesi doctoral. No s'autoritza la seva reproducció o altres formes d'explotació efectuades amb finalitats de lucre ni la seva comunicació pública des d'un lloc aliè al servei TDX. Tampoc s'autoritza la presentació del seu contingut en una finestra o marc aliè a TDX (framing). Aquesta reserva de drets afecta tant als continguts de la tesi com als seus resums i índexs.

ADVERTENCIA. El acceso a los contenidos de esta tesis doctoral y su utilización debe respetar los derechos de la persona autora. Puede ser utilizada para consulta o estudio personal, así como en actividades o materiales de investigación y docencia en los términos establecidos en el art. 32 del Texto Refundido de la Ley de Propiedad Intelectual (RDL 1/1996). Para otros usos se requiere la autorización previa y expresa de la persona autora. En cualquier caso, en la utilización de sus contenidos se deberá indicar de forma clara el nombre y apellidos de la persona autora y el título de la tesis doctoral. No se autoriza su reproducción u otras formas de explotación efectuadas con fines lucrativos ni su comunicación pública desde un sitio ajeno al servicio TDR. Tampoco se autoriza la presentación de su contenido en una ventana o marco ajeno a TDR (framing). Esta reserva de derechos afecta tanto al contenido de la tesis como a sus resúmenes e índices.

WARNING. Access to the contents of this doctoral thesis and its use must respect the rights of the author. It can be used for reference or private study, as well as research and learning activities or materials in the terms established by the 32nd article of the Spanish Consolidated Copyright Act (RDL 1/1996). Express and previous authorization of the author is required for any other uses. In any case, when using its content, full name of the author and title of the thesis must be clearly indicated. Reproduction or other forms of for profit use or public communication from outside TDX service is not allowed. Presentation of its content in a window or frame external to TDX (framing) is not authorized either. These rights affect both the content of the thesis and its abstracts and indexes.

UNIVERSITAT ROVIRA I VIRGILI

Development and Mechanistic Understanding of Photochemical Reactions

Ana Bahamonde Jiménez



**UNIVERSITAT
ROVIRA I VIRGILI**

Development and Mechanistic Understanding of Photochemical Reactions

Ana Bahamonde Jiménez



**DOCTORAL THESIS
2017**

English

This doctoral thesis describes the development and mechanistic understanding of photochemical organocatalytic reactions. Initially, I focused on designing new chemical transformations that relied on the formation of electron-donor acceptor (EDA) complexes. Specifically, we developed an enamine-mediated enantioselective photochemical α -alkylation of ketones with electron-poor alkyl bromides. Subsequently, we expanded this EDA complex-mediated strategy to the photochemical alkylation of indoles with electron-poor alkyl bromides.

The second part of my PhD work was characterized by a progressive transition from reaction development towards a mechanistically-oriented approach. In particular, I focused on detailed mechanistic studies of some photochemical enantioselective transformations previously developed in the group. We studied the mechanism of the enamine-mediated photochemical α -alkylation of aldehydes. Quantum yield measurements revealed that a radical chain mechanism was operative. Moreover, kinetic studies established the trapping of the carbon-centered radical by the enamine, to form the carbon-carbon bond, as the turnover-limiting step. Additionally, we uncovered the turnover-limiting step of the iminium ion-mediated radical conjugate addition to β,β -disubstituted cyclic enones which had been previously developed by the group.

Español

Esta tesis doctoral describe el desarrollo y los estudios del mecanismo de reacciones fotoquímicas organocatalíticas. Inicialmente, nos centramos en el diseño de nuevas transformaciones químicas que dependían de la formación de complejos dadores-aceptores de electrones (EDA). En este contexto, se desarrolló una alquilación fotoquímica enantioselectiva en la posición alfa de cetonas con bromuros de alquilo pobres en electrones a través de la formación de enaminas. Posteriormente, ampliamos esta estrategia, mediada por la formación de complejos EDA, a la alquilación fotoquímica de indoles con bromuros de alquilo pobres en electrones.

Una transición progresiva desde el desarrollo de nuevas reacciones hacia un enfoque centrado en los estudios del mecanismo de reacción caracterizó la segunda parte de mi doctorado. En esta parte nos focalizamos en un estudio detallado de los mecanismos de reacción de algunas transformaciones fotoquímicas enantioselectivas previamente

desarrolladas en el grupo. En concreto, se estudió el mecanismo de la alquilación fotoquímica de aldehídos en la posición alfa a través de la formación de enaminas. Por un lado, las ediciones del rendimiento cuántico de la reacción revelaron que ésta se desarrollaba mediante un mecanismo radicalario en cadena. Por otro lado, los estudios cinéticos establecieron que el paso en el que la enamina reacciona con el radical centrado en el carbono, para formar el enlace carbono-carbono, era el paso limitante de la velocidad de reacción. Además, también se descubrió cual era el paso limitante de la velocidad de reacción de la adición conjugada de radicales a enonas cíclicas β,β -disustituidas mediada por la formación de iones iminio; reacción que había sido previamente desarrollada en el grupo.

Català

Aquesta tesi doctoral descriu el desenvolupament i l'estudi del mecanisme de reaccions fotoquímiques organocatalítiques. Inicialment, ens centrem en el disseny de noves transformacions químiques promogudes per la formació de complexos donadors-acceptors d'electrons (EDA). En aquest context, es va desenvolupar una alquilació fotoquímica enantioselectiva en la posició alfa de cetones amb bromurs d'alquil pobres en electrons mitjançant la formació d'enamines. Posteriorment, vam ampliar aquesta estratègia, mitjançant la formació de complexos EDA, a l'alquilació fotoquímica d'indols amb bromurs d'alquil pobres en electrons.

La segona part del meu doctorat es va caracteritzar per una progressiva transició des del desenvolupament de noves reaccions cap a un enfocament centrat en els estudis de mecanisme de reacció. En particular, vam realitzar un estudi detallat del mecanisme de reacció d'algunes transformacions fotoquímiques enantioselectives prèviament desenvolupades en el grup. Es va estudiar el mecanisme de l'alquilació fotoquímica d'aldehíds en la posició alfa mitjançant la formació d'enamines. El rendiment quàntic d'aquesta va revelar que es desenvolupava mitjançant un mecanisme en cadena radical. A més, estudis cinètics van establir que el pas en què l'enamina reacciona amb el radical centrat en el carboni, per formar l'enllaç carboni-carboni, era el pas limitant de la velocitat de reacció. Addicionalment, es va descobrir quin era el pas limitant de la velocitat de reacció de l'addició conjugada de radicals a enones cícliques β,β -disubstituídes mitjançant la formació d'ions imini; reacció prèviament desenvolupada en el grup.

Long Summary

My doctorate studies aimed at using the photochemical activity of transient intermediates or molecular aggregations, such as electron donor-acceptor (EDA) complexes, to enable unconventional reactivities. An EDA complex is a ground-state association characterized by the appearance of a new absorption band, the charge transfer band, which generally falls in the visible region. The irradiation of the charge transfer band of an EDA complex is related with a single-electron transfer from the donor to the acceptor. As a result, the EDA photoexcitation with visible light triggers the formation of radical species. I focused on the synthetic potential of this photochemical strategy, and on the mechanistic understanding of the developed photochemical reactions.

Chapter III of this dissertation describes my first project where we focused on expanding the photochemical strategy for the enantioselective α -alkylation of aldehydes, previously described by the group, to include ketones as substrates. This transformation relies on the generation of EDA complexes, formed between enamines, generated upon condensation of a primary amine and a ketone, and electron-poor alkyl halides. The resulting methodology provided a rare example of direct enantioselective α -alkylation of unmodified ketones.

Subsequently, Chapter IV describes a further expansion of the EDA-based alkylation methodology. Specifically, we used the ability of indoles to act as donor counterpart for the formation of EDA complexes with electron-poor alkyl bromides. Conceptually, this study demonstrated that other molecules than enamines could serve as suitable donors in EDA complex formation. Synthetically, the photochemical activity of the indole-based EDA complexes promoted the formation of indole alkylation products. Mechanistically, we could isolate and fully characterize, by X-ray crystallographic analysis, the EDA complex that was promoting this photochemical transformation.

The second part of my PhD work was characterized by a progressive transition from reaction development towards a mechanistically-oriented approach. In particular, I focused on detailed mechanistic studies of some photochemical enantioselective transformations previously developed in the group.

Initially, I focused on studying the mechanism of the photochemical α -alkylation of aldehydes. As discussed in Chapter V, I used a combination

of conventional photophysical investigations, nuclear magnetic resonance (NMR) spectroscopy, and kinetic studies to gain a better understanding of the factors governing these enantioselective photochemical catalytic processes. We found that these α -alkylation reactions rely on the generation of open-shell species via two different enamine-based photochemical mechanisms: the direct photo-excitation of the enamine or the excitation of a photoactive EDA complex, generated between enamines and electron-poor alkyl halides. Quantum yield measurements revealed that a radical chain mechanism was operative. In addition, kinetic studies established the trapping of the carbon-centered radical by the enamine, to form the carbon-carbon bond, was the turnover-limiting step.

Our group recently developed an iminium ion-mediated radical conjugate addition to β,β -disubstituted cyclic enones. The last chapter of this thesis will detail how a combination of spectroscopic and kinetic studies have been used to elucidate the key mechanistic aspects of this transformation. The chemistry exploits the ability of the chiral primary amine catalyst, purposely adorned with a redox-active carbazole moiety, to facilitate the stereoselective interception of photochemically generated carbon-centered radicals by means of an electron-relay mechanism. Our studies uncovered an unanticipated turnover-limiting step.

UNIVERSITAT ROVIRA I VIRGILI

Development and Mechanistic Understanding of Photochemical Reactions

Ana Bahamonde Jiménez

UNIVERSITAT ROVIRA I VIRGILI

Development and Mechanistic Understanding of Photochemical Reactions

Ana Bahamonde Jiménez

Ana Bahamonde Jiménez

Development and Mechanistic Understanding of Photochemical Reactions

Doctoral Thesis

Supervised by Prof. Paolo Melchiorre

ICIQ – Institut Català d'Investigació Química



UNIVERSITAT ROVIRA I VIRGILI

Tarragona

2017

UNIVERSITAT ROVIRA I VIRGILI

Development and Mechanistic Understanding of Photochemical Reactions

Ana Bahamonde Jiménez



UNIVERSITAT ROVIRA I VIRGILI

Prof. Paolo Melchiorre, ICREA Research Professor & ICIQ Group Leader

I STATE that the present study, entitled “Development and Mechanistic Understanding of Photochemical Reactions”, presented by ANA BAHAMONDE JIMÉNEZ for the award of the degree of Doctor, has been carried out under my supervision at the Institut Català d'Investigació Química (ICIQ).

Tarragona, May the 18th 2017

Doctoral Thesis Supervisor

Prof. Paolo Melchiorre

UNIVERSITAT ROVIRA I VIRGILI

Development and Mechanistic Understanding of Photochemical Reactions

Ana Bahamonde Jiménez

Acknowledgements

Looking back to these past years in the Melchiorre group, I can easily see how many extraordinary people I have had the honor to get to know and work with. I am extremely grateful to all the past and present members of the group.

Without any doubt I would not have become the chemist and scientist that I am now if it wasn't for Paolo Melchiorre. He gave me the opportunity to join his research group for my Master studies and to remain in the group for conducting my PhD. This thesis will show how I moved from reaction development towards focusing on mechanistic studies. The potential for conducting mechanistic studies that Paolo saw in me will probably change the fate of my career as a chemist, *grazie* Paolo.

Additionally, I had been extremely lucky to work with incredibly talented chemists among which I would like to highlight Elena Arceo and John Murphy. Elena worked with me for several years. She became one of my best friends and taught me to how to dig deep when thinking about chemistry as well as how to think outside the box, *gracias* Elenita. John took Elena's position when she left; with him I had lots of chemistry discussions and I also got invaluable lessons on how to pour a real pint of Guinness, *go raibh maith agat* John.

There are other group members that I have shared great moments with. David Bastida, the most Catalan guy on Earth, *gràcies per tot* Dávide. Giulia Bergonzini, who worked with me during my first months in the group and with whom I shared a lot, *grazie mille* Giu. Eva Raluy, she has been in the group for quite a long time now and has become a good friend, *moltes gràcies* Eva. Luca Buzzetti, he is always joking in the lab and sometime this makes the difference, *grazie mille* Luchino. Alberto Vega, quite a nice guy for being a Barça supporter, *un abrazo manito*. Zhong-Yan Cao, one of the funniest and most sincere people I know, 谢谢. Łukasz Wozniak, for the unforgettable *troompets*, *dziękuję* Łukasz. Lorna Piazzzi, for the administrative support and for pushing me to go out to run together, *grazie mille* Lorna. Sandeep Kandukuri, who worked with me on the indole project, thanks Sandeep. In addition, I am grateful to the group as a whole for the great atmosphere. Working with you feels like I am truly "standing on the shoulders of giants".

I would also like to thank all the research support units at ICIQ, specially the NMR section where I spent a lot of time.

On the other hand, there are several people that have directly contributed on the writing of this manuscript and I want to thank them for proofreading: Zhong-Yan Cao, Hamish Hepburn, Catherine Holden and Yannick Rey.

During these years, I had the opportunity to go to Utah as a visiting student and work in the group of Matt Sigman. When I arrived in Utah I had already been working on mechanistic studies for a while but Matt's passion for physical organic chemistry was a big encouragement for continuing focusing on this line of research. I was really happy during the four months I spent there and I would like to thank him for the opportunity and his group, especially Jamie Allen a talented chemist that I had the pleasure to work with, for the chemistry and the incredible atmosphere.

Finally I would like to thank the people that have been with me outside the lab. Mi padre, who always encouraged me to become a scientist, taught me how to think and has been with me during these years. Y a Jaime, who is always there to listen to all my complaints from the bad days and always manages to bring a smile to my face.

Gijón is an important part of my life. It is where my friends and family lives and where I was born and lived for more than 20 years. That is why the cover of this manuscript shows a picture of one of Gijón's sculptures (I am grateful to José Rodríguez for allowing me to use his picture). I studied Chemistry in little town nearby Gijón, I would also like to acknowledge the Facultad de Química of the Universidad de Oviedo and specially the members of the Organic Department for their support during these years and the outstanding chemistry lessons that they taught me.

I would also like to acknowledge the financial support from the Institute of Chemical Research of Catalonia (ICIQ), MINECO for support through the Severo Ochoa Excellence Accreditation 2014-2018 (SEV-2013-0319) and from the European Research Council for the ERC starting grant (278541-ORGA-NAUT) and ERC consolidator grant (681840-CATA-LUX).

Additionally, I am personally grateful to:

- ICIQ Foundation for a first year predoctoral fellowship (ref. 03/12-7)
- Ministry of Education, Culture and Sport of Spain for a FPU predoctoral fellowship (FPU13/02402)



List of Publications

Some of the results presented in this thesis have been published:

- Ana Bahamonde, John J. Murphy, Marika Savarese, Éric Brémond, Andrea Cavalli and Paolo Melchiorre “Studies on the enantioselective iminium ion trapping of radicals triggered by an electron-relay mechanism” *J. Am. Chem. Soc.* **2017**, *139*, 4559.
- Ana Bahamonde and Paolo Melchiorre “On the mechanism of the stereoselective α -alkylation of aldehydes driven by the photochemical activity of enamines” *J. Am. Chem. Soc.* **2016**, *138*, 8019.
- Sandeep Kandukuri, Ana Bahamonde, Indranil Chatterjee, Igor D. Jurberg, Eduardo C. Escudero-Adán and Paolo Melchiorre “X-ray characterization of an EDA complex which drives the photochemical alkylation of indoles” *Angew. Chem. Int. Ed.* **2015**, *54*, 1485.
- Elena Arceo,[†] Ana Bahamonde,[†] Giulia Bergonzini and Paolo Melchiorre “Enantioselective direct α -alkylation of cyclic ketones by means of photo-organocatalysis” *Chem. Sci.* **2014**, *5*, 2438.

[†] These authors contributed equally

UNIVERSITAT ROVIRA I VIRGILI

Development and Mechanistic Understanding of Photochemical Reactions

Ana Bahamonde Jiménez

UNIVERSITAT ROVIRA I VIRGILI

Development and Mechanistic Understanding of Photochemical Reactions

Ana Bahamonde Jiménez

A mi padre, mi madre y Jaime

UNIVERSITAT ROVIRA I VIRGILI

Development and Mechanistic Understanding of Photochemical Reactions

Ana Bahamonde Jiménez

Table of Contents

1. General overview	1
1.1 Enantioselective organocatalysis.....	1
1.1.1 Activation modes in aminocatalysis.....	2
1.2 Photochemistry.....	5
1.3 General objectives and summary.....	8
1.3.1 Alkylation reactions driven by the photochemical activity of EDA complexes.....	8
1.3.2 Mechanistic studies of the stereoselective α -alkylation of aldehydes driven by the photochemical activity of enamines.....	10
1.3.3 Mechanistic studies of the of iminium ion trapping of radicals <i>via</i> asymmetric electron-relay catalysis	11
2. EDA complexes: characteristics and uses	13
2.1 Introduction.....	13
2.2 Enamine-mediated α -alkylation of aldehydes.....	14
2.2.1 α -Alkylation of aldehydes mediated by the photochemical activity of EDA complexes	16
2.3 Historical background.....	18
2.4 EDA complex characterization.....	20
2.4.1 X-Ray crystallographic analysis.....	20
2.4.2 Determination of the association constant of an EDA complex.....	21
2.5 Characteristics that govern the complex strength and SET rate.....	22
2.5.1 Solvent effect on the stability of an EDA complex.....	23
2.6 Synthetic applications of EDA complexes	24
3. Enantioselective direct α-alkylation of cyclic ketones by means of photo-organocatalysis	29
3.1 Introduction.....	29
3.1.1 Enantioselective α -alkylation of ketones.....	31
3.1.2 Aminocatalytic α -functionalization of ketones	35
3.2 Target of the project	39
3.3 Results and discussion	40
3.3.1 Reaction scope.....	46
3.3.2 Mechanistic insights.....	50
3.4 Conclusions and remarks	56
3.5 Experimental section	57

4. X-Ray characterization of an EDA complex that drives the photochemical alkylation of indoles	69
4.1 Introduction.....	69
4.1.1 EDA complexes with indoles	70
4.1.2 Indole-based EDA complexes relevant for synthetic transformations	72
4.2 Target of the project	74
4.3 Optimization studies and reaction scope	75
4.3.1 Optimization studies	75
4.3.2 Reaction scope.....	77
4.4 Mechanistic insights	82
4.4.1 Absorption spectra	82
4.4.2 Mulliken's correlation.....	83
4.4.3 Determination of the stoichiometry of the complex in solution.....	84
4.4.4 Determination of the association constant.....	85
4.4.5 X-Ray characterization of the EDA complex IIa	88
4.4.6 Quantum yield determination	89
4.4.7 Proposed mechanisms.....	90
4.5 Conclusions and remarks	92
4.6 Experimental section	93
4.6.1 Quantum yield measurements	93
5. Studies on the enantioselective α-alkylation of aldehydes driven by the photochemical activity of enamines.....	99
5.1 Introduction.....	99
5.2 Target of the project	101
5.3 Results and discussion	101
5.3.1 Spectroscopic studies	103
5.3.2 Quantum yield measurements	112
5.3.3 Proposed mechanism	115
5.3.4 Studies of the concentration of enamine in solution.....	121
5.3.5 Kinetic studies	129
5.4 Conclusions and remarks	137
5.5 Experimental section	139
5.5.1 Quantum yield measurements	141
5.5.2 Evolution of the catalyst concentration over time.....	149
5.5.3 Kinetic studies	154
5.5.4 Cyclic voltammetry	171
5.5.5 Synthesis and characterization of iminium ion IX	172

6. Studies on the iminium ion trapping of radicals triggered by an electron-relay mechanism	173
6.1 Introduction.....	173
6.1.1 The unexpected result	177
6.2 Target of the project	179
6.3 Results and discussion	179
6.3.1 Light intensity/reactivity correlation studies.....	181
6.3.2 Rate dependence on the electronic properties of different aminocatalysts	182
6.3.3 Rate order assessment	185
6.3.4 Photophysical studies	192
6.4 Conclusions and remarks	197
6.5 Experimental section	198
6.5.1 Synthesis of the aminocatalysts	201
6.5.2 Kinetic studies	205
6.5.3 Characterization of the intermediates involved in iminium ion formation.....	214
6.5.4 Cyclic voltammetry	217

UNIVERSITAT ROVIRA I VIRGILI

Development and Mechanistic Understanding of Photochemical Reactions

Ana Bahamonde Jiménez

Chapter I

General overview

1.1 Enantioselective organocatalysis

The aim of this doctoral thesis was the development and mechanistic understanding of new enantioselective organocatalytic photochemical transformations. The core of the investigations relies on the use of chiral organic molecules to catalyze enantioselective reactions; consequently, the definition of catalyst is provided. A catalyst is a compound which increases the rate of a process without modifying the overall standard Gibbs energy change (ΔG^0). Furthermore, a catalyst takes part in a reaction but is not consumed; as a result, it can be employed in sub-stoichiometric amounts.¹ The use of efficient catalysts in organic synthesis can enable the realization of otherwise elusive transformations, providing alternative pathways that reduce the originally large energy activation barriers that would prevent these reactions from proceeding.

Another important target of synthetic chemistry is to develop methodologies that can control the stereochemistry of the final chiral products. This is because enantiomers of a given biomolecule can exhibit dramatically different biological activities. Catalysis can provide a game-changing strategy in this endeavor, since a chiral catalyst can yield the target product of a chemical transformation enantioselectively. The fact that valuable chiral catalysts could be used in a sub-stoichiometric amount greatly reduces the cost of the process.²

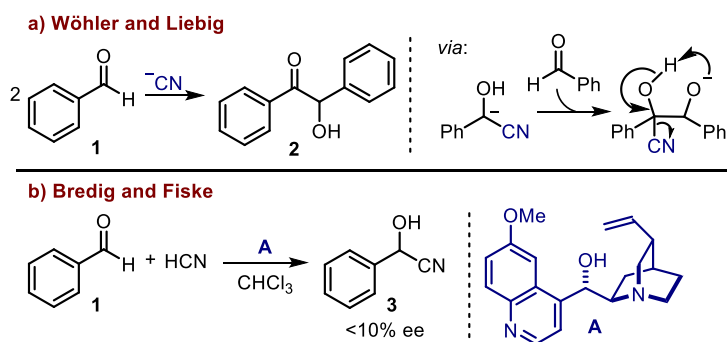
Organocatalysis is a field of enantioselective chemistry which uses small chiral organic molecules as catalysts. The low cost, low toxicity, and generally high stability of the organocatalysts allow the use of simple setups, thus avoiding the need for a controlled atmosphere or dry solvents. Nowadays, organocatalysis has reached a level of efficiency and reliability to be considered an established tool of modern asymmetric synthesis, complementing bio- and metal-based enantioselective catalysis.³

¹ Laidler, K. J. "A glossary of terms used in chemical kinetics, including reaction dynamics (IUPAC Recommendations 1996)" *Pure and App. Chem.* **1996**, *68*, 149.

² Noyori, R. "Asymmetric catalysis: science and opportunities (Nobel Lecture)" *Angew. Chem. Int. Ed.* **2002**, *41*, 2008.

³ Bertelsen, S.; Jørgensen, K. A. "Organocatalysis-after the gold rush" *Chem. Soc. Rev.* **2008**, *38*, 2178.

The cyanide-catalyzed benzoin condensation reaction, reported by Wöhler in 1832, can be considered the first report of an organocatalytic reaction (Scheme 1.1a).⁴ The first asymmetric variant was developed as early as 1912, when Bredig and Fiske published the enantioselective hydrocyanation of benzaldehyde.⁵ As depicted in Scheme 1.1b, the authors obtained the final product **3** with a moderate enantiomeric excess when conducting the reaction in the presence of the natural cinchona alkaloid quinidine (**A**).



Scheme 1.1 First examples of organocatalysis.

1.1.1 Activation modes in aminocatalysis

Aminocatalysis is a specific research area within organocatalysis that deals with the enantioselective functionalization of unmodified carbonyl compounds.⁶ This approach relies on the formation of transient active intermediates, enamines and iminium ions, generated upon condensation of chiral amine catalysts with a carbonyl compound. These reactive intermediates can participate in many reaction types imparting consistently high enantioselectivity. As a result, they provide two different activation modes of aminocatalysis: enamine and iminium ion activation.⁷

In enamine-mediated reactions, a chiral aminocatalyst condenses with an enolizable carbonyl compound, generating an iminium ion (**I**) which contains a highly acidic α -proton (Scheme 1.2). The deprotonation of **I** generates enamine **II**, the synthetic equivalent of an enol. The formation of enamines increases the energy of the highest occupied molecular orbital (HOMO) with respect to the enol form of the carbonyl, thus enhancing the nucleophilicity of the α -carbon. The chiral enamines can stereoselectively

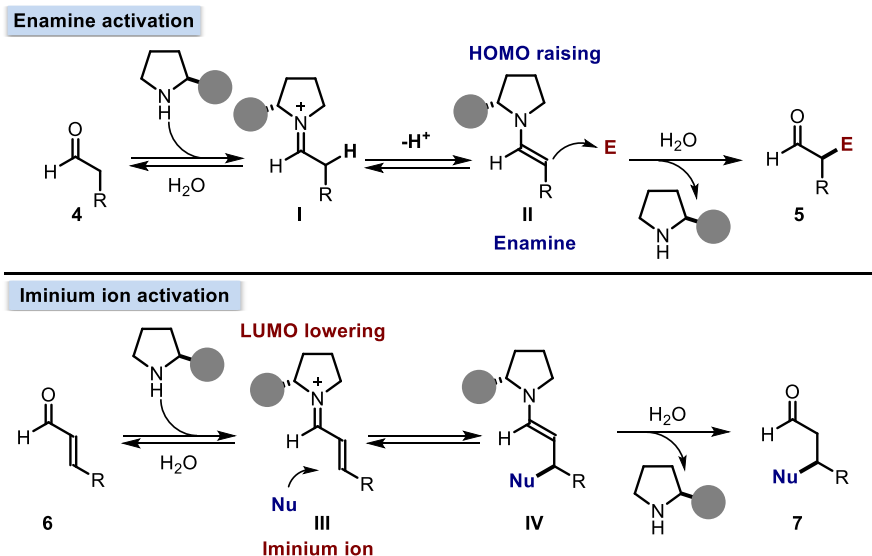
⁴ Wöhler, F.; Liebig, J. "Untersuchungen über das radikal der benzoessäure" *Ann. Der. Pharm.* **1832**, 3, 249.

⁵ Bredig, G; Fiske, P. S. "Asymmetric synthesis caused by catalysts" *Biochem. Z.* **1912**, 46, 7.

⁶ Melchiorre, P.; Marigo, M.; Carlone, A.; Bartoli, G. "Asymmetric aminocatalysis-gold rush in organic chemistry" *Angew. Chem. Int. Ed.* **2008**, 47, 6138.

⁷ MacMillan, D. W. "The advent and development of organocatalysis" *Nature* **2008**, 455, 304.

trap a variety of electrophiles providing, after catalyst release, enantioenriched α -functionalized carbonyl compounds **5**. Synthetically, this approach allows for the direct activation and stereoselective functionalization of unmodified carbonyl substrates.



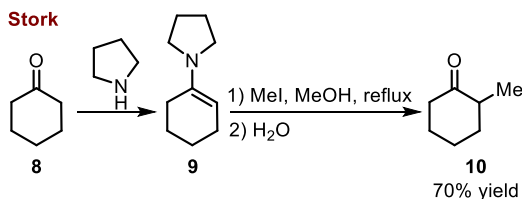
Scheme 1.2 Enamine and iminium ion activations. Protonation-deprotonation steps (aside from the one between **I** and **II**) are not reported for brevity. The filled grey circle represents a bulky substituent on the chiral amine catalyst. Nu = nucleophile; E = electrophile.

In iminium ion-mediated reactions, the condensation of a chiral amine with an α,β -unsaturated carbonyl compound **6** generates the cationic iminium ion **III**.⁸ The formation of this intermediate reduces the energy of the lowest occupied molecular orbital (LUMO) compared to the starting unsaturated carbonyl substrate **6**, therefore increasing the electrophilicity. For conjugated π -systems, the electronic redistribution induced by the formation of the iminium ion intermediate facilitates nucleophilic additions and pericyclic reactions. As a result, this activation mode allows the asymmetric β -functionalization of carbonyl compounds. It should be noted that metal-based Lewis acid catalysis, another classical activation strategy in enantioselective chemistry, is also based on the same LUMO-lowering principle. As a result, the coordination of a Lewis acid to an α,β -

⁸ Although the most accurate nomenclature for these species is ene-iminium ions, they will be referred to as iminium ion intermediates throughout the whole thesis, in consonance with the established literature of the aminocatalysis field.

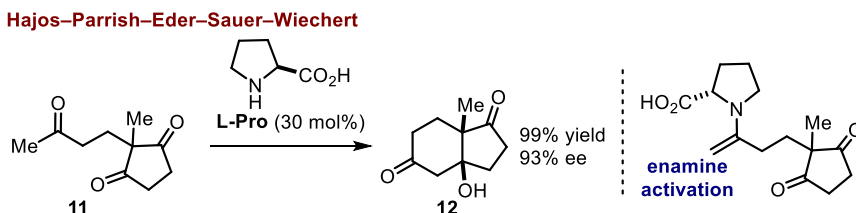
unsaturated carbonyl compound causes a similar effect, thus rendering analogous reactivity.

In 1954, Stork reported the first use of an enamine to promote the α -alkylation of ketones.⁹ In this early report, the preformed stoichiometric enamine **9** facilitated the functionalization of the starting ketone **8** through a two-step strategy (Scheme 1.3).



Scheme 1.3 Use of the preformed enamine **9** to promote the α -alkylation of ketones, an early example of enamine-mediated transformation.

The first use of a chiral amine in a sub-stoichiometric amount to catalyze an aldol reaction was reported by two independent groups: Hajos and Parrish and Eder, Sauer, and Wiechert. In the early 1970s, they described an intramolecular L-proline-catalyzed aldol desymmetrization process (Scheme 1.4).¹⁰



Scheme 1.4 Hajos-Parrish-Eder-Sauer-Wiechert reaction, an early example of enamine-mediated asymmetric organocatalysis.

The field of enantioselective aminocatalysis continued to grow slowly until 2000, when the seminal works reported by List, Lerner, and Barbas III¹¹ and MacMillan¹² encouraged

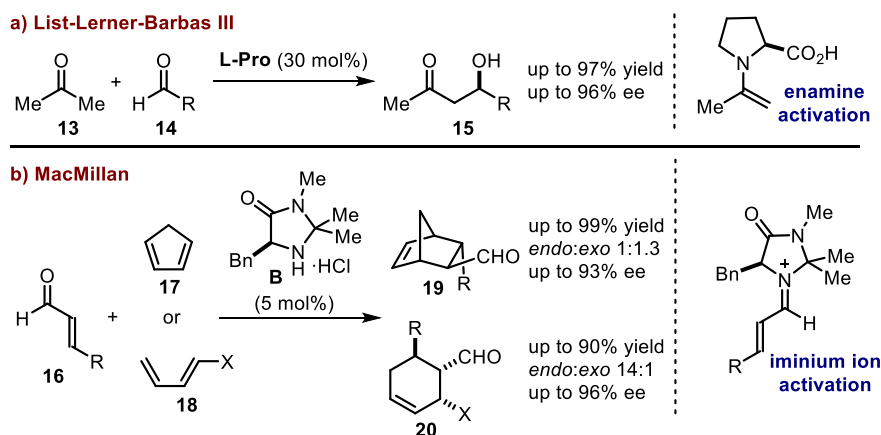
⁹ Stork, G.; Terrell, R.; Szmuszkovicz, J. "A new synthesis of 2-alkyl and 2-acyl ketones" *J. Am. Chem. Soc.* **1954**, *76*, 2029.

¹⁰ a) Eder, U.; Sauer, G.; Wiechert, R. "New type of asymmetric cyclization to optically active steroid CD partial structures" *Angew. Chem. Int. Ed.* **1971**, *10*, 496. b) Hajos, Z. G.; Parrish, D. R. "Asymmetric synthesis of bicyclic intermediates of natural product chemistry" *J. Org. Chem.* **1974**, *39*, 1615.

¹¹ List, B.; Lerner, R. A.; Barbas III, C. F. "Proline-catalyzed direct asymmetric aldol reactions" *J. Am. Chem. Soc.* **2000**, *122*, 2395.

¹² Ahrendt, K. A.; Borths, C. J.; MacMillan, D. W. C. "New strategies for organic catalysis: the first highly enantioselective organocatalytic Diels-Alder reaction" *J. Am. Chem. Soc.* **2000**, *122*, 4243.

numerous researchers to explore the potential of this novel metal-free approach, establishing organocatalysis as a new powerful strategy.³ These two reports showed the potential of aminocatalysis to facilitate the enantioselective functionalization of unmodified carbonyl compounds *via* enamine and iminium ion-mediated reactions. List, Lerner and Barbas reported a L-proline-catalyzed intermolecular enantioselective aldol reaction driven by the *in situ* formation of a chiral enamine (Scheme 1.5a). On the other hand, MacMillan described the use of the L-phenylalanine-derived imidazolidinone **B** as chiral aminocatalyst for a Diels-Alder iminium ion-mediated transformation (Scheme 1.5b).



Scheme 1.5 Seminal works for the modern era of asymmetric organocatalysis: a) enamine-mediated intermolecular asymmetric aldol; b) iminium ion-mediated Diels-Alder reactions.

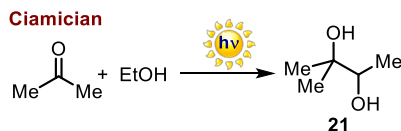
1.2 Photochemistry

The necessity of alternative energy sources that would allow humankind to move away from the finite fossil fuels is currently a general concern. As early as 1912, Giacomo Ciamician, a pioneer of photochemistry, suggested the use of light as an alternative energy source for chemical processes.¹³ He used light to promote chemical reactions, establishing photochemistry as a new branch of organic synthesis. The reductive alkylation of ketones activated by light serves as an example of Ciamician's early work (Scheme 1.6).¹⁴ It shows the potential of light-driven transformations, which enabled the product formation in the absence of any added base or heating. The inexhaustibility, cleanliness, and the extraordinary quantities of light that reaches our planet from the sun's

¹³ Ciamician, G. "The photochemistry of the future" *Science* **1912**, *36*, 385.

¹⁴ Ciamician, G.; Silber, P. "Chemische lichtwirkungen" *Ber. Dtsch. Chem. Ges.* **1910**, *43*, 945.

irradiation every day, makes Ciamician's original idea one of the most intriguing and potentially beneficial research fields of our era.



Scheme 1.6 Early example of photochemistry, developed by Ciamician.

Photochemistry is now an established branch of chemistry, which studies the chemical effects of light.¹⁵ Upon light absorption, a chemical species undergoes an electronic transition and an excited-state of the molecule is reached. The excited-state molecule differs from the corresponding ground-state not only in terms of energy content, but also in its electronic distribution. For this reason, the excited molecule should not be considered as a “hot” ground-state molecule, but as a new chemical species, with an inherently different chemical and physical behavior.¹⁶

The photochemistry field has been gradually growing ever since; however, initially only specialized groups have focused on the development of this area. The photochemical transformations were, in most of the cases, achieved utilizing very specialized equipment able to generate high energy photons (UV irradiation), like mercury lamps, or photo-boxes. Such harsh conditions prevented a fast growth of the field as functional group compatibility was limited.

In the past decade, the seminal works by MacMillan,¹⁷ Yoon¹⁸ and Stephenson,¹⁹ along with other contributions, stimulated a massive interest in the development of new visible light-driven photoredox transformations. Central to this synthetic approach is the use of photoredox catalysts that, under visible light irradiation, can generate radicals from stable precursors. The possibility of accessing radical reactivity under very mild conditions allowed the use of traditional tools of enantioselective catalysis, which were very successful in classical polar processes (like organocatalysis, not compatible with the previous harsh reaction conditions), within radical reactivity patterns. The rediscovery of

¹⁵ McNaught, A. D.; McNaught, A. D. “Compendium of chemical terminology” *The Gold Book 2nd Ed.* **1997**, Oxford: Blackwell Science.

¹⁶ Balzani, V.; Ceroni, P.; Juris, A. “Photochemistry and photophysics: concepts, research, applications” **2014**, Chapter 4, p. 103, Wiley & Sons.

¹⁷ Nicewicz, D. A.; MacMillan, D. W. C. “Merging photoredox catalysis with organocatalysis: the direct asymmetric alkylation of aldehydes” *Science* **2008**, *322*, 77.

¹⁸ Ischay, M. A.; Anzovino, M. E.; Du, J.; Yoon, T. P. “Efficient visible light photocatalysis of [2+2] enone cycloadditions” *J. Am. Chem. Soc.* **2008**, *130*, 12886.

¹⁹ Narayanam, J. M.; Tucker, J. W.; Stephenson, C. R. “Electron-transfer photoredox catalysis: development of a tin-free reductive dehalogenation reaction” *J. Am. Chem. Soc.* **2009**, *131*, 8756.

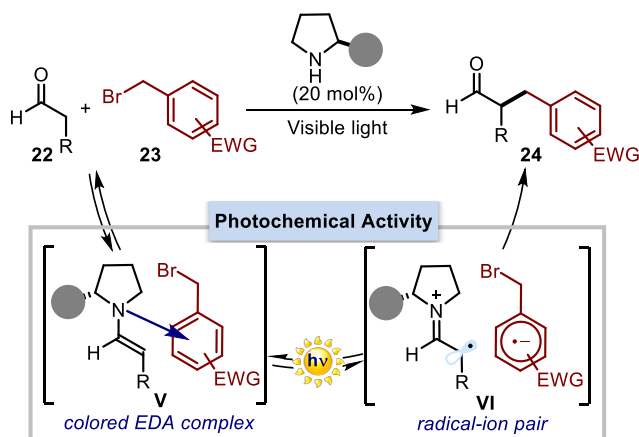
organic photochemistry has attracted the attention of numerous research groups; this scientific interest has led to the development of new powerful methodologies and concepts, extending the number of transformations available in organic chemistry.²⁰

The use of a photoredox catalyst for the generation of open-shell species has been the most commonly employed strategy. However, the Melchiorre group has recently found that radicals can be formed by using the photochemistry of transient organocatalytic chiral intermediates, without the necessity of employing any external photoredox catalyst. Specifically, it was discovered that the stereocontrolled enamine-mediated α -alkylation of aldehydes could be accomplished by simple irradiation of the reaction mixture with visible light, but without an external photocatalyst. The photoactive species was an enamine-based electron donor-acceptor (EDA) complex (Scheme 1.7).²¹ An EDA complex is a ground-state association characterized by the appearance of a new absorption band, the charge-transfer (CT) band, which generally falls in the visible region.²² The irradiation of the CT band of an EDA complex is related with a single-electron transfer (SET) from the donor, in our case the chiral enamine (*in situ* formed by the condensation of a chiral secondary amine and an aldehyde **22**), to the acceptor, the electron-poor alkyl halide **23**. As a result, the EDA photoexcitation with visible light afforded the radical species required for this transformation to take place.

²⁰ Prier, C. K.; Rankic, D. A.; MacMillan, D. W. C. "Visible light photoredox catalysis with transition metal complexes: applications in organic synthesis" *Chem. Rev.* **2013**, *113*, 5322.

²¹ Arceo, E.; Jurberg, I. D.; Álvarez-Fernández, A.; Melchiorre, P. "Photochemical activity of a key donor-acceptor complex can drive stereoselective catalytic α -alkylation of aldehydes" *Nat. Chem.* **2013**, *5*, 750.

²² a) Mulliken, R. S. "Molecular compounds and their spectra. II" *J. Am. Chem. Soc.* **1952**, *74*, 811. b) Foster, R. "Electron donor-acceptor complexes" *J. Phys. Chem.* **1980**, *84*, 2141. c) Rosokha, S. V.; Kochi, J. K. "Fresh look at electron-transfer mechanisms *via* the donor/acceptor bindings in the critical encounter complex" *Acc. Chem. Res.* **2008**, *41*, 641.



Scheme 1.7 Organocatalytic asymmetric α -alkylation of aldehydes driven by the photochemical activity of a key EDA complex. The filled grey circle represents a bulky substituent on the chiral amine catalyst.

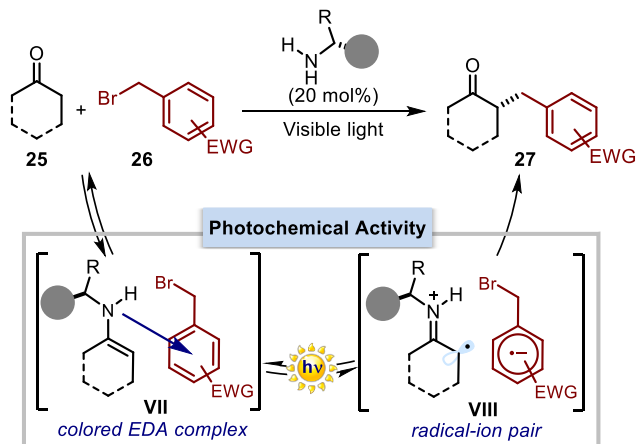
The characterization and the photochemical activity of EDA complexes had a central role in my doctoral studies. I have been involved on various projects related to the development and mechanistic study of light-triggered transformations based on the EDA complex activation strategy.

1.3 General objectives and summary

My doctorate studies aimed at using the photochemical activity of transient intermediates or molecular aggregations, such as EDA complexes, to enable unconventional reactivities. I focused on the synthetic potential of this photochemical strategy, and also on the mechanistic understanding of the developed photochemical reactions.

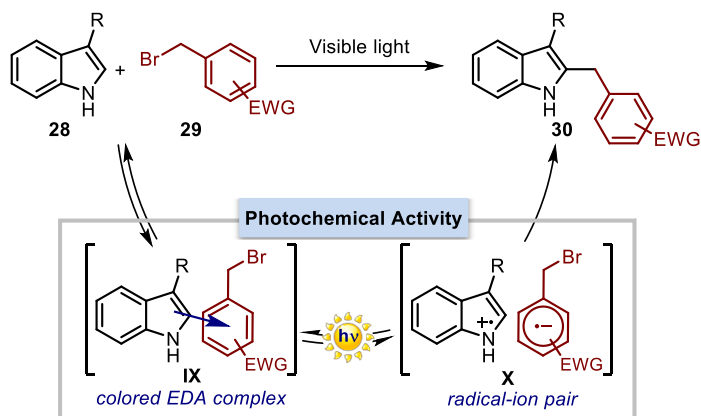
1.3.1 Alkylation reactions driven by the photochemical activity of EDA complexes

Chapter III of this dissertation describes how it was possible to expand the photochemical strategy for the enantioselective α -alkylation of aldehydes²¹ to include ketones as substrates. This transformation relies on the generation of the EDA complex VII, formed between enamines, generated upon condensation of a primary amine and a cyclic ketone 25, and electron-poor alkyl halides 26 (Scheme 1.8). The resulting methodology provided a rare example of direct enantioselective α -alkylation of unmodified ketones.



Scheme 1.8 Photo-organocatalytic asymmetric α -alkylation of cyclic ketones *via* EDA complex activation. The filled grey circle represents a bulky substituent on the chiral amine catalyst.

This work was conducted in collaboration with Dr. Elena Arceo, who run the first reaction and greatly collaborated in the discussion of the optimization studies and analysis of the scope, and Dr. Giulia Bergonzini, who was involved in the initial optimization studies. Chapter IV describes a further expansion of the EDA-based alkylation methodology. Specifically, we used the ability of indoles **28** to act as donor counterpart for the formation of EDA complexes with electron-poor alkyl bromides (Scheme 1.9). Conceptually, this study demonstrated that other molecules than enamines could serve as suitable donors in EDA complex formation. Synthetically, the photochemical activity of the indole-based EDA complexes promoted the formation of the indole alkylation product **30**. Mechanistically, we could isolate and fully characterize, by X-ray crystallographic analysis, the EDA complex **IX**.



Scheme 1.9 Photo-organocatalytic alkylation of indoles *via* EDA complex activation.

This work was conducted in collaboration with Dr. Sandeep Kandukuri, who isolated crystals of the EDA complex **IX**, and, together with Dr. Indranil Chatterjee, optimized the method while evaluating the reaction scope. I mainly focused on the mechanistic aspects of the photochemical transformation.

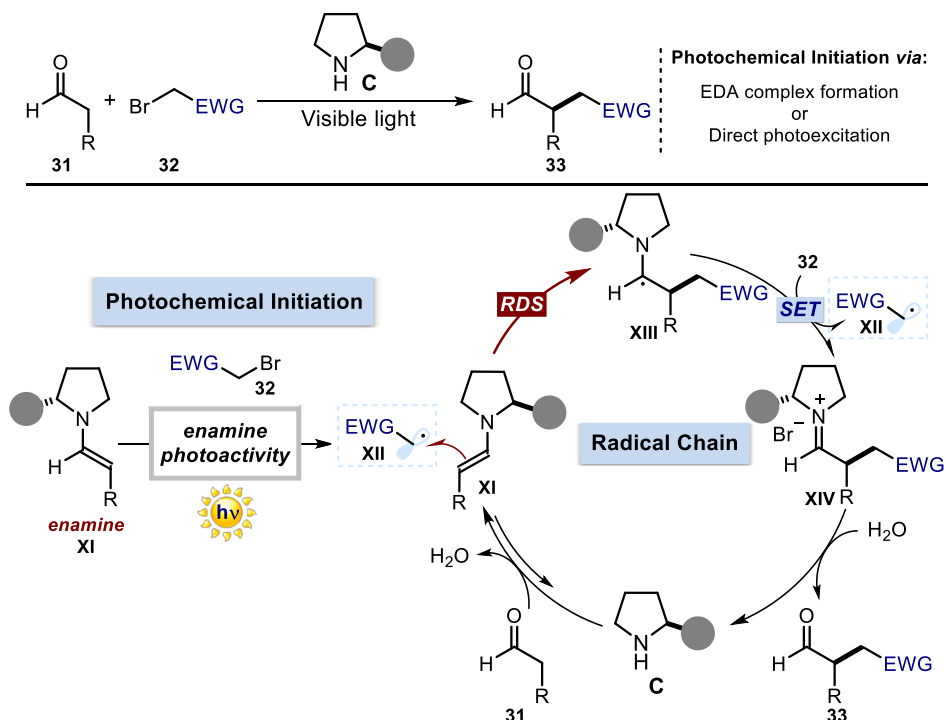
1.3.2 Mechanistic studies of the stereoselective α -alkylation of aldehydes driven by the photochemical activity of enamines

The second part of my PhD work was characterized by a progressive transition from reaction development towards a mechanistically-oriented approach. In particular, I focused on detailed mechanistic studies of some photochemical enantioselective transformations previously developed in the group. A deep understanding of a reaction mechanism is essential for the optimization of the system as well as to uncover the real possibilities that a methodology might provide. As Christopher Ingold said in 1934, “*no longer can one just mix things: sophistication in physical chemistry is the base from which all chemists, including the organic chemist, must start*”.²³

I focused on studying the mechanism of the photochemical α -alkylation of aldehydes.^{21,24} As discussed in Chapter V, I used a combination of conventional photophysical investigations, nuclear magnetic resonance (NMR) spectroscopy, and kinetic studies to gain a better understanding of the factors governing these enantioselective photochemical catalytic processes. We found that these α -alkylation reactions rely on the generation of open-shell species **XII** *via* two different enamine-based photochemical mechanisms: the direct photo-excitation of the enamine **XI** or the excitation of a photoactive EDA complex, generated between enamines and electron-poor alkyl halides **32** (Scheme 1.10). In addition, measurements of the quantum yield revealed that a radical chain mechanism was operative, while kinetic studies established the trapping of the carbon-centered radical by the enamine, to form the carbon-carbon bond, as the turnover-limiting step.

²³ Ingold, C. K.; quoted by Barton, D. H. R. “Ingold, Robinson, Winstein, Woodward, and I” *Bull. Hist. Chem.* **1996**, *19*, 43.

²⁴ Silvi, M.; Arceo E.; Jurberg, I. D.; Cassani, C.; Melchiorre, P. “Enantioselective organocatalytic alkylation of aldehydes and enals driven by the direct photoexcitation of enamines” *J. Am. Chem. Soc.* **2015**, *137*, 6120.

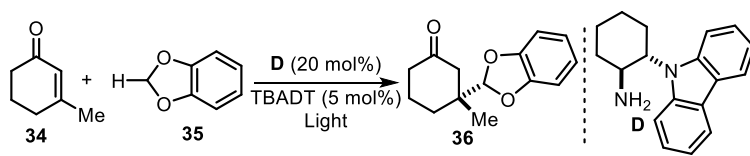


Scheme 1.10 Mechanistic studies of the photo-organocatalytic asymmetric α -alkylation of aldehydes *via* EDA complex activation and direct photoexcitation of enamines. The filled grey circle represents a bulky substituent on the chiral amine catalyst; RDS: rate-determining step.

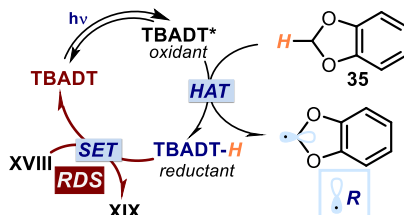
1.3.3 Mechanistic studies of the of iminium ion trapping of radicals *via* asymmetric electron-relay catalysis

Our group recently developed an iminium ion-mediated radical conjugate addition to β,β -disubstituted cyclic enones (**34**).²⁵ The last chapter of this thesis details how a combination of spectroscopic and kinetic studies served to elucidate the key mechanistic aspects of this transformation. The chemistry exploits the ability of the chiral primary amine catalyst **D**, purposely adorned with a redox-active carbazole moiety, to facilitate the stereoselective interception of photochemically-generated carbon-centered radicals by means of an electron-relay mechanism (Scheme 1.11). An unanticipated turnover-limiting step has been uncovered, for it is the reduction of the carbazole radical cation within intermediate **XVIII** and the regeneration of the photocatalyst (tetrabutylammonium decatungstate, TBADT) that dictates the overall rate of the process.

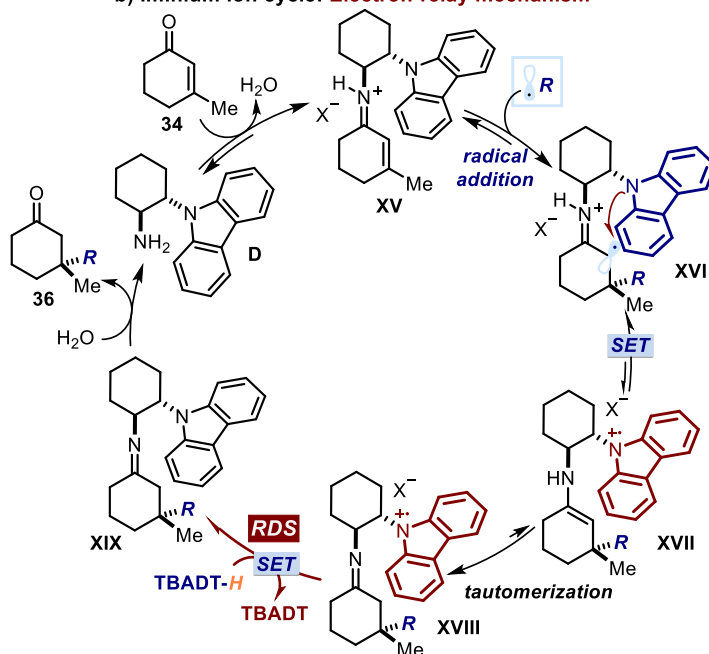
²⁵ Murphy, J. J.; Bastida, D.; Paria, S.; Fagnoni, M.; Melchiorre, P. "Asymmetric catalytic formation of quaternary carbons by iminium ion trapping of radicals" *Nature* **2016**, *532*, 218.



a) Photoredox Cycle: TBADT - HAT mechanism



b) Iminium ion cycle: Electron-relay mechanism



Scheme 1.11 Mechanism for the enantioselective catalytic radical conjugated addition to enones. a) TBADT-mediated photoredox cycle, which affords the carbon-centered radical from benzodioxole precursors **35** by means of a HAT mechanism. b) The electron-relay mechanism underlying the iminium-ion-mediated enantioselective radical conjugate addition to enone **34**. RDS: rate-determining step; SET = single-electron transfer; HAT: hydrogen-atom transfer.

This work was conducted in collaboration with Dr. John Joseph Murphy, who developed the catalytic system and greatly collaborated in the mechanistic discussion and the experiment design.

Chapter II

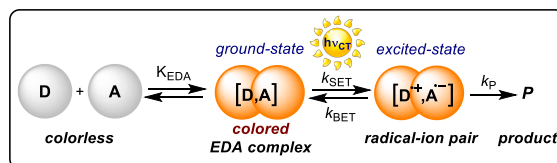
EDA complexes: characteristics and uses

Target

Photochemical generation of radicals under mild conditions.

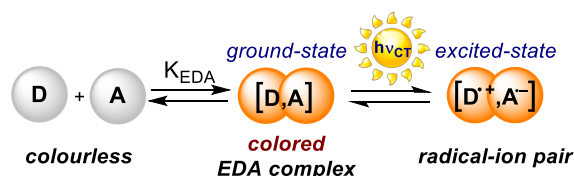
Tool

Photochemical activity of electron donor-acceptor (EDA) complexes.



2.1 Introduction

This chapter provides a thorough description of electron donor-acceptor (EDA) complexes, molecular aggregations that play a central role for the reactivity discussed in this doctoral thesis. As shown in Scheme 2.1, an EDA complex is a ground-state association of an electron-rich substrate (a donor **D** with a low ionization potential, IP) with an electron-accepting molecule (an acceptor **A** having a high electronic affinity, EA). EDA complexes are characterized by physical properties that differ from those of the separated substrates. This is because new molecular orbitals are formed, emerging from the electronic coupling of the **D** and **A** frontier orbitals (HOMO/LUMO). The main peculiarity of EDA complexes is that their formation is accompanied by the appearance of a new absorption band, the charge-transfer band ($h\nu_{CT}$), associated with an intracomplex single-electron transfer (SET) from the donor to the acceptor. In many cases, the energy of this transition lies within the visible range.



Scheme 2.1 Formation and excitation of an EDA complex. **D** = donor; **A** = acceptor; K_{EDA} = association constant of the complex.

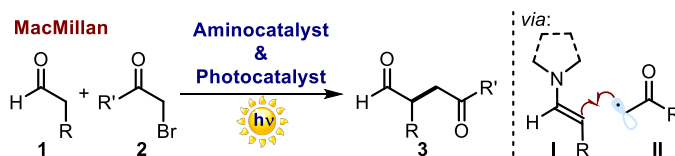
These molecular aggregations have been known since the 1940's¹ and extensive studies have been reported describing their properties and characterization ever since. Recently,

¹ Benesi, H. A.; Hildebrand, J. H. "A spectrophotometric investigation of the interaction of iodine with aromatic hydrocarbons" *J. Am. Chem. Soc.* **1949**, *71*, 2703.

our group discovered the intermediacy of these complexes while studying the photochemical enamine-mediated α -alkylation of aldehydes with electron-poor alkyl halides.²

2.2 Enamine-mediated α -alkylation of aldehydes

Gilbert Stork reported in the 1950's that preformed enamines can facilitate the S_N2 -type α -alkylation of ketones with alkyl halides.³ However despite extensive efforts, mainly conducted during the renaissance of enantioselective organocatalysis, it was not possible to accomplish these enamine-mediated alkylation reactions using a catalytic amount of chiral amines. It was only in 2008 when MacMillan addressed this difficult synthetic target by merging two powerful strategies of molecule activation: aminocatalysis and photoredox catalysis (Scheme 2.2).⁴ The last approach was used to access radical reactivity manifolds under mild conditions. By these means, carbon-centered radicals (**II**) were generated upon reduction of the alkyl halides **2**. Concomitantly, these reactive intermediates **II** were trapped by catalytic *in situ* generated enamines **I** affording the new carbon-carbon bond. This report demonstrated that the enamine-mediated α -alkylation of aldehydes with alkyl halides could be successfully performed when employing a catalytic amount of the chiral enamine **I** through radical pathways.



Scheme 2.2 Photochemical enamine-mediated α -alkylation of aldehydes combining amino and photoredox catalysis.

Key for success was the use of photoredox catalysis to generate open-shell species under mild conditions.⁵ A photoredox catalyst is a molecule capable of undergoing a redox reaction in the excited-state. Generally, it is also involved in a subsequent redox process

² Arceo, E.; Jurberg, I. D.; Álvarez-Fernández, A.; Melchiorre, P. "Photochemical activity of a key donor-acceptor complex can drive stereoselective catalytic α -alkylation of aldehydes" *Nat. Chem.* **2013**, *5*, 750.

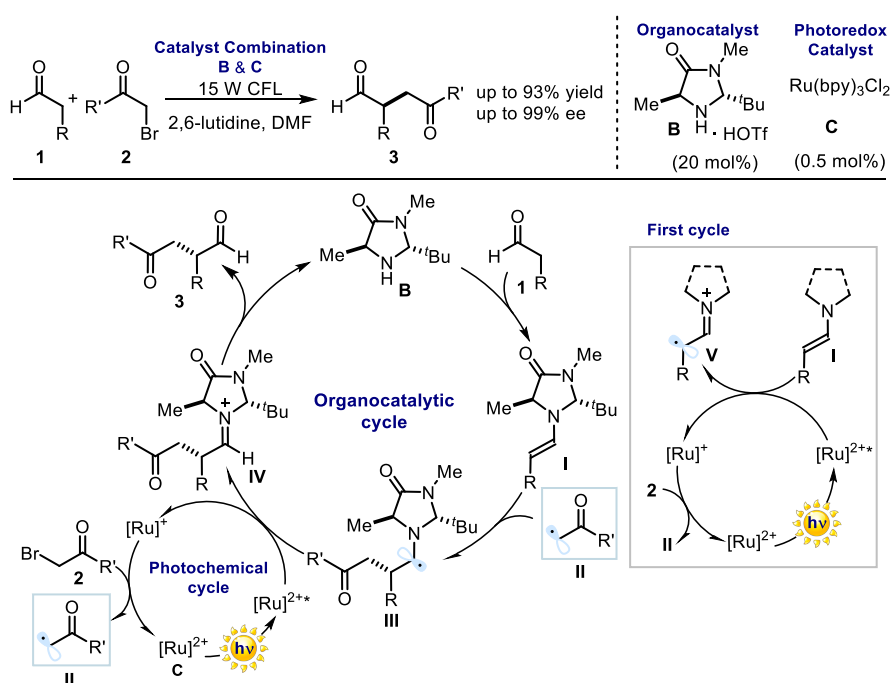
³ a) Stork, G.; Terrell, R.; Szmuszkovicz, J. "A new synthesis of 2-alkyl and 2-acyl ketones" *J. Am. Chem. Soc.* **1954**, *76*, 2029. b) Stork, G.; Brizzolara, A.; Landesman, H.; Szmuszkovicz, J.; Terrell, R. "The enamine alkylation and acylation of carbonyl compounds" *J. Am. Chem. Soc.* **1963**, *85*, 207.

⁴ Nicewicz, D. A.; MacMillan, D. W. C. "Merging photoredox catalysis with organocatalysis: the direct asymmetric alkylation of aldehydes" *Science* **2008**, *322*, 77.

⁵ Prier, C. K.; Rankic, D. A.; MacMillan, D. W. C. "Visible light photoredox catalysis with transition metal complexes: Applications in organic synthesis" *Chem. Rev.* **2013**, *113*, 5322.

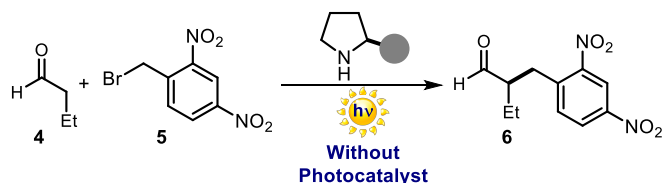
that regenerates the original photocatalyst, enabling its participation in light-mediated catalytic redox transformations.

The catalytic cycle proposed by MacMillan for the α -alkylation of aldehydes is shown in Scheme 2.3.⁴ On one side, the nucleophilic enamine **I** is formed upon condensation of aminocatalyst **B** with aldehyde **1**. Simultaneously, the photocatalyst **C** would reduce the starting alkyl halide **2** generating a highly reactive radical anion. This step would render, upon irreversible fragmentation of the carbon-halogen bond, the carbon centered radical **II**. The chiral enamine **I**, which is not nucleophilic enough to directly react with the starting alkyl halide **2** through a polar pathway, is however able to trap the carbon-centered radical **II** generating the α -aminoradical **III**. A single-electron transfer (SET) from the excited ruthenium photocatalyst eventually oxidizes this intermediate, closing the photoredox cycle and generating the iminium ion of the final product (**IV**). After hydrolysis, the final product as well as the aminocatalyst are released. The first equivalent of carbon-centered radical **II** would be furnished after an initial reduction of the ruthenium photocatalyst **C** carried out by a sacrificial equivalent of the enamine **I**.



Scheme 2.3 Proposed mechanism by MacMillan and coworkers for the asymmetric α -alkylation of aldehydes combining photoredox and organocatalysis. CFL = compact fluorescent light; DMF = dimethylformamide.

The report by MacMillan stimulated further investigations from our group on the enamine-mediated photochemical α -alkylation of aldehydes. By means of a control experiment, the unanticipated and surprising observation was made that the transformation with 2,4-dinitrobenzyl bromide (**5**) could proceed upon light irradiation but in the absence of any external photocatalyst (Scheme 2.4). This unexpected result brought the group's attention to elucidate the photochemical mechanism which enabled this transformation without the necessity of an external photocatalyst.²

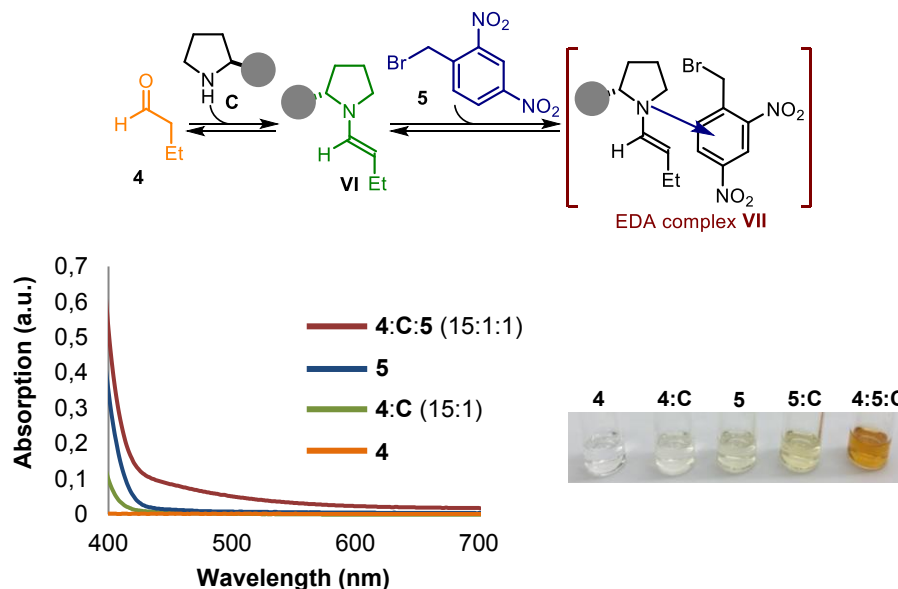


Scheme 2.4 Enamine-mediated photochemical α -alkylation of aldehydes in the absence of any photocatalyst. The filled grey circle represents a bulky substituent on the chiral amine catalyst.

2.2.1 α -Alkylation of aldehydes mediated by the photochemical activity of EDA complexes

The enamine-mediated asymmetric α -alkylation of aldehydes was found to be completely suppressed in the absence of light irradiation, thus confirming the photochemical nature of the transformation. Furthermore, inhibition of the reactivity was also observed under an aerobic atmosphere or in the presence of TEMPO (1 equiv.), the latter observation being consonant with a radical mechanism. It was found that such radical reactivity was achieved by the photochemical activity of EDA complexes **VII** (see Scheme 2.5) generated *in situ* between the electron-rich enamines (formed upon condensation of the aminocatalyst **E** and the starting aldehyde **4**), which acted as a donor, and the electron-poor alkyl halide **5**, which played the role of acceptor.

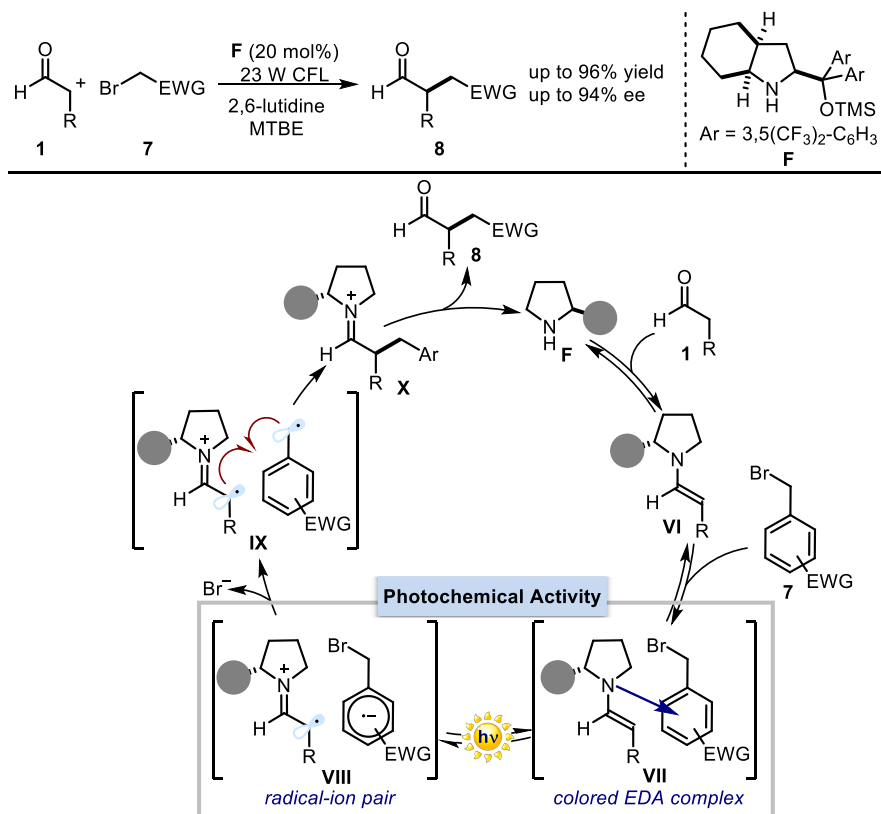
As it is shown in Scheme 2.5, achromatic solutions are obtained from the separate reaction components. However, a marked yellow color can be observed immediately after mixing a methyl *tert*-butyl ether (MTBE) solution of the enamine **VI**, generated *in situ* upon condensation of butanal **4** (15 equiv.) with the aminocatalyst **E** (1 equiv.), with 2,4-dinitrobenzyl bromide **5** (1 equiv.). This color change is characteristic of the formation of an EDA complex **VII**.



Scheme 2.5 Optical absorption spectra, recorded in MTBE in 1 mm path quartz cuvettes using a Shimadzu 2401PC UV-visible spectrophotometer, and visual appearance of the separate reaction components and of the colored EDA complex in the alkylation of 2,4-dinitrobenzyl bromide **5**; $[4] = 3 \text{ M}$; $[5] = [E] = 0.2 \text{ M}$. The filled grey circle represents a bulky substituent on the chiral amine catalyst.

The thorough mechanistic study of this transformation, which is triggered by the photochemical activity of enamine-based EDA complexes, is the main focus of Chapter V. Here, a brief introduction of our original mechanistic hypothesis is given (Scheme 2.6). Upon visible light absorption, the colored EDA complex **VII** forms the radical-ion pair **VIII**. The facile fragmentation of the bromide anion from the ion pair **VIII** would productively render the positively charged intermediate **IX**. Concomitantly, an in-cage radical-radical coupling could be invoked to account for the new carbon-carbon bond formation, which leads to the final product after hydrolysis of the iminium ion **X**.⁶

⁶ Recent studies on the mechanism of this transformation established that a radical chain propagation mechanism is operative, while the photo-activity of the enamine-based EDA complex serves as the initiation step. For details, see Chapter V and: Bahamonde, A.; Melchiorre, P. "Mechanism of the stereoselective α -alkylation of aldehydes driven by the photochemical activity of enamines" *J. Am. Chem. Soc.* **2016**, *138*, 8019.



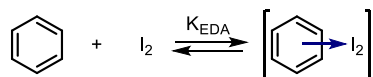
Scheme 2.6 Photo-organocatalytic asymmetric α -alkylation of aldehydes *via* EDA complex activation. CFL = compact fluorescent light; EWG = electron-withdrawing group. The filled grey circle represents a bulky substituent on the chiral amine catalyst.

Our studies established the involvement of photoactive EDA complexes in the enamine-mediated α -alkylation of aldehydes.² Despite synthetic applications of EDA complexes were rare, their formation and structural/photophysical characterization had been extensively studied for decades.

2.3 Historical background

The appearance of strong colour after bringing together two colourless organic compounds is not an uncommon observation for a chemist. In 1949, Benesi and Hildebrand reported a thorough study of the UV-Vis absorption spectra of different solutions of aromatic compounds and molecular iodine in CCl₄ (Scheme 2.7).¹ This study showed the appearance of new absorption bands and suggested the formation of a complex between iodine and the aromatic molecules. The authors associated the nature

of this complex to “an interaction in the electron-donor sense”, in which iodine would function as the electron-acceptor and the aromatic compound would act as the donor.



Scheme 2.7 EDA complex formed between I₂ and aromatic compounds in a 1:1 ratio.

Furthermore, this report described a methodology to calculate the extinction coefficient (ϵ_0) of the new absorption band and the association constant (K_{EDA}) of complexes that present a 1:1 ratio between donor and acceptor (see Section 2.4.2 for details).

Mulliken related these findings to his molecular orbital theory and supported the Benesi and Hildebrand’s idea that this new band is not associated to the iodine molecule or the arenes but rather to the complex as a whole. In addition, Mulliken proposed that the electronic excitations associated to this new absorption band were related to a charge redistribution in the complex.⁷

The wavelength (color) of this new charge-transfer band (λ_{CT}) was correlated by Mulliken to the electronics of the acceptor and donor (Equation 2.1, where IP is the ionization potential of the donor, EA is the electron affinity of the acceptor, and ω is related to the donor-acceptor distance).⁹ According to Equation 2.1, the complex presents an absorption band at a higher wavelength the more electron-rich the donor (lower IP) and the more electron-poor the acceptor (higher EA). Furthermore, a more tightly bonded complex will present a smaller HOMO-LUMO gap and therefore the charge-transfer band will appear at a higher wavelength.

$$\frac{hc}{\lambda_{\text{CT}}} = IP - EA - \omega \quad (\text{Eq. 2.1})$$

Mulliken related the formation of these complexes to the availability of accessible molecular orbitals, which should be both energetically and geometrically allowed to overlap.⁸ Additionally, a detailed generalized theory was developed to explain the ground

⁷ Mulliken, R. S. “Structures of complexes formed by halogen molecules with aromatic and with oxygenated solvents” *J. Am. Chem. Soc.* **1950**, 72, 600.

⁸ Orgel, L. E.; Mulliken, R. S. “Molecular complexes and their spectra. VII. The spectrophotometric study of molecular complexes in solution; contact charge-transfer spectra 1” *J. Am. Chem. Soc.* **1957**, 79, 4839.

and excited-state wave functions (ψ_{GS} in Equation 2.2 and ψ_{ES} in Equation 2.3, respectively) of EDA complexes.⁹

$$\psi_{GS} = a \cdot \psi_{D,A} + b \cdot \psi_{D^+ \cdot A^-} \quad (\text{Eq. 2.2})$$

$$\psi_{ES} = b \cdot \psi_{D,A} - a \cdot \psi_{D^+ \cdot A^-} \quad (\text{Eq. 2.3})$$

Equation 2.2 shows that the ground-state wave function of these complexes ψ_{GS} presents a partial charge delocalization, prior to excitation, due to a contribution from $\psi_{D^+ \cdot A^-}$. This ground-state delocalization is described by the degree of charge-transfer (q), which roughly corresponds to the normalized b/a ratio (where a and b are the coefficients from Equation 2.2 and 2.3) and varies from 0 to 1 (Equation 2.4). A tightly bonded EDA complex possesses a high degree of charge-transfer prior to any irradiation (some illustrative values are depicted in Figure 2.1b). The degree of charge-transfer is also related to the temperature: the radical-ion pair form becomes more prominent at high temperatures.

$$q \approx \frac{b}{a} \quad (0 \leq q \leq 1) \quad (\text{Eq. 2.4})$$

Mulliken's studies provided an insightful description of EDA complexes, conceptualizing the theory of EDA aggregations.¹⁰

2.4 EDA complex characterization

Most of the studies concerning EDA complexes focus on their characterization, the determination of the association constants, and the isolation of these molecular aggregations as crystalline salts.

2.4.1 X-Ray crystallographic analysis

The obtainment of a crystal of an EDA complex can be particularly informative as it displays the orientation of the complex, which clarifies the orbitals involved in the stabilization, provides donor-acceptor distances, and permits to estimate the charge distribution on the aggregate. Furthermore, the isolation of a crystal provides a direct evidence for the formation of an EDA complex.

⁹ a) Mulliken, R. S. "Molecular compounds and their spectra. II" *J. Am. Chem. Soc.* **1952**, *74*, 811.

b) Mulliken, R. S.; Person, W. B. "Molecular compounds and their spectra. XXI. Some general considerations" *J. Am. Chem. Soc.* **1969**, *91*, 3409.

¹⁰ Foster, R. "Electron donor-acceptor complexes" *J. Phys. Chem.* **1980**, *84*, 2141.

Although the intermolecular interactions of most EDA complexes are moderate, some of these aggregations are sufficiently stable to allow their isolation as crystalline salts amenable to direct X-ray structure analysis. These crystals usually reveal a significantly larger distance between donor and acceptor (r_{DA}) than any covalent bond. However, such distances, approximately 3.0–3.3 Å for most complexes, are closer than the sum of their Van der Waals radii, corroborating the presence of a weak attractive interaction. Figure 2.1a depicts the structure of some isolated intermolecular EDA complexes.¹¹

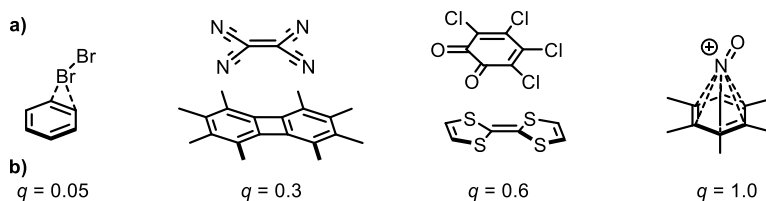
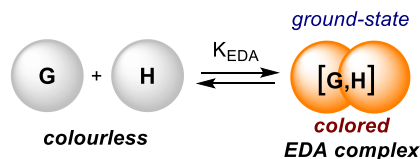


Figure 2.1 (a) X-Ray structure; (b) degree of charge-transfer (q) of some EDA complexes.

2.4.2 Determination of the association constant of an EDA complex

The majority of the studies describing the characterization of EDA complexes report their association constants (K_{EDA} , see Scheme 2.8). This thermodynamic parameter characterizes the equilibrium between free donor and acceptor and the complex (**G** and **H** in Scheme 2.8) and describes the strength of the EDA complex. The most commonly employed methodology for the determination of the association constant of an EDA complex was established by Benesi and Hildebrand.¹ According to this procedure, a series of solutions containing a constant concentration of one species, either the donor or the acceptor (**G**), and an increasing excess of the other partner (**H**) should be prepared. The absorbance of these solutions at a wavelength where only the complex is absorbing should be measured. A straight line is obtained when the reciprocal of the absorbance is plotted against the reciprocal of the concentration of the partner in excess **H**. The extinction coefficient of the absorption band and association constant of the complex can be calculated from the slope and intercept (Equation 2.5; A is the absorption and l is the optical path-length of the irradiation cell).

¹¹ Rosokha, S. V.; Kochi, J. K. "Fresh look at electron-transfer mechanisms *via* the donor/acceptor bindings in the critical encounter complex" *Acc. Chem. Res.* **2008**, *41*, 641.



Scheme 2.8 Formation of an EDA complex between **G** and **H**; K_{EDA} = association constant of the complex.

$$\text{when } [H] \gg [G] \quad \frac{1}{A} = \frac{1}{[G] \cdot l \cdot \varepsilon_0 \cdot K_{EDA}} \cdot \left(\frac{1}{[H]} \right) + \frac{1}{[G] \cdot l \cdot \varepsilon_0} \quad (\text{Eq. 2.5})$$

It should be noted that the methodology developed by Benesi and Hildebrand is widely employed nowadays for the spectroscopic calculation of association constants of various types of molecular aggregations.¹²

2.5 Characteristics that govern the complex strength and SET rate

The association constants measured for different EDA complexes vary from 10^{-1} to 10^5 M^{-1} and are subjected to both electronic and steric interactions. An extended π -system and the lack of bulky groups, which would interfere with a good orbital overlap between donor and acceptor, are ideal.¹¹

On the other hand, from an electronic point of view, the best donor-acceptor couple is achieved when the energy of the single-electron transfer (ΔG_{SET}^0) is minimized. As shown in Equation 2.6, a lower energy for the SET is achieved the more similar the E_{ox}^0 of the donor is to E_{red}^0 of the acceptor. As a result, a strong oxidant will make a tightly bonded complex ($K_{EDA} > 10^2$ M^{-1}) with a strong reductant but not with a soft reductant, which would rather make a complex with another soft reductant.¹³

$$\Delta G_{SET}^0 = F \cdot (E_{ox}^0 - E_{red}^0) \quad (\text{Eq. 2.6})$$

Furthermore, in a tightly bounded EDA complex ($r_{DA} \approx 3.0\text{--}3.3$ Å), the SET caused by the irradiation of the charge transfer band proceeds through an inner-sphere mechanism and displays a virtually barrierless transition state. This is because the molecules of donor, acceptor, and solvent display a spatial and electronic organization upon complex formation that favors the SET. As a result, no molecular or electronic reorganization is required to stabilize the radical-ion pair formed after the SET.¹¹

¹² Wang, R.; Yu, Z. "Validity and reliability of Benesi-Hildebrand method" *Acta Phys. Chim. Sin.* **2007**, *23*, 1353.

¹³ Rosokha, S. V.; Sun, D.; Kochi, J. K. "Reversible interchange of charge-transfer *versus* electron-transfer states in organic electron transfer *via* cross-exchanges between diamagnetic (donor/acceptor) dyads" *J. Phys. Chem. B* **2007**, *111*, 6555.

On the other hand, for hindered EDA complexes, where the interplanar distance between the components varies from 5 to 6 Å, the SET follows an outer-sphere mechanism. In these cases, the SET activation energy becomes significant and the Marcus theory for the SET can be applied.¹⁴ As a result, the rate of electron-transfer is also influenced by the reorganization energy (λ). λ is defined as the energy needed for a vertical electron transition without changes in the nuclear configuration, thus satisfying the Franck-Condon principle.¹⁵ In addition, such EDA complexes are not significantly stabilized by resonance, thus making its formation constant (K_{EDA}) small.

2.5.1 Solvent effect on the stability of an EDA complex

The strength of these molecular aggregations in solution is also affected by the solvent. As a general trend, the formation of EDA complexes is favored in non-polar solvents.^{11,16} A lower solvation of the generally polarized donor and acceptor allows for an easier encounter of the species within the solvent. Furthermore, the *solvent cage*, which surrounds these molecular aggregations, is less prone to be disrupted after the photo-induced SET. In contrast, a polar solvent would stabilize the non-bonded EDA partners, because the solvent-solute interactions compete with complex formation. In addition, the back-electron transfer (BET) from the radical anion is partially inhibited facilitating an *out of the cage* solvation of both radical ions separately.¹⁷

However, this tendency is inverted for EDA complexes where ion-pair interactions contribute significantly to the ground-state. Therefore, complexes with a high degree of charge-transfer might present higher association constants in polar media. The interactions of complex formation would be favored in more polar solvents, because charge separation is supported by a higher dielectric constant.¹⁸

¹⁴ Marcus, R. A. "Tutorial on rate constants and reorganization energies" *J. Electroanal. Chem.* **2000**, 483, 2.

¹⁵ Franck-Condon principle is the approximation that an electronic transition is most likely to occur without changes in the positions of the nuclei in the molecular entity and its environment. It is a consequence of the Born-Oppenheimer approximation: electronic transfers occur much faster than nuclear vibrations. McNaught, A. D.; McNaught, A. D. "Glossary of terms used in photochemistry (IUPAC Recommendations 1996) Compendium of chemical terminology" *Pure and App. Chem* **1997**, 68, 2223.

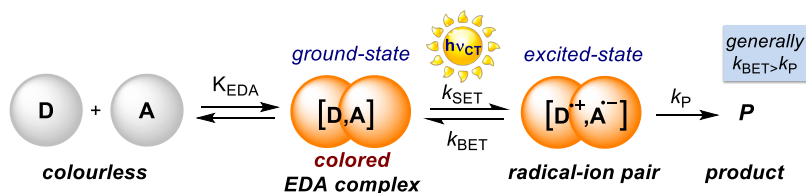
¹⁶ McKim, W. D.; Ray, J.; Arnold, B. R. "Analysis of the association constants for charge-transfer complex formation" *J. Mol. Struct.* **2013**, 1033, 131.

¹⁷ Foster, R.; Fyfe, C. A. "Interaction of electron acceptors with bases. Part 20.-Application of an NMR method to determination of stability of some organic charge-transfer complexes in solution" *Trans. Faraday Soc.* **1966**, 62, 1400.

¹⁸ Singh, N.; Khan, I. M.; Ahmad, A.; Javed, S. "Preparation, spectral investigation and spectrophotometric studies of proton transfer complex of 2, 2'-bipyridine with 3, 5-dinitrobenzoic acid in various polar solvents" *J. Mol. Struct.* **2014**, 1065, 74.

2.6 Synthetic applications of EDA complexes

Upon irradiation of the charge-transfer band, the ground-state EDA generates the radical-ion pair ($[D^+, A^-]$). However, this reactive intermediate, in most of the cases, regenerates the original complex due to a rapid back-electron transfer. This is because the BET is generally faster than other possible processes leading to products **P** ($k_{\text{BET}} > k_{\text{P}}$, with k being rate constants, Scheme 2.9), thus preventing further reactivity. This is the main reason why, although there are numerous reports on the characterization of EDA complexes, their use in chemical synthesis has found very limited applications.¹¹ However, in a reduce number of cases other processes are fast enough to compete with the BET, allowing different reaction pathways to take place. Rearrangements, additions or eliminations, or examples where the radical ions escape the solvent cage have been reported. Herein, we will discuss some selected examples of these reactions.¹⁹



Scheme 2.9 Formation and excitation of an EDA complex. D = donor; A = acceptor; K_{EDA} = association constant of the complex. k_{SET} , k_{BET} , k_{P} are kinetic constants.

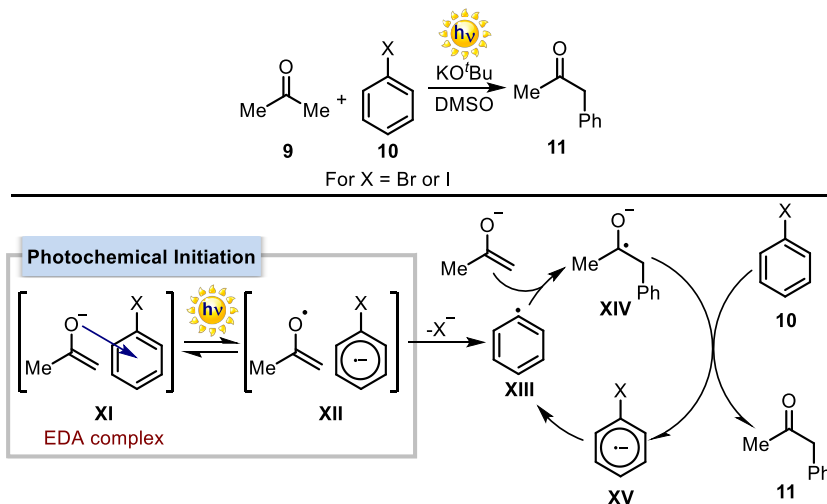
Several contributions have been reported regarding the initiation of radical transformations that present a $\text{S}_{\text{RN}}1$ -type chain propagation cycle. An $\text{S}_{\text{RN}}1$ is a process through which nucleophilic substitution is achieved on aromatic and aliphatic compounds that bear a suitable leaving group and that do not react through polar nucleophilic mechanisms. This class of transformations is characterized by an innate chain mechanism involving electron-transfer steps with radical ions as intermediates.²⁰ One of the first examples of this transformation was the reaction between acetone enolate and bromo and iodobenzene.²¹ As depicted in Scheme 2.10, the reaction is initiated by the photochemical

¹⁹ For a review on EDA complex reactivity see: Lima, C. G.; de M. Lima, T.; Duarte, M.; Jurberg, I. D.; Paixão, M. W. "Organic synthesis enabled by light-irradiation of EDA complexes: theoretical background and synthetic applications" *ACS Catal.* **2016**, *6*, 1389.

²⁰ a) Rossi, R. A.; Pierini, A. B.; Peñeñory, A. B. "Nucleophilic substitution reactions by electron transfer" *Chem. Rev.* **2003**, *103*, 71. b) Rossi, R. A.; Guastavino, J. F.; Budén, M. E. "Arene chemistry: reaction mechanisms and methods for aromatic compounds" **2015**, Chapter 10, p. 243, John Wiley & Sons.

²¹ a) Rossi, R. A.; Bunnett, J. F. "Photostimulated aromatic $\text{S}_{\text{RN}}1$ reactions" *J. Org. Chem.* **1973**, *38*, 1407. b) Bunnett, J. F.; Scamehorn, R. G.; Traber, R. P. "Solvents for aromatic $\text{S}_{\text{RN}}1$ reactions" *J. Org. Chem.* **1976**, *41*, 3677. c) Fox, M. A.; Younathan, J.; Fryxell, G. E. "Photoinitiation of the

excitation of the EDA complex **XI** where the enolate of acetone acts as the donor and the benzene halide behaves as the acceptor. Consequently, the reaction proceeds through a classical $S_{RN}1$ ²⁰ mechanism where the C-X bond of the radical anion cleaves affording the carbon-centered radical **XIII**. Afterwards, a nucleophilic trapping of this radical generates the new carbon-carbon bond forming the ketyl radical **XIV**. A subsequent reduction of another molecule of the benzene halide **10** restarts the radical chain and releases the final product **11**.

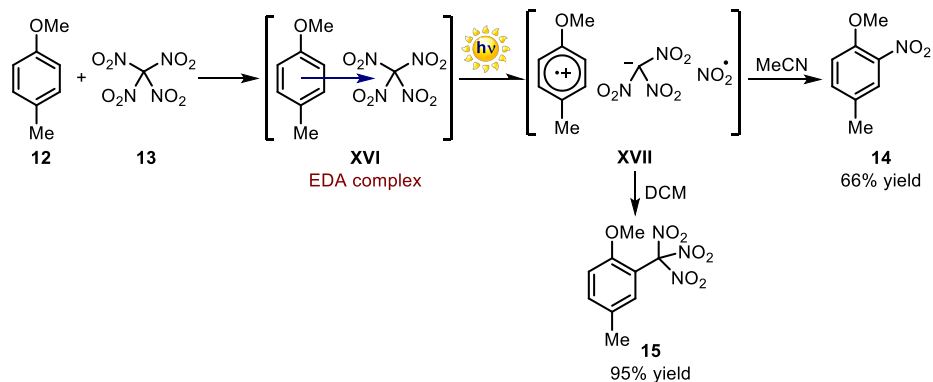


Scheme 2.10 $S_{RN}1$ reactions between acetone enolate and bromo and iodobenzene initiated by the excitation of an EDA complex. DMSO = dimethyl sulfoxide.

Scheme 2.11 shows a reaction that produces selectively two different products depending on the solvent. This example highlights the role a solvent may play in these reactions: it does not only influence the formation and stability of the EDA complex (as discussed in Section 2.5.1), but it can also affect the reaction outcome. This transformation demonstrates how the reactivity of an EDA complex-mediated reaction relies on the prevention of the back-electron transfer from the radical-ion pair. In this case, this is achieved by either a fast in-cage reaction in dichloromethane, leading to the alkylation product **15**; or the out-of-cage solvation of the intermediates, which preferentially takes place in a more polar solvent such as acetonitrile, leading to the nitration product **14**.

$S_{RN}1$ reaction by excitation of charge-transfer complexes" *J. Org. Chem.* **1983**, *48*, 3109. d) Kornblum, N. "Substitution reactions which proceed *via* radical anion intermediates" *Angew. Chem. Int. Ed.* **1975**, *14*, 734.

The transformation begins with the excitation of the EDA complex **XVI**, which leads to the formation of the triad **XVII** that, depending on the solvent, affords the nitration or the alkylation of *p*-methylanisole (Scheme 2.11).²²

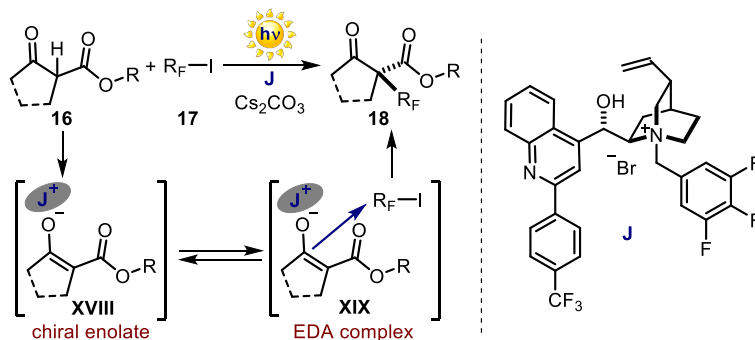


Scheme 2.11 Nitration and alkylation of *p*-methyl anisole driven by the formation of the same EDA complex in different solvents. DCM = dichloromethane.

A further contribution was reported by our research group. As already discussed, we combined the photochemical activity of EDA complexes with asymmetric catalysis. Initially, the enamine-mediated α -alkylation of aldehydes was reported (see Section 2.2.1).² Subsequently, phase-transfer catalysis was used to promote the enantioselective photo-organocatalytic perfluoroalkylation of β -ketoesters (Scheme 2.12).²³ The latter transformation proceeds *via* a radical chain mechanism. The chain reaction is initiated by the photochemical activity of the EDA complex **XIX**, formed upon the aggregation of the chiral enolate **XVIII** with the perfluorinated compound **17**. Subsequently, the final products are afforded with high yields and enantiomeric excesses.

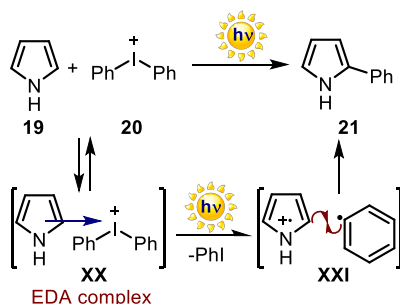
²² Sankararaman, S.; Haney, W. A.; Kochi, J. K. "Annihilation of aromatic cation radicals by ion-pair and radical pair collapse. Unusual solvent and salt effects in the competition for aromatic substitution" *J. Am. Chem. Soc.* **1987**, *109*, 7824.

²³ Woźniak, Ł.; Murphy, J. J.; Melchiorre, P. "Photo-organocatalytic enantioselective perfluoroalkylation of β -ketoesters" *J. Am. Chem. Soc.* **2015**, *137*, 5678.



Scheme 2.12 Phase-transfer catalyzed asymmetric perfluoroalkylation of enolates triggered by the photochemical activity of an EDA complex.

In the last years, the synthetic potential of EDA complexes has also been exploited by others. The Chatani's biaryl coupling should be highlighted (Scheme 2.13).²⁴ This transformation is promoted by the excitation of the EDA complex **XX**, generated between pyrrole and diphenyliodonium salt **20**, which affords the positively charged intermediate **XXI**. Concomitantly, a radical-radical coupling leads to the formation of the final product **21**.



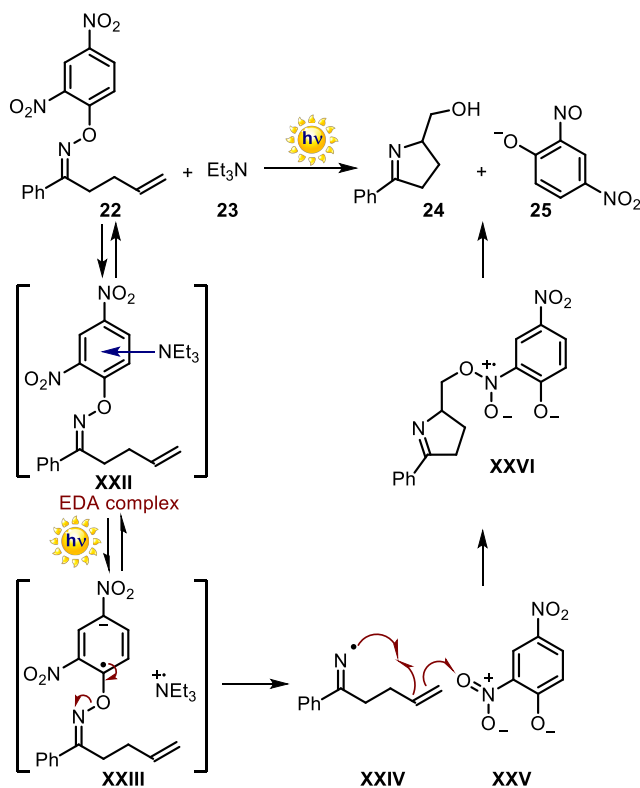
Scheme 2.13 Biaryl coupling mediated by the photochemical activity of EDA complex **XX**.

A cyclization reaction of a nitrogen-centered radical triggered by the excitation of EDA complex **XXII** was reported by Leonori (Scheme 2.14).²⁵ Upon irradiation of the charge-transfer band of **XXII**, the radical-ion pair **XXIII** is generated. A subsequent cleavage of

²⁴ Tobisu, M.; Furukawa, T.; Chatani, N. "Visible light-mediated direct arylation of arenes and heteroarenes using diaryliodonium salts in the presence and absence of a photocatalyst" *Chem. Lett.* **2013**, *42*, 1203.

²⁵ Davies, J.; Booth, S. G.; Essafi, S.; Dryfe, R. A. W.; Leonori, D. "Visible-light-mediated generation of nitrogen-centered radicals: metal-free hydroimination and iminohydroxylation cyclization reactions" *Angew. Chem. Int. Ed.* **2015**, *54*, 14017.

the nitrogen-oxygen bond affords the intermediate **XXIV**, which undergoes a 5-*exo*-dig cyclization. Concomitantly, the carbon-centered radical formed after the cyclization is trapped by **XXV** generating the intermediate **XXVI**. Finally, cleavage of the nitrogen-oxygen of **XXVI** leads to the formation of the final products **24** and **25**.



Scheme 2.14 Radical cyclization reactions mediated by the photochemical activity of EDA complex **XXII**.

The employment and investigations of EDA complexes have been the central point of my doctoral studies. The development of new photochemical EDA-based transformations led to the projects discussed in Chapter III and IV (photochemical alkylation of ketones and indoles, respectively). A special emphasis was placed on the characterization of the EDA complex responsible for the photochemical indole alkylation. Additionally, a thorough mechanistic study on the role of an EDA complex in the enamine-based enantioselective α -alkylation of aldehydes is detailed in Chapter V.

Chapter III

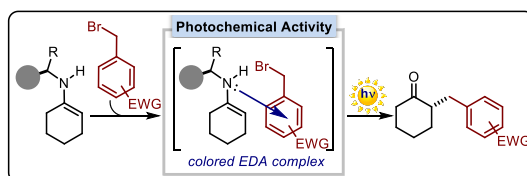
Enantioselective direct α -alkylation of cyclic ketones by means of photo-organocatalysis

Target

Developing a rare example of enantioselective catalytic direct α -alkylation of ketones with alkyl halides.

Tools

The ability of a cinchona-based primary amine catalyst to guide both the stereoselectivity-defining event and – by means of the transient formation of photon-absorbing chiral electron donor-acceptor (EDA) complexes – the photo-activation of the substrates.¹



3.1 Introduction

The aim of this project was to further expand the synthetic potential of the EDA complex-mediated reactions to develop novel, sustainable, enantioselective transformations driven by visible light. The previous studies developed by the group on the enamine-mediated α -alkylation of aldehydes **1** with alkyl halides **2** triggered by the photochemical activity of an *in situ* generated EDA complex **I**,² prompted us to expand this strategy to the α -alkylation of ketones **4** (Scheme 3.1).

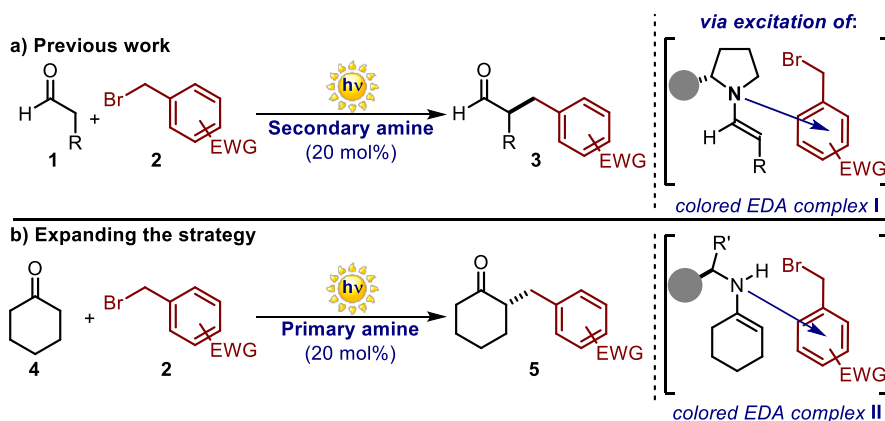
The extension of the previously developed aldehyde-alkylation strategy to include the functionalization of ketones may seem trivial due to the superficial similarities between these substrates. However, ketones present larger steric impediments that generally limit the use of chiral secondary amine catalysts for enamine formation. As a result, the less encumbered primary amines, which favor the condensation with the carbonyl moiety, are often used for the functionalization of ketones (Scheme 3.1b).³ However, this option brings about also some drawbacks. Secondary enamines, obtained by the condensation of

¹ The work discussed in this chapter has been published: Arceo, E.; Bahamonde, A.; Bergonzini, G.; Melchiorre, P. "Enantioselective direct α -alkylation of cyclic ketones by means of photo-organocatalysis" *Chem. Sci.* **2014**, *5*, 2438.

² Arceo, E.; Jurberg, I. D.; Álvarez-Fernández, A.; Melchiorre, P. "Photochemical activity of a key donor-acceptor complex can drive stereoselective catalytic α -alkylation of aldehydes" *Nat. Chem.* **2013**, *5*, 750.

³ Hine, J. "Bifunctional catalysis of alpha-hydrogen exchange of aldehydes and ketones" *Acc. Chem. Res.* **1978**, *11*, 1.

a primary amine and a carbonyl compound, spontaneously rearrange to the imine form.⁴ As a result of this unfavorable imine-enamine equilibrium, there is a reduced concentration of enamine in solution. Since the enamine would be the donor species of the crucial EDA complex **II**, the formation of this key photo-active intermediate can be difficult. In addition, a suitable ionization potential of the transient secondary enamine⁵ is required for the formation of this ground-state aggregation. Finally, an effective chiral primary amine catalyst, capable of conferring a high level of stereocontrol during the carbon-carbon bond forming event, would be required.



Scheme 3.1 Expanding the EDA complex activation strategy from aldehydes to ketones. a) Previously reported enantioselective α -alkylation of aldehydes driven by the photochemical activity of an enamine-based EDA complex **I**. b) Enantioselective α -alkylation of ketones mediated by the photo-activity of EDA complex **II**. EWG: electron-withdrawing group.

The filled grey circle represents a bulky substituent on the chiral amine catalyst.

Synthetically, developing an asymmetric α -alkylation of ketones is interesting because of the limited number of methodologies available to access the final enantioenriched compounds **5** in a direct manner, without the necessity of prefunctionalizing the substrate.

⁴ Enamines are normally stable only when the nitrogen atom does not bear a hydrogen; otherwise, the imine form predominates, see: Clark, R. A.; Parker, D. C. "Imine-enamine tautomerism. I. 2-(*N*-Cyclohexylimino)-1,3-diphenylpropane" *J. Am. Chem. Soc.* **1971**, *93*, 7257.

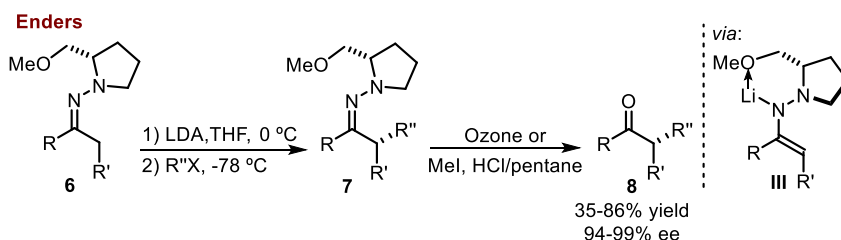
⁵ a) Müller, K.; Previdoli, F.; Desilvestro, H. "Enamines. II. A theoretical and photoelectron spectroscopic study of the molecular and electronic structures of aliphatic enamines" *Helv. Chim. Acta* **1981**, *64*, 2497. b) Domelsmith, N.; Houk, K. N. "Photoelectron spectra of cyclopentanone and cyclohexanone enamines" *Tetrahedron Lett.* **1977**, *18*, 1984. c) Schoeller, W. W.; Niemann, J.; Rademacher, P. "On the electrochemical oxidation of enamines" *J. Chem. Soc.-Perkin Trans. 2*, **1988**, 369.

3.1.1 Enantioselective α -alkylation of ketones

The enantioselective functionalization of carbonyl compounds has historically offered a potent synthetic way of producing valuable chiral molecules.⁶ Different asymmetric strategies have been described to prepare the final enantioenriched α -alkylated ketones. However, in most cases, these approaches required the use of chiral auxiliaries or other stoichiometric methodologies, the preformation of metal enolates, or the synthesis of other intermediates.

Chiral auxiliaries and stoichiometric methodologies

The utilization of chiral auxiliaries to promote the enantioselective α -alkylation of ketones with alkyl halides was extensively explored by Enders. In 1976, he reported the diastereoselective α -alkylation of ketones employing (*S*)-1-amino-2-methoxymethylpyrrolidine (SAMP) hydrazones.⁷ As depicted in Scheme 3.2, this transformation, which today is considered a classic of asymmetric synthesis, proceeds in a highly diastereoselective manner: the original products, formed upon deprotonation of the hydrazone **6** and S_N2 alkylation of alkyl halides, can be easily converted into the α -functionalized ketone **8** with high enantiomeric purity. Moreover, the configuration of the final product can be predicted; the reaction proceeds through the formation of the rigid intermediate **III**, where the lithium atom is bonded to the methoxy group of the chiral auxiliary, which controls the stereoselectivity of the alkylation by shielding one of the prochiral faces.⁸



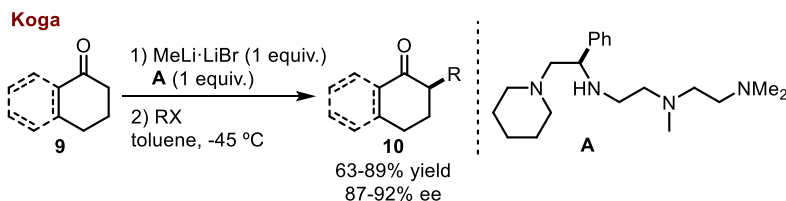
Scheme 3.2 Seminal report of the diastereoselective α -alkylation of ketones employing chiral hydrazones. LDA: lithium diisopropylamide; THF: tetrahydrofuran; X = halide.

⁶ a) Carey, F. A.; Sundberg, R. J. "Alkylation of enolates and other carbon nucleophiles" *Advanced Organic Chemistry Part B: Reactions and Synthesis*, 5th Ed. **2007**, p. 1-62, Springer. b) Carreira, E. M.; Kvaerno, L. "Classics in Stereoselective Synthesis" Weinheim, **2007**, Chapter 3, Wiley-VCH.

⁷ Enders, D.; Eichenauer, H. "Asymmetric synthesis of α -substituted ketones by metalation and alkylation of chiral hydrazones" *Angew. Chem. Int. Ed.* **1976**, *15*, 549.

⁸ Job, A.; Janecek, C. F.; Bettray, W.; Peters, R.; Enders, D. "The SAMP-/RAMP-hydrazone methodology in asymmetric synthesis" *Tetrahedron* **2002**, *58*, 2253.

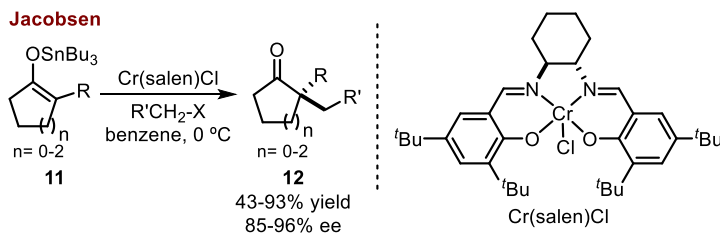
Stoichiometric chiral amines **A** have also been used to form chiral lithium enolates, generated upon deprotonation of ketones, which facilitate the stereoselective α -alkylation (Scheme 3.3).⁹ The reaction proceeds *via* nucleophilic attack of the enolate, formed by mixing the chiral lithium amide derived from **A** and the starting ketone **9**, to the alkyl halide.



Scheme 3.3 Stoichiometric methodology for the asymmetric α -alkylation of ketones.

Catalytic indirect strategies

Enantioselective catalytic methodologies based on the pre-functionalization of the ketones, requiring the synthesis of metal enolates or other intermediates, have also been developed. As shown in Scheme 3.4, Jacobsen reported in 2005 the use of chiral chromium salen complexes to promote the enantioselective alkylation of preformed tin enolates **11**.¹⁰ This strategy enabled the α -alkylation of α -branched ketones, affording highly enantioenriched products **12** with quaternary stereocenters.



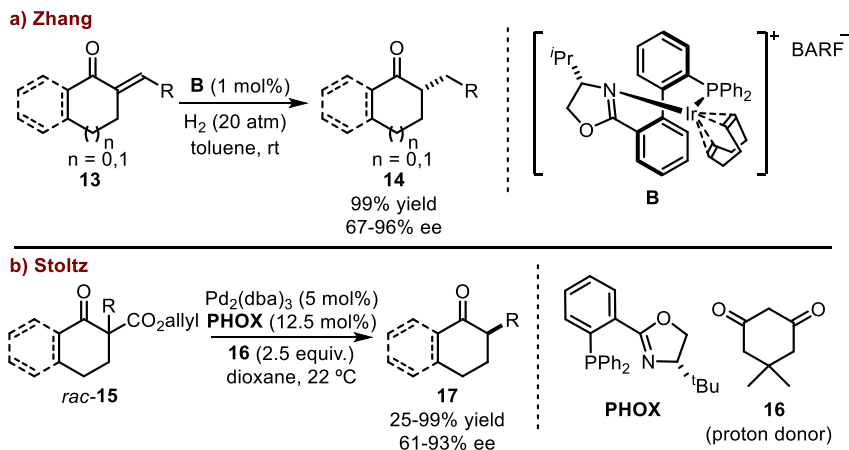
Scheme 3.4 Catalytic asymmetric alkylation of tin enolates.

Other indirect strategies, which do not rely upon a S_N2 manifold, have also been used to access enantioenriched α -alkylated ketones. An example is the organometallic approach based on an iridium-catalyzed asymmetric hydrogenation of α,β -unsaturated ketones **13**

⁹ Murakata, M.; Yasukata, T.; Aoki, T.; Nakajima, M.; Koga, K. "Stereoselective reactions. 30. Enantioselective alkylation of the lithium enolates of six-membered cyclic ketones using tetradentate chiral amines in the presence of lithium bromide" *Tetrahedron* **1998**, *54*, 2449.

¹⁰ Doyle, A. G.; Jacobsen, E. N. "Enantioselective alkylations of tributyltin enolates catalyzed by Cr(salen)Cl: Access to enantiomerically enriched all-carbon quaternary centers" *J. Am. Chem. Soc.* **2005**, *127*, 62.

leading to the reduced adducts **14** (Scheme 3.5a).¹¹ Similar products (**17**) have alternatively been accessed from racemic allyl β -ketoesters by means of a Pd-catalyzed enantioselective decarboxylative-protonation sequence, as shown in Scheme 3.5b.¹²



Scheme 3.5 Asymmetric strategies for the indirect α -alkylation of ketones based on: a) reduction of enones **13**, and b) decarboxylation of β -keto esters **15**; rt: room temperature; BARF: tetrakis[(3,5-trifluoromethyl)phenyl]borate; dba: dibenzylideneacetone.

Catalytic direct strategies

The most desirable approach to access enantioenriched α -alkylated ketones would rely on a direct method, which avoids any pre-functionalization of the substrate while employing a sub-stoichiometric amount of a chiral catalyst.

One effective catalytic strategy for the direct alkylation of ketones is phase-transfer catalysis. In this approach, the enantioselectivity is induced by chiral quaternary ammonium salts – the phase-transfer catalysts – which form chiral ion-pairs with transiently generated enolates.¹³ In these reactions, the deprotonation required for the enolate formation and the subsequent S_N2 alkylation with alkyl halides take place in different phases (immiscible liquids or solid and liquid phases). The phase-transfer catalyst transfers one reactant across the interface into the other phase so that reaction can

¹¹ Tian, F.; Yao, D.; Liu, Y.; Xie, F.; Zhang, W. "Iridium-catalyzed highly enantioselective hydrogenation of exocyclic α,β -unsaturated carbonyl compounds" *Adv. Synth. Catal.* **2010**, *352*, 1841.

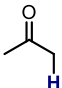
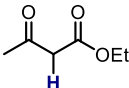
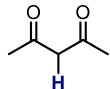
¹² Marinescu, S. C.; Nishimata, T.; Mohr, J. T.; Stoltz, B. M. "Homogeneous Pd-catalyzed enantioselective decarboxylative protonation" *Org. Lett.* **2008**, *10*, 1039.

¹³ Hashimoto, T.; Maruoka, K. "Recent development and application of chiral phase-transfer catalysts" *Chem. Rev.* **2007**, *107*, 5656.

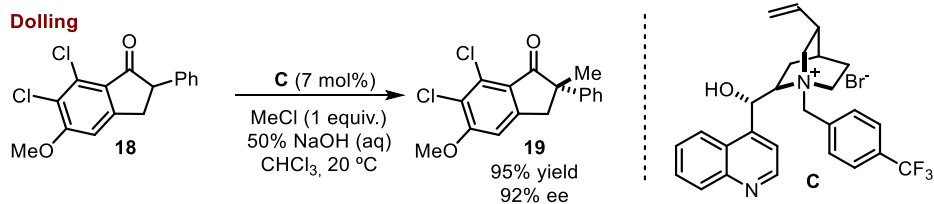
proceed. The phase-transfer agent is not consumed but performs the transport function repeatedly.¹⁴

Various methodologies for the enantioselective α -alkylation of unmodified ketones have been reported based on phase-transfer catalysis. However, the key deprotonation event leading to the enolate requires substrates with suitable high acidity of the carbonyl α -protons. As a result, most of the reports are limited to the use of β -ketoesters or 1,3-diketones (Table 3.1).

Table 3.1 pKa values in DMSO of different ketones¹⁵

Entry	Ketone	pKa
1		26.5
2		14.2
3		13.3

The first phase-transfer approach for the enantioselective alkylation of an inactivated ketone was reported by Dolling (Scheme 3.6).¹⁶ However, this methodology is restricted to the methylation of the depicted indanone derivative **18**.



Scheme 3.6 Enantioselective direct methylation of indanone **18** via phase-transfer catalysis.

¹⁴ a) McNaught, A. D.; Wilkinson, A. "Compendium of chemical terminology" *The Gold Book 2nd Ed.* **1997**, Oxford: Blackwell Science. b) Starks, C. M. "Phase-transfer catalysis. I. Heterogeneous reactions involving anion transfer by quaternary ammonium and phosphonium salts" *J. Am. Chem. Soc.* **1971**, *93*, 195.

¹⁵ Ripin, D. H.; Evans, D. A. "pKa's of Inorganic and Oxo-Acids" **2005**.

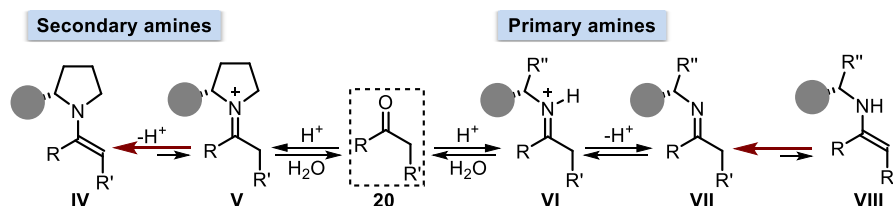
¹⁶ Dolling, U. H.; Davis, P.; Grabowski, E. J. "Efficient catalytic asymmetric alkylations. 1. Enantioselective synthesis of (+)-indacrinone via chiral phase-transfer catalysis" *J. Am. Chem. Soc.* **1984**, *106*, 446.

3.1.2 Aminocatalytic α -functionalization of ketones

The aminocatalytic approaches for the α -functionalization of carbonyl compounds have mainly focused on the use of aldehydes. This is because ketones are sterically more demanding. Consequently, their functionalization is more difficult since their condensation with chiral aminocatalysts is hampered.

Secondary amines, especially chiral pyrrolidine derivatives, are commonly employed for the functionalization of non-hindered carbonyl compounds, since the cyclic structure of these amines imparts a high nucleophilicity, which facilitates the condensation step. However, the condensation of these catalysts with carbonyl compounds is sensitive to steric factors. In contrast, primary amines are less influenced by the structural features of the carbonyl compounds. Therefore, the strategies developed for the functionalization of sterically demanding substrates, like ketones or α -branched aldehydes, usually rely on the use of primary amines as catalysts.

However, some drawbacks are associated with the use of primary amines. In contrast to secondary amines, primary amines present unfavorable imine-enamine equilibria. Generally, secondary enamines **VIII**, derived from the condensation of a primary amine and a carbonyl compound, tautomerize to the more stable imine **VII** (Scheme 3.7). Furthermore, primary amines condense more slowly than secondary amines due to the decreased nucleophilicity of the amino group.^{17, 4}



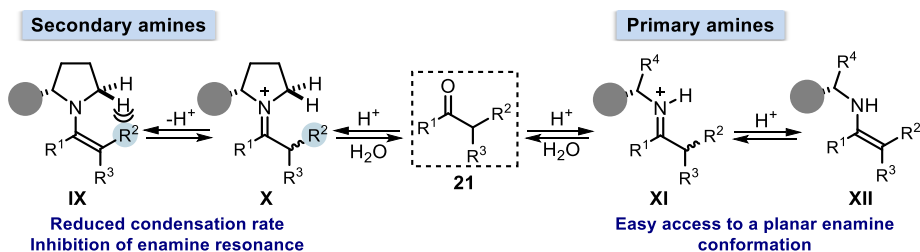
Scheme 3.7 Secondary *vs.* primary amines in condensation with non-hindered carbonyls. The filled grey circle represents a bulky substituent on the chiral amine catalyst.

However, a comparison of the reactivity of primary and secondary amines, when condensing with hindered aldehydes and ketones,¹⁸ shows a different trend (Scheme 3.8).

¹⁷ Hine, J.; Evangelista, R. A. "Iminium-ion formation and deuterium exchange by acetone in the presence of pyrrolidine, pyrazolidine, isoxazolidine, and their acyclic analogs" *J. Am. Chem. Soc.* **1980**, *102*, 1649.

¹⁸ a) Hine, J.; Menon, B. C.; Jensen, J. H.; Mulders, J. "Catalysis of α -hydrogen exchange. II. isobutyraldehyde-2-d exchange *via N*-methyliminium ion formation" *J. Am. Chem. Soc.* **1966**, *88*, 3367. b) Hine, J.; Via, F. A. "Kinetics of the formation of imines from isobutyraldehyde and primary aliphatic amines with polar substituents" *J. Am. Chem. Soc.* **1972**, *94*, 190. c) Hine, J.; Mulders, J. "Isobutyraldehyde and secondary amines. Addition and catalysis of deuterium exchange" *J. Org. Chem.* **1967**, *32*, 2200.

The equilibrium constants for iminium ion formation (deduced by rate constants for catalysis of the deuterium exchange of deuterated carbonyls) indicated how steric factors strongly influence the reactivity of secondary amines, while primary amines are less affected. Indeed, in spite of the particular rapidity of iminium ion formation from acetone, pyrrolidine is less effective than primary amines in condensation with a α -branched aldehyde such as isobutyraldehyde.



Scheme 3.8 Secondary *vs.* primary amines in condensation with sterically hindered carbonyls. The filled grey circle represents a bulky substituent on the chiral amine catalyst.

In addition, it was demonstrated that secondary enamines (**XII**) hydrolyzed (thus, reacted) much faster than the corresponding tertiary enamines (**IX**), derived from the condensation of a secondary amine and a carbonyl.¹⁹ Again, this can be attributed to steric factors, since bulky substituents on the double bond and the nitrogen make it difficult for the resulting enamine system to achieve a near to planar conformation; this geometry is required to maximize the overlap between the π -orbital of the carbon-carbon double bond and the lone pair orbital on the nitrogen (Scheme 3.8).²⁰ The steric inhibition is more pronounced for tertiary than for secondary enamines, since the latter always bear a small hydrogen substituent on the nitrogen that secures π -conjugation, thus minimizing the allylic 1,3-strain.

Among the primary amines used to promote enamine and iminium ion-mediated reactions, cinchona-based primary amines (Figure 3.1) stand out.²¹ This family of aminocatalysts has been reported to promote the stereoselective functionalization of a variety of sterically hindered carbonyl compounds, which could not be functionalized using secondary amines. These primary amines are easily prepared in a single step by

¹⁹ Capon, B.; Wu, Z. P. "Comparison of the tautomerization and hydrolysis of some secondary and tertiary enamines" *J. Org. Chem.* **1990**, *55*, 2317.

²⁰ a) Johnson, F. "Allylic strain in six-membered rings" *Chem. Rev.* **1968**, *68*, 375. b) Anderson, J. E.; Casarini, D.; Lunazzi, L. "Conformational studies by dynamic NMR. part 36.: The steric barrier and the π -barrier to rotation in simple enamines: diethylaminocyclohexenes" *Tetrahedron Lett.* **1988**, *29*, 3141.

²¹ Melchiorre, P. "Cinchona-based primary amine catalysis in the asymmetric functionalization of carbonyl compounds" *Angew. Chem. Int. Ed.* **2012**, *51*, 9748.

conversion of the hydroxyl moiety of readily available natural cinchona alkaloids by means of a Mitsunobu reaction into the amine.²² It should be noted that the catalysts derived from quinidine (**D-F**) and quinine (**G-I**) are diastereomers, as only two of the four stereogenic centers are inverted. However, in many catalytic enantioselective reactions, they act as pseudoenantiomeric catalysts, promoting the reactions to access either enantiomer of the final product with similar (but not equal) yet opposite stereoselectivity.

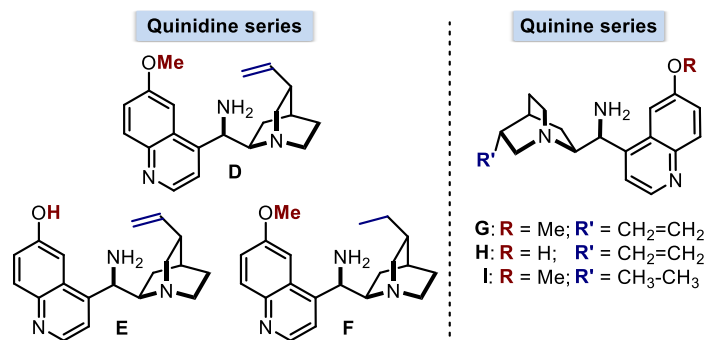


Figure 3.1 9-amino-9-deoxy-*epi*-cinchona alkaloids derived from (hydro)quinidine and (hydro)quinine.

Chen²³ and our group,²⁴ almost simultaneously, demonstrated the ability of cinchona-based primary amines to act as aminocatalysts, utilizing this scaffold in an iminium ion-mediated Michael addition. The first example of the use of a cinchona-based primary amine to promote an enamine-mediated transformation was reported by Connon.²⁵ The catalyst was used in the enantioselective Michael addition of ketones and α -branched aldehydes to nitroolefins with high yields and excellent enantio and diastereocontrol (Scheme 3.9).²⁶

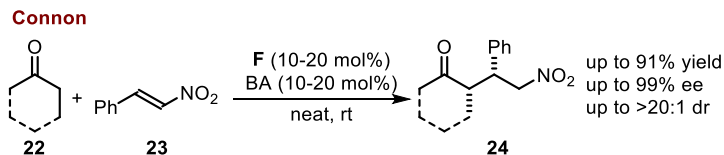
²² Cassani, C.; Martín-Rapún, R.; Arceo, E.; Bravo, F.; Melchiorre, P. "Synthesis of 9-amino(9-deoxy)epi cinchona alkaloids, general chiral organocatalysts for the stereoselective functionalization of carbonyl compounds" *Nat. Protocols* **2013**, *8*, 325.

²³ Xie, J. W.; Chen, W.; Li, R.; Zeng, M.; Du, W.; Yue, L.; Chen, Y. C.; Wu, Y.; Zhu, J.; Deng, J. G. "Highly asymmetric Michael addition to α,β -unsaturated ketones catalyzed by 9-amino-9-deoxyepiquinine" *Angew. Chem. Int. Ed.* **2007**, *46*, 389.

²⁴ Bartoli, G.; Bosco, M.; Carlone, A.; Pesciaioli, F.; Sambri, L.; Melchiorre, P. "Organocatalytic asymmetric Friedel-Crafts alkylation of indoles with simple α,β -unsaturated ketones" *Org. Lett.*, **2007**, *9*, 1403.

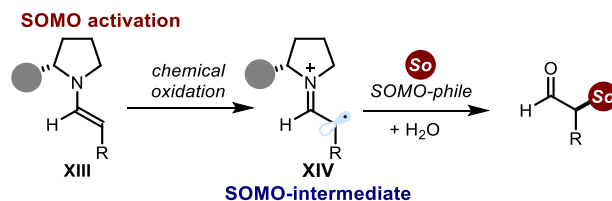
²⁵ McCooney, S. H.; Connon, S. J. "Readily accessible 9-*epi*-amino cinchona alkaloid derivatives promote efficient, highly enantioselective additions of aldehydes and ketones to nitroolefins" *Org. Lett.* **2007**, *9*, 599.

²⁶ Kwiatkowski, P.; Beeson, T. D.; Conrad, J. C.; MacMillan, D. W. "Enantioselective organocatalytic α -fluorination of cyclic ketones" *J. Am. Chem. Soc.* **2011**, *133*, 1738.



Scheme 3.9 First report of enamine-promoted transformations catalyzed by a cinchona-based primary amine. Addition of ketones to nitroolefins. BA: benzoic acid.

Additionally, there are some examples of the use of secondary amines for the enamine-mediated functionalization of ketones. Specifically, an interesting α -alkylation of ketones was recently described by MacMillan,²⁷ who used a strategy based on the formation of α -iminyl radical cations (**XIV**, SOMO-intermediates) generated upon oxidation of *in situ* generated enamines (**XIII**, Scheme 3.10).²⁸ The α -iminyl radical cation intermediate can react with nucleophilic species (SOMO-philes, *e.g.* allyl silanes) to afford α -functionalized carbonyl compounds. Consequently, this strategy provides an *umpolung*²⁹ approach for the α -functionalization of ketones and aldehydes.



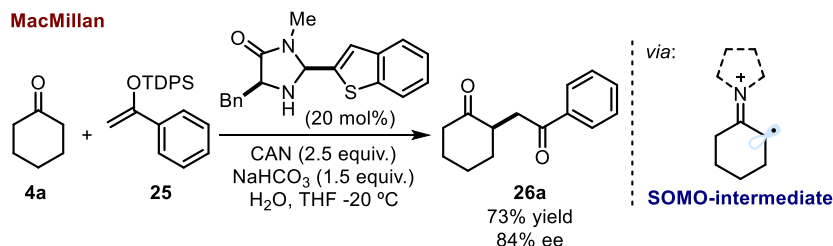
Scheme 3.10 Use of enamines as radical precursors upon single-electron chemical oxidation. So: SOMO-ophile that can intercept the enamine radical cation. The filled grey circle represents a bulky substituent on the chiral amine catalyst.

The formation of SOMO-intermediates was applied to the enantioselective trapping of the silyl enol ether **25**,²⁷ thus providing an example of the capability of this strategy to afford α -acylated ketones (Scheme 3.11).

²⁷ Mastracchio, A.; Warkentin, A. A.; Walji, A. M.; MacMillan, D. W. C. "Direct and enantioselective α -alkylation of ketones *via* singly occupied molecular orbital (SOMO) catalysis" *Proc. Natl. Acad. Sci.* **2010**, *107*, 20648.

²⁸ For seminal work see: Beeson, T. D.; Mastracchio, A.; Hong, J. B.; Ashton, K.; MacMillan, D. W. "Enantioselective organocatalysis using SOMO activation" *Science* **2007**, *316*, 582.

²⁹ Seebach, D. "Methods of reactivity *umpolung*" *Angew. Chem. Int. Ed.* **1979**, *18*, 239.

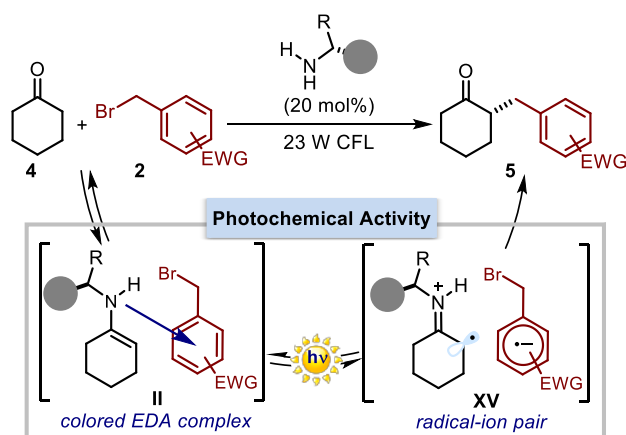


Scheme 3.11 Enantioselective synthesis of the α -phenacyl ketone **26a** through a radical-based methodology. CAN: ceric ammonium nitrate.

Despite these advances, there are no reports, also using enamine-mediated processes, for the stereocontrolled direct α -alkylation of ketones with alkyl halides. Therefore the development of an enamine-mediated alkylation reaction with an alkyl halide was a motivating objective.

3.2 Target of the project

The aim of this project was the development of a methodology for the direct enantioselective α -alkylation of ketones with alkyl halides (Scheme 3.12). Our previous report on the enamine-mediated photochemical α -alkylation of aldehydes² based on the formation of EDA complexes prompted us to follow a similar strategy. Accordingly, we envisioned that a primary amine could play a dual crucial role: first, it can guide, through the transient formation of a secondary enamine upon condensation with a ketone, the generation of a photoactive EDA complex with the electron-poor alkyl halides **2**: second, it can direct the stereoselectivity-defining event that would render the enantioenriched α -alkylation products **5**.



Scheme 3.12 Target of the project: implementing a direct photo-organocatalytic enantioselective α -alkylation of cyclic ketones. CFL = compact fluorescent light.

3.3 Results and discussion

We focused on the direct organocatalytic α -benzylation of cyclohexanone (**4a**) using 2,4-dinitrobenzyl bromide (**2a**). The model reaction has been conducted using a household 23 W compact fluorescent light (CFL) bulb to irradiate the mixture (Table 3.2).³⁰

First, we sought to identify a chiral amine able to efficiently catalyze the α -benzylation reaction. A series of 9-amino(9-deoxy)-*epi*-cinchona alkaloid-based primary amines were tested (entries 1-3). In the model reaction, the quinidine-derived catalyst **D** and its pseudo-enantiomeric counterpart **G**, derived from quinine, provided similar results but leading to the two enantiomers of the product **5a** (entries 1 and 2). Both primary amines catalyzed the formation of **5a** with high enantiomeric excess and a 45% NMR yield³¹ after 3 days of reaction. These experiments were conducted in the presence of trifluoroacetic acid (TFA, 2:1 acid to amine ratio) since it is established that an acid co-catalyst is generally needed to facilitate the imine protonation (affording the iminium ion) required for enamine formation (details on the acid effect are provided in Table 3.5). 6'-hydroxy-9-amino-9-deoxyepiquinidine **E**, bearing a hydroxyl moiety, was also tested as catalyst (entry 3). The presence of an additional hydrogen bond donor can alter the catalytic ability of amine **E**, which can be regarded as a bifunctional catalyst capable of simultaneously activating both the electrophilic and nucleophilic components.³² However, **E** did not promote the desired reaction to any extent. The less hindered primary amine **J** (entry 4) also catalyzed the benzylation of cyclohexanone, but without reaching the level of stereoselectivity inferred by catalyst **D**.

³⁰ As previously discussed, the polar enamine-mediated S_N2 -type alkylation of aldehydes with alkyl halides is not an effective strategy for the α -alkylation of these substrates (see Section 2.2 of Chapter II). This lack of reactivity is also observed when a cinchona-based primary amine is used as catalyst for the α -alkylation of ketones with alkyl halides, which does not proceed in the absence of light.

³¹ The yield of the final product **5a** was calculated by ¹H NMR employing 1,3,5-trimethoxybenzene as the internal standard.

³² a) Chen, W.; Du, W.; Duan, Y.; Wu, Y.; Yang, S.-Y.; Chen, Y.-C. "Enantioselective 1,3-dipolar cycloaddition of cyclic enones catalyzed by multifunctional primary amines: beneficial effects of hydrogen bonding" *Angew. Chem. Int. Ed.* **2007**, *46*, 7667. b) Bergonzini, G.; Vera, S.; Melchiorre, P. "Cooperative organocatalysis for the asymmetric γ -alkylation of α -branched enals" *Angew. Chem. Int. Ed.* **2010**, *49*, 9685.

Table 3.2 Catalyst screening

Reaction scheme showing the α -alkylation of cyclic ketone **4a** (4 equiv.) with 2,4-dinitrobenzyl bromide **2a** (0.1 mmol) using a catalyst (20 mol%), TFA (40 mol%), 23 W CFL, NaOAc (2 equiv.), toluene, 25 °C, 45 h to yield product **5a**.

Catalyst structures shown below the reaction:

- D**: R = Me
- E**: R = H
- G**: [Structure]
- J**: [Structure]
- K**: [Structure]

Entry	Catalyst	NMR yield ^a (%)	ee ^b (%)
1	D	45	88
2	G	45	84 ^c
3	E	<5	n.d.
4	J ^d	90	18
5	K ^d	45	42

^a Determined by ¹H NMR analysis of the crude reaction mixture employing 1,3,5-trimethoxybenzene as internal standard. ^b Enantiomeric excess determined by HPLC analysis on a Daicel Chiralpak IC column. ^c Reaction leading to the (*R*) enantiomer of **5a**. ^d Reaction performed with 20 mol% of benzoic acid instead of 40 mol% of TFA. TFA: trifluoroacetic acid; NaOAc: sodium acetate; n.d.: not determined.

The primary amine-urea bifunctional catalyst **K** was also tested (entry 5). We hypothesized that the nitro moieties on the 2,4-dinitrobenzyl bromide **2a** could engage in productive hydrogen bonding interactions with the acidic hydrogen atoms of the urea scaffold, potentially leading to a simultaneous activation of both substrates.³³ By these means, a single catalyst could activate the ketone by formation of the enamine and also orient the reaction partner **2a** in proximity to the enamine, possibly favoring the formation of a more structured transition state assembly.³⁴ However, catalyst **K** did not provide synthetically useful results. In addition, as expected, more encumbered secondary amine-based catalysts were not able to promote the reaction (data not shown).

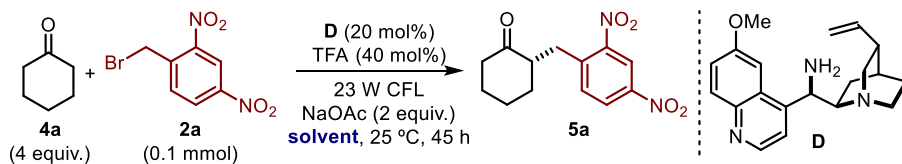
We then evaluated the effect of the solvent on the model reaction (Table 3.3). When using solvents of low dielectric constant, the final product **5a** was obtained in moderated yields (entries 1 and 2). However, remarkably low reactivity was observed in either chlorinated

³³ Okino, T.; Hoashi, Y.; Takemoto, Y. "Enantioselective Michael reaction of malonates to nitroolefins catalyzed by bifunctional organocatalysts" *J. Am. Chem. Soc.* **2003**, *125*, 12672.

³⁴ Huang, H.; Jacobsen, E. N. "Highly enantioselective direct conjugate addition of ketones to nitroalkenes promoted by a chiral primary amine-thiourea catalyst" *J. Am. Chem. Soc.* **2006**, *128*, 7170.

or polar solvents (entries 3 to 5). Toluene was identified as the solvent of choice (entry 1).

Table 3.3 Solvent screening

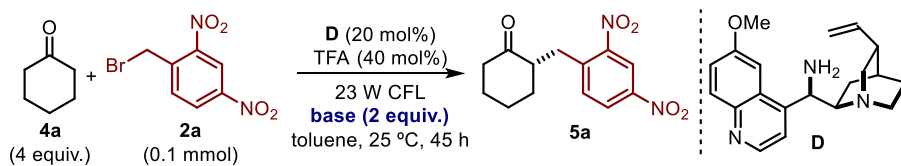


Entry	Solvent	NMR yield ^a (%)	ee ^b (%)
1	toluene	45	88
2	MTBE	19	68
3	chloroform	6	n.d.
4	DMSO	<5	n.d.
5	CH₃CN	<5	n.d.

^a Determined by ¹H NMR analysis of the crude reaction mixture employing 1,3,5-trimethoxybenzene as internal standard. ^b Enantiomeric excess determined by HPLC analysis on a Daicel Chiralpak IC column. MTBE: methyl *tert*-butyl ether; DMSO: dimethyl sulfoxide.

The presence of a base within the catalytic system is needed to neutralize the HBr generated during the reaction. Table 3.4 reports the results obtained with different bases. This study showed that not all the bases are competent to promote the benzylation. The soluble organic base 2,6-lutidine gave good results (entry 2), but could not outperform the results provided by the heterogeneous system based on the use of the partially soluble sodium acetate (entry 1). The possibility of lowering the amount of base was also investigated. As shown in entry 4, when one equivalent of sodium acetate was used instead of two, the reaction did not progress further after 20 hours. An experiment in the absence of the base (entry 5) confirmed the need of neutralizing the HBr generated during the process.

Table 3.4 Base screening



Entry	Base	NMR yield ^a (%)	ee ^b (%)
1	NaOAc	45	88
2	2,6-lutidine	35	75
3	K ₂ CO ₃	<10	65
4	NaOAc ^c	23	n.d.
5	none	13	n.d.

^a Determined by ¹H NMR analysis of the crude reaction mixture employing 1,3,5-trimethoxybenzene as internal standard. ^b Enantiomeric excess determined by HPLC analysis on a Daicel Chiralpak IC column. ^c 1 equivalent of base.

An acidic co-catalyst (generally 2 equivalents with respect to the amine) is commonly used with cinchona-based primary amines. It serves the dual role of protonating the quinuclidine moiety while a second equivalent is usually needed to facilitate the condensation of the primary amine with the carbonyl moiety.

On this basis, different acids were tested as additives in the model reaction. As shown in Table 3.5, TFA provided the best results in terms of reactivity and stereocontrol (entry 1). All the other acids, including trichloroacetic acid (TCA, entry 2) or benzoic acid derivatives, provided worse results. When the relative amount of TFA was lowered (20 mol%), both enantiocontrol and NMR yield were reduced (entry 6, Table 3.5). This indicated that a second equivalent of TFA was needed to achieve an effective catalytic system. Furthermore, the absence of any acid (entry 7) resulted in a sluggish reaction and a lower stereocontrol.

Table 3.5 Acid screening

Entry	Acid	NMR yield ^a (%)	ee ^b (%)
1	TFA	45	88
2	TCA	47	70
3	benzoic acid	20	72
4	4-nitrobenzoic acid	26	72
5	3,5-dimethoxybenzoic acid	44	81
6	TFA ^c	29	84
7	none	20	75

^a Determined by ¹H NMR analysis of the crude reaction mixture employing 1,3,5-trimethoxybenzene as internal standard. ^b Enantiomeric excess determined by HPLC analysis on a Daicel Chiralpak IC column. ^c Reaction performed with 20 mol% of TFA.

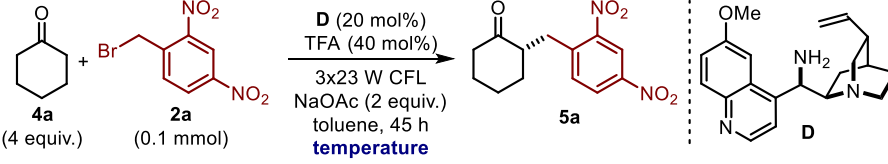
During the optimization studies, we observed that the rate of the model reaction catalyzed by the amine **D** was dramatically reduced after twelve hours (40% yield was obtained overnight while 45% of yield was reached after 45 hours). Additionally, the aminocatalyst **D** could not be detected in the reaction media after 45 hours by either ¹H NMR or GC analysis. During the course of the reaction, it was also observed that an orange precipitate was being generated. Mass analysis of this precipitate showed the presence of the cinchona scaffold, suggesting the possibility of a catalyst degradation pathway being operative under the reaction conditions. Various possible deactivation pathways of catalyst **D** can be foreseen, in particular involving the bridgehead nitrogen in the quinuclidine. This nucleophilic nitrogen can easily react *via* S_N2 with the benzyl bromide to afford the *N*-benzylated catalyst. As a matter of fact, many effective phase-transfer catalysts are prepared by means of *N*-alkylation of cinchona alkaloids with the corresponding alkyl halides upon heating in toluene at reflux.³⁵ However, despite many efforts, we could not unambiguously identify the degradation byproducts containing the catalyst.

We eventually found that the formation of the precipitate could be avoided by performing the reaction under cryogenic conditions (0 °C). These conditions also preserved the catalyst efficiency, allowing the isolation of the final benzylated product **5a** in a good chemical yield and with a slightly improved optical purity (60% yield, 90% ee, entry 2,

³⁵ a) O'Donnell, M. J. "The enantioselective synthesis of α -amino acids by phase-transfer catalysis with achiral Schiff base esters" *Acc. Chem. Res.* **2004**, *37*, 506. b) Maruoka, K. "Asymmetric phase transfer catalysis" **2008**, John Wiley & Sons.

Table 3.6). The use of the pseudo-enantiomeric primary amine catalyst **G**, derived from quinine, granted access to the opposite enantiomer of the benzylated product **5a** (entry 3).

Table 3.6 Temperature screening

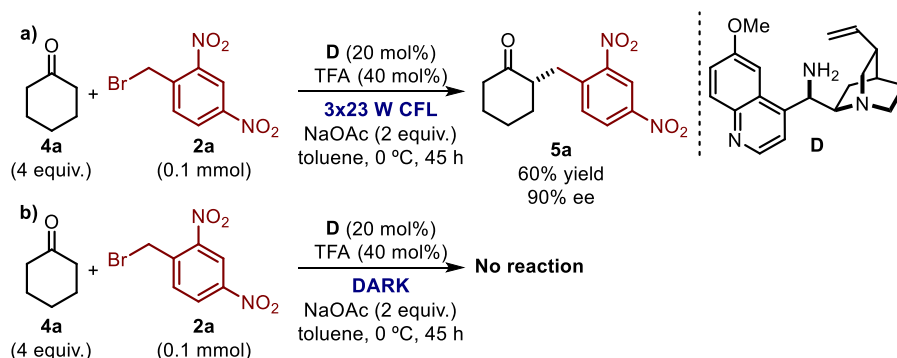


Entry	Temperature (°C)	NMR yield ^a (%)	ee ^b (%)
1	15	68	88
2	0	60 ^c	90
3	0	50 ^c	90 ^d

^a Determined by ¹H NMR analysis of the crude reaction mixture employing 1,3,5-trimethoxybenzene as internal standard. ^b Enantiomeric excess determined by HPLC analysis on a Daicel Chiralpak IC column. ^c Yield of the isolated product **5a** after purification on silica gel. ^d Reaction performed with catalyst **G** leading to the (*R*) enantiomer of **5a**. 3 x 23 W CFL: 3 compact fluorescent light bulbs.

The optimized conditions resulting from the optimization studies are depicted in entry 2, Table 3.6. To control the temperature, the reaction vessel was positioned in the middle of a Dewar flask containing an EtOH bath at 0 °C. This set up hampered the irradiation of the sample, impeding close positioning of the lamps. As a result, more lamps were required to ensure an effective illumination. Finally, 3 light sources at approximately 10 cm were utilized to irradiate the solutions.

As shown in Scheme 3.13, the photochemical nature of the transformation was tested by performing a control experiment under the final reaction conditions but carefully excluding the presence of light. Under these conditions, no product formation was observed.

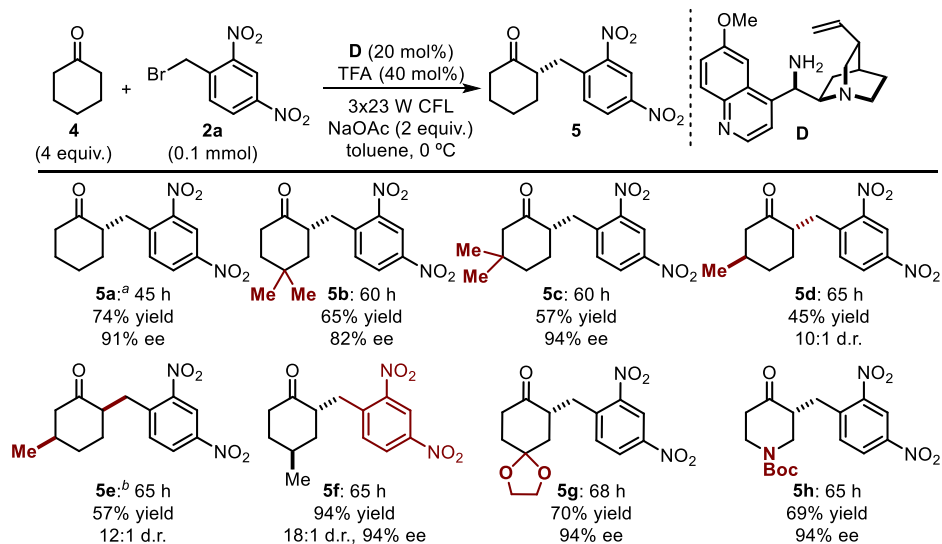


Scheme 3.13 Control experiment in the absence of light under the optimized reaction conditions for the photochemical α -benzylation of ketones.

3.3.1 Reaction scope

The optimized conditions were then applied to achieve the enantioselective α -benzylation of different cyclic six-membered ketones leading to adducts **5a-5h** (82-94% ee, Scheme 3.14). A hindered ketone, bearing a geminal dimethyl pattern at the 4-position of the cyclohexane ring, was effectively alkylated yielding the final ketone **5b** with a moderate yield and enantioselectivity. Substitution at the cyclohexanone 3-position was also tolerated, affording the final product exclusively benzylated at the α -carbon atom more distant from the encumbered site (>20:1 regio-control, products **5c-5e**). Remarkably, a highly diastereoselective α -benzylation of the enantiopure (*R*)-3-methylcyclohexanone was achieved when using both pseudo-enantiomeric catalysts **D** and **G**, granting access to the *trans*- and *cis*-alkylated ketones respectively (**5d** and **5e**). These results illustrate the ability of the cinchona-based catalyst to override the inherent bias of the resident stereogenicity of the starting enantiopure ketone. Moreover, high enantio- and diastereo-control was achieved in the desymmetrization of 4-methyl-cyclohexanone, leading to the corresponding benzylated product **5f**.

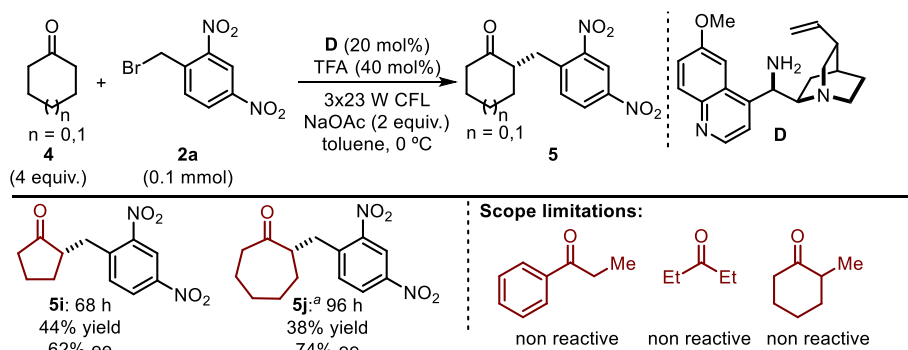
In addition, the reaction showed a good functional group tolerance, providing the desired α -alkylated ketones in good yields and high enantiomeric excess even in the presence of ketals (**5g**) or Boc-protected amines (**5h**).



Scheme 3.14 Scope of the enantioselective photochemical ketone α -benzylation: six-membered ring ketones. ^a Reaction performed on a 1 mmol scale. ^b Using catalyst **G**.

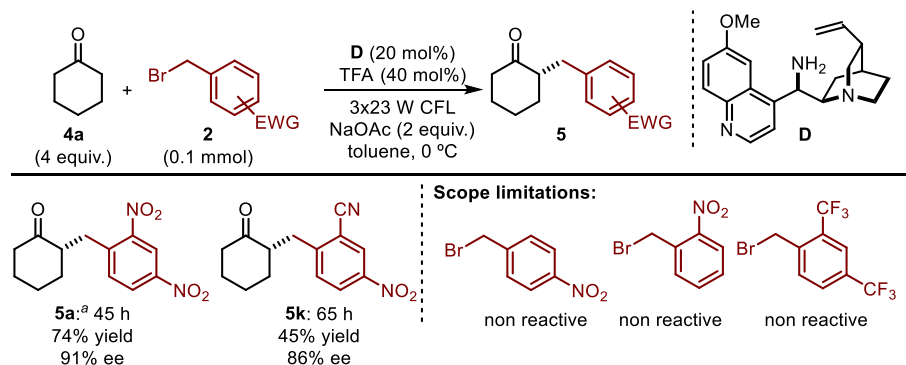
As shown in Scheme 3.15, when using cyclic ketones of different ring sizes (five- and seven-membered cyclic ketones), the efficiency of the process was lowered (products **5i**

and **5j**). Additionally, linear and α -branched ketones were unsuitable substrates for they did not react at all.



Scheme 3.15 Scope of the enantioselective photochemical ketone α -benzylation: different ketone scaffolds. ^a 10 equiv. of the starting ketone **4j** was used.

The scope for electron-deficient benzylic systems was limited to the use of the 2,4-dinitrobenzyl bromide **2a** and 2-cyano-4-nitrobenzyl bromide. The last substrate, when submitted to the optimized reaction conditions, provided the final product **5k** with a moderate yield and good enantiomeric excess (Scheme 3.16). However, our attempts of employing other benzyl bromides failed (Scheme 3.16).

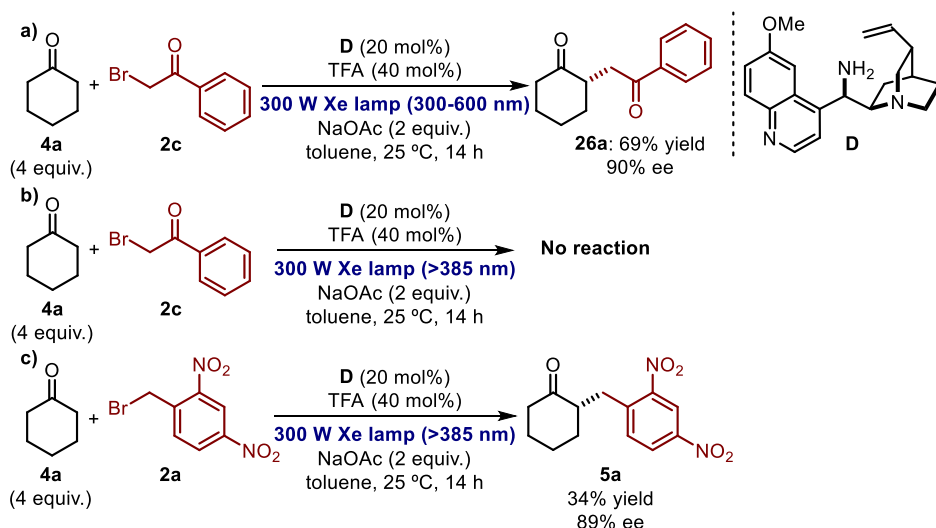


Scheme 3.16 Scope of the enantioselective photochemical ketone α -benzylation: the ketone component. ^a Reaction performed on a 1 mmol scale.

Nevertheless, a number of phenacyl bromides were found to be competent substrates for the enantioselective photochemical alkylation of cyclic ketones (adducts **26a-26h**; Scheme 3.18). In contrast to the reaction with benzyl bromides, phenacyl bromides did not yield the α -alkylated ketones upon visible light irradiation with a 23 W CFL. We were surprised by the lack of reactivity as it was in disagreement with the behavior observed

in the EDA-mediated α -alkylation of aldehydes² where both families of substrates reacted under the same conditions. As a result, further optimization studies were conducted.

As shown in Scheme 3.17a, using a more powerful light source, specifically a 300 W xenon lamp (irradiation from 300 to 600 nm), the α -alkylated ketone **26a** could be obtained in a moderate yield when reacting phenacyl bromide **2c** and cyclohexanone **4a**.

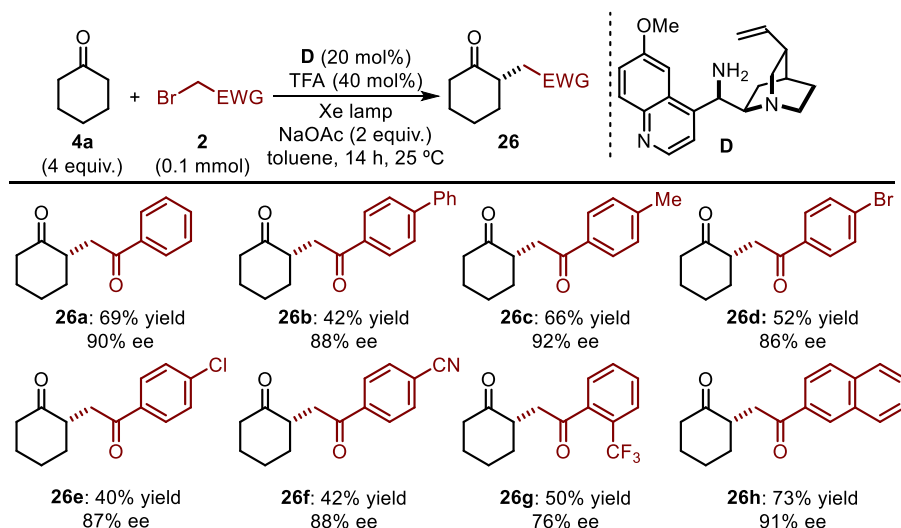


Scheme 3.17 Control experiments irradiating with different wavelengths. Reactions between cyclohexanone **4a** and: a) phenacyl bromide **2c** irradiating with wavelengths from 300 to 600 nm, b) phenacyl bromide **2c** irradiating with wavelengths higher than 385 nm and c) benzyl bromide **2a** irradiating with wavelengths higher than 385 nm.

Intrigued by this behavior, we studied whether the transformation was successful because of the higher irradiation power employed³⁶ or because the photochemical alkylation of cyclohexanone with phenacyl bromide **2c** required the use of higher energy photons. For this purpose, the reaction mixture was irradiated with a 300 W Xe lamp equipped with a cut-off filter, which allowed irradiation only with wavelengths higher than 385 nm. Under these conditions, no product formation was detected when using **2c** (Scheme 3.17b). This indicates that the absorption of wavelengths within the visible region is not sufficient for this reaction to occur. In contrast, the use of this light source was found to be suitable for the photochemical benzylation of cyclohexanone with **2a**, which provided the final product **5a** in a moderate yield (Scheme 3.17c).

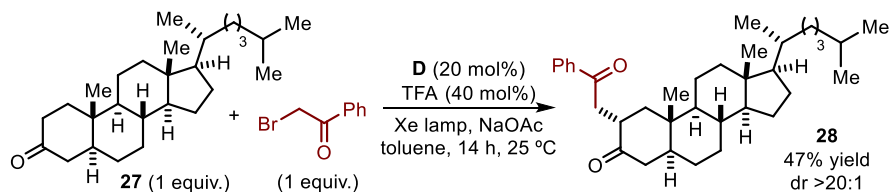
³⁶ The irradiance (related to the number of photons per seconds) of the 300 W xenon lamp is 590 mW/cm², whereas for the 23 W CFL the irradiance is 8 mW/cm².

Consequently, an irradiation system which allowed for the illumination of the sample with wavelengths lower than those of the visible region (<400 nm) was required to promote the photochemical alkylation of cyclohexanone with phenacyl bromides. The reaction could be successfully performed upon irradiation of either a 15 W black light CFL bulb ($\lambda_{\text{max}} = 360$ nm) or a 300 W xenon lamp (300-600 nm). However, the use of the 300 W xenon lamp provided for a faster and effective reaction. We use this illumination system for studying the scope of the photochemical α -alkylation of **4a** with a variety of phenacyl bromides, leading to the corresponding products **26** with high enantiomeric excess after 14 hours of irradiation at ambient temperature (products **26a-h**, 76-92% ee, Scheme 3.18).



Scheme 3.18 Scope of the enantioselective photochemical ketone α -alkylation: phenacyl bromides.

Finally, this strategy was successfully applied for the α -alkylation of the steroid 5 α -cholestan-3-one (**27**). The reaction proceeded smoothly leading to the final product **28** in a moderate yield but with excellent regio- and stereocontrol (Scheme 3.19). This transformation shows the feasibility of applying our methodology for late-stage functionalization of natural products.



Scheme 3.19 Application of our enantioselective photochemical α -alkylation ketones to a natural product functionalization.

Control experiments, performed by excluding light illumination for all the reactions presented here, led to no product formation.

3.3.2 Mechanistic insights

A series of experiments were designed and performed in order to study the mechanism of this photochemical asymmetric α -alkylation of ketones.³⁷

Absorption Spectra

In order to investigate the formation of an EDA complex, we measured the optical absorption spectra of the separate reaction components involved in this alkylation.

Absorption spectra of samples in the presence or the absence of the acid co-catalyst were recorded. In the spectra obtained without the acid, no evidence for the EDA complex formation was collected (the red line results from the addition of the absorption of **2a**, blue line, and the free catalyst **D**, black-dashed line, Figure 3.2). This result is consonant with the notion that the enamine formation is greatly retarded in the absence of any acid (see overlap between the dashed-black spectrum, corresponding to the amine, and the green spectrum corresponding to the mixture of the primary amine and the ketone), a condition which does not allow the formation an enamine-based EDA complex. This is in agreement with the extremely low reactivity observed in the reactions performed with exclusion of the acidic additive (entry 7, Table 3.5).

³⁷ Our current understanding of the EDA-mediated photochemical alkylation of aldehydes, gathered after the extensive mechanistic studies recently performed (see Chapter V and: Bahamonde, A.; Melchiorre, P. "Mechanism of the stereoselective α -alkylation of aldehydes driven by the photochemical activity of enamines" *J. Am. Chem. Soc.* **2016**, *138*, 8019.), influenced most of the conclusions described in this section. As a result, some of the discussions and conclusions reported in the original study (Ref. 1) have been modified.

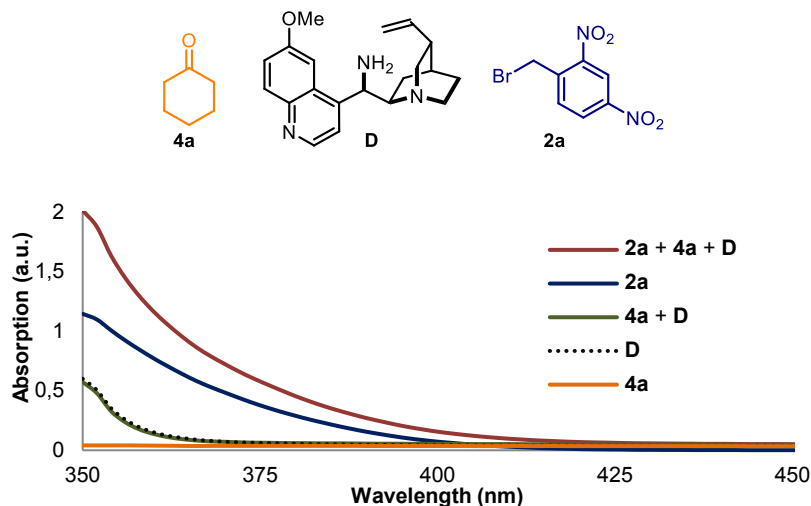


Figure 3.2 Optical absorption spectra recorded in toluene in 1 mm path quartz cuvettes using a Shimadzu 2401PC UV-visible spectrophotometer. $[D] = [2a] = 0.04$ M; $[4a] = 2$ M.

We then added TFA to facilitate the condensation of the primary amine catalyst **D** with the carbonyl moiety of the cyclohexanone (**4a**), so as to increase the amount of the transiently generated active enamine intermediate. As shown in Figure 3.3, the absorption of the protonated catalyst (dashed-black spectrum) and the solution containing also cyclohexanone (green spectrum) do not overlay any longer, suggesting the formation of such a covalent intermediate.

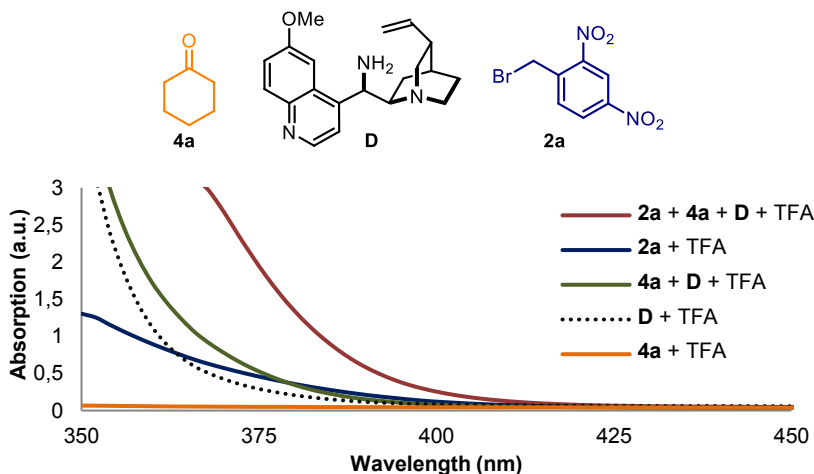


Figure 3.3 Optical absorption spectra recorded in toluene in 1 mm path quartz cuvettes using a Shimadzu 2401PC UV-visible spectrophotometer. $[D] = [2a] = 0.04$ M; $[4a] = 2$ M; $[TFA] = 0.08$ M.

Furthermore, a marked yellow color was observed when catalyst **A**, cyclohexanone **4a**, and the electron-poor benzyl bromide **2a** were mixed in the presence of TFA. The absorption spectra of this mixture (red line) showed a bathochromic displacement in the visible region, diagnostic of the formation of an EDA complex.³⁸

In contrast, the appearance of a new absorption band could not be observed when the same experiments were repeated mixing phenacyl bromide **26a** with cyclohexanone and the cinchona-based primary amine **D** under acidic conditions.³⁹

Effect of aerobic conditions and radical scavengers

The effect of oxygen on this transformation was tested performing a reaction under aerobic conditions. The reaction mixture was not degassed,⁴⁰ thus there was oxygen dissolved in the solvent. The reaction carried out between cyclohexanone **4a** and the electron-poor benzyl bromide **2a** was completely inhibited in the presence of oxygen. The presence of oxygen might result in the quenching of the triplet excited-state of the EDA complex, interrupting the single-electron transfer that generates the contact radical-ion pair from the ground-state EDA.

The aerobic conditions were tested when using both the chiral catalyst **D** and benzylamine, a catalyst that was effective to promote the racemic transformation (useful to produce the racemic sample needed for HPLC analyses). This lack of reactivity was also observed when the model reaction (see Scheme 3.13a) was performed in the presence of 0.5 equivalents of TEMPO (2,2,6,6-tetramethylpiperidine-1-oxyl), a known radical scavenger.

The absence of reactivity observed in the presence of these radical scavengers is consonant with a radical mechanism being operative.

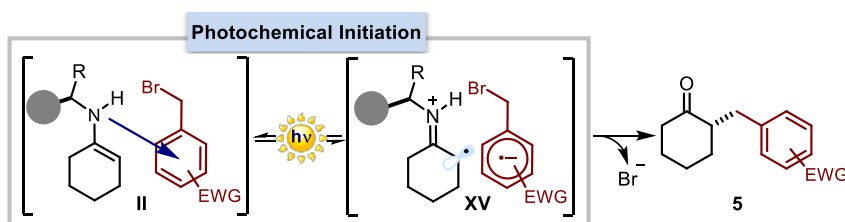
³⁸ The ¹H NMR spectroscopic analysis of the mixture excluded the formation of any reaction product.

³⁹ This suggests that the photoactive species in the enamine-mediated α -alkylation of cyclohexanone with phenacyl bromides might be other than an EDA complex. This process might be initiated by an alternative photochemical mechanism. In analogy with the studies developed by the group for the enamine-mediated photochemical alkylation of aldehydes (see ref. 37), the direct photoexcitation of the enamine **XVI** could also be envisioned as an alternative radical generation manifold (more details about this alternative initiation will be given in Chapter V). Photophysical studies that would unambiguously establish this alternative light-triggered pathway are complicated by the difficulties of isolating the secondary enamine derived by the condensation of the primary amine catalyst and ketones.

⁴⁰ The model reaction is generally performed under anaerobic conditions, since the reaction mixture is degassed *via* freeze-pump-thaw.

Proposed mechanism for the α -benzylation of ketones

The studies described in this section point towards the formation of an EDA complex between the transient enamine, generated upon condensation of the chiral amine **D** and the ketone **4**, and the electron-poor benzyl bromide **2a**. Furthermore, the control experiment depicted in Scheme 3.17c shows that the reaction between **2a** and **4a** is operative when irradiated with wavelengths higher than 385 nm, where the EDA complex **II** is the major photo-active species (see Figure 3.3). This suggests that the irradiation of the charge-transfer band of the complex is responsible for the reactivity. Such absorption would render a radical-ion pair (**XV**) prone to undergo a fast back-electron transfer regenerating the ground-state EDA complex (Scheme 3.20). Key to the success of this transformation is the presence of a leaving group in the acceptor that facilitates the fragmentation of the radical anion to give the carbon-centered radical, preventing the back-electron transfer and allowing the reaction to proceed.



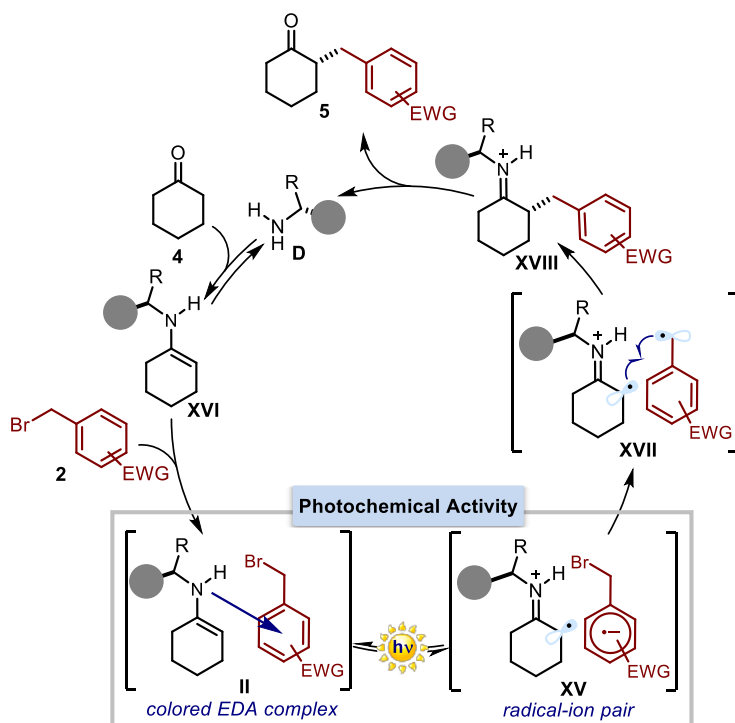
Scheme 3.20 EDA complex excitation and fragmentation of the radical anion to promote the formation of the α -alkylated ketones **5**.

As for the overall mechanism of the transformation, two catalytic cycles can be envisioned: a cycle which closely resembles the one previously proposed for the α -alkylation of aldehydes,² where a radical-radical coupling would forge the new bond (Scheme 3.21), and a $S_{RN}1$ -type radical chain mechanism (Scheme 3.22).⁴¹

Originally, a catalytic cycle based on the in-cage radical-radical coupling was suggested for this transformation (Scheme 3.21).¹ According to this proposal, the excitation *via* visible light irradiation of the colored EDA complex **II** would induce a single-electron transfer to generate a radical-ion pair **XV**. A fast fragmentation of the bromide ion from the ion-pair **XV** would consequently afford a positively charged intermediate **XVII**, bringing two radicals within a geometrically restricted chiral space and in very close proximity. This condition should facilitate a stereocontrolled radical combination within

⁴¹ For an example of an EDA-initiated $S_{RN}1$ radical chain reaction see: Fox, M. A.; Younathan, J.; Fryxell, G. E. "Photoinitiation of the $S_{RN}1$ reaction by excitation of charge-transfer complexes" *J. Org. Chem.* **1983**, *48*, 3109. Depicted in Scheme 2.10 in Chapter II.

the solvent cage (between the carbon-centered radical derived from **2** and the transient radical cation of the *in situ* generated enamine) to form a new carbon-carbon bond while forging the stereogenic centre. Subsequently, the iminium ion **XVIII** derived from this coupling would be hydrolyzed, releasing the amino catalyst **D** and the product **5**. Therefore the catalyst is regenerated and the catalytic cycle can restart.

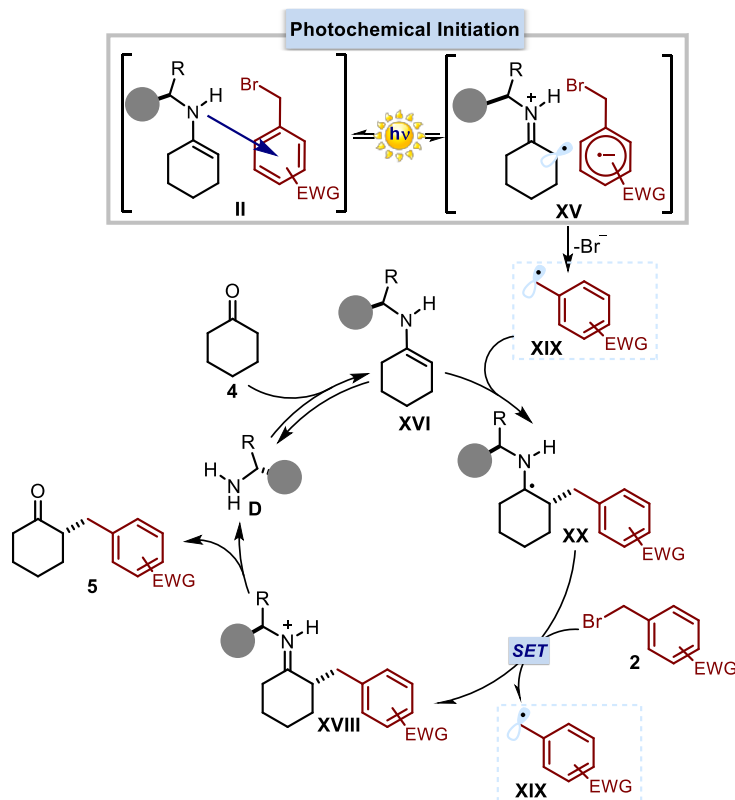


Scheme 3.21 Proposed mechanism for the photochemical enantioselective α -benzylation of ketones driven by the photochemical activity of EDA complexes.

As detailed in Scheme 3.22, a radical chain mechanism can be alternatively proposed as electron-poor benzyl bromides are suitable substrates for chain pathways.⁴² In this mechanistic scenario, the photoexcitation of the EDA complex will serve only to initiate the self-propagating radical chains. The radical-ion pair **XV**, generated after the photoactivation of the EDA complex **II**, would provide the carbon-centered radical **XIX** after fragmentation of the carbon-halogen bond of the acceptor. Out-of-cage diffusion of the electrophilic radical **XIX** will consequently start the radical chain. Trapping of the electrophilic radical **XIX** by the transiently generated nucleophilic enamine **XVI**

⁴² Kornblum, N. "Substitution reactions which proceed *via* radical anion intermediate" *Angew. Chem. Int. Ed.* **1975**, *14*, 734.

enantioselectively forms the new carbon-carbon bond while generating the α -amino radical **XX**. This highly reducing radical could propagate the radical chain *via* single-electron transfer to the electron-poor benzyl bromide **2a** ($E_p^{\text{red}} = -0.66$ V) regenerating the electrophilic radical **XIX**, which can restart the chain, along with the iminium ion **XVIII**. Finally, hydrolysis of **XVIII** releases the alkylation product while liberating the aminocatalyst allowing the cycle to restart.



Scheme 3.22 Alternative chain propagation mechanism for the photochemical enantioselective α -benzylation of ketones - here the photochemical activity of the EDA complex would serve as the initiation step.

Based on the extensive studies on the enamine-mediated photochemical α -alkylation of aldehydes, which will be thoroughly discussed in Chapter V, we have learnt that this type of processes generally takes place through radical chain mechanisms.³⁷ By analogy, we believe that the mechanism depicted in Scheme 3.22 is more likely. In this mechanistic hypothesis, the single-electron transfer within the EDA complex would serve as the initiation step that starts a radical chain. Thus, while in our initially proposed mechanism the enamine radical cation within the ion pair **XV** is actively involved in the carbon-

carbon bond forming event, in the alternative mechanistic hypothesis it would be an unproductive species.

A quantum yield measurement, which relates the number of molecules formed with the number of absorbed photons, is generally a useful tool to investigate if radical chain propagations are operative.⁴³ This experiment would have allowed us to discriminate between these two possible mechanisms. However, the heterogeneous nature of the reaction, not compatible with these measurements, prevented us from measuring the quantum yield of this reaction.

3.4 Conclusions and remarks

A new methodology for the direct enantioselective catalytic synthesis of α -benzyl and α -phenacyl cyclic ketones (Scheme 3.13a and 3.17a, respectively) has been developed. The process is triggered by the photoexcitation of a transiently generated EDA complex between an *in situ* formed enamine and a series of electron-poor alkyl bromides. This study further demonstrates the synthetic potential of EDA-mediated photochemical reactions.

⁴³ For an extensive discussion on the use and experimental measurement of the quantum yield see the following chapter.

3.5 Experimental section

General information: The ^1H and ^{13}C NMR spectra were recorded at 400 MHz or 500 MHz for ^1H and at 100 MHz or 125 MHz for ^{13}C , respectively. The chemical shifts (δ) for ^1H and ^{13}C are given in ppm relative to residual signals of the solvents (CHCl_3 @ 7.26 ppm ^1H NMR, 77.0 ppm ^{13}C NMR). Coupling constants are given in Hz. When necessary, ^1H and ^{13}C signals were assigned by means of g-COSY 2D-NMR sequence. The following abbreviations are used to indicate the multiplicity: s, singlet; d, doublet; t, triplet; q, quartet; qn, quintet; m, multiplet; bs, broad signal.

Mass spectra (high and low resolution) were obtained from the ICIQ High Resolution Mass Spectrometry Unit on a Bruker Maxis Impact (QTOF) or Waters Micromass LCT-Premier (TOF) in Electrospray Ionization (ESI) by direct infusion.

Optical rotations were measured on a Polarimeter Jasco P-1030 and are reported as follows: $[\alpha]_{\text{D}}$ rt (*c* in g per 100 mL, solvent).

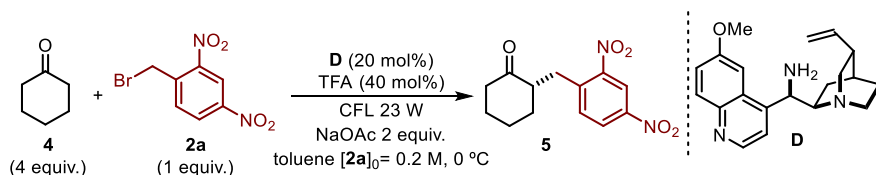
The ^1H , ^{13}C NMR spectra and the HPLC traces are available in the literature¹ and are not reported in the present thesis.

General Procedures. All reactions were set up under an argon atmosphere in oven-dried glassware using standard Schlenk techniques, unless otherwise stated. Synthesis grade solvents were used as purchased and the reaction mixtures were deoxygenated by three cycles of freeze-pump-thaw. Chromatographic purification of products was accomplished using force-flow chromatography (FC) on silica gel (35-70 mesh). For thin layer chromatography (TLC) analysis throughout this work, Merck precoated TLC plates (silica gel 60 GF₂₅₄, 0.25 mm) were employed, using UV light as the visualizing agent and an acidic mixture of para-anisaldehyde or basic aqueous potassium permanganate (KMnO_4) stain solutions, and heat as developing agents. Organic solutions were concentrated under reduced pressure on a Büchi rotatory evaporator.

Determination of Enantiomeric Purity. HPLC analysis on chiral stationary phase was performed on an Agilent 1200-series instrumentation. Daicel Chiralpak IC and IB columns with hexane:PrOH as the eluent were used. HPLC traces were compared to racemic samples prepared using a) a catalytic amount of benzylamine (20 mol%) and irradiation with a 23 W compact fluorescent bulb for the α -benzylation of ketones (products **5a** to **5k**) or b) one equivalent of a preformed enamine (1-pyrrolidino-1-cyclohexene, Aldrich) and irradiation with a 15 W-black light CFL for the phenacylation of cyclic ketones (products **26a** to **26h**).

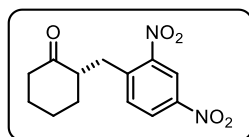
Materials. Reagents were purchased at the highest commercial quality and used without further purification, unless otherwise stated. Chiral primary amine catalysts **D**, **E**, and **G** were synthesized by a Mitsunobu reaction from the commercially available cinchona alkaloids, according to the reported procedure.²² The bifunctional catalyst **K** was synthesized following a one-step procedure from commercially available (1*R*,2*R*)-1,2-diphenylethylenediamine, according to the literature procedure.⁴⁴ All the cyclic ketones (**4**) used are commercially available, as well as most of the alkyl halides used within the study. 2-Cyano-4-nitrobenzyl bromide was prepared by brominating the commercially available 2-methyl-5-nitrobenzonitrile, according to the literature.⁴⁵

General procedure for the photochemical α -asymmetric benzylation of ketones



A 10 mL Schlenk tube was charged with the aminocatalyst **D** (20 mol%), toluene (0.2 M referring to the alkyl bromide **2**), trifluoroacetic acid, TFA, (40 mol%), the ketone **4** (4 equiv.), sodium acetate (2 equiv.), and the alkylating agent **2** (1 equiv.). The reaction mixture was degassed *via* freeze-pump-thaw (x 3 cycles), and the vessel refilled with nitrogen. After the reaction mixture was thoroughly degassed, the vial was sealed and positioned approximately in the middle of a Dewar flask containing an EtOH bath at 0 °C, 10 cm away from 3 light sources. Three household full spectrum 23 W compact fluorescent light (CFL) bulbs were used for irradiating the reaction mixture. After stirring for the indicated time, the crude mixture was purified by flash column chromatography to afford the title compound **5** in the stated yield and optical purity.

(*S*)-2-(2,4-dinitrobenzyl)cyclohexanone (**5a**)



The reaction was carried out following the general procedure to furnish the crude product after 45 h of irradiation. Purification by flash column chromatography (gradient eluent from pure

⁴⁴ Yu, F.; Jin, Z.; Huang, H.; Ye, T.; Liang, X.; Ye, J. "A highly efficient asymmetric Michael addition of α,α -disubstituted aldehydes to maleimides catalyzed by primary amine thiourea salt" *Org. Biomol. Chem.* **2010**, *8*, 4767.

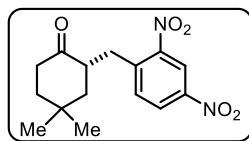
⁴⁵ Makhija, M. T.; Kasliwal, R. T.; Kulkarni, V. M.; Neamati, N. "De novo design and synthesis of HIV-1 integrase inhibitors" *Bioorg. Med. Chem.* **2004**, *12*, 2317.

pentane to 10:1 pentane:AcOEt mixture) afforded the title compound (16.5 mg, 60 % yield, 90 % ee) as a yellow oil.

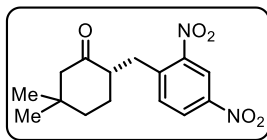
A larger scale reaction was performed according to the general procedure using the amino catalyst **D** (0.2 mmol, 65 mg, 20 mol%), toluene (0.2 M, 5 mL), trifluoroacetic acid (0.4 mmol, 30 μ L, 40 mol%), sodium acetate (2 mmol, 164 mg, 2 equiv.), cyclohexanone **4a** (4 mmol, 420 μ L, 4 equiv.) and 2,4-dinitrobenzyl bromide **2a** (1 mmol, 260 mg, 1 equiv.). Time of irradiation: 45 h. Purification by flash column chromatography (gradient eluent from pure hexane to 10:1 hexane:AcOEt mixture) afforded the title compound (206.1 mg, 74 % yield, 91 % ee) as a yellow oil.

The enantiomeric excess was determined by HPLC analysis on a Daicel Chiralpak IC column, 70:30 hexane:iPrOH, flow rate 1.00 mL/min, $\lambda = 254$ nm: $\tau_{\text{major}} = 22.1$ min, $\tau_{\text{minor}} = 27.5$ min. $[\alpha]_{\text{D}}^{28} = -42.6 \pm 0.7$ ($c = 1.0$, CHCl_3 , 90 % ee). **HRMS**: calculated for $\text{C}_{13}\text{H}_{14}\text{N}_2\text{O}_5$ ($\text{M}+2\text{Na}$): 301.0795, found: 301.0802. **^1H (CDCl₃, 400 MHz)**: δ 8.79 (d, = 2.4Hz, 1H), 8.36 (dd, = 2.4Hz, $J = 8.6\text{Hz}$, 1H), 7.79 (d, $J = 8.6\text{Hz}$, 1H), 3.53 (dd, $J = 7.6\text{Hz}$, $J = 13.5\text{Hz}$, 1H), 2.88 (dd, $J = 5.1\text{Hz}$, $J = 13.5\text{Hz}$, 1H), 2.70-2.69 (m, 1H), 2.48-2.41 (m, 1H), 2.37-2.27 (m, 1H), 2.24-2.01 (m, 2H), 1.97-1.89 (m, 1H), 1.75-1.65 (m, 2H), 1.60-1.51 (m, 1H). **^{13}C (CDCl₃, 100 MHz)**: δ 211.2, 149.3, 146.4, 143.0, 135.0, 126.6, 129.2, 51.7, 42.3, 34.9, 33.1, 28.1, 25.4.

(S)-2-(2,4-dinitrobenzyl)-4,4-dimethylcyclohexanone (**5b**)

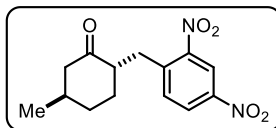


The reaction was carried out following the general procedure to furnish the crude product after 60 h of irradiation. Purification by flash column chromatography (eluent 2:1 DCM:hexane mixture) afforded the title compound (15.0 mg, 65 % yield, 82 % ee) as an orange solid. The enantiomeric excess was determined by HPLC analysis on a Daicel Chiralpak IC column, 70:30 hexane:iPrOH, flow rate 1.00 mL/min, $\lambda = 254$ nm: $\tau_{\text{major}} = 16.9$ min, $\tau_{\text{minor}} = 19.9$ min. $[\alpha]_{\text{D}}^{28} = -32 \pm 2$ ($c = 1.0$, CHCl_3 , 82 % ee). **HRMS**: calculated for $\text{C}_{15}\text{H}_{20}\text{N}_2\text{O}_5$ ($\text{M}+2\text{Na}$): 329.1108, found: 329.1110. **^1H (CDCl₃, 400 MHz)**: δ 8.79 (d, $J = 2.8\text{Hz}$, 1H), 8.36 (dd, $J = 2.4\text{Hz}$, $J = 8.5\text{Hz}$, 1H), 7.81 (d, $J = 8.5\text{Hz}$, 1H), 3.51 (dd, $J = 7.8\text{Hz}$, $J = 13.1\text{Hz}$), 2.94-2.85 (m, 1H), 2.77 (dd, $J = 4.8\text{Hz}$, $J = 13.1\text{Hz}$, 1H), 2.53-2.46 (m, 1H), 2.32-2.25 (m, 1H), 1.83-1.74 (m, 2H), 1.73-1.63 (m, 1H), 1.54 (t, $J = 13.0$ Hz 1H), 1.22 (s, 3H), 1.01 (s, 3H). **^{13}C (CDCl₃, 100 MHz)**: δ 211.7, 143.0, 135.0, 126.6, 120.2, 47.5, 47.4, 40.2, 38.4, 33.0, 31.2, 31.1, 29.7, 24.2.

(S)-2-(2,4-dinitrobenzyl)-5,5-dimethylcyclohexanone (5c)

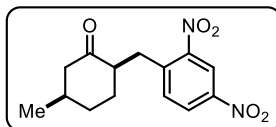
The reaction was carried out following the general procedure to furnish the crude product after 60 h of irradiation. Purification by flash column chromatography (eluent 2:1 DCM:hexane mixture) afforded the title compound (17.6 mg, 57 % yield, 94 % ee) as a yellow oil.

The enantiomeric excess was determined by HPLC analysis on a Daicel Chiralpak IC column, 70:30 hexane:iPrOH, flow rate 1.00 mL/min, $\lambda = 254$ nm: $\tau_{\text{major}} = 15.6$ min, $\tau_{\text{minor}} = 20.1$ min. $[\alpha]_{\text{D}}^{28} = -28 \pm 1$ ($c = 1.0$, CHCl_3 , 94 % ee). **HRMS**: calculated for $\text{C}_{15}\text{H}_{20}\text{N}_2\text{O}_5$ ($\text{M}+2\text{Na}$): 329.1108, found: 329.1110. **^1H (CDCl_3 , 400 MHz)**: δ 8.79 (d, $J = 2.3\text{Hz}$, 1H), 8.36 (dd, $J = 2.3\text{Hz}$, $J = 8.5\text{Hz}$, 1H), 7.80 (d, $J = 8.5\text{Hz}$, 1H), 3.55-3.47 (m, 1H), 2.88 (dd, $J = 5.1\text{Hz}$, $J = 13.6\text{Hz}$, 1H), 2.72-2.61 (m, 1H), 2.25 (d, $J = 12.7\text{Hz}$, 1H), 2.13 (dd, $J = 2.2\text{Hz}$, $J = 12.7\text{Hz}$, 1H), 2.10-2.03 (m, 1H), 1.73-1.59 (m, 3H), 1.09 (s, 3H), 0.90 (s, 3H). Residual peaks of benzene and water at δ 7.38 and 1.29. **^{13}C (CDCl_3 , 100 MHz)**: δ 210.7, 149.3, 146.4, 143.0, 135.0, 126.6, 102.3, 55.1, 50.7, 38.3, 37.4, 32.9, 31.8, 30.5, 29.7, 25.0.

(2S,5R)-2-(2,4-dinitrobenzyl)-5-methylcyclohexanone (5d)

The reaction was carried out following the general procedure to furnish the crude product after 65 h of irradiation. Purification by flash column chromatography (eluent from pure hexane to 10:1 hexane:EtOAc mixture) afforded the

title compound (12.8 mg, 43 % yield, 10:1 d.r) as a yellow oil. The diastereomeric ratio was determined by ^1H NMR. $[\alpha]_{\text{D}}^{28} = -10 \pm 1$ ($c = 0.5$, CHCl_3) **HRMS**: calculated for $\text{C}_{14}\text{H}_{16}\text{N}_2\text{O}_5$ ($\text{M}-\text{H}$): 291.0986, found: 291.0992. **^1H (CDCl_3 , 400 MHz)**: δ 8.79 (d, $J = 2.4$ Hz, 1H), 8.36 (dd, $J = 8.6$, 2.4 Hz, 1H), 7.80 (d, $J = 8.6$ Hz, 1H), 3.51 (dd, $J = 13.6$, 7.6 Hz, 1H), 2.87 (dd, $J = 13.6$, 5.1 Hz, 1H), 2.74 – 2.61 (m, 1H), 2.44 – 2.37 (m, 1H), 2.21 – 2.12 (m, 1H), 2.03 (dd, $J = 12.74$, 12.78 Hz, 1H), 1.97 – 1.85 (m, 2H), 1.52 (td, $J = 12.5$, 11.8, 2.6 Hz, 1H), 1.47 – 1.39 (m, 1H), 1.05 (d, $J = 6.2$ Hz, 3H). **^{13}C (CDCl_3 , 100 MHz)**: δ 210.5, 149.3, 146.3, 143.0, 135.0, 126.6, 120.2, 50.8, 50.3, 35.8, 33.9, 33.6, 32.9, 22.2.

(2R,5R)-2-(2,4-dinitrobenzyl)-5-methylcyclohexanone (5e)

The reaction was carried out following the general procedure employing the pseudoenantiomer of the catalyst **G** to furnish the crude product after 65 h of irradiation. Purification by flash column chromatography (eluent 3:2 hexane:DCM

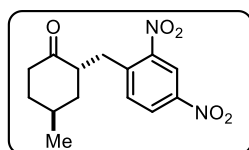
mixture) afforded the title compound (16.6 mg, 57 % yield, 12:1 d.r) as a yellow oil. The

diastereomeric ratio was determined by ^1H NMR. $[\alpha]^{27}_{\text{D}} = +38 \pm 1$ ($c = 1.0$, CHCl_3)
HRMS: calculated for $\text{C}_{14}\text{H}_{16}\text{N}_2\text{O}_5$ (M-H): 291.0986, found: 291.0994. **^1H (CDCl_3 , 400 MHz)**: δ 8.78 (d, $J = 2.4$ Hz, 1H), 8.36 (dd, $J = 8.5, 2.4$ Hz, 1H), 7.77 (d, $J = 8.6$ Hz, 1H), 3.51 (dd, $J = 13.6, 7.8$ Hz, 1H), 2.91 (dd, $J = 13.6, 5.2$ Hz, 1H), 2.80 – 2.68 (m, 1H), 2.53 (dd, $J = 13.0, 5.4$ Hz, 1H), 2.50 – 2.41 (m, 1H), 2.24 – 2.16 (m, 1H), 2.09 – 1.91 (m, 3H), 1.84 – 1.71 (m, 1H), 1.71 – 1.63 (m, 1H), 0.98 (d, $J = 7.1$ Hz, 3H). **^{13}C (CDCl_3 , 100 MHz)**: δ 211.1, 146.4, 142.8, 134.8, 126.6, 120.2, 51.2, 48.3, 33.1, 32.3, 30.6, 29.7, 18.7.

All proton signals of compounds **5d** and **5e** were unambiguously assigned using traditional 1D and 2D NMR methods. Identification of *alpha* proton signals was performed by selective 1D-NOESY by correlation between the substituted *alpha* proton and the *alpha'* proton in the same face (H^a) [when $\text{CO-CH}(\text{CH}_2\text{Ar})$ is irradiated $\text{CO-CH}^a\text{H}^b\text{-CH}(\text{Me})$ is correlated].

To determine if proton in $\text{CH}(\text{Me})$ is in equatorial or axial position, coupling constants of $\text{CH}(\text{Me})$ and $\text{CO-CH}^a\text{H}^b$ were compared between **5d** and **5e**. $\text{CO-CH}^a\text{H}^b$ appears as a double doublet with a geminal coupling and large diaxial coupling of 12.74, 12.78 Hz in **5d**, consistent with geminal and axial-axial couplings for a six-membered ring, requiring axial orientations for $\text{CO-CH}^a\text{H}^b$, $\text{CH}(\text{Me})$, and $\text{CO-CH}(\text{CH}_2\text{Ar})$, and enabling assignment of the relative stereochemistry shown. On the other hand, compound **5e**, $\text{CO-CH}^a\text{H}^b$ appears as a double doublet with a geminal coupling and smaller axial-equatorial coupling of 13.0, 5.4 Hz, consistent with geminal and axial-equatorial couplings for a six-membered ring, and enabling assignment of the relative stereochemistry shown in the drawing.

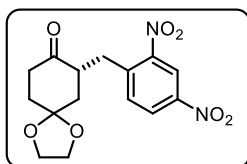
(2*S*,4*S*)-2-(2,4-dinitrobenzyl)-4-methylcyclohexanone (**5f**)



The reaction was carried out following the general procedure to furnish the crude product after 65 h of irradiation. Purification by flash column chromatography (eluent 20:1 hexane:EtOAc mixture) afforded the title compound (28.4 mg, 94 % yield, 18:1 d.r, 94 % ee) as a brown. The enantiomeric excess was determined by HPLC analysis on a Daicel Chiralpak IC column, 85:15 hexane:iPrOH, flow rate 1.00 mL/min, $\lambda = 254$ nm: $\tau_{\text{major}} = 31$ min, $\tau_{\text{minor}} = 37$ min. $[\alpha]^{28}_{\text{D}} = -67 \pm 1$ ($c = 1.0$, CHCl_3 , 94 % ee). **HRMS**: calculated for $\text{C}_{14}\text{H}_{16}\text{N}_2\text{O}_5$ (M+Na): 315.0951, found: 315.0953. **^1H (CDCl_3 , 400 MHz)**: δ 8.79 (d, $J = 2.4$ Hz, 1H), 8.36 (dd, $J = 8.5, 2.4$ Hz, 1H), 7.77 (d, $J = 8.5$ Hz, 1H), 3.53 – 3.46 (m, 1H), 2.99 – 2.87 (m, 2H), 2.53 – 2.44 (m, 1H), 2.35 (dt, $J = 14.3, 5.0$ Hz, 1H), 2.23 – 2.15 (m, 1H), 2.00 – 1.90 (m, 2H), 1.87 – 1.77 (m, 2H), 1.19 (d, $J = 7.0$ Hz, 3H). **^{13}C (CDCl_3 , 100 MHz)**: δ 211.3, 149.2, 146.4, 143.0, 135.0, 126.1, 120.2, 50.5, 42.8, 41.4, 35.9, 33.0, 32.1, 21.0.

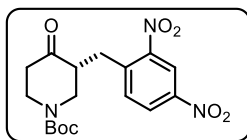
The relative stereochemistry was determined by selective 1D-NOESY correlation between the substituted *alpha* proton and the methyl group in position 4 [when CO-CH(CH₂Ar) is irradiated 4-Me is correlated].

(S)-7-(2,4-dinitrobenzyl)-1,4-dioxaspiro[4.5]decan-8-one (5g)



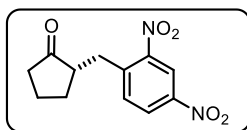
The reaction was carried out following the general procedure to furnish the crude product after 68 h of irradiation. Purification by flash column chromatography (eluent 10:1 hexane: AcOEt mixture) afforded the title compound (23.5 mg, 70 % yield, 94 % ee) as a yellow oil. The enantiomeric excess was determined by HPLC analysis on a Daicel Chiralpak IC column, 75:25 hexane:iPrOH, flow rate 1.00 mL/min, $\lambda = 254$ nm: $\tau_{\text{minor}} = 38$ min, $\tau_{\text{major}} = 41$ min. $[\alpha]_{\text{D}}^{28} = -58 \pm 2$ ($c = 1.0$, CHCl₃, 94 % ee). **HRMS**: calculated for C₁₅H₁₆N₂O₇ (M-H): 335.0885, found: 335.0885. **¹H (CDCl₃, 400 MHz)** δ 8.81 (d, $J = 2.4$ Hz, 1H), 8.37 (dd, $J = 8.5, 2.4$ Hz, 1H), 7.77 (d, $J = 8.5$ Hz, 1H), 4.20 – 3.92 (m, 4H), 3.56 (dd, $J = 13.7, 7.6$ Hz, 1H), 3.24 – 3.08 (m, 1H), 2.84 (dd, $J = 13.7, 5.2$ Hz, 1H), 2.65 (m, 1H), 2.41 (m, 1H), 2.15 (m, 1H), 2.12 – 1.95 (m, 2H), 1.89 (t, $J = 13.2$ Hz, 1H). **¹³C (CDCl₃, 100 MHz)**: δ 209.7, 149.3, 146.5, 142.5, 134.7, 126.7, 120.3, 106.9, 64.8, 64.6, 47.5, 41.2, 38.1, 34.7, 32.5.

(S)-tert-butyl 3-(2,4-dinitrobenzyl)-4-oxopiperidine-1-carboxylate (5h)



The reaction was carried out following the general procedure to furnish the crude product after 65 h of irradiation. Purification by flash column chromatography (eluent 2:1 DCM:hexane mixture) afforded the title compound (26.0 mg, 69 % yield, 94 % ee) as a yellow solid. The enantiomeric excess was determined by HPLC analysis on a Daicel Chiralpak IC column, 90:10 hexane:iPrOH, flow rate 1.00 mL/min, $\lambda = 254$ nm: $\tau_{\text{minor}} = 86$ min, $\tau_{\text{major}} = 92$ min. $[\alpha]_{\text{D}}^{27} = -22 \pm 2$ ($c = 1.0$, CHCl₃, 94 % ee). **HRMS**: calculated for C₁₇H₂₁N₃O₇ (M-H): 378.1307, found: 378.1309. **¹H (CDCl₃, 400 MHz)**: δ 8.83 (d, $J = 2.4$ Hz, 1H), 8.39 (dd, $J = 8.5, 2.4$ Hz, 1H), 7.81 (bs, 1H), 4.68 – 4.01 (m, 1H), 3.53 (bs, 1H), 3.24 (bs, 1H), 3.06 – 2.72 (m, 3H), 2.67 – 2.34 (m, 2H), 1.50 (s, 10H). **¹³C (CDCl₃, 100 MHz)**: δ 154.2, 149.2, 146.6, 141.7, 134.8, 126.9, 120.5, 80.9, 44.0, 41.3, 30.1, 28.2.

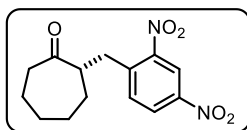
(S)-2-(2,4-dinitrobenzyl)cyclopentanone (5i)



The reaction was carried out following the general procedure to furnish the crude product after 68 h of irradiation. Purification by flash column chromatography (eluent 2:1 DCM:hexane mixture) afforded the title compound (10.8 mg, 44 % yield, 62

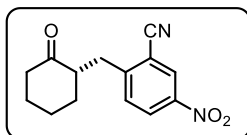
% ee) as a yellow oil. The enantiomeric excess was determined by HPLC analysis on a Daicel Chiralpak IC column, 70:30 hexane:iPrOH, flow rate 1.00 mL/min, $\lambda = 254$ nm: $\tau_{\text{minor}} = 25$ min, $\tau_{\text{major}} = 30$ min. $[\alpha]_{\text{D}}^{28} = +31 \pm 1$ ($c = 1.0$, CHCl_3 , 62 % ee). **HRMS**: calculated for $\text{C}_{12}\text{H}_{12}\text{N}_2\text{O}_5$ (M-H): 263.0673, found: 263.0673. **^1H (CDCl₃, 400 MHz)**: δ 8.80 (d, $J = 2.4$ Hz, 1H), 8.39 (dd, $J = 8.5, 2.4$ Hz, 1H), 7.68 (d, $J = 8.5$ Hz, 1H), 3.50 (dd, $J = 13.8, 6.1$ Hz, 1H), 3.02 (dd, $J = 13.8, 7.6$ Hz, 1H), 2.58 – 2.46 (m, 1H), 2.46 – 2.35 (m, 1H), 2.26 – 2.00 (m, 4H), 1.91 – 1.74 (m, 1H), 1.70 – 1.52 (m, 1H). **^{13}C (CDCl₃, 100 MHz)**: δ 218.1, 149.3, 146.5, 142.4, 134.1, 126.8, 120.3, 49.8, 37.4, 32.5, 29.6, 20.4.

(S)-2-(2,4-dinitrobenzyl)cycloheptanone (5j)



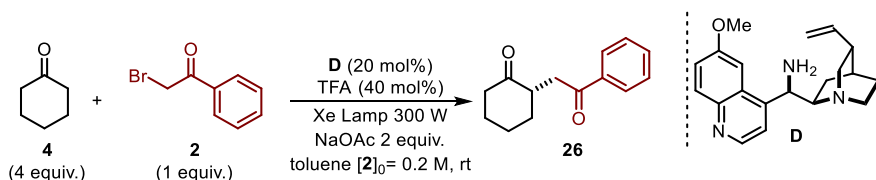
The reaction was carried out following the general procedure to furnish the crude product after 96 h of irradiation. Purification by flash column chromatography (eluent 10:1 hexane:EtOAc mixture) afforded the title compound (11.1 mg, 38 % yield, 74 % ee) as a yellow oil. The enantiomeric excess was determined by HPLC analysis on a Daicel Chiralpak IC column, 80:20 hexane:iPrOH, flow rate 1.00 mL/min, $\lambda = 254$ nm: $\tau_{\text{major}} = 21$ min, $\tau_{\text{minor}} = 29$ min. $[\alpha]_{\text{D}}^{28} = -80 \pm 1$ ($c = 2.0$, CHCl_3 , 74 % ee). **HRMS**: calculated for $\text{C}_{14}\text{H}_{16}\text{N}_2\text{O}_5$ (M-H): 291.0986, found: 291.0985. **^1H (CDCl₃, 400 MHz)**: δ 8.79 (d, $J = 2.4$ Hz, 1H), 8.35 (dd, $J = 8.5, 2.4$ Hz, 1H), 7.66 (d, $J = 8.5$ Hz, 1H), 3.54 – 3.41 (m, 1H), 3.10 – 2.96 (m, 2H), 2.50 – 2.43 (m, 2H), 1.99 – 1.79 (m, 5H), 1.73 – 1.43 (m, 3H), 1.39 – 1.23 (m, 3H). **^{13}C (CDCl₃, 100 MHz)**: δ 213.4, 149.3, 146.4, 142.6, 134.6, 126.6, 120.3, 52.4, 43.2, 34.9, 32.0, 28.7, 23.5.

(S)-5-nitro-2-((2-oxocyclohexyl)methyl)benzotrile (5k)



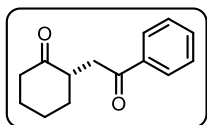
The reaction was carried out following the general procedure to furnish the crude product after 65 h of irradiation. Purification by flash column chromatography (gradient eluent from pure hexane to 10:1 hexane:AcOEt mixture) afforded the title compound (11.6 mg, 45 % yield, 86 % ee) as a yellow solid. The enantiomeric excess was determined by HPLC analysis on a Daicel Chiralpak IB column, 70:30 hexane:iPrOH, flow rate 1.00 mL/min, $\lambda = 254$ nm: $\tau_{\text{minor}} = 44.6$ min, $\tau_{\text{major}} = 32.9$ min. $[\alpha]_{\text{D}}^{26} = -19 \pm 1$ ($c = 1.0$, CHCl_3 , 86 % ee). **HRMS**: calculated for $\text{C}_{14}\text{H}_{14}\text{N}_2\text{O}_3$ (M+Na): 281.0885, found: 281.0897. **^1H (CDCl₃, 400 MHz)**: δ 8.49 (d, $J = 2.4$ Hz, 1H), 8.35 (dd, $J = 8.6, 2.4$ Hz, 1H), 7.68 (d, $J = 8.6$ Hz, 1H), 3.47 (dd, $J = 13.8, 7.2$ Hz, 1H), 2.86 (dd, $J = 13.8, 6.0$ Hz, 1H), 2.82 – 2.73 (m, 1H), 2.53 – 2.43 (m, 1H), 2.42 – 2.28 (m, 1H), 2.20 – 2.10 (m, 2H), 1.98 – 1.87 (m, 1H), 1.82 – 1.64 (m, 2H), 1.64 – 1.50 (m, 2H). **^{13}C (CDCl₃, 100 MHz)**: δ 210.5, 152.0, 146.2, 132.2, 127.7, 127.0, 116.0, 114.21, 51.6, 42.1, 34.6, 34.4, 27.9, 25.2.

General procedure for the photochemical α -asymmetric phenacylation of ketones



A 10 mL Schlenk tube was charged with the aminocatalyst **D** (20 mol%), toluene (0.2 M referring to the alkyl bromide **2**), trifluoroacetic acid, TFA, (40 mol%), cyclohexanone **4a** (4 equiv.), sodium acetate (2 equiv.), and the alkylating agent **2** (1 equiv.). The reaction mixture was degassed *via* freeze-pump-thaw (x 3cycles), and the vessel refilled with nitrogen. After the reaction mixture was thoroughly degassed, the flask was sealed and positioned approximately 10 cm away from the light source. The mixture was irradiated with a 300 W Xe lamp (*Asashi* Spectra Co., Ltd.) for 14 h under magnetic stirring. The temperature of the reaction mixture was maintained at room temperature by a water bath during the reaction. After stirring for the indicated time, the crude mixture was purified by flash column chromatography to afford the title compound **26** in the stated yield and optical purity.

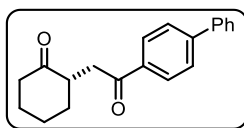
(*S*)-2-(2-oxo-2-phenylethyl)cyclohexanone (**26a**)



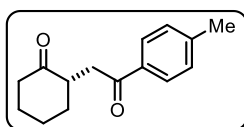
The reaction was carried out following the general procedure to furnish the crude product after 14 h of irradiation. Purification by flash column chromatography (gradient eluent from pure hexane to 10:1 hexane:AcOEt mixture) afforded the title compound (15.0 mg, 69 % yield, 90 % ee) as a yellow oil. The enantiomeric excess was determined by HPLC analysis on a Daicel Chiralpak IC column, 85:15 hexane:iPrOH, flow rate 1.00 mL/min, $\lambda = 254$ nm: $\tau_{\text{major}} = 20$ min, $\tau_{\text{minor}} = 33$ min. $[\alpha]_{\text{D}}^{28} = -50 \pm 2$ ($c = 1.0$, CHCl_3 , 90 % ee).

Literature value for (*R*)-2-(2-oxo-2-phenylethyl)cyclohexanone $[\alpha]_{\text{D}} = +57.8$ ($c = 1$, CHCl_3 , for 84% ee). The (*S*)-absolute configuration for compound **26a** was inferred by comparison of the optical rotation with the value reported in the literature.²⁷

HRMS: calculated for $\text{C}_{14}\text{H}_{16}\text{O}_2$ ($\text{M}+\text{Na}$): 239.1043, found: 239.1047. **^1H (CDCl_3 , 400 MHz):** δ 8.07 – 7.93 (m, 1H), 7.66 – 7.53 (m, 1H), 7.53 – 7.42 (m, 1H), 3.63 (dd, $J = 17.7, 6.6$ Hz, 1H), 3.28 – 3.14 (m, 1H), 2.71 (dd, $J = 17.7, 5.7$ Hz, 1H), 2.54 – 2.41 (m, 1H), 2.31 – 2.09 (m, 1H), 1.98 – 1.62 (m, 2H), 1.48 (qd, $J = 12.8, 3.9$ Hz, 1H). **^{13}C (CDCl_3 , 125 MHz):** δ 211.5, 198.6, 137.0, 133.0, 128.5, 128.0, 46.4, 41.9, 38.3, 34.3, 27.9, 25.3.

(S)-2-(2-((1,1'-biphenyl)-4-yl)-2-oxoethyl)cyclohexanone (26b)

The reaction was carried out following the general procedure to furnish the crude product after 14 h of irradiation. Purification by flash column chromatography (gradient eluent from pure hexane to 10:1 hexane:AcOEt mixture) afforded the title compound (17.3 mg, 60 % yield, 87 % ee) as a white solid. The enantiomeric excess was determined by HPLC analysis on a Daicel Chiralpak IC column, 85:15 hexane:iPrOH, flow rate 1.00 mL/min, $\lambda = 254$ nm: $\tau_{\text{minor}} = 20$ min, $\tau_{\text{major}} = 29$ min. $[\alpha]_{\text{D}}^{27} = -44 \pm 2$ ($c = 1.0$, CHCl_3 , 87 % ee). HRMS: calculated for $\text{C}_{20}\text{H}_{20}\text{O}_2$ ($\text{M}+\text{Na}$): 315.1356, found: 315.1356. ^1H (CDCl_3 , 400 MHz): δ 8.12 – 8.06 (m, 2H), 7.73 – 7.69 (m, 2H), 7.68 – 7.62 (m, 2H), 7.55 – 7.46 (m, 2H), 7.46 – 7.40 (m, 1H), 3.66 (dd, $J = 17.6$, 6.6 Hz, 1H), 3.34 – 3.10 (m, 1H), 2.74 (dd, $J = 17.6$, 5.7 Hz, 1H), 2.56 – 2.42 (m, 2H), 2.31 – 2.12 (m, 2H), 2.00 – 1.90 (m, 1H), 1.90 – 1.75 (m, 1H), 1.75 – 1.64 (m, 1H), 1.50 (qd, $J = 12.8$, 3.9 Hz, 1H). ^{13}C (CDCl_3 , 100 MHz): δ 211.5, 198.2, 145.7, 139.9, 135.8, 128.9, 128.6, 128.1, 127.2, 127.2, 46.5, 42.0, 38.3, 34.3, 28.0, 25.4.

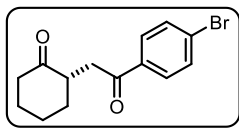
(S)-2-(2-oxo-2-(p-tolyl)ethyl)cyclohexanone (26c)

The reaction was carried out following the general procedure to furnish the crude product after 14 h of irradiation. Purification by flash column chromatography (gradient eluent from pure hexane to 10:1 hexane:AcOEt mixture) afforded the title compound (15.5 mg, 66 % yield, 92 % ee) as a white solid. The enantiomeric excess was determined by HPLC analysis on a Daicel Chiralpak IC column, 85:15 hexane:iPrOH, flow rate 1.00 mL/min, $\lambda = 254$ nm: $\tau_{\text{major}} = 26$ min, $\tau_{\text{minor}} = 38$ min.

$[\alpha]_{\text{D}}^{28} = -68 \pm 2$ ($c = 1.0$, CHCl_3 , 92 % ee). ^1H (CDCl_3 , 400 MHz): δ 7.91 (d, $J = 8.2$ Hz, 2H), 7.30 – 7.24 (d, $J = 8.2$ Hz, 2H), 3.60 (dd, $J = 17.6$, 6.4 Hz, 1H), 3.23 (dq, $J = 12.2$, 6.0 Hz, 1H), 2.69 (dd, $J = 17.6$, 6.0 Hz, 1H), 2.50 – 2.44 (m, 2H), 2.43 (s, 3H), 2.28 – 2.11 (m, 2H), 1.95 – 1.87 (m, 1H), 1.87 – 1.64 (m, 2H), 1.46 (qd, $J = 12.7$, 3.9 Hz, 1H). ^{13}C (CDCl_3 , 100 MHz): δ 211.6, 198.2, 143.7, 134.6, 129.2, 128.2, 46.4, 42.0, 38.1, 34.3, 28.0, 25.3, 21.6.

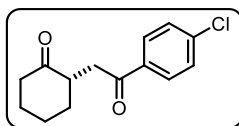
Characterization data in agreement with the literature.⁴⁶

⁴⁶ Yasu, Y.; Koike, T.; Akita, M. "Sunlight-driven synthesis of γ -diketones via oxidative coupling of enamines with silyl enol ethers catalyzed by $[\text{Ru}(\text{bpy})_3]^{2+}$ " *Chem. Comm.* **2012**, 48, 5355.

(S)-2-(2-(4-bromophenyl)-2-oxoethyl)cyclohexanone (26d)

The reaction was carried out following the general procedure to furnish the crude product after 14 h of irradiation. Purification by flash column chromatography (gradient eluent from pure hexane to 10:1 hexane:AcOEt mixture) afforded the title compound (15.4 mg, 52 % yield, 86 % ee) as a yellow solid. The enantiomeric excess was determined by HPLC analysis on a Daicel Chiralpak IC column, 95:5 hexane:iPrOH, flow rate 1.00 mL/min, $\lambda = 254$ nm: $\tau_{\text{minor}} = 36$ min, $\tau_{\text{major}} = 41$ min.

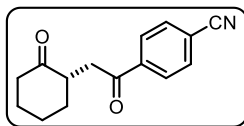
$[\alpha]_{\text{D}}^{27} = -40 \pm 1$ ($c = 1.0$, CHCl_3 , 86 % ee). ^1H (CDCl_3 , 500 MHz): δ 7.87 (d, $J = 8.7$ Hz, 2H), 7.63 (d, $J = 8.8$ Hz, 2H), 3.58 (dd, $J = 17.6, 6.9$ Hz, 1H), 3.26 – 3.13 (m, 1H), 2.64 (dd, $J = 17.6, 5.4$ Hz, 1H), 2.52 – 2.41 (m, 2H), 2.33 – 2.11 (m, 2H), 1.97 – 1.89 (m, 1H), 1.87 – 1.75 (m, 1H), 1.75 – 1.65 (m, 1H), 1.48 (qd, $J = 12.8, 3.9$ Hz, 1H). ^{13}C (CDCl_3 , 125 MHz): δ 211.3, 197.6, 135.8, 131.8, 129.6, 128.1, 46.5, 41.9, 38.3, 34.3, 27.9, 25.3. Characterization data in agreement with the literature.⁴⁶

(S)-2-(2-(4-chlorophenyl)-2-oxoethyl)cyclohexanone (26e)

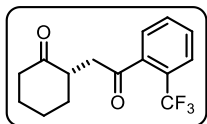
The reaction was carried out following the general procedure to furnish the crude product after 14 h of irradiation. Purification by flash column chromatography (gradient eluent from pure hexane to 10:1 hexane:AcOEt mixture) afforded the title compound (10 mg, 40 % yield, 87 % ee) as a yellow solid. The enantiomeric excess was determined by HPLC analysis on a Daicel Chiralpak IB column, 95:5 hexane:iPrOH, flow rate 1.00 mL/min, $\lambda = 254$ nm: $\tau_{\text{major}} = 9$ min, $\tau_{\text{minor}} = 10$ min. $[\alpha]_{\text{D}}^{27} = -55 \pm 2$ ($c = 1.0$, CHCl_3 , 87 % ee). ^1H (CDCl_3 , 400 MHz): δ 7.95 (d, $J = 8.6$ Hz, 2H), 7.45 (d, $J = 8.6$ Hz, 2H), 3.58 (dd, $J = 17.6, 6.9$ Hz, 1H), 3.30 – 3.08 (m, 1H), 2.64 (dd, $J = 17.6, 5.4$ Hz, 1H), 2.52 – 2.40 (m, 2H), 2.31 – 2.10 (m, 2H), 1.98 – 1.88 (m, 1H), 1.88 – 1.75 (m, 1H), 1.75 – 1.64 (m, 1H), 1.48 (qd, $J = 12.8, 3.8$ Hz, 1H). ^{13}C (CDCl_3 , 100 MHz): δ 211.4, 197.4, 139.4, 135.4, 129.5, 128.8, 46.5, 41.9, 38.3, 34.3, 27.9, 25.3.

Characterization data in agreement with the literature.⁴⁷

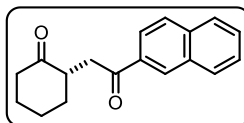
⁴⁷ Xie, J.; Huang, Z. Z. "The cascade carbo-carbonylation of unactivated alkenes catalyzed by an organocatalyst and a transition metal catalyst: a facile approach to γ -diketones and γ -carbonyl aldehydes from arylalkenes under air" *Chem. Comm.* **2010**, 46, 1947.

(S)-4-(2-(2-oxocyclohexyl)acetyl)benzonitrile (26f)

The reaction was carried out following the general procedure to furnish the crude product after 14 h of irradiation. Purification by flash column chromatography (gradient eluent from pure hexane to 10:1 hexane:AcOEt mixture) afforded the title compound (10.2 mg, 42 % yield, 88 % ee) as a yellow solid. The enantiomeric excess was determined by HPLC analysis on a Daicel Chiralpak IC column, 70:30 hexane:iPrOH, flow rate 1.00 mL/min, $\lambda = 254$ nm: $\tau_{\text{major}} = 34$ min, $\tau_{\text{minor}} = 38$ min. $[\alpha]_{\text{D}}^{28} = -72 \pm 2$ ($c = 1.0$, CHCl_3 , 88 % ee). **HRMS**: calculated for $\text{C}_{15}\text{H}_{15}\text{NO}_2$ ($\text{M}+\text{Na}$): 264.0995, found: 264.0996. **^1H (CDCl₃, 400 MHz)**: δ 8.09 (d, $J = 8.4$ Hz, 2H), 7.79 (d, $J = 8.4$ Hz, 2H), 3.59 (dd, $J = 17.6$, 7.5 Hz, 1H), 3.32 – 3.13 (m, 1H), 2.64 (dd, $J = 17.6$, 5.0 Hz, 1H), 2.55 – 2.38 (m, 2H), 2.32 – 2.13 (m, 2H), 2.06 – 1.87 (m, 1H), 1.88 – 1.76 (m, 1H), 1.76 – 1.64 (m, 1H), 1.51 (qd, $J = 12.9$, 3.8 Hz, 1H). **^{13}C (CDCl₃, 100 MHz)**: δ 211.2, 197.4, 140.5, 140.1, 132.4, 128.5, 117.9, 116.2, 46.7, 41.8, 38.7, 34.2, 27.9, 25.3.

(S)-2-(2-oxo-2-(2-(trifluoromethyl)phenyl)ethyl)cyclohexanone (26g)

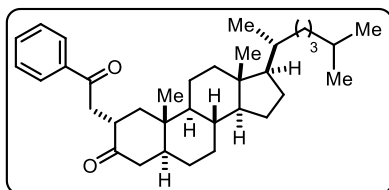
The reaction was carried out following the general procedure to furnish the crude product after 14 h of irradiation. Purification by flash column chromatography (gradient eluent from pure hexane to 10:1 hexane:AcOEt mixture) afforded the title compound (13.9 mg, 50 % yield, 76 % ee) as a yellow oil. The enantiomeric excess was determined by HPLC analysis on a Daicel Chiralpak IC column, 95:5 hexane:iPrOH, flow rate 1.00 mL/min, $\lambda = 254$ nm: $\tau_{\text{major}} = 16$ min, $\tau_{\text{minor}} = 20$ min. $[\alpha]_{\text{D}}^{28} = -14 \pm 1$ ($c = 0.5$, CHCl_3 , 76 % ee). **HRMS**: calculated for $\text{C}_{15}\text{H}_{15}\text{F}_3\text{O}_2$ ($\text{M}+\text{Na}$): 307.0916, found: 307.0928. **^1H (CDCl₃, 400 MHz)**: δ 7.78 – 7.69 (m, 2H), 7.68 – 7.62 (m, 1H), 7.61 – 7.53 (m, 1H), 3.42 (dd, $J = 18.2$, 7.5 Hz, 1H), 3.26 – 3.21 (m, 1H), 2.59 (dd, $J = 18.2$, 5.0 Hz, 1H), 2.50 – 2.43 (m, 2H), 2.29 – 2.22 (m, 1H), 2.22 – 2.14 (m, 1H), 1.98 – 1.91 (m, 1H), 1.87 – 1.76 (m, 1H), 1.75 – 1.63 (m, 1H), 1.55 – 1.40 (m, 1H). **^{13}C (CDCl₃, 100 MHz)**: δ 211.2, 202.8, 131.8, 129.8, 127.6, 126.4 (m, 1C, CF_3), 46.5, 43.0, 43.0, 41.8, 33.8, 27.9, 25.3.

(S)-2-(2-(naphthalen-2-yl)-2-oxoethyl)cyclohexanone (26h)

The reaction was carried out following the general procedure to furnish the crude product after 14 h of irradiation. Purification by flash column chromatography (gradient eluent from pure hexane to 10:1 hexane:AcOEt mixture) afforded the title compound (19.4 mg, 73 % yield, 91 % ee) as a white solid. The enantiomeric excess was determined by HPLC analysis on a Daicel Chiralpak IC column, 85:15 hexane:iPrOH, flow rate 1.00 mL/min, $\lambda = 254$ nm: $\tau_{\text{minor}} = 26$ min, $\tau_{\text{major}} = 29$ min. $[\alpha]_{\text{D}}^{28} = -19 \pm 1$ ($c =$

0.5, CHCl_3 , 91 % ee). **HRMS**: calculated for $\text{C}_{18}\text{H}_{18}\text{O}_2$ ($\text{M}+\text{Na}$): 289.1199, found: 289.1199. **^1H (CDCl_3 , 400 MHz)**: δ 8.55 (s, 1H), 8.07 (dd, $J = 8.6, 1.8$ Hz, 1H), 8.01 – 7.97 (m, 1H), 7.94 – 7.87 (m, 2H), 7.68 – 7.54 (m, 2H), 3.78 (dd, $J = 17.5, 6.5$ Hz, 1H), 3.26 (dq, $J = 11.8, 5.8$ Hz, 1H), 2.85 (dd, $J = 17.6, 5.9$ Hz, 1H), 2.54 – 2.44 (m, 2H), 2.35 – 2.23 (m, 1H), 2.18 (m, 1H), 2.00 – 1.90 (m, 1H), 1.90 – 1.65 (m, 2H), 1.65 – 1.45 (m, 1H). **^{13}C (CDCl_3 , 100 MHz)**: δ 211.6, 198.6, 135.6, 134.4, 132.5, 129.7, 129.5, 128.3, 128.3, 127.7, 126.7, 123.8, 46.6, 42.0, 38.4, 34.4, 28.0, 25.4.

(*S*)-2-(2-oxo-2-phenylethyl)cyclohexanone (**28**)



The reaction was carried out following the general procedure to furnish the crude product after 14 h of irradiation. Purification by flash column chromatography (gradient eluent from pure hexane to 20:1 hexane:AcOEt mixture) afforded

the title compound (23 mg, 47 % yield, >20:1 r.r., >20:1 d.r.) as a white solid.

HRMS: calculated for $\text{C}_{35}\text{H}_{52}\text{O}_2$ ($\text{M}+\text{Na}$): 527.3881, found: 527.3860. **^1H (CDCl_3 , 400 MHz)**: δ 8.00 (dd, $J = 8.4, 1.4$ Hz, 2H), 7.68 – 7.53 (m, 1H), 7.53 – 7.43 (m, 2H), 3.61 (dd, $J = 17.7, 6.3$ Hz, 1H), 3.33 – 3.26 (m, 1H), 2.70 (dd, $J = 17.7, 5.5$ Hz, 1H), 2.54 – 2.40 (m, 1H), 2.21 – 2.11 (m, 2H), 2.04 – 1.94 (m, 1H), 1.84 (ddd, $J = 9.6, 5.7, 3.7$ Hz, 1H), 1.78 – 1.67 (m, 1H), 1.64 – 0.96 (m, 28H), 0.96 – 0.82 (m, 10H), 0.82 – 0.71 (m, 1H), 0.70 (s, 3H). **^{13}C (CDCl_3 , 100 MHz)**: δ 211.3, 198.6, 137.1, 132.9, 128.5, 128.0, 56.2, 56.2, 53.9, 48.1, 46.3, 44.6, 42.6, 42.5, 39.9, 39.5, 38.4, 36.6, 36.1, 35.7, 35.2, 31.7, 29.7, 28.8, 28.2, 28.0, 24.2, 23.8, 22.8, 22.5, 21.5, 18.6, 12.42, 12.0.

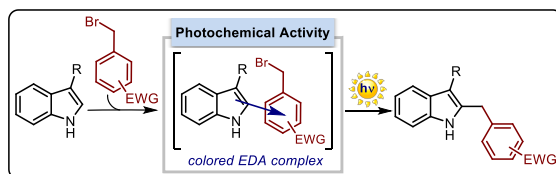
The assignment of the relative stereochemistry shown in the drawing was performed by selective 1D-NOESY by correlation between the substituted *alpha* proton and the methyl group in position 4 [when $\text{CO}-\text{CH}(\text{CH}_2\text{Ar})$ is irradiated $\text{CO}-\text{CH}(\text{CH}_2\text{Ar})-\text{CH}_2-\text{C}(\text{Me})$ is correlated].

Chapter IV

X-Ray characterization of an EDA complex that drives the photochemical alkylation of indoles

Target

Developing a straightforward method for the direct benzylation and phenacylation of substituted 1*H*-indoles, which requires mild conditions in order to proceed.



Tools

Accessing radical reactivity manifolds through the photochemical activity of EDA complexes, formed upon mixing readily available indoles and electron-accepting benzyl or phenacyl bromides.¹

4.1 Introduction

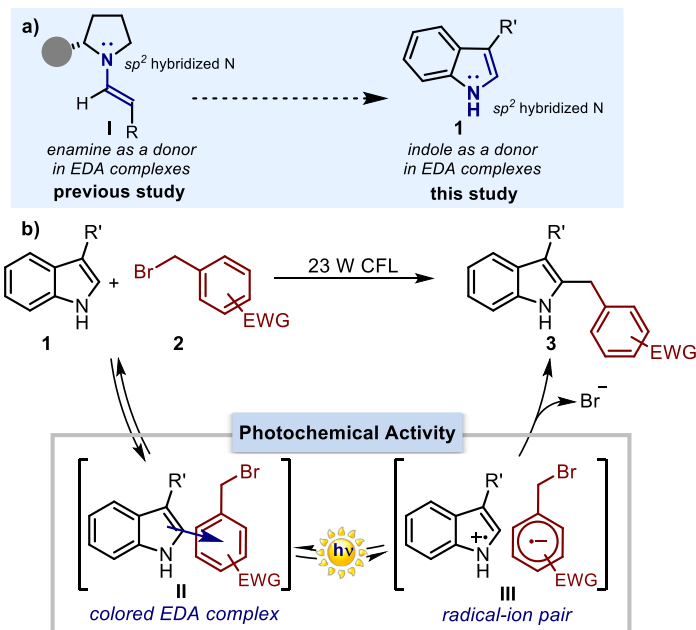
The successful development of the photochemical α -alkylation of carbonyl compounds driven by the formation of electron donor-acceptor (EDA) complexes between chiral enamines and electron-poor alkyl halides,² prompted us to expand the synthetic potential of EDA complex-mediated reactions to other class of donors. The electronic similarities between 1*H*-indoles (**1**) and enamines **I**, along with the numerous precedents describing the ability of indoles to engage in EDA complex formation (Section 4.1.1), encouraged us to test these hetero-aromatic compounds as donors (Scheme 4.1a). While precedents in the literature demonstrate the indole tendency toward EDA associations, the potential of productively using the photo-activity of indole-based EDA complexes in synthetic chemistry is limited to a few examples (detailed in Section 4.1.2).

We hypothesized that EDA complexes would be generated between indoles **1** and electron-poor alkyl bromides **2**. Subsequently, visible light irradiation of these complexes

¹ The work discussed in this chapter has been published, see: Kandukuri, S. R.; Bahamonde, A.; Chatterjee, I.; Jurberg, I. D.; Escudero-Adán, E. C.; Melchiorre, P. "X-Ray characterization of an electron donor-acceptor complex that drives the photochemical alkylation of indoles" *Angew. Chem. Int. Ed.* **2015**, *54*, 1485.

² a) Arceo, E.; Jurberg, I. D.; Álvarez-Fernández, A.; Melchiorre, P. "Photochemical activity of a key donor-acceptor complex can drive stereoselective catalytic α -alkylation of aldehydes" *Nat. Chem.* **2013**, *5*, 750. b) Arceo, E.; Bahamonde, A.; Bergonzini, G.; Melchiorre, P. "Enantioselective direct α -alkylation of cyclic ketones by means of photo-organocatalysis." *Chem. Sci.* **2014**, *5*, 2438.

II might induce an electron-transfer, affording the contact radical pair **III**. Concomitantly, the presence of bromine as a suitable leaving group within the radical anion partner may trigger an irreversible and rapid fragmentation, preventing the back-electron transfer and facilitating the formation of the alkylated indole scaffolds **3** (Scheme 4.1b).



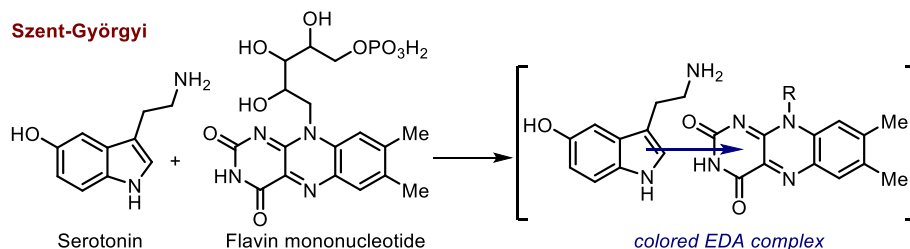
Scheme 4.1 a) Expanding the EDA-complex activation strategy to include indoles as donors. b) The alkylation of indoles driven by the photochemical activity of the EDA complex **II**. CFL = compact fluorescent light; EWG: electron-withdrawing group.

4.1.1 EDA complexes with indoles

The study of indole-based EDA complexes started with the investigations of Albert Szent-Györgyi, who was awarded the Nobel Prize in Physiology or Medicine in 1937 for his studies on oxidation and energy transfer of vitamin C. Györgyi's research related the formation of indole-containing EDA complexes to the activity of tranquilizing drugs.³ He also reported in 1960 the first characterization of an EDA complex, where an indole (serotonin) acted as donor. Flavine mononucleotide served as the acceptor partner (Scheme 4.2).⁴

³ a) Isenberg, I.; Szent-Györgyi, A. "Free radical formation in riboflavin complexes" *Proc. Natl. Acad. Sci.* **1958**, *44*, 857. b) Karreman, G.; Isenberg, I.; Szent-Györgyi, A. "On the mechanism of action of chlorpromazine" **1959**, *Science*, *130*, 1191.

⁴ Isenberg, I.; Szent-Györgyi, A.; Baird, S. L. "Spin resonance study of serotonin-FMN interaction" *Proc. Natl. Acad. Sci.* **1960**, *46*, 1307.



Scheme 4.2 First described indole-based EDA complex.

These investigations pointed out the remarkable ability of indoles to act as electron donors in the formation of EDA complexes with various acceptors, including molecular iodine, electron-poor arenes, and a series of quinones.⁵ Subsequently, other groups studied the electrochemical properties⁶ and the association constants⁷ of these indole-based complexes. Which orbitals of the indole scaffold are involved in the charge-transfer interaction was a topic that attracted a great deal of interest. Initially, it was suggested by Szent-Györgyi that the π -electrons at both C2 and C3 of the indole moiety were responsible for this interaction.⁵ This hypothesis was based on the comparison between the donor abilities of indoles and carbazoles: despite the superficial similarities, carbazoles were not able to engage in the formation of EDA complexes. This was an unexpected result as carbazoles have a more extended π -system; therefore, their ability as donors was supposed to be greater. However, carbazoles lack the presence of highly negatively charged carbons, in contrast to indoles, where C2 and C3 positions are polarized. This hypothesis was corroborated by quantum mechanics calculations.⁸ Additionally, the effect of the steric interactions on the association constant and the spatial disposition of indole-based EDA complex have also been investigated.⁹ The measurement of the association constants of several methoxy-substituted indoles with trinitrobenzene (**5**) and tetracyanoethylene (**6**) suggested that the three-dimensional arrangement of the complexes in solution depends on the acceptor. In the EDA complex generated between indole **4** and **5**, the acceptor appears to be slightly inclined towards the indole C2 and C7

⁵ Szent-Györgyi, A.; Isenberg, I.; McLaughlin, J. "Local and π - π interactions in charge transfer" *Proc. Natl. Acad. Sci.* **1961**, *47*, 1089.

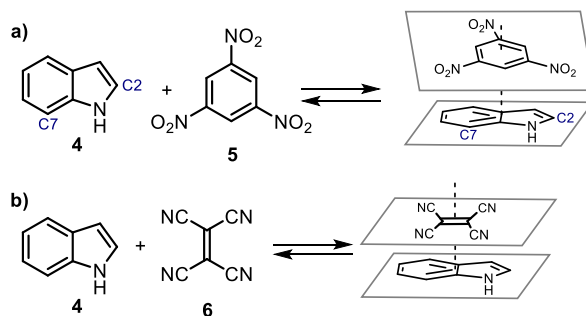
⁶ Smaller, B.; Isenberg, I.; Baird, S. L. "Spin resonance and electrical conductivity of indole-iodine" *Nature* **1961**, *191*, 168.

⁷ Foster, R.; Fyfe, C. A. "Electron-donor-acceptor complex formation by compounds of biological interest. Part III. Indole complexes" *J. Chem. Soc. B* **1966**, 926.

⁸ Green, J. P.; Malrieu, J. P. "Quantum chemical studies of charge-transfer complexes of indoles" *Proc. Natl. Acad. Sci.* **1965**, *54*, 659.

⁹ Sung, M. T.; Parker, J. A. "Molecular complexes of methoxyindoles with 1,3,5-trinitrobenzene and tetracyanoethylene" *Proc. Natl. Acad. Sci.* **1972**, *69*, 1196.

positions (both molecules are not positioned in parallel planes, Scheme 4.3a) and the effect of steric interactions on the complex formation are not significant. However, in the complex formed with **6**, the steric hindrance plays a significant role on the value of the association constant and the acceptor seems to be positioned above the indole nucleus (Scheme 4.3b).



Scheme 4.3 Spatial dispositions of indole-based EDA complexes.

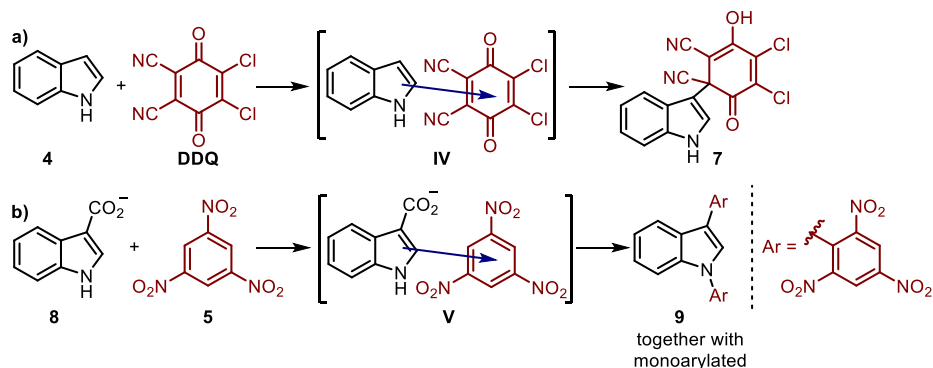
4.1.2 Indole-based EDA complexes relevant for synthetic transformations

The theoretical studies and the reports describing the association constants and properties of EDA complexes where an indole acts as acceptor are numerous. However, the application of these molecular associations in synthesis has remained largely unexplored. Only two thermally-driven and two photochemical reactions have been described where the intermediacy of indole-based EDA complexes was proposed to drive the overall process.

As depicted in Scheme 4.4a, a mixture of indole **4** and 2,3-dichloro-5,6-dicyano-1,4-benzoquinone (DDQ) has been reported to form an EDA complex.¹⁰ This complex can be isolated as a solid, when prepared in apolar solvents like dichloromethane, or it can lead to the formation of the C3-alkylated indole **7** in polar protic solvents, like water or ethanol, following a thermal path. Moreover, it has been described that a solution of indole **8**, bearing a carboxylate moiety in the 3-position, and 1,3,5-trinitrobenzene (**5**) in dimethylsulfoxide affords a mixture of the diarylated adduct **9**, together with the monoarylated products (Scheme 4.4b).¹¹ However, when the same mixture is prepared in MeOH, the EDA complex **V** could be isolated by precipitation.

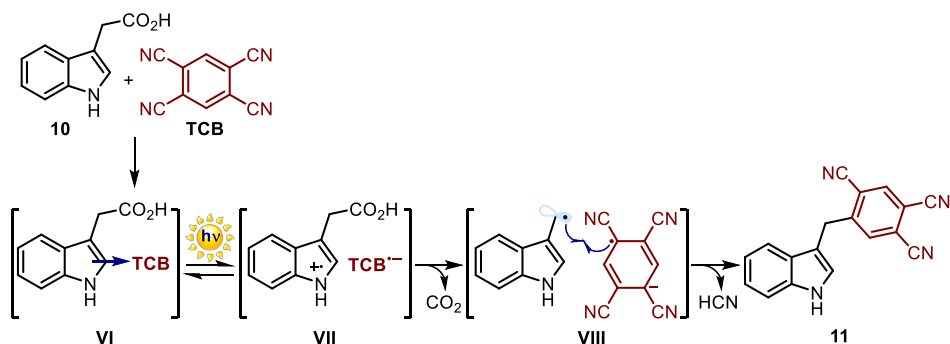
¹⁰ Bergman, J.; Carlsson, R.; Misztal, S. "The reaction of some indoles and indolines with 2,3-dichloro-5,6-dicyano-1,4-benzoquinone" *Acta Chem. Scand.* **1976**, *30*, 853.

¹¹ Sepulcri, P.; Goumont, R.; Hallé, J. C.; Buncel, E.; Terrier, F. "The first isolation of a π -complex precursor in Meisenheimer complex formation" *Chem. Commun.* **1997**, *8*, 789.



Scheme 4.4 Thermally-driven reactions mediated by the formation of an indole-based EDA complex.

A solid-state reaction, mediated by an indole-based EDA complex, has also been reported.¹² The formation of the arylation product **11** can be triggered by the irradiation of the crystals of the EDA complex **VI**, formed between 3-indoleacetic acid (**10**), which acts as a donor, and 1,2,4,5-tetracyanobenzene, who plays the role of acceptor (Scheme 4.5). This transformation has been proposed to proceed *via* a radical-radical coupling. Upon excitation of the crystals of **VI**, the radical-ion pair **VII** extrudes CO₂ yielding two radicals in close proximity, which would then couple. A subsequent elimination of hydrogen cyanide would render the final product **11**.

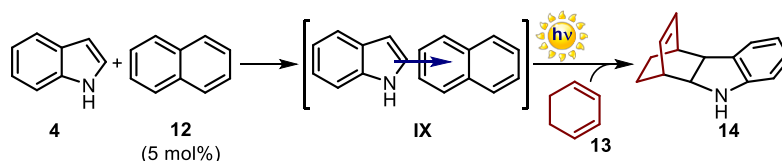


Scheme 4.5 Solid-state photochemical decarboxylative coupling of indole **10** with tetracyanobenzene mediated by the formation of an indole-based EDA complex.

¹² Koshima, H.; Ding, K.; Chisaka, Y.; Matsuura, T.; Ohashi, Y.; Mukasa, M. "Solid-state photodecarboxylation induced by exciting the CT bands of the complexes of arylacetic acids and 1,2,4,5-tetracyanobenzene" *J. Org. Chem.* **1996**, *61*, 2352.

This study reported a rare example demonstrating the synthetic potential of the photochemical properties of an indole-based EDA complex. Quite remarkably, it was also possible to obtain the structural characterization, by X-ray crystallographic analysis, of the photoactive EDA complex directly involved in the chemical reaction. There are few studies describing the X-ray structure of EDA complexes that are relevant for a chemical transformation. Only the characterization of complexes that can undergo Diels-Alder reactions¹³ and the isolation of the aggregation between bromine and benzene or toluene, which subsequently provides the electrophilic aromatic bromination of the arene, have been reported.¹⁴

In addition, the photochemical activity of another indole-based EDA complex **IX**, generated between naphthalene **12** and indole **4**, was exploited to promote a [4+2] cycloaddition (Scheme 4.6).¹⁵ Interestingly, naphthalene is used in catalytic amounts to trigger the formation of an EDA complex that, upon excitation, promotes the reaction between the indole contained within the complex and an external cyclohexadiene **13** within a Diels-Alder cycloaddition manifold.



Scheme 4.6 Photochemical Diels-Alder reaction mediated by the formation of an indole-based EDA complex.

4.2 Target of the project

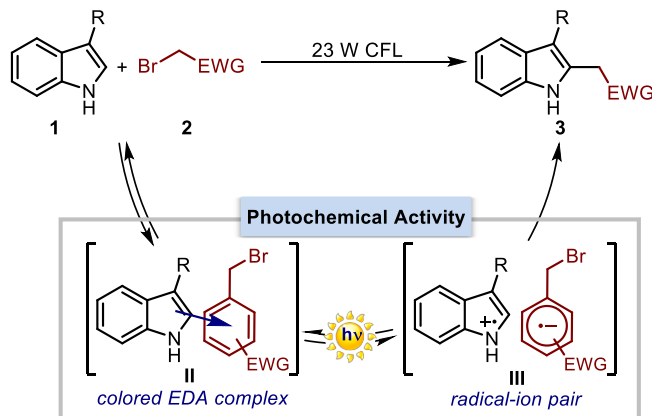
The aim of this project was to further expand the scope of the EDA complex-mediated reactions by designing other synthetically useful transformations. Specifically, we exploited the tendency of indoles **1** to act as donors in EDA complex formation with

¹³ a) Kim, J. H.; Lindeman, S. V.; Kochi, J. K. "Charge-transfer forces in the self-assembly of heteromolecular reactive solids: successful design of unique (single-crystal-to-single-crystal) Diels-Alder cycloadditions" *J. Am. Chem. Soc.* **2001**, *123*, 4951. b) Kim, J. H.; Hubig, S. M.; Lindeman, S. V.; Kochi, J. K. "Diels-Alder topochemistry *via* charge-transfer crystals: novel (thermal) single-crystal-to-single-crystal transformations" *J. Am. Chem. Soc.* **2001**, *123*, 87. c) Berionni, G.; Bertelle, P. A.; Marrot, J.; Goumont, R. "X-Ray structure of a CT complex relevant to Diels-Alder reactivity of anthracenes" *J. Am. Chem. Soc.* **2009**, *131*, 18224.

¹⁴ Vasilyev, A. V.; Lindeman, S. V.; Kochi, J. K. "Molecular structures of the metastable charge-transfer complexes of benzene (and toluene) with bromine as the pre-reactive intermediates in electrophilic aromatic bromination" *New J. Chem.* **2002**, *26*, 582.

¹⁵ González-Béjar, M.; Stiriba, S. E.; Miranda, M. A.; Pérez-Prieto, J. "Positive photocatalysis of a Diels-Alder reaction by quenching of excited naphthalene-indole charge-transfer complex with cyclohexadiene" *Org. Lett.* **2007**, *9*, 453.

electron-accepting benzyl and phenacyl bromides. Subsequently, the photochemical activity of such complexes **II** promotes the formation of the indole alkylation product **3** (Scheme 4.7).



Scheme 4.7 Photo-organocatalytic alkylation of indoles *via* EDA complex activation.

The EDA complex **II** is formed by two stable molecules, in contrast to our previous studies based on the use of transient enamines as donors. This situation allowed us to thoroughly study the nature and properties of these aggregations. The characterization of the complex **II** was a main target of the project and the focus of my work.

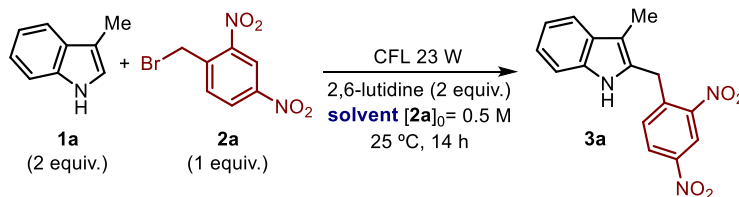
4.3 Optimization studies and reaction scope

The optimization of the best reaction conditions and the exploration of the substrate scope were conducted by Dr. Sandeep R. Kandukuri and Dr. Indranil Chatterjee. Thus, only a brief discussion of these aspects will be provided.

4.3.1 Optimization studies

The light-triggered benzylation of 3-methyl *1H*-indole (**1a**) with 2,4-dinitrobenzyl bromide (**2a**) was chosen as the model reaction (Table 4.1). A household 23 W compact fluorescent light (CFL) bulb was used to irradiate the reaction mixture. Initial optimization studies showed a higher reactivity in polar protic solvents (entries 6 to 8) with respect to the use of solvents with lower polarity (entries 1 to 3) or polar aprotic solvents (entries 4 and 5). Methanol was identified as the solvent of choice (entry 8). Additionally, the presence of a base, required to neutralize the HBr generated during the process, was found to be essential for this transformation (entry 9).

Table 4.1 Optimization studies



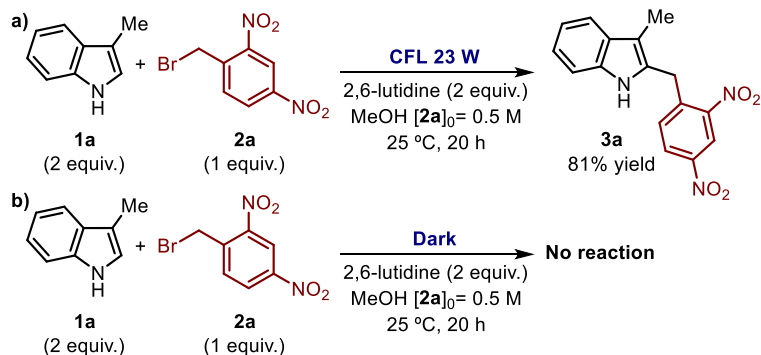
Entry	Solvent	Conversion ^a (%)
1	CHCl ₃	52
2	MTBE	58
3	toluene	67
4	DMSO	43
5	CH ₃ CN	67
6	EtOH	83
7	DMF	89
8	MeOH	92
9	MeOH (without base)	0

^a Determined by ¹H NMR analysis of the crude reaction mixture. MTBE: methyl *tert*-butyl ether; DMSO: dimethyl sulfoxide; DMF: *N,N*-dimethylformamide.

The optimized conditions, depicted in Scheme 4.8a, afforded the C2-benzylated indole **3a** in 81% yield after 20 hours of irradiation. A control experiment, carried out by performing the reaction in the dark, did not provide any reactivity. This testifies to the photochemical nature of the transformation (Scheme 4.8b).

The radical nature of the transformation was tested by carrying out the reaction between **1a** and **2a** (Scheme 4.8a) under aerobic conditions. The reaction mixture was not degassed, therefore there was oxygen dissolved in the solvent. Under these conditions, no product formation was observed. This observation can be rationalized when considering that molecular oxygen may quench the excited triplet-state of the EDA complex, resulting in an interruption of the single-electron transfer process, which is needed to generate the radical-ion pair **III** (Scheme 4.1).

The radical mechanism was further corroborated by the experiments conducted in the presence of 0.5 equivalents of 2,6-di-*tert*-butyl-4-methylphenol (BHT), a known radical scavenger. No product formation was detected after prolonged exposure to light, suggesting again the presence of radical intermediates in this reaction.



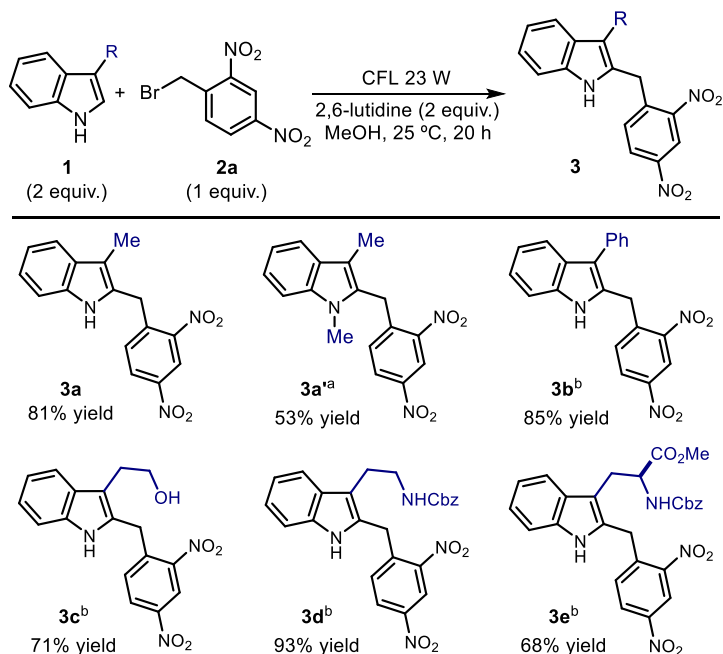
Scheme 4.8 a) Optimized reaction conditions for the EDA-mediated photochemical alkylation of indoles. b) Control experiment in the absence of irradiation.

4.3.2 Reaction scope

As shown in Scheme 4.9, a series of 3-substituted 1*H*-indoles could be selectively benzylated by **2a** at the C2 position. Importantly, *N*-Cbz (carboxybenzyl) protected tryptophan and tryptamine could also be employed affording the final products in good yields (adducts **3d** and **3e**). Furthermore, the fact that an alcohol was also tolerated testifies to the high chemoselectivity of the reaction (product **3c**).

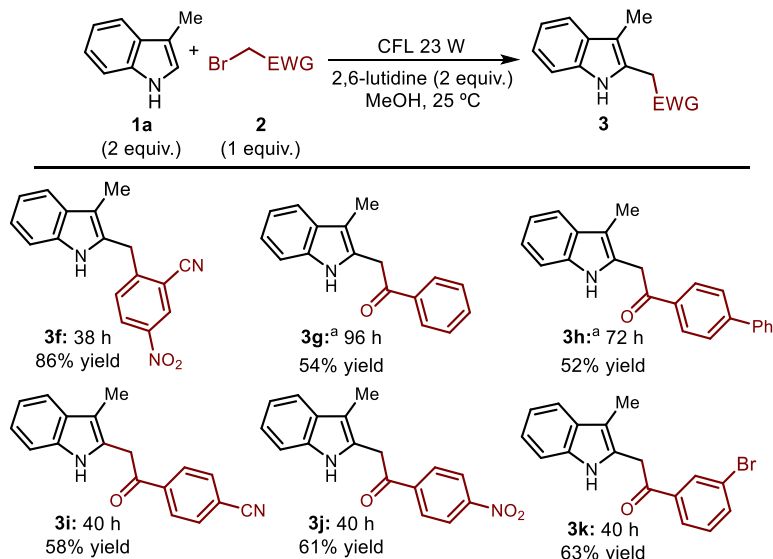
In addition, I was involved in evaluating the necessity of having a free N–H for the reaction to proceed by submitting an *N*-methyl protected indole derivative to the reactions conditions. It was found that *N*-methyl protected indole was also a competent substrate leading to the formation of **3a'** in a moderate yield.

In some occasions, three 15 W black light CFL bulbs ($\lambda_{\text{max}}=360$ nm) were used to illuminate the reaction vessel because they provided a slightly better yield (about 10% higher) than 23 W CFL bulbs.



Scheme 4.9 Scope of the photochemical C2-selective alkylation of different 3-substituted-1H-indoles. ^a Reaction irradiated for 40 h. ^b Three 15 W black light CFL bulbs ($\lambda_{\text{max}}=360$ nm) were used to illuminate the reaction vessel.

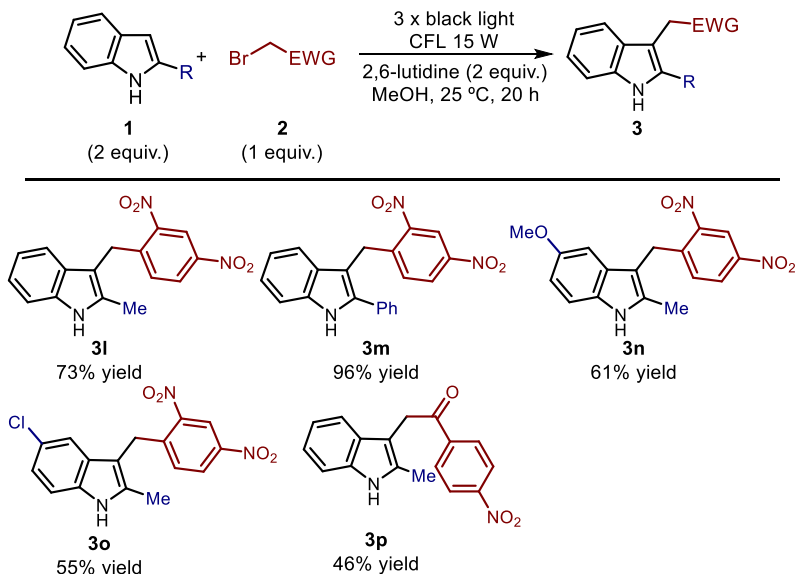
Moreover, we found that other bromide-containing acceptors productively combined with 1H-indoles to give photon-absorbing EDA associations (Scheme 4.10). The benzylation strategy could be extended to the use of 2-cyano-4-nitrobenzyl bromide, leading to the formation of product **3f**. In addition, a number of phenacyl bromides were also demonstrated as suitable alkylating agents for the photochemical C2-alkylation of **1a** (products **3g-k**).



Scheme 4.10 Scope of the photochemical C2-selective alkylation of 3-methyl-1H-indole employing different alkyl bromides. ^a Three 15 W black light CFL bulbs ($\lambda_{\text{max}} = 360 \text{ nm}$) were used to illuminate the reaction vessel.

The scope concerning the indole moiety was found not to be limited to the use of 3-substituted scaffolds, but 2-substituted 1H-indoles also effectively underwent the photochemical transformation. A series of 2-substituted 1H-indoles, bearing a variety of substituents at 2 and 5 positions, were successfully employed to selectively yield the C3-benzylated products **3l-o** (Scheme 4.11) upon reaction with **2a**. Furthermore, the reaction between 2-methyl 1H-indole and *p*-nitrophenacyl bromide afforded the final product **3p** with a moderate yield.

As a limitation of the method, the unsubstituted 1H-indole reacted sluggishly with **2a** to afford a mixture of C3- and C2-alkylation products in a 1.1:1 ratio and in a low overall yield of 14% after 36 hours.



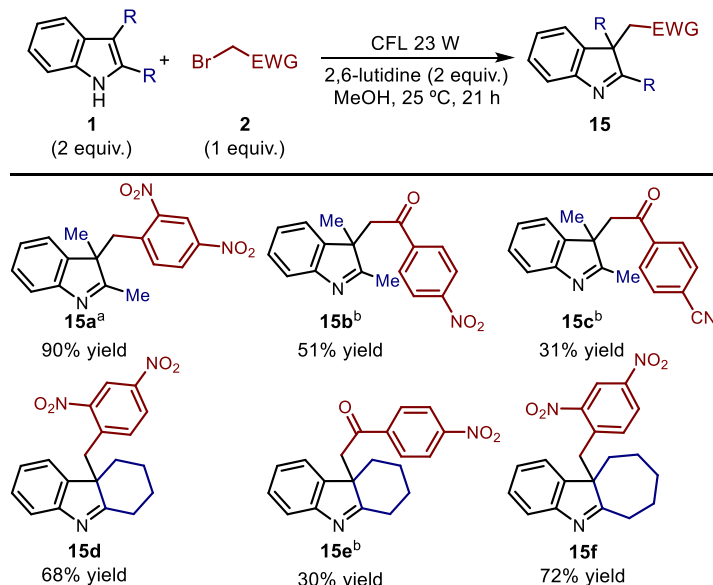
Scheme 4.11 Scope of the photochemical C3-selective alkylation of 2-substituted-1H-indoles. Three 15 W black light CFL bulbs ($\lambda_{\text{max}}=360$ nm) were used to illuminate the reaction vessel.

We next examined the possibility of extending the photo-alkylation strategy to include 2,3-disubstituted-1H-indoles. This methodology provides a direct access to valuable indolenine products through a dearomatization pathway.¹⁶

As shown in Scheme 4.12, different 2,3-disubstituted indoles successfully reacted with high regioselectivity, the C3-alkylated adducts being exclusively produced. This methodology allows the construction indolenines **15a-f** bearing a quaternary stereocenter *via* photochemical alkylation with **2a** or phenacyl bromides. Notably, while few metal-mediated protocols exist for the C3-benylation of 2,3-disubstituted-1H-indoles,¹⁷ the direct construction of indolenines adorned with a phenacyl moiety at C3 (**15b-c** and **15e**) was unknown.

¹⁶ a) Roche, S. P.; Porco, J. A. "Dearomatization strategies in the synthesis of complex natural products" *Angew. Chem. Int. Ed.* **2011**, *50*, 4068. For an early example of indolines containing quaternary stereocenters, see: b) Trost, B. M.; Quancard, J. "Palladium-catalyzed enantioselective C-3 allylation of 3-substituted-1H-indoles using trialkylboranes" *J. Am. Chem. Soc.* **2006**, *128*, 6314.

¹⁷ a) Zhu, Y.; Rawal, V. H. "Palladium-catalyzed C3-benylation of indoles" *J. Am. Chem. Soc.* **2012**, *134*, 111. b) Lin, A.; Yang, J.; Hashim, M. "N-Indolyltriethylborate: a useful reagent for synthesis of C3-quaternary indolenines" *Org. Lett.* **2013**, *15*, 1950.

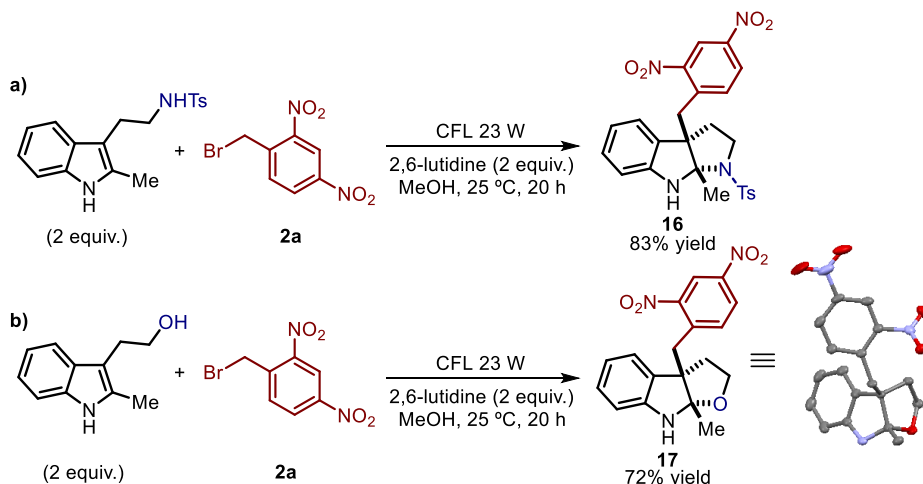


Scheme 4.12 Scope of the photochemical C3-selective alkylation of 2,3-disubstituted-1H-indoles. ^a Reaction irradiated for 36 h. ^b Three 15 W black light CFL bulbs ($\lambda_{\text{max}}=360$ nm) were used to illuminate the reaction vessel.

The substrates with a pendant nucleophile are especially interesting as they were found to cyclize onto the imine under the reaction conditions. Specifically, *N*-tosyl (Ts) tryptamine and tryptophol effectively yielded the corresponding *cis*-fused pyrrolo- and furano-indolines **16** and **17**,¹⁸ respectively, in high yields as single diastereomers (Scheme 4.13). These scaffolds are commonly found in numerous natural products.¹⁹

¹⁸ CCDC 1025726 contains the supplementary crystallographic data for **17**. These data can be obtained free of charge from The Cambridge Crystallographic Data Centre via www.ccdc.cam.ac.uk/data_request/cif.

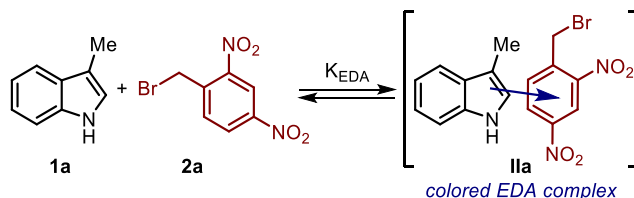
¹⁹ Repka, L. M.; Reisman, S. E. "Recent developments in the catalytic, asymmetric construction of pyrroloindolines bearing all-carbon quaternary stereocenters" *J. Org. Chem.* **2013**, *78*, 12314.



Scheme 4.13 Scope of the photochemical indole alkylation: dearomatization-annulation strategy.

4.4 Mechanistic insights

I was mainly involved in performing a series of experiments to investigate the mechanism of the photochemical alkylation of indoles. A special emphasis was placed on the characterization of the EDA complex **IIa**, formed upon mixing two stable molecules such as 3-methylindole **1a** and 2,4-dinitrobenzyl bromide **2a** (Scheme 4.14).



Scheme 4.14 Generation of EDA complex **IIa** upon mixing **1a** and **2a**. K_{EDA} = association constant of the EDA complex.

In our previous investigations of EDA complexes, an enamine, transiently generated in solution, was acting as donor. In contrast, in this case, both EDA partners are stable intermediates. This aspect greatly facilitated the EDA complex characterization.

4.4.1 Absorption spectra

Optical absorption spectra of the separate reaction components were recorded. As shown in Figure 4.1, the absorption spectrum of the solution containing both reagents (**1a** and **2a**) in methanol showed a bathochromic displacement above 430 nm, where neither substrate absorbs (red spectrum). This points towards the formation of a colored EDA

complex, where the indole **1a** acts as the acceptor and the electron-poor benzyl bromide **2a** as the donor.

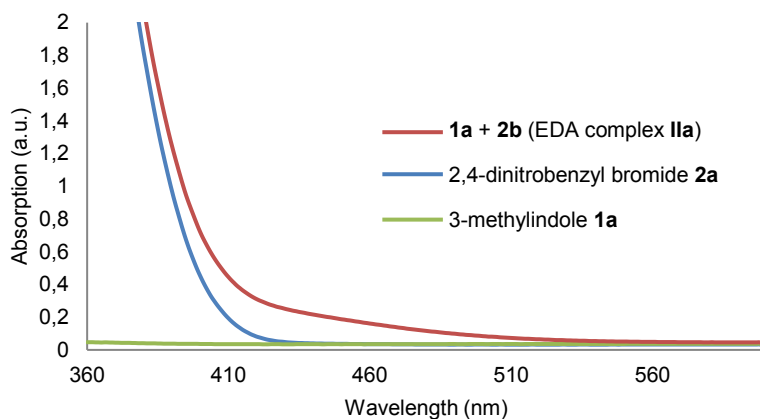


Figure 4.1 Optical absorption spectra recorded in MeOH in 1 mm path quartz cuvettes using a Shimadzu 2401PC UV-visible spectrophotometer. $[1\mathbf{a}] = [2\mathbf{a}] = 0.1$ M.

4.4.2 Mulliken's correlation

Mulliken's correlation establishes a relation between the wavelength of the charge-transfer band (λ_{CT}), the ionization potential (IP) of the donor, and the electron affinity (EA) of the acceptor (Equation 4.1).²⁰

$$\frac{h \cdot c}{\lambda_{CT}} = IP - EA - \omega \quad (\text{Eq. 4.1})$$

Our system was tested for an adherence to this correlation. A series of absorption spectra of solutions of the same donor (**2a**) and 2-methylindole derivatives with different electronic properties (different ionization potentials) were measured. As shown in Figure 4.2, it was observed that the charge-transfer absorption band undergoes a hypsochromic shift when electron-withdrawing groups are introduced at the 5 position of the indole nucleus (substituent = chlorine, blue spectrum of the plot). Furthermore, we also observed a bathochromic shift when an electron-donating group (MeO) was introduced (green spectrum). These results show the adherence of the EDA complexes generated by mixing these 2-methyl indoles with **2a** to Mulliken's correlation.

²⁰ a) Mulliken, R. S. "Molecular compounds and their spectra. II" *J. Am. Chem. Soc.* **1952**, *74*, 811.
b) Mulliken, R. S.; Person, W. B. "Molecular compounds and their spectra. XXI. Some general considerations" *J. Am. Chem. Soc.* **1969**, *91*, 3409.

The absorption spectra were acquired with a Shimadzu 2401PC UV-Vis spectrophotometer in 1 mm path quartz cuvettes. Methanol was used as the solvent; the concentration of 2,4-dinitrobenzyl bromide **2a** was 0.1 M and the concentration of the different 2-methylindoles was 0.4 M.

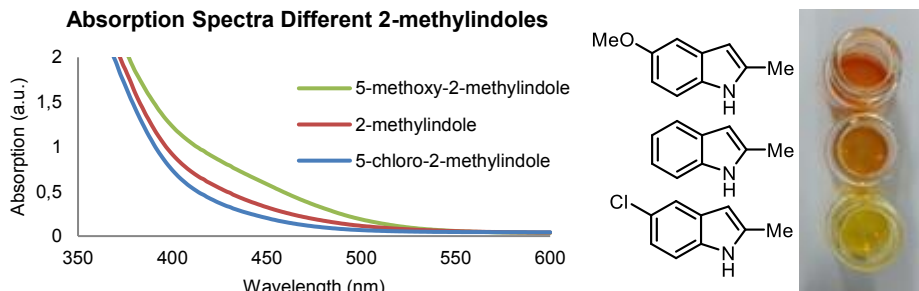


Figure 4.2 Mulliken correlation studies. Optical absorption spectra and visual appearance of solutions containing a mixture of 2,4-dinitrobenzyl bromide **2a** and a series of 2-methylindole derivatives with different electronic properties. [**2a**] = 0.1 M; [2-methylindoles] = 0.4M.

4.4.3 Determination of the stoichiometry of the complex in solution

The stoichiometry of the EDA complex in solution between the 2,4-dinitrobenzyl bromide **2a** and 3-methylindole **1a** was evaluated utilizing the Job's methodology (Figure 4.3).²¹ The absorption at 450 nm of methanol solutions with different donor/acceptor ratios, but constant total concentration of the two components ($[1a] + [2a] = 0.2$ M), was measured. All the absorption spectra were recorded in 1 mm path quartz cuvettes using a Shimadzu 2401PC UV-visible spectrophotometer. The absorbance values are plotted against the molar fraction (%) of 3-methylindole **1a**. The maximum absorbance is obtained with a 1:1 mixture, indicating that this is the stoichiometry of the EDA complex in solution.

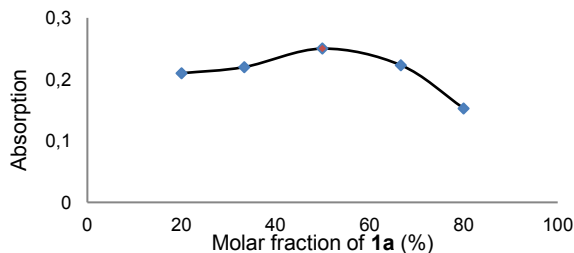
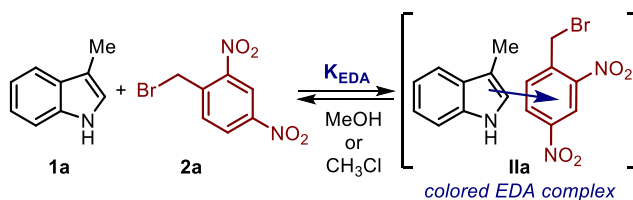


Figure 4.3 Job's plot in MeOH.

²¹ Job, P. "Formation and stability of inorganic complexes in solution" *Ann. Chem.* **1928**, *9*, 113.

4.4.4 Determination of the association constant

Having established that a 1:1 complex is formed in solution, we focused on the calculation of the association constant of the EDA complex (K_{EDA}) formed between **2a** and **1a** (Scheme 4.15). Two different solvents were employed for the measurements (methanol and chloroform), since this could allow us to rationalize why the process was faster in polar protic solvents.



Scheme 4.15 Generation of EDA complex **IIa** upon mixture of **1a** and **2a**.

Determination of the association constant by photochemical measurements

The Hildebrand-Benesi methodology²² was used to spectrophotometrically measure the association constant of the EDA complex formed between 2,4-dinitrobenzyl bromide **2a** and 3-methylindole **1a**. The study was done both in methanol and chloroform. The absorption at 450 nm of solutions with constant concentration of the 2,4-dinitrobenzyl bromide (0.05 M), but increased donor/acceptor ratios, was measured adding an excess of the indole **1a**. All the absorption spectra were recorded in 1 mm path quartz cuvettes. According to the methodology, a straight line is obtained when the reciprocal of the absorbance is plotted against the reciprocal of the concentration of the partner in excess (Equation 4.2). The plots, obtained for the methanol and chloroform solutions, are displayed below (Figure 4.4). The association constant (K_{EDA}), calculated dividing the intercept by the slope, is $0.88 \pm 0.02 \text{ M}^{-1}$ for the solution in methanol, and $0.60 \pm 0.02 \text{ M}^{-1}$ when using chloroform as the solvent.

$$\text{when } [1a] \gg [2a] \quad \frac{1}{A} = \frac{1}{[2a] \cdot l \cdot \epsilon_0 \cdot K_{EDA}} \cdot \left(\frac{1}{[1a]} \right) + \frac{1}{[2a] \cdot l \cdot \epsilon_0} \quad (\text{Eq. 4.2})$$

²² Benesi, H. A.; Hildebrand, J. H. "A spectrophotometric investigation of the interaction of iodine with aromatic hydrocarbons" *J. Am. Chem. Soc.* **1949**, *71*, 2703.

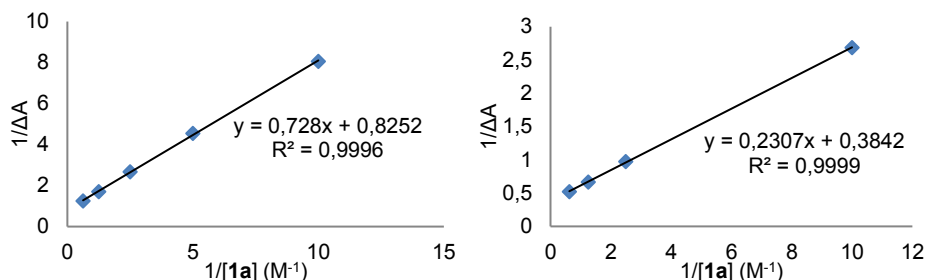


Figure 4.4 Hildebrand-Benesi plots in methanol (*left*) and chloroform (*right*).

Determination of the association constant by ¹H NMR spectroscopy measurements

The association constant of the EDA complex (K_{EDA}) was also determined utilizing the method described by Foster.²³ According to this approach, the differences in chemical shifts measured by ¹H NMR spectroscopy can be used to calculate K_{EDA} by means of Equation 4.3.

$$\text{when } [D] \gg [A] \quad \frac{\Delta}{[D]} = -\Delta \cdot K_{EDA} + \Delta_0 \cdot K_{EDA} \quad (\text{Eq. 4.3})$$

[D] and [A] are the concentrations of the donor and the acceptor; K_{EDA} is the association constant for the complex formation; Δ indicates the difference between the chemical shift of the acceptor in the presence of excess concentrations of the donor and the chemical shift of that specific proton in the absence of the donor; and Δ_0 indicates the difference between the chemical shift of the acceptor in the pure EDA complex (donor/acceptor in 1:1 ratio) and the chemical shift of that specific proton in the absence of the donor. A plot of $\Delta/[D]$ against Δ should be linear, with the slope gives the value of $-1 \cdot K_{EDA}$.

NMR samples with constant concentration of 2,4-dinitrobenzyl bromide **2a** (the acceptor, $[2a] = 0.1$ M), and different concentrations of 3-methylindole **1a** (the donor, $[1a]$ from 0.3 M to 1.5 M), were prepared in $CDCl_3$ and CD_3OD . The change in chemical shift (in ppm) of each peak of 2,4-dinitrobenzyl bromide **2a** was calculated by comparing the complexed **2a** in the corresponding solvent. The association constants were measured from the slope of the plots (Figure 4.5).

²³ a) Hanna, M. W.; Ashbaugh, A. L. "Nuclear magnetic resonance study of molecular complexes of 7,7,8,8-tetracyanoquinodimethane and aromatic donors" *J. Phys. Chem.* **1964**, *68*, 811. b) Foster, R.; Fyfe, C. A. "Interaction of electron acceptors with bases. Part 15.-Determination of association constants of organic charge-transfer complexes by NMR spectroscopy" *Trans. Faraday. Soc.* **1965**, *61*, 1626.

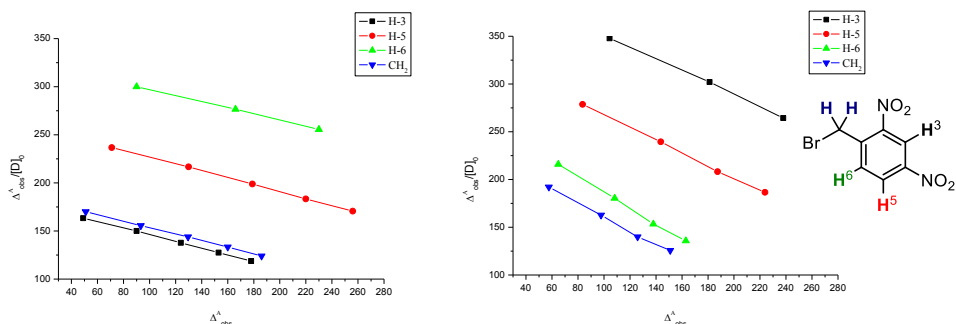


Figure 4.5 Plots of $\Delta/[1a]$ versus Δ in CDCl_3 (left) CD_3OD (right)

The association constants measured using the spectroscopic method are congruent with the ones calculated by optical methods. A comparison is provided in Table 4.2.

Table 4.2 Comparison between the K_{EDA} of **IIa** measured with the different methods.

Proton	K_{EDA} (M^{-1})	K_{EDA} (M^{-1})	K_{EDA} (M^{-1})	K_{EDA} (M^{-1})
	CDCl_3 <i>NMR</i>	CDCl_3 <i>Optical</i>	CD_3OMe <i>NMR</i>	CD_3OMe <i>Optical</i>
H-3	0.35		0.62	
H-5	0.36		0.66	0.88
H-6	0.32	0.60	0.83	
CH₂	0.34		0.72	

The results obtained with both methodologies indicate a slightly higher association constant for the EDA complex formation in methanol than in chloroform. This is in line with the optimization studies, which indicated that methanol was the best solvent for the EDA-mediated indole alkylation process.

A higher association constant is observed in the more polar solvent ($\epsilon(\text{CHCl}_3) = 4.81$; $\epsilon(\text{MeOH}) = 32.7$).²⁴ These results contradict the general trend that EDA complex formation is usually favored in apolar media, since the solvent-solute interactions barely compete with the complex formation. However, it has been reported that solvents capable of stabilizing the complex *via* hydrogen bonding can favor EDA complex formation.²⁵

²⁴ Smallwood, I. "Handbook of organic solvent properties" **2012**, Butterworth-Heinemann.

²⁵ Alghanmi, R. M.; Habeeb, M. M. "Spectral and solvation effect studies on charge transfer complex of 2, 6-diaminopyridine with chloranilic acid" *J. Mol. Liq.* **2013**, *181*, 20.

4.4.5 X-Ray characterization of the EDA complex **IIa**

The formation of an EDA complex between 2,4-dinitrobenzyl bromide **2a** and 3-methylindole **1a** was unambiguously established by the isolation of stable dark-orange crystals, suitable for an X-ray diffraction analysis (Figure 4.6).²⁶ The crystals were grown by Dr. Kandukuri by liquid diffusion of *n*-hexane into a dichloromethane solution of the EDA complex **IIa** at 0 °C and in the dark. X-Ray structural determination confirmed the formation of **IIa** as a face-to-face π - π complex with a 1:1 donor/acceptor ratio. The cofacially oriented indole and 2,4-dinitrobenzyl moieties afford infinite alternate stacks along the crystallographic *b* axis. The average interplanar distance, measured between the centroid of the planar core of the 2,4-dinitrobenzyl or the indole and the plane containing its respective counterpart, is 3.33 Å. This interplanar spacing is significantly less than the Van der Waals separation for aromatic molecules (3.40 Å),²⁷ which is consistent with the presence of intermolecular binding forces in the solid-state.

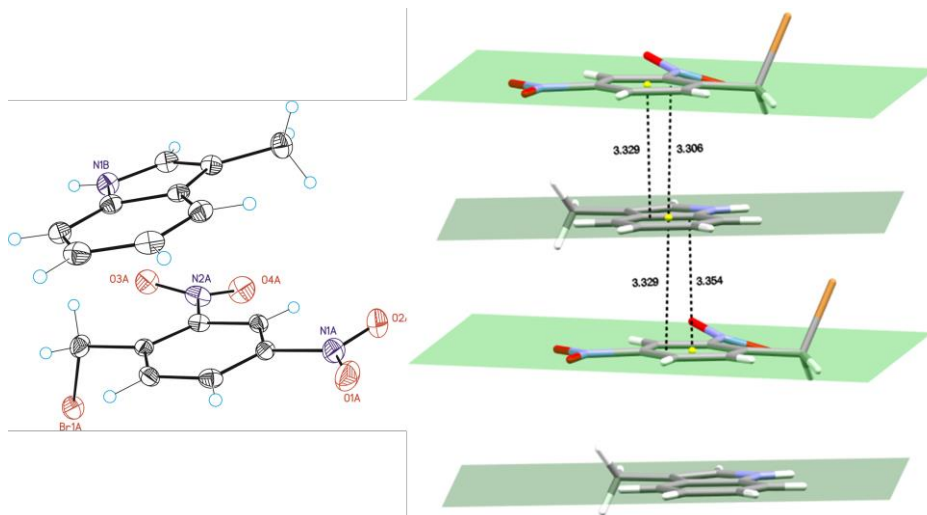


Figure 4.6 ORTEP plot (50% probability) of EDA complex **IIa** (*left*). Projection of the crystal structure along the *b* axis and distances used for calculating the average interplanar spacing (*right*). Disorder has been omitted for clarity. C gray, H white, Br orange, N blue, O red.

²⁶ CCDC 1025725 contains the supplementary crystallographic data for **IIa**. These data can be obtained free of charge from The Cambridge Crystallographic Data Centre via www.ccdc.cam.ac.uk/data_request/cif.

²⁷ a) Pauling, L. "The nature of the chemical bond" **1942**, p. 192, Cornell University Press. b) Bondi, A. "Van der Waals volumes and radii" *J. Phys. Chem.* **1964**, *68*, 441. c) Álvarez, S. "A cartography of the Van der Waals territories" *Dalton Trans.* **2013**, *42*, 8617.

Furthermore, the solid-state optical absorption spectrum of the EDA complex **IIa** (red line in Figure 4.7) showed a similar profile to the absorption spectrum measured from a solution of the **1a** and **2a** in methanol (Figure 4.1).

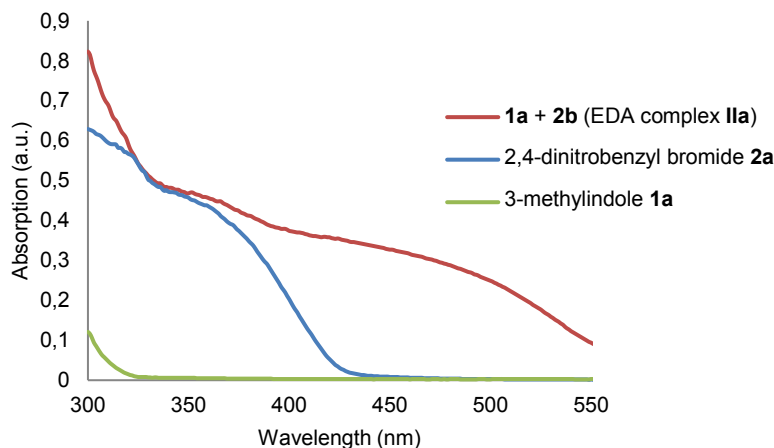


Figure 4.7 Optical absorption spectrum of the EDA complex **IIa** in the crystalline state.

After the characterization of the EDA complex **IIa**, we focused on ascertain whether the transformation proceeds *via* a radical chain mechanism. Consequently, we calculated the quantum yield of the model transformation, which relates the number of photons absorbed by the EDA complex with the molecules of product generated.

4.4.6 Quantum yield determination

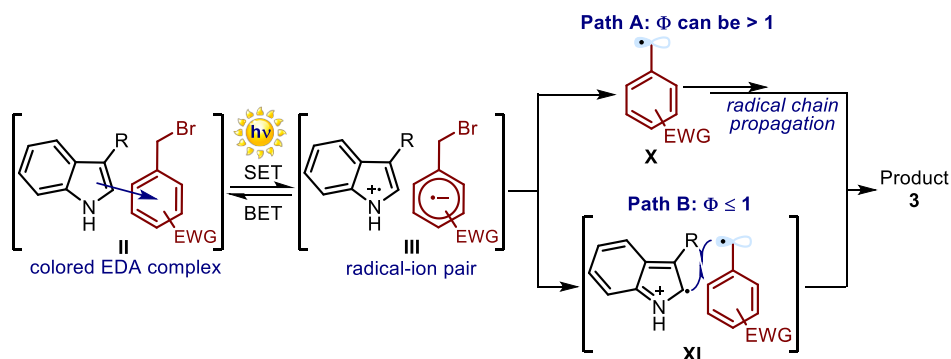
The quantum yield ($\Phi(\lambda)$) is defined by the IUPAC as the number of events (molecules changed, formed, or destroyed) per the number of photons absorbed at a particular wavelength (λ) in the same period of time (Equation 4.4).²⁸

$$\Phi(\lambda) = \frac{\text{molecules generated}}{\text{absorbed photons}} \quad (\text{Eq. 4.4})$$

Quantum yield measurements are a convenient method to discriminate whether radical chain mechanisms are taking place. In chain processes initiated by light absorption, one photon can form several molecules of product, resulting in a quantum yield larger than one. Consequently, a quantum yield greater than one can only be explained if a chain pathway initiated by light absorption is present. In this scenario, the EDA photochemical

²⁸ Kuhn, H. J.; Braslavsky, S. E.; Schmidt, R. "Chemical actinometry" *Pure and App. Chem.* **2004**, *76*, 2105.

activity would serve as an initiation event to generate radicals which are fed into a self-propagation manifold (Scheme 4.16, Path A, full mechanistic details in Scheme 4.18). However, a value of Φ equal or less than one is inconclusive, since it does not exclude a possible radical chain mechanism (Scheme 4.16, Path B, full mechanistic details in Scheme 4.17). This is because of potential non-productive energy wasting photochemical processes. Upon light absorption, a molecule can undergo several unproductive relaxation processes, resulting in a lower quantum yield value. For example, a back-electron transfer (BET) from the ion pair **III** (Scheme 4.16) would unproductively restore the ground-state EDA complex **II**.



Scheme 4.16 Role of the photochemical activity of EDA complex **II**. Path A: initiation of a radical chain. Path B: generation of intermediate **XI** which directly leads to the product formation.

The quantum yield of the photoreaction between 2,4-dinitrobenzyl bromide **2a** and 3-methylindole **1a** at 450 nm ($\Phi_{\text{reac}}(450 \text{ nm})$) was measured following the procedure detailed in Section 4.6.1. The experiment was conducted twice providing similar quantum yield values of **0.2** and **0.3**.

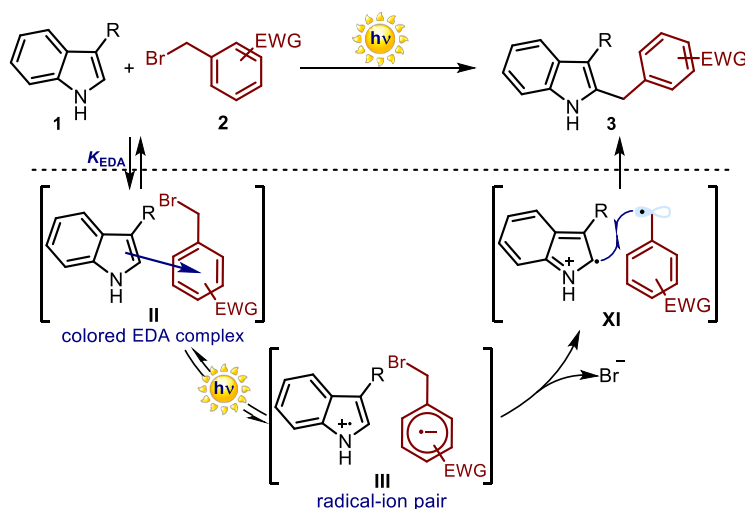
As previously mentioned, quantum yield values lower than one are mechanistically not conclusive because they can be caused by either the absence of a radical chain or by an initiation step with a low efficiency.

4.4.7 Proposed mechanisms

The studies described in this chapter point towards the formation of an EDA complex between indole **1** and the electron-poor alkyl halide **2**. Furthermore, the alkylation product **3** has only been observed upon visible light irradiation with wavelengths at which the EDA complex **II** is the only photoactive species (Scheme 4.8b). The inhibition of the reactivity in the presence of radical scavengers suggests the formation of radical intermediates during the course of the reaction. Consequently, we envision that this

photochemical alkylation of indoles starts upon excitation of the complex **II** and formation of the radical-ion pair **III**. Subsequently, two different mechanisms can be proposed for the product formation: a direct radical-radical coupling (Scheme 4.17) and a radical chain propagation (Scheme 4.18).

The quantum yield calculations suggests that a mechanism lacking a chain propagation pathway could be operative (Scheme 4.17). Accordingly, it can be foreseen that the radical anion, generated from the acceptor **2**, can trigger a carbon-bromine bond cleavage fast enough to compete with the back-electron transfer, which would regenerate the starting ground-state complex **II**. A radical-radical coupling in the solvent cage between the resulting carbon-centered radical and the positively charged radical intermediate within **XI**, followed by rearomatization, would generate the final product **3**.

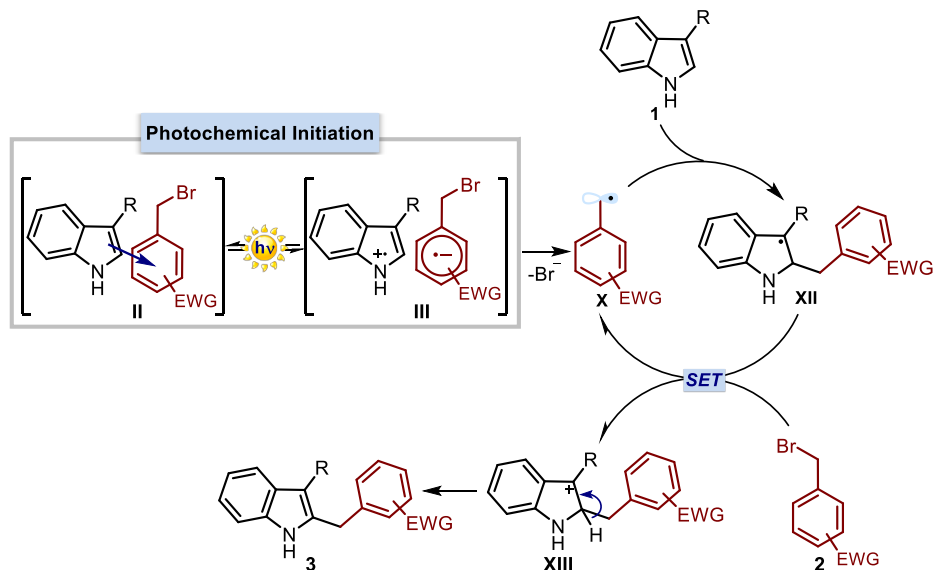


Scheme 4.17 Proposed mechanism for the EDA-mediated photochemical alkylation of indoles based on a radical-radical coupling.

However, the numerous reports of $S_{RN}1$ radical chain reactions described with the electron-deficient alkyl bromides **2** used in this study,²⁹ suggest that the photoexcitation of EDA complex **II** might be the initiation step of a short-lived chain propagation pathway (Scheme 4.18). Consequently, out-of-cage diffusion of carbon-centered radical **X**, generated upon mesolysis of the carbon-bromine bond within the radical anion, would

²⁹ a) Kornblum, N. "Substitution reactions which proceed *via* radical anion intermediates" *Angew. Chem. Int. Ed.* **1975**, *14*, 734. b) Rossi, R. A., Pierini, A. B., Peñéñory, A. B. *Chem. Rev.* **2003**, *103*, 71.

start a $S_{RN}1$ -type mechanism.³⁰ Trapping of the electrophilic radical by indole **1** would generate intermediate **XII** that can propagate the radical chain *via* single-electron transfer to the alkyl halide **2**. The oxidation of **XII** would generate a positively charged species **XIII**, which quickly aromatizes to afford the final product **3**.



Scheme 4.18 $S_{RN}1$ -type mechanism for the EDA-mediated photochemical alkylation of indoles.

4.5 Conclusions and remarks

We have described a methodology for the alkylation of indoles driven by the photochemical activity of a transiently generated EDA complex. The development of this transformation shows that the applications of EDA complex excitation within chemical synthesis can be broadened. A special emphasis has been placed on the characterization of the reaction intermediate: the isolation of a crystal structure of **IIa** provided direct evidence of the formation of the complex.

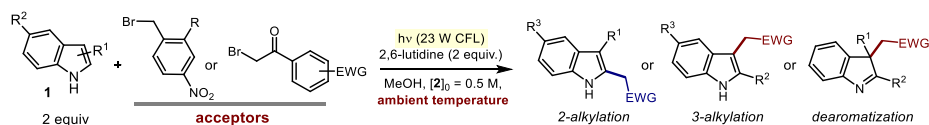
Furthermore, during this project, I performed quantum yield measurements, a valuable tool for the mechanistic elucidation of photochemical reactions. The knowledge accumulated during these studies was functional to the development of the research endeavors discussed in the following chapters.

³⁰ For an example of an EDA complex-initiated $S_{RN}1$ radical chain reaction, see: Fox, M. A.; Younathan, J.; Fryxell, G. E. "Photoinitiation of the $S_{RN}1$ reaction by excitation of charge-transfer complexes" *J. Org. Chem.* **1983**, *48*, 3109. Depicted in Scheme 2.10 in Chapter II.

4.6 Experimental section

The general procedure for the photochemical alkylation of substituted 1*H*-indoles is detailed herein. However, the details for the synthesis of the starting materials and the full characterization of products are not provided, since these studies were performed by Sandeep R. Kandukuri and Indranil Chatterjee. Please refer to the supporting information of the published manuscript for further details.¹

General Procedure for the Photochemical Alkylation of Substituted-1*H*-Indoles:



A 10 mL Schlenk tube was charged with the appropriate substituted 1*H*-indole **1** (0.2 mmol), methanol (0.2 mL, 0.5 M referring to **2**), the alkyl bromide **2** (0.1 mmol, 1 equiv.) and 2,6-lutidine (0.2 mmol, 2 equiv.). The reaction mixture was degassed via freeze pump thaw (x 3 cycles), and the vessel refilled with nitrogen. After the reaction mixture was thoroughly degassed, the vial was sealed and positioned approximately 5 cm away from a household full spectrum 23 W compact fluorescent light (CFL). For specific entries (as detailed in Section 4.3.2), three commercially available 15 W black light CFL bulb ($\lambda_{\text{max}} = 360$ nm) were used to illuminate the reaction vessel, since they provided slightly better yield (about 10% higher) than the use of 23 W CFL bulbs. After stirring for the indicated time, the solvent was removed under reduced pressure and the crude mixture charged on a flash column and purified by chromatography on silica gel to afford the title compound **3**, **15**, **16** and **17** in the stated yield. Results represent the average of two runs per substrate.

4.6.1 Quantum yield measurements

The quantum yield for the reaction between 2,4-dinitrobenzyl bromide **2a** and 3-methylindole **1a** was measured. A ferrioxalate solution was used as the actinometer; it was prepared by following the Hammond variation of the Hatchard and Parker procedure outlined in *Handbook of Photochemistry*.³¹ The ferrioxalate actinometer solution measures the decomposition of ferric ions to ferrous ions, which are complexed by 1,10-phenanthroline and monitored by UV/Vis absorbance at 510 nm.

An actinometer is a chemical system whose quantum yield is known. It is used to calculate the incident photons per unit of time (photon flux, $q_{\text{n,p}}^0$) that the reaction under study is irradiated with. The experiment is conducted in a way to assure that the incident light on

³¹ Murov, S. L. "Handbook of Photochemistry" 1973 Marcel Dekker.

the actinometer solution and on the reaction under study is equal. Accordingly, the reactions were placed next to each other at approximately 4 cm from the light source, and were irradiated simultaneously with a 300 W xenon lamp equipped with a 450 ± 5 nm band-pass filter (Figure 4.8). To ensure that both reactions were exposed to an identical surface of irradiation from the light beam, solutions with the same volume, in identical quartz cuvettes, and unstirred were used for the measurements. Furthermore, homogeneous solutions are needed to avoid any light scattering.



Figure 4.8 Picture of the set-up used for the quantum yield measurements.

Equations used for the quantum yield calculation

The quantum yield of the actinometer solution is a known parameter that relates the photons absorbed by this system with the molecules generated. A measurement of the product formation provides the absorbed photons by the actinometer in a certain period of time (see Equation 4.5, rearranged Equation 4.4).

$$\text{absorbed photons}_{acti}/dt = \frac{\text{molecules generated}_{acti}/dt}{\Phi_{acti}(\lambda)} \quad (\text{Eq. 4.5})$$

However, for our measurements, the total received incident photons are required. Therefore, the light absorbed by the actinometer solution must be related to incident photons. Equations 4.6 shows the relation between these parameters.

$$\text{absorbed photons} = \text{incident photons} \cdot \frac{\text{absorbed photons}}{\text{incident photons}} \quad (\text{Eq. 4.6})$$

The ratio between the absorbed and the incident photons can be calculated using Equation 4.7, where T is the transmittance of the solution. Although the transmittance can be directly measured with a spectrophotometer, the absorbance (A), derived from the Lambert-Beer law, is the most commonly used parameter to measure the ratio of the light intensity transmitted after interaction with the solution (I) with respect to intensity received (I_0 , Equation 4.8).

$$\text{absorbed photons} = \text{incident photons} \cdot (1 - T) \quad (\text{Eq. 4.7})$$

$$T = \frac{I}{I_0} = 10^{-A} \quad (\text{Eq. 4.8})$$

Equation 4.9 can thus be derived from Equations 4.7 and 4.8.

$$\text{absorbed photons}/dt = \text{incident photons}/dt \cdot \left(1 - 10^{-A(\lambda)}\right) \quad (\text{Eq. 4.9})$$

A combination of Equations 4.5 and 4.9 gives Equation 4.10 where: $\Phi_{\text{acti}}(\lambda)$ is the quantum yield of the actinometer (a known parameter), $A_{\text{acti}}(\lambda)$ is the absorbance of the actinometer reaction at the wavelength utilized to measure the quantum yield, and $q_{n,p}^0$ is the photon flux. Equation 4.10 was employed for the calculation of the photon flux of the experiment.³²

$$\text{incident photons}/dt = q_{n,p}^0 = \frac{\text{molecules generated}_{\text{acti}}/dt}{\Phi_{\text{acti}}(\lambda) \cdot (1 - 10^{-A_{\text{acti}}(\lambda)})} \quad (\text{Eq. 4.10})$$

Following calculation of the photon flux, Equation 4.11 - derived by the rearrangement of Equation 4.10 - can be used to calculate the quantum yield of the reaction under study ($\Phi_{\text{reac}}(\lambda)$). $A_{\text{reac}}(\lambda)$ is the absorbance of the reaction under study, at the wavelength used to carry out the experiments.

$$\Phi_{\text{reac}}(\lambda) = \frac{\text{molecules generated}_{\text{reac}}/dt}{q_{n,p}^0 \cdot (1 - 10^{-A_{\text{reac}}(\lambda)})} \quad (\text{Eq. 4.11})$$

³² a) Braslavsky, S. E. "Glossary of terms used in photochemistry, (IUPAC Recommendations 2006)" *Pure and App. Chem.* **2007**, 79, 293. b) Sun, L.; Bolton, J. R. "Determination of the quantum yield for the photochemical generation of hydroxyl radicals in TiO₂ suspensions" *J. Phys. Chem.* **1996**, 100, 4127.

Solutions used for the measurements of the quantum yield

The solutions were prepared and stored in a dark laboratory (red light):

1. Potassium ferrioxalate solution: 589.5 mg of potassium ferrioxalate (commercially available from Alfa Aesar) and 278 μL of sulfuric acid (96%) added to a 100 mL volumetric flask and diluted to a total volume of 100 mL with water (HPLC grade).
2. Phenantroline solution: 0.2% by weight of 1,10-phenanthroline in water (200 mg in 100 mL of water).
3. Buffer solution: 4.104 g of NaOAc and 1.0 mL of sulfuric acid (96%) were added to a 100 mL volumetric flask and diluted to a total volume of 100 mL with water (HPLC grade).
4. Model reaction solution: 650 mg of 2,4-dinitrobenzyl bromide **2a** (0.5 mmol), 650 mg of 3-methylindole **1a** (1 mmol, 2 equiv.) and 600 μL of 2,6-lutidine (1 mmol, 2 equiv.) were added to a 5.0 mL volumetric flask and diluted to a total volume of 5.0 mL with methanol (HPLC grade).

Procedure for the sample irradiation:

1 mL of the actinometer solution was added to a quartz cuvette ($l = 1$ cm). The cuvette was placed 4 cm away from the lamp along with a sample solution (1 mL in a similar cuvette) whose quantum yield has to be measured (our model reaction). The sample and actinometer solutions were irradiated with 300 W xenon lamp (50% of light intensity, 450 ± 5 nm band-pass filter high transmittance) for specified time intervals (10.0, 12.5, 15.0, 17.5) min (Figure 4.8).

Photon flux calculation:

The photon flux was determined according to Equation 4.10. After irradiation, the actinometer solution was removed and placed in a 10 mL volumetric flask containing 0.5 mL of 1,10-phenanthroline solution and 2 mL of buffer solution. This flask was filled to the mark with water (HPLC grade). The UV-Vis spectra of the complexed actinometer samples were recorded for each time interval. The absorbance of the complexed actinometer solution was monitored at 510 nm. The moles of Fe^{2+} formed for each time interval are determined according to Beer's Law (Eq. 4.12):

$$\text{moles } \text{Fe}^{+2} = \frac{V_1 \cdot V_3 \cdot \Delta A (510 \text{ nm})}{10^3 \cdot V_2 \cdot l \cdot \epsilon (510 \text{ nm})} \quad (\text{Eq. 4.12})$$

where V_1 is the irradiated volume (1 mL), V_2 is the aliquot of the irradiated solution taken for the determination of the ferrous ions (1 mL), V_3 is the final volume after complexation

with phenanthroline (10 mL), l is the optical path-length of the irradiation cell (1 cm), $\Delta A(510 \text{ nm})$ the optical difference in absorbance between the irradiated solution and the one stored in the dark, $\varepsilon(510 \text{ nm})$ is that of the complex $\text{Fe}(\text{phen})_3^{2+}$ ($11100 \text{ L mol}^{-1} \text{ cm}^{-1}$). The moles of Fe^{2+} formed are plotted as a function of time to obtain the numerator of Equation 4.10 as the slope of this line.

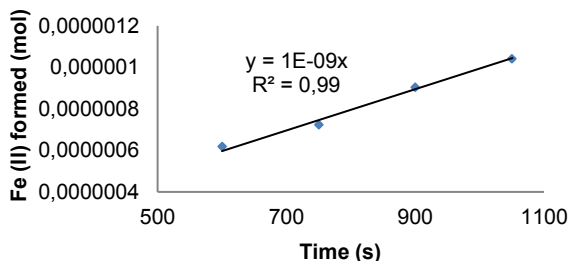


Figure 4.9 Relation between the moles of Fe (II) formed and the reaction time for the potassium ferrioxalate actinometer reaction.

Finally, the denominator of Equation 4.10 can be calculated from the quantum yield for the actinometer at 450 nm ($\Phi_{\text{acti}}(450 \text{ nm}) = 0.9$)³³ and $A_{\text{acti}}(450)$. The absorbance was measured using a Shimadzu 2401PC UV-Vis spectrophotometer in 1 mm path quartz cuvettes in the presence of the same bandpass filter of 450 nm used to perform the measurements. An absorbance of 0.15 was obtained. And therefore, the photon flux ($q_{\text{n,p}}^0$) was determined to be $4.74 \cdot 10^{-9} \text{ einstein s}^{-1}$.

Quantum yield calculation:

The quantum yield of the reaction under study was determined according to Equation 4.11. The moles of products formed (reaction performed by irradiating the sample alongside with the actinometer solution) were determined by GC measurement (FID detector) using 2,4-dinitrotoluene as reference standard. The number of moles of product was plotted as a function of time to obtain the numerator of Equation 4.11.

³³ Hamai, S.; Hirayama, F. "Actinometric determination of absolute fluorescence quantum yields" *J. Phys. Chem.* **1983**, *87*, 83.

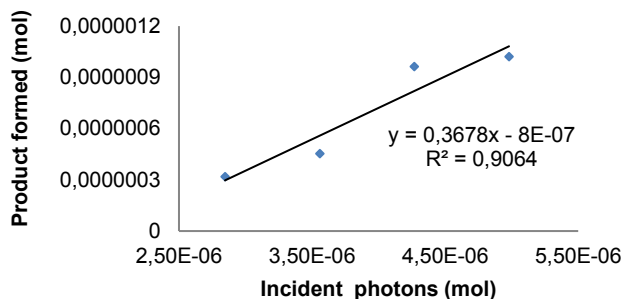


Figure 4.10 Relation between the moles of product formed and the moles of incident photons for the reaction between **1a** and **2a**.

The denominator of Equation 4.11 can be calculated from the previously obtained photon flux ($q_{n,p}^0$) and $A_{\text{reac}}(450)$. The absorbance was measured using a Shimadzu 2401PC UV-Vis spectrophotometer in 1 mm path quartz cuvettes in the presence of the bandpass filter of 450 nm.

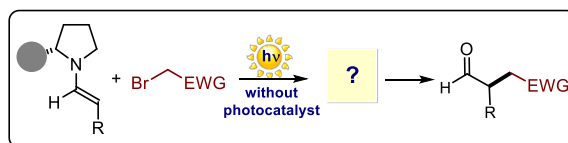
Finally, the quantum yield of the reaction between 2,4-dinitrobenzyl bromide **2a** and 3-methylindole **1a** at 450 nm was calculated ($\Phi_{\text{reac}}(450 \text{ nm})$). A value of **0.2** was obtained and a similar value of **0.3** was obtained when the experiment was repeated a second time. For the second experiment, 100% power of the xenon lamp was used, double power than in the first experiment. The photon flux measured ($9.43 \cdot 10^{-9} \text{ einstein s}^{-1}$) by the actinometer solution was consistent with the higher power employed. This indicates that the actinometer solution was not saturated with the amount of light because it proceeded faster when a higher irradiance was used. Furthermore, the quantum yield obtained was in line with the previous measurement, which indicates that the reaction under study was also not saturated with the amount of light. As a result, these experiments suggest that both reactions were light-limited under these conditions. It is important that the experiments are conducted under light-limiting conditions, not under saturation of light, for both reactions as this ensures that the product formation is directly related to the number of photons irradiated by the xenon lamp. As a result, the number of photons absorbed by the actinometer and by the reaction under study can be accurately correlated to the photon flux. Alternatively, if the experiment was conducted under light saturation conditions, the reactions would provide similar yields after being irradiated for the same time with different photon fluxes.

Chapter V

Studies on the enantioselective α -alkylation of aldehydes driven by the photochemical activity of enamines

Target

A mechanistic study of the α -alkylation of aldehydes driven by the direct excitation of enamines or by the photo-activity of transiently generated enamine-based EDA complexes.



Tools

Photophysical techniques, NMR spectroscopy, kinetic studies and quantum yield measurements.¹

5.1 Introduction

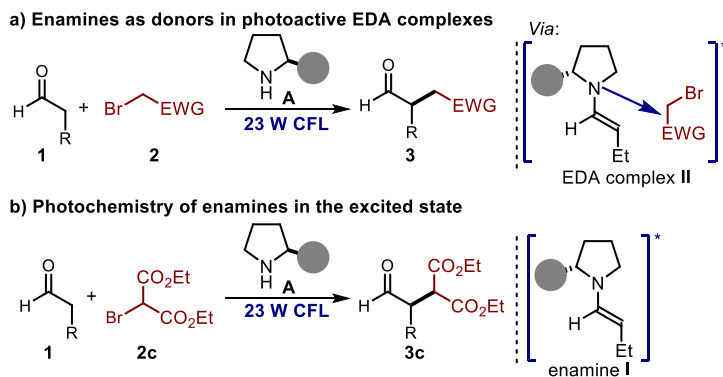
Studies developed in our group demonstrated that the photochemical properties of enamines can be employed to promote the α -alkylation of aldehydes with some electron-poor alkyl halides.² We revealed that enamines, generated upon condensation of a diarylprolinol silyl ether catalyst (**A**)³ with an aldehyde, can actively participate in the photoexcitation of substrates and trigger the formation of reactive open-shell species from organic halides. At the same time, ground-state chiral enamines can provide effective stereochemical control over the enantioselective radical trapping process. This strategy, where stereoinduction and photoactivation merges in a sole chiral organocatalyst, enables light-driven enantioselective transformations that cannot be realized using the thermal reactivity of enamines. Specifically, we used this approach to develop the α -alkylation of

¹ The work discussed in this chapter has been published, see: Bahamonde, A.; Melchiorre, P. "Mechanism of the stereoselective α -alkylation of aldehydes driven by the photochemical activity of enamines" *J. Am. Chem. Soc.* **2016**, *138*, 8019.

² a) Arceo, E.; Jurberg, I. D.; Álvarez-Fernández, A.; Melchiorre, P. "Photochemical activity of a key donor-acceptor complex can drive stereoselective catalytic α -alkylation of aldehydes" *Nat. Chem.* **2013**, *5*, 750. b) Silvi, M.; Arceo E.; Jurberg, I. D.; Cassani, C.; Melchiorre, P. "Enantioselective organocatalytic alkylation of aldehydes and enals driven by the direct photoexcitation of enamines" *J. Am. Chem. Soc.* **2015**, *137*, 6120.

³ Donslund, B. S.; Johansen, T. K.; Poulsen, P. H.; Halskov, K. S.; Jørgensen, K. A. "The diarylprolinol silyl ethers: ten years after" *Angew. Chem. Int. Ed.* **2015**, *54*, 13860.

aldehydes **1**⁴ with electron-deficient benzyl and phenacyl bromides **2** (Scheme 5.1a)^{2a} and bromomalonate derivatives **2c** (Scheme 5.1b).^{2b} The reactions were conducted at ambient temperature using household compact fluorescence light (CFL) bulbs as the light source.



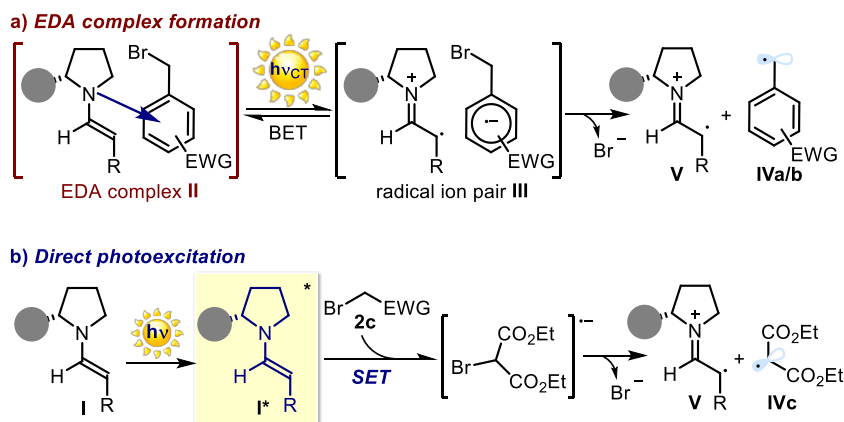
Scheme 5.1 Enamine-mediated photochemical enantioselective α -alkylation of aldehydes *via* a) formation of EDA complex **II** or b) the direct photoexcitation of enamine **I**. The filled grey circle represents a bulky substituent on the chiral amine catalyst; CFL: compact fluorescence light; EWG: electron-withdrawing group.

At first glance, both processes depicted in Scheme 5.1 may seem to be classical substitution reactions of enamines proceeding through a S_N2 manifold. However, no product formation is observed when the reactions are performed in the absence of light irradiation. Crucial for reactivity was the ability of enamines to trigger the photochemical formation of radicals (**IV**) from the alkyl halides **2** under mild conditions (Scheme 5.2). Despite the superficial similarities between the two chemical transformations, they profoundly diverge in the radical generation mechanism. The first strategy (Scheme 5.2a) relied on the formation of photon-absorbing electron donor-acceptor (EDA) complexes,⁵ where the electron-rich enamine **I** acts as donor and the electron-deficient benzyl and phenacyl bromides plays the role of acceptor. Visible light irradiation of the charge-transfer (CT) band of the colored EDA complex **II** induces a single-electron transfer

⁴ Prior to our studies, similar enamine-mediated enantioselective alkylations of aldehydes were realized using an external photoredox catalyst, which served to generate the radical species from alkyl halides, see: a) Nicewicz, D. A.; MacMillan, D. W. C. "Merging photoredox catalysis with organocatalysis: the direct asymmetric alkylation of aldehydes" *Science* **2008**, 322, 77. b) Shih, H.-W.; Vander Wal, M. N.; Grange, R. L.; MacMillan, D. W. C. "Enantioselective α -benzylation of aldehydes *via* photoredox organocatalysis" *J. Am. Chem. Soc.* **2010**, 132, 13600.

⁵ a) Mulliken, R. S. "Molecular compounds and their spectra. II" *J. Am. Chem. Soc.* **1952**, 74, 811. b) Foster, R. "Electron donor-acceptor complexes" *J. Phys. Chem.* **1980**, 84, 2141. c) Rosokha, S. V.; Kochi, J. K. "Fresh look at electron-transfer mechanisms *via* the donor/acceptor bindings in the critical encounter complex" *Acc. Chem. Res.* **2008**, 41, 641.

(SET), allowing access to the reactive open-shell intermediates. In the second approach (Scheme 5.2b), we used the capability of the chiral enamine **I** to directly reach an electronically excited state (**I***), upon light absorption, and then to act as effective photo-reductant. Upon SET, the reductive cleavage of the bromomalonate **2c** induces the formation of the carbon-centered radical (**IVc**).



Scheme 5.2 Radical generation strategy based on the formation of a) EDA complex **II** or b) the direct photoexcitation of the chiral enamine **I**. The filled grey circle represents a bulky substituent on the chiral amine catalyst.

5.2 Target of the project

Our aim was to study the mechanistic analogies and differences of these enamine-mediated photochemical enantioselective alkylations of aldehydes with electron-poor alkyl halides. A combination of photophysical investigations, nuclear magnetic resonance (NMR) spectroscopy, kinetic studies, and quantum yield measurements were used for achieving these goals.

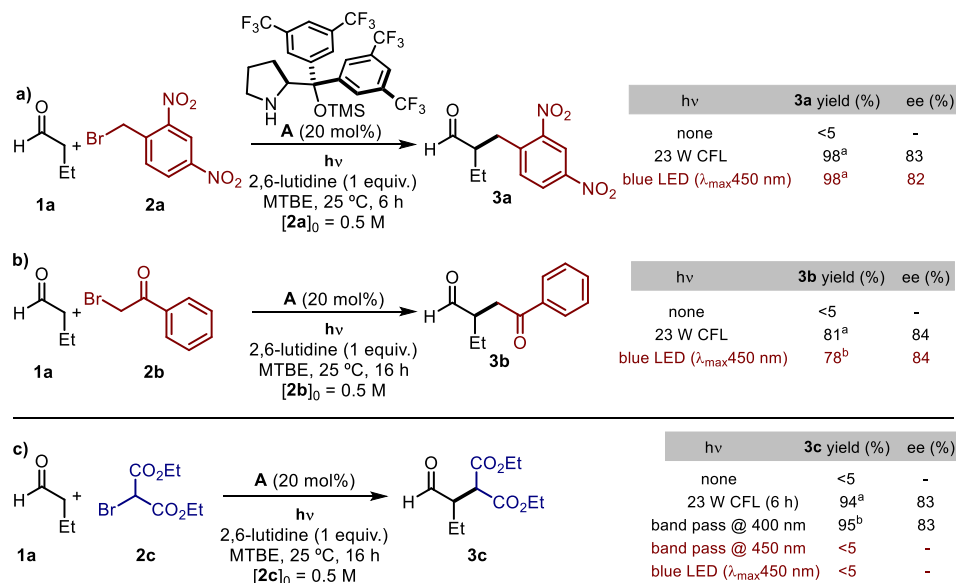
5.3 Results and discussion

Our recent studies² established that enamines **I** can interact with visible light in two different ways, serving either as donors in photoactive EDA complex formation (Scheme 5.2a) or as photo-reductants upon direct excitation (Scheme 5.2b). As the prototypical reactions for mechanistic analysis, we selected the alkylations of butanal (**1a**) with 2,4-dinitrobenzyl bromide (**2a**, Scheme 5.3a), phenacyl bromide (**2b**, Scheme 5.3b), and diethyl bromomalonate (**2c**, Scheme 5.3c),⁶ all promoted by the commercially available

⁶ The reactions required the presence of 1 equiv. of a base (2,6-lutidine and NaOAc giving similar results) to perform well. Removing the base additive, trace amounts of the alkylation products **3** were formed (<15%), while reagent decomposition along with acidification of the reaction medium

diarylprolinol silyl ether catalyst **A** (20 mol%).³ The reactions with **2a** and **2b** are representative of the EDA complex activation strategy,^{2a} while the chemistry in Scheme 5.3c is triggered by the direct photoexcitation of the enamine **I**.^{2b}

These alkylation reactions shared the intermediacy of radical species, as they were quenched in the presence of radical scavengers such as TEMPO. Furthermore, the alkylation product **3** was only detected when the reactions were conducted under light irradiation.



Scheme 5.3 The model photochemical alkylations of butanal **1a** catalyzed by the chiral secondary amine **A** employing: a) 2,4-dinitrobenzyl bromide **2a**, b) phenacyl bromide **2b** and c) diethyl bromomalonate **2c** as alkylating agents. MTBE: methyl *tert*-butyl ether.

^a Yield of the isolated products **3**. ^b Yield of **3** determined by ¹H NMR spectroscopic analysis of the crude reaction mixture using 1,1,2-trichloroethene as the internal standard.

Along with these similarities, the light-triggered reactions in Scheme 5.3 showed striking differences too. The reactivity of the three processes remained unaltered when the experiments were conducted under illumination by a 300 W xenon lamp equipped with a cut-off filter at 385 nm and a band-pass filter at 400 nm (irradiation at λ ≥ 385 nm and λ = 400 nm, respectively). However, only the EDA-mediated reactions (Scheme 5.3a and b) could be triggered by irradiation with a blue LED (λ_{max} at 450 nm). In sharp contrast,

was observed. The likely role of 2,6-lutidine is to quench the acid generated during the process, as testified to by the formation of the insoluble lutidinium bromide salt generated during the reaction. The presence of 2,6-lutidine does not contribute to the absorption in the visible region to any extent.

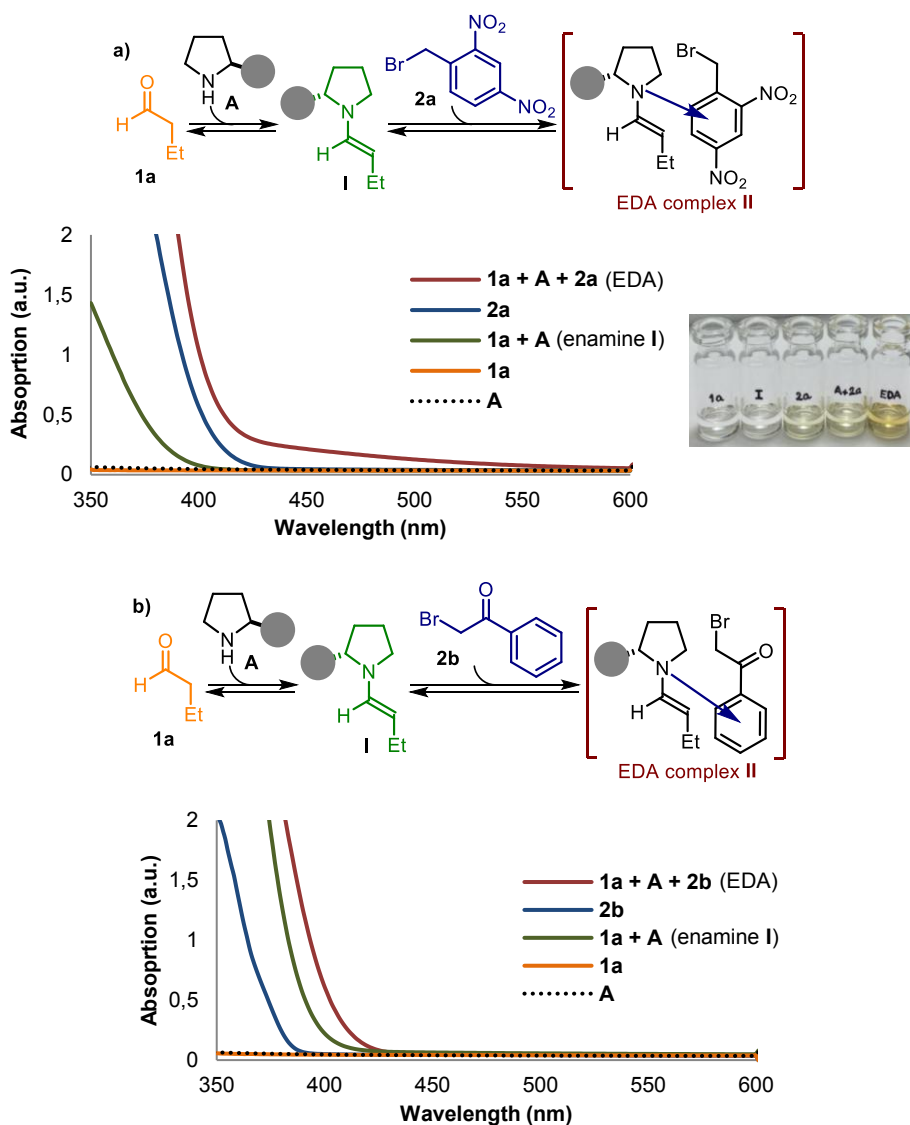
no product formation was observed for the alkylation reaction with bromomalonate **2c** when the mixture was irradiated with wavelengths higher than 400 nm (Scheme 5.3c). As a result, we decided to conduct spectroscopic investigations to rationalize the different light-wavelength/reactivity correlation profiles while elucidating the origins of the photochemical activity of the enamine.

5.3.1 Spectroscopic studies

Immediately after mixing an MTBE solution of the enamine, generated *in situ* upon condensation of butanal **1a** (3 equiv.) with 20 mol% of catalyst **A**, with either 2,4-dinitrobenzyl bromide **2a** or phenacyl bromide **2b** (1 equiv.), we observed that the achromatic solution turned to a marked yellow color (Scheme 5.4a). The color change was further confirmed by measuring the optical absorption spectra of these mixtures. As depicted in Scheme 5.4, the spectra recorded from solutions containing **1a**, **A**, and either **2a** or **2b** showed a bathochromic displacement in the visible spectral region where none of the substrates absorbs (red lines). The new absorption bands, which in the case of **2a** reaches the green region of the visible range (550 nm), cannot be accounted for by the addition of the absorption of the separate compounds, which can barely absorb visible light. This observation is in line with the formation of an EDA complex **II**. As enamines are electron-rich species with low ionization potential,⁷ **I** would act as donor in these molecular aggregations and the acceptor would be the electron-deficient 2,4-dinitrobenzyl bromide **2a** ($E_p^{\text{red}} = -0.66$ V vs. Ag/Ag⁺ in CH₃CN, see Scheme 5.52) and phenacyl bromide **2b** ($E_p^{\text{red}} = -1.35$ V vs. Ag/Ag⁺ in CH₃CN, see Scheme 5.53).⁸

⁷ Enamines have a low ionization potential; for example 1-(but-1-enyl)pyrrolidine has an IP of 7.2 eV, see: Müller, K.; Previdoli, F.; Desilvestro, H. "Enamines. II. A theoretical and photoelectron spectroscopic study of the molecular and electronic structures of aliphatic enamines" *Helv. Chim. Acta* **1981**, *64*, 2497.

⁸ The electron-donor property of a donor molecule is indicated by the magnitude of its ionization potential (*IP* in the gas phase) or its oxidation potential (E_p^{ox} in solution). Conversely, the viability of a compound as an acceptor is indicated by the magnitude of its electron affinity (*EA* in the gas phase) or its reduction potential (E_p^{red} in solution). E_p^{ox} and E_p^{red} , which can be estimated by cyclic voltammetry measurements, can help in predicting the suitability of a given substrate to undergo EDA complex formation.



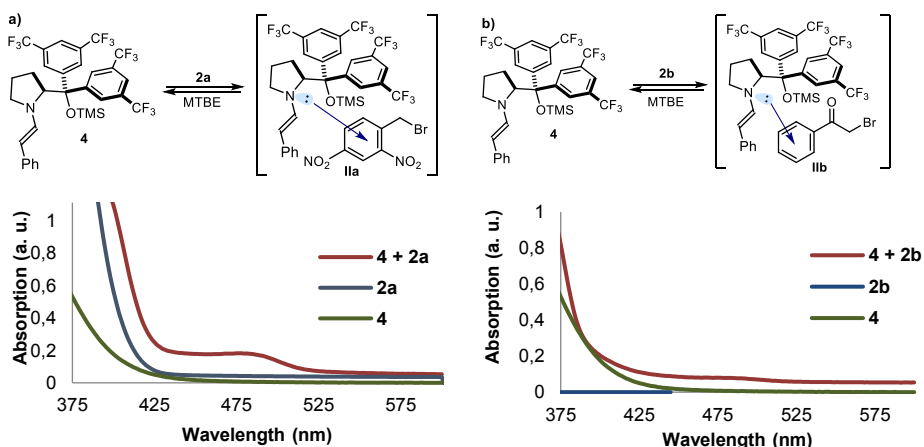
Scheme 5.4 Optical absorption spectra, recorded in MTBE in 1 mm path quartz cuvettes using a Shimadzu 2401PC UV-visible spectrophotometer, and visual appearance of the separate reaction components and of the colored EDA complex with: a) 2,4-dinitrobenzyl bromide **2a**; [**1a**] = 1.5 M; [**2a**] = 0.5 M; [**A**] = 0.1 M. and b) phenacyl bromide **2b**; [**1a**] = 1.5 M; [**2b**] = 0.5 M; [**A**] = 0.1 M. The filled grey circle represents a bulky substituent on the chiral amine catalyst.

To further examine the implication of the enamine in the formation of photoactive EDA complexes, we synthesized the enamine **4**, derived from the condensation of catalyst **A**

with 2-phenylacetaldehyde, according to the literature.^{2b} 2-Phenylacetaldehyde is a competent substrate of the photo-organocatalytic reaction with **2a**, **2b**, and **2c** which provides full conversion into the corresponding α -alkylation products under the conditions set out in Scheme 5.3. However, a low level of enantioselectivity was observed (below 30% ee), a consequence of the lability of the resulting benzylic stereocenter.

Absorption spectra of EDA complexes with preformed enamine **4**

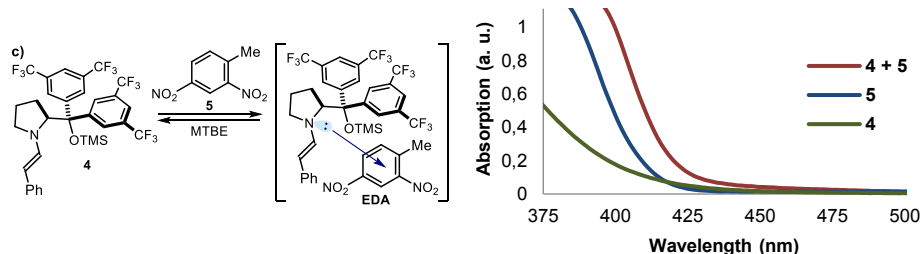
Initially, we confirmed that the preformed enamine **4** could form EDA complexes with 2,4-dinitrobenzyl bromide **2a** and phenacyl bromide **2b** as acceptors (Scheme 5.5). Accordingly, a solution containing the enamine **4** was prepared by diluting 1 mL of a 0.4 M solution of **4** in MTBE into 10 mL, affording a 0.04 M solution of **4** in MTBE. Subsequently, aliquots of this solution were utilized for the preparation of the samples containing **4** and the acceptors. The absorption spectra of the resulting mixtures showed the formation of new absorption bands diagnostic of EDA complex formation (red lines in Scheme 5.5).



Scheme 5.5 Optical absorption spectra, recorded in MTBE in 1 mm path quartz cuvettes using a Shimadzu 2401PC UV-visible spectrophotometer of the mixtures of enamine **4** with: a) 2,4-dinitrobenzyl bromide **2a** and b) phenacyl bromide **2b** showing the formation of EDA complexes (red lines); [**4**] = 0.04 M; [**2a**] = [**2b**] = 0.5 M.

Furthermore, 2,4-dinitrotoluene (**5**), analogous to **2a** but lacking the presence of a suitable leaving group, was tested as substrate for the formation of an EDA with **4** (Scheme 5.6). The absorption spectra of the mixture of **4** and **5** showed the appearance of new absorption bands, characteristic of the formation of an EDA complex (red line). It should be noted that the irradiation of this mixture does not lead to any product formation as there is no leaving groups that can promote any reactivity. In consequence, upon light illumination,

this aggregation just leads to a fast back-electron transfer that regenerates the ground-state complex.

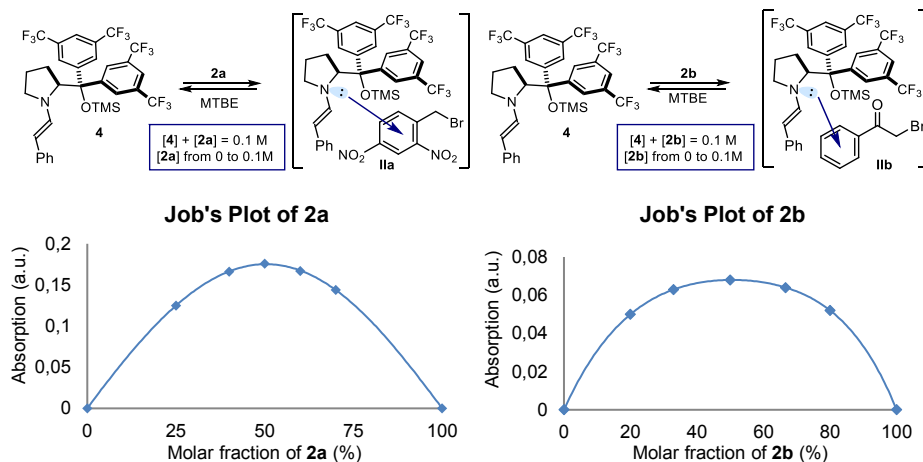


Scheme 5.6 Optical absorption spectra, recorded in MTBE in 1 mm path quartz cuvettes using a Shimadzu 2401PC UV-visible spectrophotometer of the mixtures of enamine **4** with 2,4-dinitrotoluene **5** showing the formation of an EDA complex (red line); $[4] = 0.04 \text{ M}$; $[5] = 0.5 \text{ M}$.

Stoichiometry of the EDA complex in solution

A Job's plot was constructed to evaluate the stoichiometry of the EDA complex⁹ between 2,4-dinitrobenzyl bromide **2a** and the preformed enamine **4** (Scheme 5.7). We measured the absorption at 470 nm of MTBE solutions with different donor/acceptor ratios but constant concentration (0.1 M) of the two components. All the absorption spectra were recorded in 1 mm path quartz cuvettes using a Shimadzu 2401PC UV-visible spectrophotometer. The absorbance values are plotted against the molar fraction (%) of 2,4-dinitrobenzyl bromide. The maximum absorbance is obtained with a 1:1 mixture, indicating that this is the stoichiometry of the EDA complex in solution. The same procedure was repeated to evaluate the stoichiometry in solution of the EDA complex between enamine **4** and phenacyl bromide **2b**, obtaining identical results.

⁹ Job, P. "Formation and stability of inorganic complexes in solution" *Ann. Chem.* **1928**, *9*, 113.

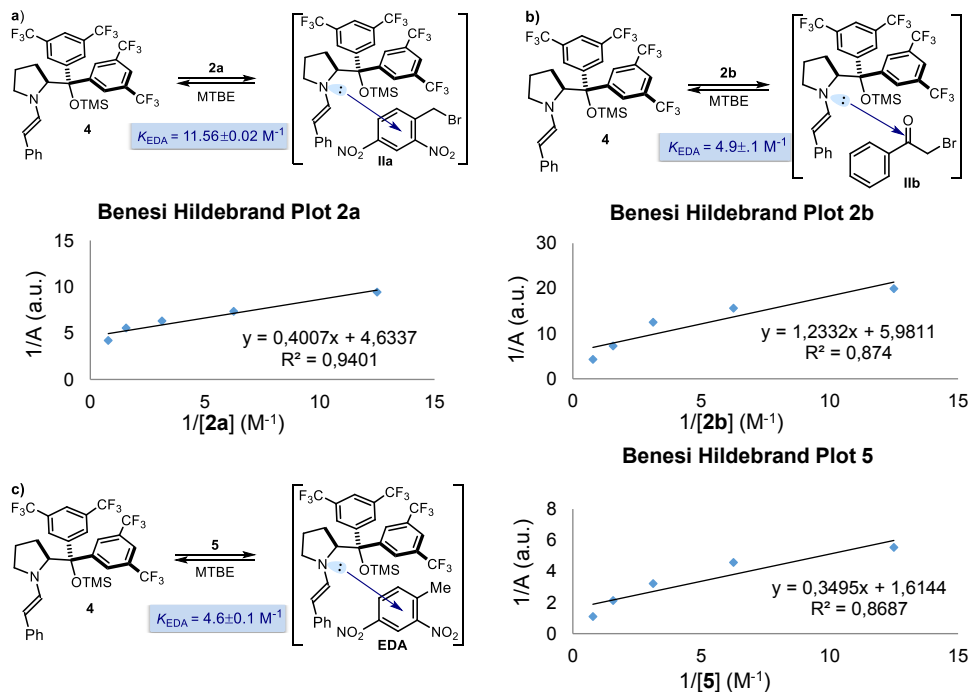


Scheme 5.7 Job's plot of the EDA complex **IIa** and **IIb** in MTBE.

Determination of the Association Constant (K_{EDA})

The association constant of the EDA complex formed between 2,4-dinitrobenzyl bromide **2a** and enamine **4** was determined spectrophotometrically in MTBE, employing the Benesi-Hildebrand methodology (Scheme 5.8).¹⁰ We measured the absorption at 470 nm of solutions with constant concentration of the enamine **4** (0.04 M) but increased donor/acceptor ratio, adding an excess of the benzyl bromide **2a**. All the absorption spectra were recorded in 1 mm path quartz cuvettes using a Shimadzu 2401PC UV-visible spectrophotometer. According to the methodology, a straight line is obtained when the reciprocal of the absorbance (A) is plotted against the reciprocal of the concentration of the partner in excess (see Equation 2.5 in Chapter II). The procedure was repeated to determine the association constants of the EDA complexes formed by mixing the enamine **4** with the acceptors **2b** and **5**. The plots, obtained for the calculation of the association constants of **2a**, **2b**, and **5** with the preformed enamine **4**, are displayed below. The following association constants (K_{EDA}), calculated dividing the intercept by the slope, were determined: $11.56 \pm 0.02 \text{ M}^{-1}$ for the **2a/4** complex; $4.9 \pm 0.1 \text{ M}^{-1}$ for the **2b/4** complex; and $4.6 \pm 0.1 \text{ M}^{-1}$ for the **5/4** complex.

¹⁰ Benesi, H. A.; Hildebrand, J. H. "A spectrophotometric investigation of the interaction of iodine with aromatic hydrocarbons" *J. Am. Chem. Soc.* **1949**, *71*, 2703.



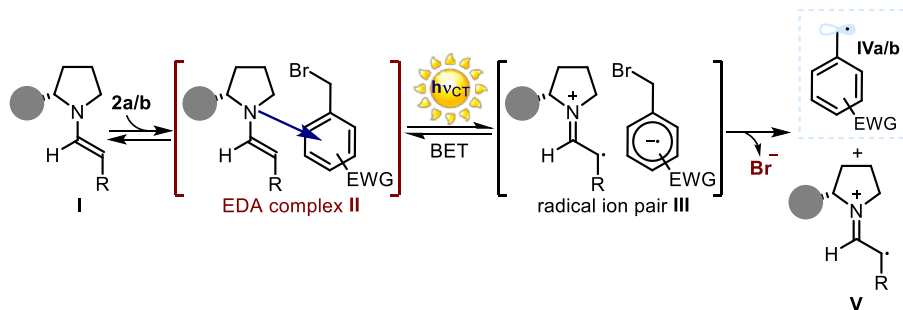
Scheme 5.8 Benesi-Hildebrand plots for the EDA complexes generated in MTBE upon association of the enamine **4** and a) 2,4-dinitrobenzyl bromide **2a**, b) phenacyl bromide **2b**, and c) 2,4-dinitrotoluene **5**.

The light-wavelength /reactivity correlation for the photochemical alkylations of butanal with **2a** and **2b** (Scheme 5.3a and Scheme 5.3b, respectively) can be rationalized on the basis of the photoactivity of the enamine-based EDA complexes **IIa** and **IIb** (which display similar absorption spectra, see Scheme 5.5, to the EDA absorption in Scheme 5.10). Irradiation of the CT band of the complex, which falls in the visible region, induces a SET from the donor enamine **I** to the acceptor alkyl bromide **2**, leading to the chiral ion-pair **III** (Scheme 5.9). Critical to reaction development is the presence of the bromide anion within the radical partner in **III**. The bromide, acting as a suitable leaving group, triggers an *irreversible* fragmentation event¹¹ rapid enough to compete with a possible back-electron transfer (BET), which would unproductively restore the ground-state EDA complex **II** instead.¹² This fragmentation productively renders two reactive

¹¹ Costentin, C.; Robert, M.; Savéant, J.-M. "Electron transfer and bond breaking: recent advances" *Chem. Physics* **2006**, *324*, 40.

¹² Although the photophysics of EDA complexes have been extensively studied (Refs 5b-c), their use in chemical synthesis has found limited applications. This is mainly because the unproductive, back-electron transfer (BET), which restores the ground-state EDA complex, is generally faster than other possible processes leading to products. For a pertinent discussion, see: Rathore, R.;

radical intermediates (the electrophilic carbon-centered radical **IV** and the α -iminyl radical cation **V**), which can initiate synthetically useful transformations, i.e. the alkylation of aldehydes. The enamine-based EDA complex activation strategy thus provides ready access to open-shell reactive species under mild conditions and without the need for any external photoredox catalyst.

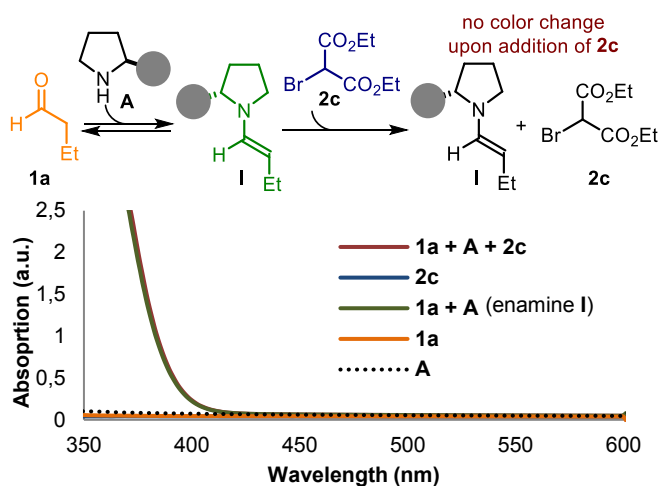


Scheme 5.9 Radical generation strategy based on the formation of EDA complex **II**. The filled grey circle represents a bulky substituent on the chiral amine catalyst.

Alternatively, the enantioselective photochemical alkylation of butanal **1a** with diethyl bromomalonate **2c** showed a profoundly different behavior. In addition to the distinct effect that the light frequency had on the reactivity (as discussed in Scheme 5.3), we did not observe any color change in the solution, which remained achromatic during the reaction progression. The absence of any photoabsorbing ground-state EDA complex was further confirmed by the optical absorption spectrum of the reaction mixture (red line in Scheme 5.10), which perfectly overlaid the absorption of the enamine, *in situ* generated upon condensation of the catalyst **A** with **1a** (green line in Scheme 5.10). In a separate experiment, we observed that the addition of a large excess of **2c** to a solution of enamines did not change the absorption.

The inhibition of reactivity observed upon irradiation with 450 nm is consistent with the lack of absorption in this spectral region (Scheme 5.10). The alkylation product **3c** is however formed upon irradiation at 400 nm. As shown in Scheme 5.10, enamine **I**, whose absorption band prolongs until 415 nm (green line), can be directly excited with this wavelength. This observation prompted us to evaluate the possibility that the direct photoexcitation of the enamine could trigger the photochemical transformation.

Kochi, J. K. "Donor/acceptor organizations and the electron-transfer paradigm for organic reactivity" *Advances Phys. Org. Chem.* **2000**, *35*, 193.



Scheme 5.10 Optical absorption spectra, recorded in MTBE in 1 mm path quartz cuvettes using a Shimadzu 2401PC UV-visible spectrophotometer of the separate reaction components and the reaction mixture with bromomalonate **2c**; [**1a**] = 1.5 M; [**2c**] = 0.5 M; [**A**] = 0.1 M. The filled grey circle represents a bulky substituent on the chiral amine catalyst.

The implication of the enamine within the photochemical regime was unambiguously established by Stern-Volmer quenching studies.^{2b} As detailed in Figure 5.1, the emission spectrum of the pre-formed enamine **4**, prepared by condensation of catalyst **A** and 2-phenylacetaldehyde, upon excitation at 365 nm, was recorded. The excited state of this enamine and its emission were effectively quenched by bromomalonate **2c** (the Stern-Volmer quenching experiments were conducted by Dr. Mattia Silvi).

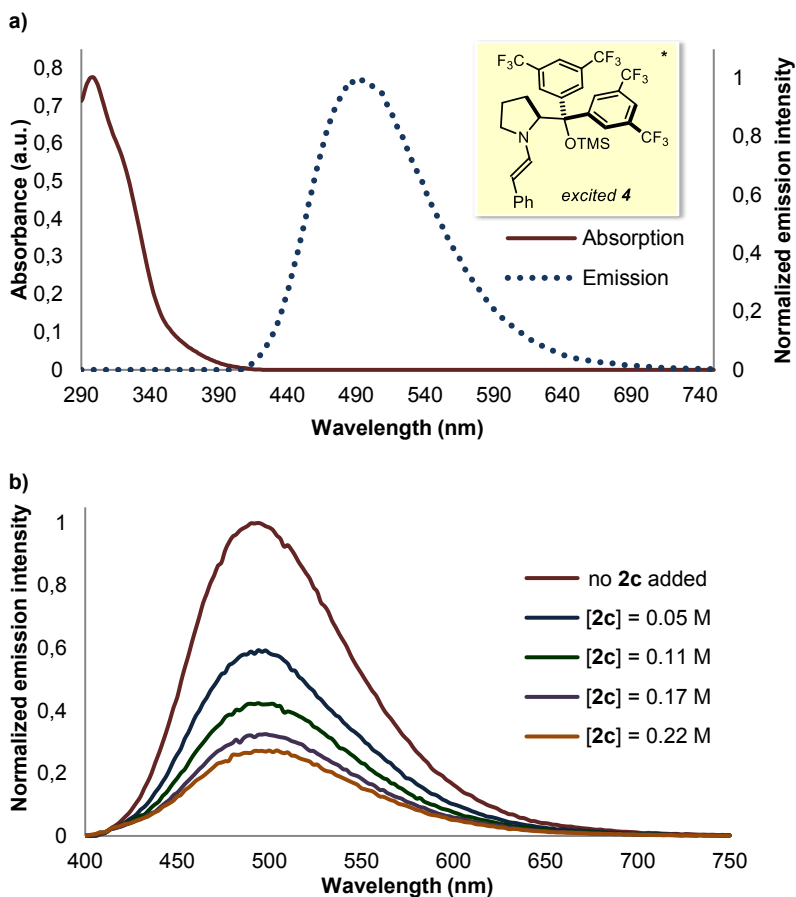
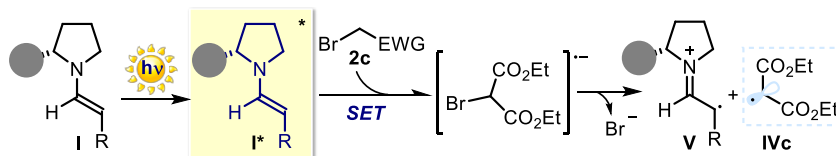


Figure 5.1 a) Emission spectrum of the enamine **4** (excitation wavelength 365 nm). b) Quenching of the enamine **4** emission ($5 \cdot 10^{-5}$ M in toluene) in the presence of increasing amounts of bromomalonate **2c**.

These observations indicate that the photochemical activity of chiral enamines and their potential for light-induced radical generation is not limited to the formation of ground-state EDA complexes. As detailed in Scheme 5.11, the enamine **I**, upon light absorption, can reach an electronically excited state (**I**^{*}) and act as a photoreductant, triggering the formation of the electron-deficient radical **IVc** through the reductive cleavage of the bromomalonate C–Br bond *via* a SET mechanism¹³ (E_{p}^{red} of **2c** = -1.69 V vs. Ag/Ag⁺ in

¹³ For examples of photoinduced reductive cleavage of C–X bonds in electron-poor alkyl halides via a SET from excited substrates, see: a) Rico, I.; Cantacuzene D.; Wakselman, C. “Condensation of CF₂Br₂, CF₂BrCl and BrCF₂CF₂Br with enamines and ynamines” *Tetrahedron Lett.* **1981**, 22, 3405. b) Iwasaki, T.; Sawada, T.; Okuyama, M.; Kamada, H. “The photochemical reaction of aromatic amines with carbon tetrachloride” *J. Phys. Chem.* **1978**, 82, 371. c) Barata-Vallejo, S.; Flesia, M. M.; Lantaño, B.; Argüello, J. E.; Peññory, A. B.; Postigo, A. “Heterogeneous

CH₃CN, see Scheme 5.54). The reduction potential of the excited enamine was estimated as <-2.0 V (vs. Ag/Ag⁺ in CH₃CN)^{2b} on the basis of electrochemical and spectroscopic measurements.¹⁴ In analogy with the EDA complex activation (Scheme 5.9), the SET event leads to both an electrophilic radical **IV** and the α -iminyl radical cation **V**.



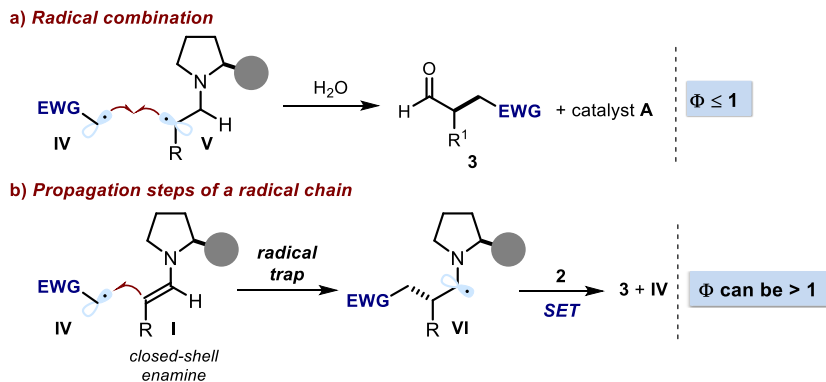
Scheme 5.11 Radical generation strategy based on the direct excitation of enamine **I**. The filled grey circle represents a bulky substituent on the chiral amine catalyst.

5.3.2 Quantum yield measurements

Our previous studies demonstrated the ability of *in situ* generated chiral enamines to promote, upon light excitation, the generation of open-shell species from electron-poor alkyl halides **2a-c**. We then focused on studying the subsequent non-photochemical steps leading to the formation of the new carbon-carbon bond and the final α -alkylated aldehyde **3**. Both enamine-mediated photochemical pathways trigger the formation of two radical species: the chiral radical cation **V** and the electrophilic radicals **IV** (Scheme 5.12). Two different mechanisms can be envisaged to account for the final product formation. One option would be a direct stereocontrolled radical-radical coupling of these two species, **IV** and **V**, affording the α -carbonyl stereogenic center within the final products **3a-c** (Scheme 5.12a). This mechanistic framework would require an enamine-mediated photochemical event for every molecule of product generated.

photoinduced homolytic aromatic substitution of electron-rich arenes with perfluoroalkyl groups in water and aqueous media – a radical-ion reaction” *Eur. J. Org. Chem.* **2013**, 998.

¹⁴ An electronically excited state possesses a much lower ionization potential (i.e. it is a better reductant) than the ground-state, see: Turro, N. J.; Ramamurthy, V.; Scaiano, J. C. “Energy transfer and electron transfer” in *Modern molecular photochemistry of organic molecules* **2010**; Chapter 7, p. 383, University Science Books. Since an excited state has an inherent propensity to form a supramolecular complex, the generation of an exciplex between the excited enamine **I*** and bromomalonate **2c** cannot be excluded; however, we could not observe any emission diagnostic of possible excited state aggregations.



Scheme 5.12 Possible pathways for the non-photochemical steps of the model reactions: a) in-cage radical-radical coupling, and b) radical chain propagation manifold. The open-shell intermediates **V** and **IV** are generated through the photochemical activity of the enamines, as detailed in Scheme 5.9 and Scheme 5.11. Φ = quantum yield.

However, it must be noted that many radical reactions generally proceed through self-propagating radical-chain pathways.¹⁵ In chain processes, product formation occurs through propagation steps that convert the open-shell intermediate (originated from the substrate precursor) into the final product while regenerating the chain-propagating radical. These reactions will occur if there is a suitable mode of initiation (that is, effective radical formation from a closed-shell substrate). Additionally, the propagation steps should be rapid enough in comparison with the possible termination pathways. In our case (Scheme 5.12b), a chain propagation sequence can be envisaged such that the nucleophilic ground-state enamine **I** would trap the photochemically-generated electrophilic radical **IV** to form the α -amino radical **VI**. Since α -aminoalkyl radicals are known to be strong reducing agents,¹⁶ **VI** would induce the reductive cleavage of the electron-poor alkyl bromide **2** through an outer-sphere SET process. As a result, the radical **IV** would be generated together with the product **3** while the aminocatalyst **A** is released (this propagation process is discussed in more detail in the following section, Scheme 5.15). In this scenario, the enamine-based photochemical radical generation strategies, which afford radicals **IV** and **V**, would serve only to initiate a radical self-propagating chain process.

¹⁵ a) Studer, A.; Curran, D. P. "Catalysis of radical reactions: a radical chemistry perspective" *Angew. Chem. Int. Ed.* **2016**, *55*, 58. b) Kärkäs, M. D.; Matsuura, B. S.; Stephenson, C. R. J. "Enchained by visible light-mediated photoredox catalysis" *Science* **2015**, *349*, 1285.

¹⁶ a) Ismaili, H.; Pitre, S. P.; Scaiano, J. C. "Active participation of amine-derived radicals in photoredox catalysis as exemplified by a reductive cyclization" *Catal. Sci. Technol.* **2013**, *3*, 935. b) Wayner, D. D. M.; Dannenberg, J. J.; Griller, D. "Oxidation potentials of α -aminoalkyl radicals: bond dissociation energies for related radical cations" *Chem. Phys. Lett.* **1986**, *131*, 189.

We determined the quantum yield (Φ)¹⁷ of the model reactions, which defines the moles of product formed per moles of photons absorbed by the system, to help distinguish between the two mechanisms.¹⁸ Using potassium ferrioxalate as the actinometer, we measured quantum yields of 25, 20, and 20 for the reactions in CH₃CN¹⁹ with **2a**, **2b**, and **2c**,²⁰ respectively ($\lambda = 450$ nm for **2a-b** and 400 nm for **2c**, details in Section 5.5.1). These results are consonant with a self-propagating radical chain mechanism as the main reaction pathways for the three enamine-mediated photochemical alkylations of butanal under study. The measured quantum yields (Φ_{measured}) are referred to the overall reactions. As such, these values do not take into account any possible non-productive energy-wasting processes,²¹ including parasitic quenching by energy or electron-transfer as well as unimolecular decay processes, which do not lead to product formation while affecting the efficiency of photo-initiation. To better estimate the actual chain length of the reactions, we measured the quantum yield of the initiation step, determining a $\Phi_{\text{initiation}}$ of 0.77, 0.68, and 0.11 for **2a**, **2b**, and **2c**, respectively ($\lambda = 450$ nm for **2a-b** and 400 nm for **2c**).²² Taking these data into account, the actual chain length of the model reactions

¹⁷ Julliard, M.; Chanon, M. "Photoelectron-transfer catalysis: its connections with thermal and electrochemical analogs" *Chem. Rev.* **1983**, *83*, 425.

¹⁸ For a process in which one photon produces only one molecule of the product, the quantum yield can be maximum 1, while for a chain process where one photon forms n molecules of product, the quantum yield is expected to be > 1 . But a value of $\Phi < 1$ does not exclude a possible radical chain mechanism. This is because of potential non-productive energy wasting photochemical processes.

¹⁹ Both the quantum yield measurements and the kinetic experiments were performed in acetonitrile to avoid the precipitation of the lutidinium bromide salt generated during the reaction (see Ref. 6), which is insoluble in MTBE instead. The presence of a precipitate would scatter the irradiating light thus precluding a reliable measurement.

²⁰ Yoon recently reported that a related enamine-mediated alkylation of octanal with bromomalonate **2c** using a polypyridyl ruthenium(II) complex as an external photoredox catalyst possesses a similar quantum yield ($\Phi = 18$), further indicating a radical chain mechanism, see: Cismesia, M. A.; Yoon, T. P. "Characterizing chain processes in visible light photoredox catalysis" *Chem. Sci.* **2015**, *6*, 5426.

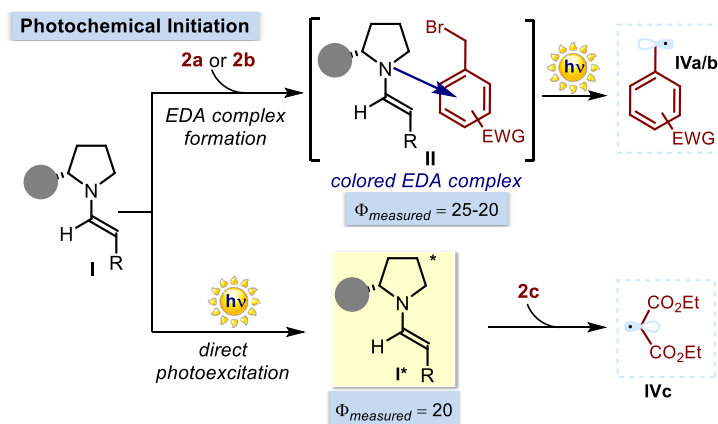
²¹ Non-productive processes can reduce the efficiency of photo-initiation, directly affecting the overall quantum yield (Φ_{measured}). For example, the photoexcited enamine could relax to the ground-state *via* either radiative or vibrational pathways without undergoing electron-transfer processes, while a back-electron transfer from the chiral ion-pair **III** (Scheme 5.9) would unproductively restore the ground-state enamine-based EDA complex **II**.

²² The quantum yield of the initiation step has been measured by monitoring the decomposition of catalyst **A**. The analysis is based on the observation (extensively discussed in the following sections of the chapter) that the enamine **I** serves as a sacrificial initiator of the chain mechanism: for any photo-induced SET event, a propagating radical **IV** is generated while a molecule of the chiral catalyst **A** is destroyed via decomposition of the intermediate **V** (Scheme 5.9 and Scheme 5.11). If a molecule of the catalyst **A** decomposes for any photo-induced initiation, the rate of catalyst degradation correlates with the efficiency of the initiation. This analysis requires that the catalyst **A** degradation is triggered by productive photochemical initiation only, and not by other secondary reactions, a scenario which is consistent with experimental observations.

($\Phi_{\text{estimated}} = \Phi_{\text{measured}} / \Phi_{\text{initiation}}$) are considerably longer, with a lower limit of 32, 29, and 182 for **2a**, **2b**, and **2c**, respectively.

5.3.3 Proposed mechanism

The quantum yield measurements point towards a radical chain propagation mechanism. The photochemical activity of the enamines, either by EDA complex activation or direct excitation, generates radicals **IV** from the closed-shell species **2a-c**.²³ This event, by feeding in radicals from outside the chain, serves as the initiation of self-propagating radical chains (Scheme 5.13).

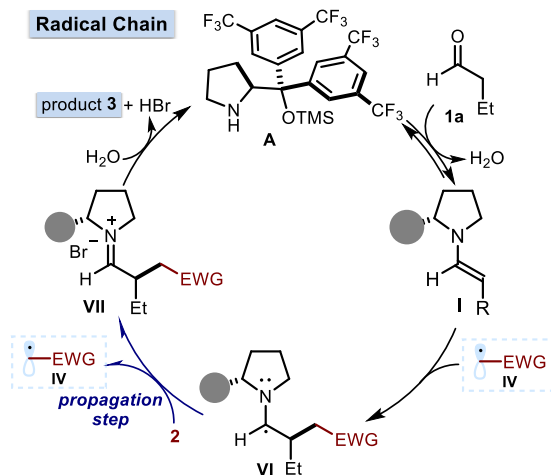


Scheme 5.13 Photochemical initiation of the α -alkylation of aldehydes *via* either EDA complex formation or direct enamine photoexcitation. The filled grey circle represents a bulky substituent on the chiral amine catalyst.

Subsequently, both regimes follow a similar propagation pathway. The ground-state enamine **I** traps the photo-generated electrophilic radical **IV**,²⁴ in a stereocontrol manner, forming the new carbon-carbon bond (Scheme 5.14). Considering the consolidated ability of catalyst **A** to infer high stereoselectivity in enamine-mediated polar reactions,³ it is no surprise that the addition of the radical **IV** to **I** proceeds in a stereocontrolled fashion. Finally, a chain propagation step would afford the iminium ion **VII** that, upon hydrolysis, releases the final product **3** and the aminocatalyst **A** resuming the cycle.

²³ The two photochemical initiation manifolds can be both operative in the alkylations of butanal with **2a** and **2b** if the reaction is conducted using a light that can be absorbed by the transiently generated enamine **I** ($\lambda < 415$ nm). As a result, to avoid any possible contribution from the direct photoexcitation of enamines, the measurements with **2a** and **2b** have been conducted using higher wavelengths of irradiation. Under these conditions, only the EDA complex activation is a viable strategy to generate radicals from **2a** and **2b**.

²⁴ Russell, G. A.; Wang, K. "Electron transfer processes. 53. Homolytic alkylation of enamines by electrophilic radicals" *J. Org. Chem.* **1991**, *56*, 3475.



Scheme 5.14 Radical chain process triggered by the radical trapping by the enamine **I**.

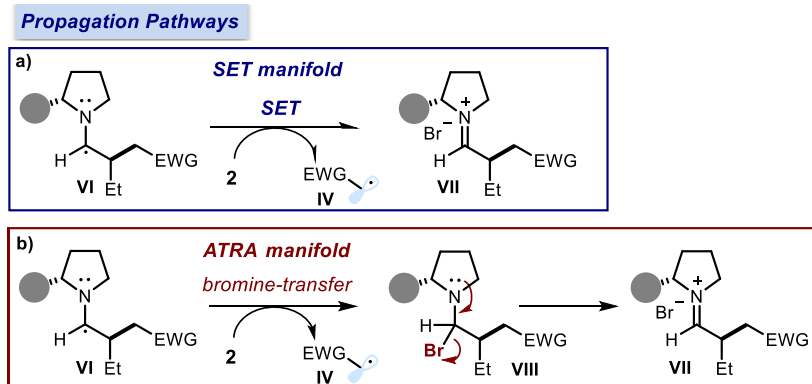
Evaluation of the propagation step

Two different pathways can be proposed for the propagation step, which would formally oxidize α -aminoalkyl radical **VI** leading to the iminium ion **VII**. An electron-transfer from the **VI** to the electron-poor alkyl halide **2** regenerates the chain-propagating radical **IV** while giving the bromide-iminium ion pair **VII** (Scheme 5.15a). The feasibility of this step is associated to the reduction potential of the alkyl halide **2**, which needs to be easier to reduce than the iminium ion **VII**, emerging from the SET.

Alternatively, an atom-transfer mechanism can be envisaged, where the α -aminoalkyl radical **VI** would abstract a bromine atom from **2**, regenerating the radical **IV** while affording an unstable α -bromo amine adduct **VIII**.²⁵ **VIII** would eventually evolve to the iminium ion **VII** (Scheme 5.15b). This pathway would provide a rare example of enantioselective catalytic atom-transfer radical addition (ATRA),²⁶ a historical methodology for functionalizing olefins with organic halides.

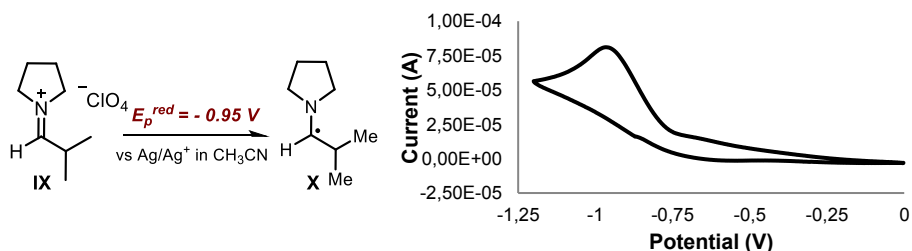
²⁵ Similar atom-transfer mechanisms have been invoked for the alkylation of enol ethers and enamides with electrophilic radicals, see: a) Curran, D. P.; Ko, S.-B. "Additions of electrophilic radicals to electron rich alkenes by the atom transfer method. Surmounting potentially reversible radical atom transfer reactions by irreversible ionic reactions" *Tetrahedron Lett.* **1998**, *39*, 6629. b) Friestad, G. K.; Wu, Y. "Intermolecular nonreductive alkylation of enamides via radical-polar crossover" *Org. Lett.* **2009**, *11*, 819. This pathway was also proposed in 15a, page 80.

²⁶ a) Kharasch, M. S.; Jensen, E. V.; Urry, W. H. "Addition of carbon tetrachloride and chloroform to olefins" *Science* **1945**, *102*, 128. b) Pintauer, T.; Matyjaszewski, K. "Encyclopedia of radicals" **2012**, Volume 4, p. 1851, Wiley.



Scheme 5.15 The two possible propagation pathways as driven either by a) the SET reduction of **2** or b) the bromine atom transfer from **2** involving the key α -amino radical **VI** intermediate.

To discriminate between the possible propagation manifolds, the iminium ion **IX** (Scheme 5.16), derived from the condensation of pyrrolidine and isovaleraldehyde, was isolated (see Section 5.5.5 for the characterization of iminium ion **IX**). **IX** mimics the actual iminium ion intermediate **VII** involved in the catalytic cycle. **VII** could not be synthesized because the steric hindrance of catalyst **A** hampers the condensation with the aldehydic product **3**.



Scheme 5.16 Evaluating the redox potential of the crucial α -aminoalkyl radical of type **VI**. Cyclic voltammogram of the iminium ion **IX** [0.02 M] in [0.1 M] TBAPF₆ in CH₃CN. Sweep rate: 10 mV/s. Pt electrode working electrode, Ag/AgCl (NaCl saturated) reference electrode, Pt wire auxiliary electrode. Irreversible reduction. $E_p^{\text{red}} = -0.95$ V.

The reduction potential of **IX** (E_p^{red} of **IX**) was measured by cyclic voltammetry in order to study the iminium/ α -aminoalkyl radical (**IX/X**) redox pair (Scheme 5.16). This measurement provides an approximation of the ability of an α -aminoalkyl radical of type **VI** to act as a reducing agent. The irreversible reduction of **IX** to give the α -aminyl radical **X** was proceeding at -0.95 V vs. Ag/Ag⁺ in CH₃CN. This value means that the α -aminyl radical of type **VI** is incapable of reducing either **2b** or **2c** (E_p^{red} of **2b** = -1.35 V vs. Ag/Ag⁺ in CH₃CN; E_p^{red} of **2c** = -1.69 V vs. Ag/Ag⁺ in CH₃CN), indicating that a bromine-

transfer mechanism is likely operative with phenacyl bromide and bromomalonate substrates (Figure 5.2b). In contrast, a SET reduction is the most likely mechanism when using **2a**, since its potential (E_p^{red} of **2a** = -0.66 V vs. Ag/Ag⁺ in CH₃CN) makes a SET reduction from intermediate **VI** feasible (Figure 5.2a).

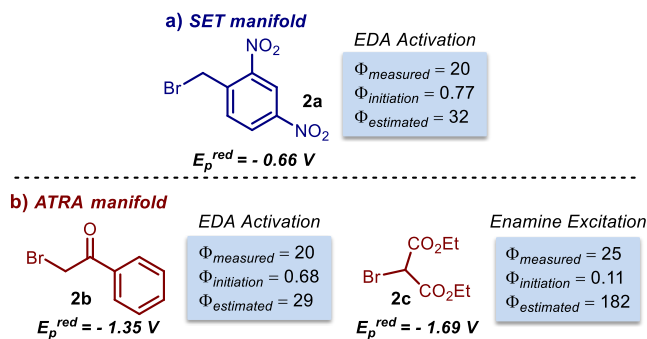


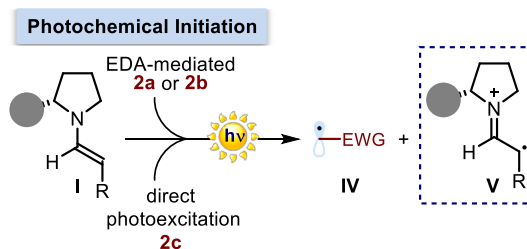
Figure 5.2 Summary of the quantum yield measurements for the three model photochemical reactions and the propagation mechanisms.

Several aspects of the mechanism proposed in Scheme 5.13-5.15 deserve comment. The underlying radical chain pathway is not surprising when considering that the transformations closely resemble ATRA processes²⁶ or a Kornblum-Russell S_{RN}I-type alkylation.²⁷ The S_{RN}I (unimolecular radical nucleophilic substitution) is a process through which nucleophilic substitution is achieved on aromatic and aliphatic compounds that bear a suitable leaving group and that do not react through polar nucleophilic mechanisms. This class of transformations is characterized by an innate chain mechanism involving electron-transfer steps with radical ions as intermediates. In some examples of S_{RN}I-type reactions, electron-rich olefins, including enamines,²⁴ efficiently trap electrophilic radicals. In addition, electron-poor benzyl²⁴ bromides are also suitable substrates for the S_{RN}I reaction manifold. Moreover, the initiation of this type of radical chain alkylations by the excitation an EDA complex have been described (see Chapter II, Scheme 2.10).²⁸ On the other side, bromomalonates and phenacyl bromides²⁵ are suitable substrates for ATRA processes, which classically proceed *via* radical chain mechanisms.²⁶

²⁷ a) Kornblum, N. "Substitution reactions which proceed *via* radical anion intermediates" *Angew. Chem. Int. Ed.* **1975**, *14*, 734. b) Rossi, R. A., Pierini, A. B., Peññory, A. B. *Chem. Rev.* **2003**, *103*, 71. c) Rossi, R. A.; Guastavino, J. F.; Budén, M. E. "Arene chemistry: reaction mechanisms and methods for aromatic compounds" **2015**, Chapter 10, p. 243, John Wiley & Sons.

²⁸ Fox, M. A.; Younathan, J.; Fryxell, G. E. "Photoinitiation of the S_{RN}I reaction by excitation of charge-transfer complexes" *J. Org. Chem.* **1983**, *48*, 3109.

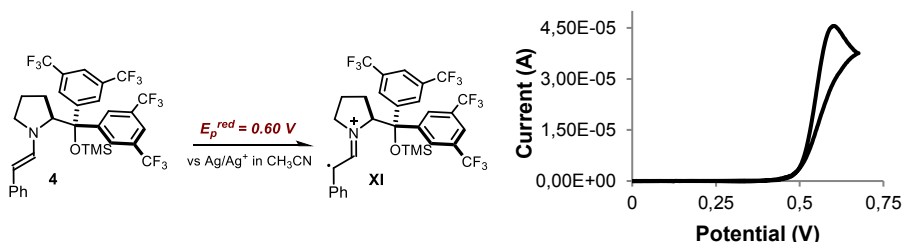
The central role of the chiral aminocatalyst **A** in these photochemical transformations deserves further comment. **A** condenses with aldehyde **1** generating *in situ* the enamine **I**. As a result, the aldehyde **1** is transformed into a nucleophilic species (**I**) able to trap electrophilic radicals and participate in the photochemical events that initiate the radical chain. Furthermore, the chiral enamine **I** is directly involved in the stereo-defining event. We focused on the initiation and the fate of the α -iminyl radical cation **V**, generated after the photo-induced SET together with the carbon-centered radical **IV** (Scheme 5.17).



Scheme 5.17 Photochemical initiation of the α -alkylation of aldehydes *via* either EDA complex formation or direct enamine photoexcitation to render carbon-centered radical **IV** and the α -iminyl radical cation **V**.

Intermediate **V** is an unproductive species, since it is not involved in the radical chain that leads to the product formation. Instead, the α -iminyl radical cation **V** collapses to give a variety of degradation products which, despite our efforts, have remained unidentified so far. Wondering whether the intermediate **V** could be reduced back to regenerate the enamine **I**, the electrochemical behavior of enamine **4** was studied (Scheme 5.18). Enamine **4** was synthesized by condensation of catalyst **A** and 2-phenylacetaldehyde in the presence of molecular sieves.²⁹ Subsequently, the α -iminyl radical cation **XI** (analogous to **V**) was electrochemically generated upon oxidation of the preformed enamine **4**. An irreversible cyclic voltammogram was obtained which suggests that α -iminyl radical cation is an unstable intermediate which cannot be reduced back to the progenitor enamine **I**.

²⁹ This study was conducted by Dr. Mattia Silvi and was originally reported in 2b.



Scheme 5.18 Cyclic voltammogram of the performed enamine **4** [0.01 M] in [0.1 M] TBAPF₆ in CH₃CN. Sweep rate: 5 mV/s. Pt electrode working electrode, Ag/AgCl (NaCl saturated) reference electrode, Pt wire auxiliary electrode. Irreversible reduction. $E_p^{\text{red}} = 0.60 \text{ V}$.

The enamine **I** serves as a sacrificial initiator of the chain mechanism³⁰ since, for any photo-induced SET event, a propagating radical **IV** is generated while a molecule of the chiral catalyst **A** is destroyed *via* decomposition of the intermediate **V**. By using both gas chromatography (GC-FID; FID = flame ionization detection) and NMR analyses,³¹ we established that the amount of catalyst **A** decreases constantly during the photochemical alkylation in correlation with the number of initiation events (further discussions in the following sections).

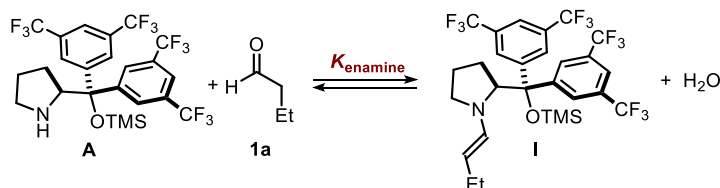
With a clearer mechanistic picture in mind, we decided to perform kinetic studies to better understand the relative importance of the initiation step and the propagation cycle for the overall rate, while establishing the turnover-limiting step of the model photochemical catalytic alkylations. But before this, we investigated whether the different photochemical pathways available to enamines for initiating the chain process (EDA complex formation *vs.* direct photoexcitation) might have an influence on the enamine formation and its concentration in solution. This matters because the amount of enamine in solution has a direct effect on the kinetic profiles of the reactions, since the enamine is involved in both initiation (Scheme 5.13) and chain propagation (Scheme 5.14).

³⁰ Interestingly, an analogous sacrificial role of the enamine was proposed to support the mechanism of the alkylation of aldehydes with bromomalonate **2c**, using a dual photoredox-organocatalytic system, see Ref. 4a.

³¹ By using an internal standard and in situ NMR spectroscopic analysis, we confirmed that the overall amount of the catalyst **A** decreased over time, further supporting the instability of the intermediate **V** generated upon photoinduced SET. Studies on the disappearance of the catalyst are reported in Figure 5.7. The same studies were repeated using gas chromatography (GC-FID); details are reported in Section 5.5.2.

5.3.4 Studies of the concentration of enamine in solution

Enamine **I** is a transient species generated *via* the reversible condensation of the chiral aminocatalyst **A** with butanal **1a** (Scheme 5.19).



Scheme 5.19 Equilibrium for the enamine **I** formation. K_{ensemble} : equilibrium constant.

This reversible process is characterized by an equilibrium constant (K_{ensemble}) given by Equation 5.1.

$$K_{\text{ensemble}} = \frac{[\text{enamine}] \cdot [\text{H}_2\text{O}]}{[\text{free catalyst}] \cdot [\text{free aldehyde}]} \quad (\text{Eq. 5.1})$$

Calculation of the equilibrium constant (K_{ensemble})

We started by determining the equilibrium constant for the formation of the enamine, generated upon condensation of the aminocatalyst **A** and butyraldehyde **1a** by ^1H NMR spectroscopy. For these measurements, three solutions containing 0.02 mmol of the catalyst **A** and of 0.02 mmol of 1,3,5-trimethoxybenzene (used as internal standard) and different amounts of **1a** (0.1 mmol, 0.25 mmol and 0.7 mmol) dissolved in 500 μL of dry CD_3CN were prepared. After mixing the components, all the solutions were kept in the dark for 15 minutes to secure equilibration. The relative amount of enamine **I** in solution with respect to the free catalyst **A** was determined by the average of the integration of the following diagnostic peaks: a doublet of doublets at 4.55 ppm ($J = 9.3, 2.0$ Hz, 1H) and a doublet of triplets at 4.09 ppm ($J = 13.6, 6.8$ Hz, 1H) for the enamine **I**; integration of a triplet at 4.40 ppm ($J = 7.2$ Hz, 1H) for catalyst **A** (Figure 5.3). The amount of water present in solution was also calculated by integration of the singlet at 2.13 ppm. The total amount of catalyst in solution was compared to the internal standard to ensure that there was no degradation.

Specifically, a stock solution containing 60 mg (0.1 mmol) of **A** and 16.8 mg (0.1 mmol) of 1,3,5-trimethoxybenzene as internal standard in 2.5 mL of CD_3CN was prepared. To 500 μL of this solution (0.04 M in **A**), 9 μL of **1a** (0.1 mmol, 0.2 M solution in **1a**) were added. The NMR analysis inferred an enamine **I**/free catalyst **A** ratio of **1.01:1** and a concentration of H_2O of 0.03 M (see Figure 5.3).

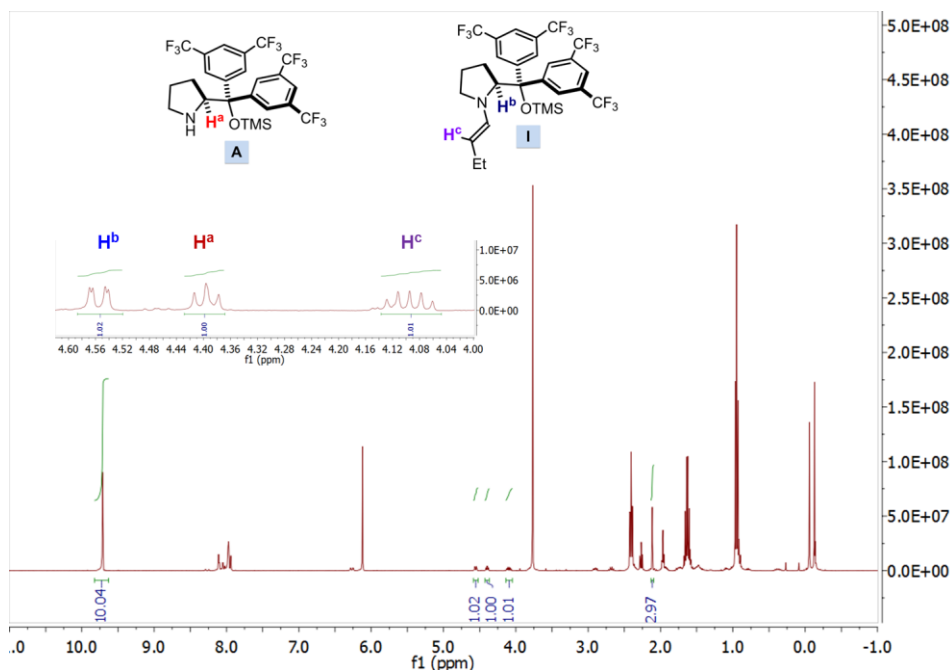
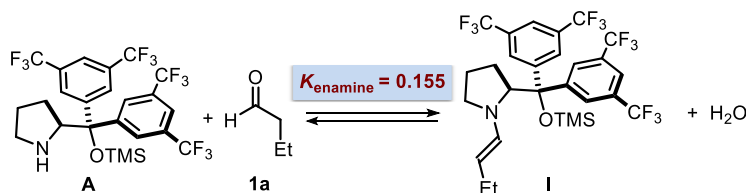


Figure 5.3 ^1H NMR spectra showing the 1.01:1 ratio of enamine **I**:free catalyst **A** for a solution containing: 0.02 mmol of **A** (0.04 M), 0.1 mmol of **1a** (0.2 M) in 0.5 mL of CD_3CN . The ^1H NMR spectral window between 4.60 and 4.00 ppm has been enlarged to show diagnostic signals for the enamine **I** and the free catalyst **A**.

Another solution was prepared from 500 μL of the stock solution 0.04 M in **A** and adding 23 μL of **1a** (0.26 mmol). A **2.32:1** ratio of **I**:**A** was observed and a concentration of H_2O of 0.036 M.

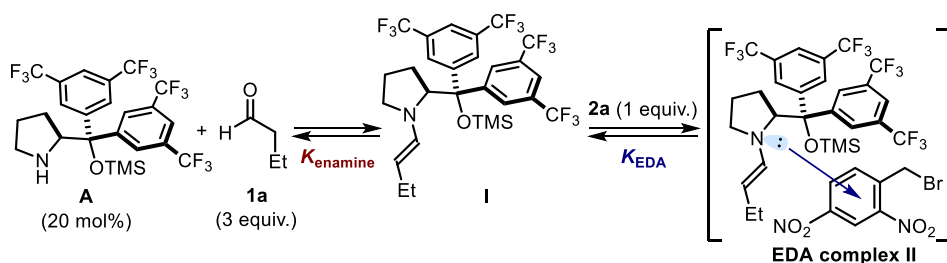
An additional solution was prepared from 500 μL of the stock solution 0.04 M in **A** and adding 65 μL (0.72 mmol of **1a**) of **1a**. A ratio of **I**:**A** of **5.47:1** was observed and a concentration of H_2O of 0.04 M.

With these data and using Equation 5.1, an equilibrium constants of $K_{\text{enamine}} = 0.155 \pm 0.002$ was determined (Scheme 5.20).



Scheme 5.20 Equilibrium constant for the enamine **I** formation (K_{enamine}).

Subsequently, we studied the effect that the addition of **2a**, a suitable acceptor for the generation of an EDA complex with enamine **I**, had on the enamine equilibrium. As all chemical equilibria, this system follows Le Châtelier's principle: "every change of one factor of an equilibrium occasions a rearrangement of the system in such a direction that the factor in question experiences a change in a sense opposite to the original change".³² Therefore it can be envisioned that the formation of an EDA complex (where K_{EDA} identifies the association constant, see Scheme 5.8), where the enamine acts as acceptor, can alter the original state of equilibrium for enamine formation. This scenario suggests that the presence of acceptor **2a** can directly influence the relative concentration of free catalyst **A** and enamine **I** in solution (Scheme 5.21).



Scheme 5.21 Influence of the EDA complex formation on the amount of enamine in solution. The equilibrium constant for the enamine **I** formation (K_{enamine}) and the following equilibrium to form an EDA complex **II** with **2a** (K_{EDA}).

To verify this possibility, we used ^1H NMR spectroscopic analysis to investigate the equilibrium of enamine formation under the reaction conditions in the presence and absence of **2a**.

Effect of the EDA complex formation with **2a** on the concentration of enamine in solution

^1H NMR analysis was made on a solution containing 11.9 mg of the aminocatalyst **A** (0.02 mmol), 27 μL of butanal (**1a**) (0.3 mmol) and 12 μL of 2,6-lutidine (0.1 mmol) in 0.5 mL of CD_3CN (Figure 5.4). Under these conditions, both enamine **I** and free catalyst **A** were detected in a ratio of 1.2:1 (red spectrum).³³ The free catalyst:enamine ratios were measured by comparing the integrals of the free catalyst peak (triplet at 4.40 ppm, $J = 7.2$

³² Le Châtelier, H. "Recherches expérimentales et théoriques sur les équilibres chimiques" *Annales des Mines* **1888**, 13, 157.

³³ ^1H NMR spectroscopic analysis did not allow us to discriminate between the free enamine **I** and the enamine which engages in EDA complex formation with **2a**. The reported **I** to **A** ratio refers to the total amount of enamine **I** present in solution.

Hz, 1H) and the diagnostic peaks of the enamine **I** (doublet of doublets at 4.55 ppm ($J = 9.3, 2.0$ Hz, 1H) and doublet of triplets at 4.09 ppm ($J = 13.6, 6.8$ Hz, 1H).

Successively, another solution containing 11.9 mg of the aminocatalyst **A** (0.02 mmol), 27 μL of butanal **1a** (0.3 mmol), 12 μL of 2,6-lutidine (0.1 mmol) and 26 mg of **2a** (0.1 mmol) in 0.5 mL of CD_3CN was prepared. This solution was degassed by three cycles of freeze-pump-thaw and its ^1H NMR spectrum was recorded (green spectrum). A 1.8:1 ratio of **I** and free catalyst **A** was observed under these conditions.

We then used a xenon lamp coupled with a monochromator which, by bringing the light in close contact with the NMR tube through an optical fiber, allowed for the *in situ* illumination of the same sample. When the EDA complex mixture was irradiated *in situ* in the NMR spectrometer ($\lambda = 470 \pm 5$ nm, irradiance = 28.8 mW/cm^2), a 3.8:1 ratio of **I**:**A** after 30 seconds of irradiation (blue spectrum). After 60 seconds of irradiation, the signals of the free catalyst **A** could no longer be detected (purple spectrum).

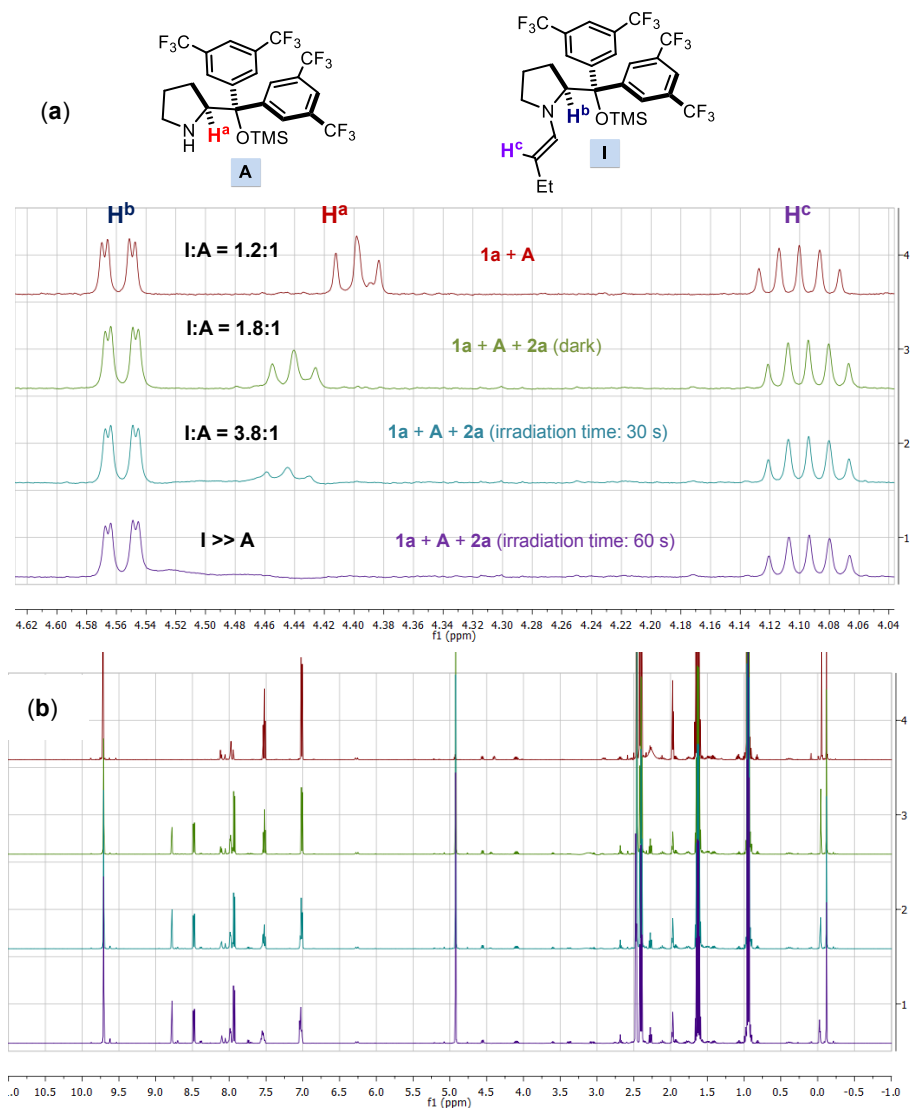
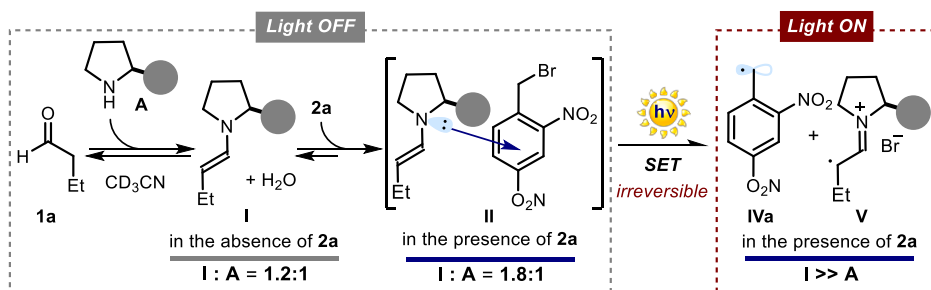


Figure 5.4 ^1H NMR spectra showing different ratios of enamine **I**:free catalyst **A**. a) Selected window of the ^1H NMR spectra between 4.62 and 4.04 ppm showing diagnostic signals for the enamine **I** and the free catalyst **A**. Red spectrum: 0.02 mmol of **A**, 0.3 mmol of **1a**, 0.1 mmol of 2,6-lutidine and 0.5 mL of CD_3CN ; green spectrum: 0.02 mmol of **A**, 0.3 mmol of **1a**, 0.1 mmol of 2,6-lutidine, 0.1 mmol of **2a** and 0.5 mL of CD_3CN without illumination; blue spectrum: same mixture as green spectrum while *in situ* irradiating for 30 seconds; purple spectrum: same mixture as green spectrum after 60 seconds of irradiation ($\lambda = 470 \pm 5$ nm, irradiance = 28.8 mW/cm^2). b) Full ^1H NMR spectra. ^1H NMR spectroscopic analysis did not allow us to discriminate between the free enamine **I** and the enamine which engages in EDA complex formation with **2a**.

These experiments show an influence of the formation of the EDA complex **II** on the concentration of enamine **I** in solution (Scheme 5.22). The displacement observed in the enamine **I** and free catalyst **A** ratio upon addition of **2a**, from a 1.2:1 to a 1.8:1 ratio, is congruent with the fact that the formation of the EDA complex, by sequestering **I**, shifts the dynamic equilibrium of enamine formation to the side that reduces the perturbation (in this case, the forward reaction).³³

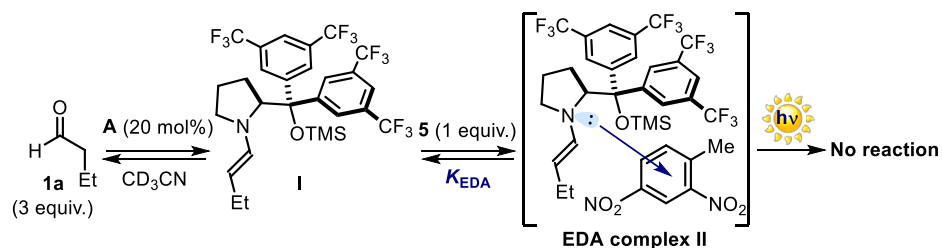


Scheme 5.22 Influence of the EDA complex formation on the amount of enamine in solution. The effect of light illumination and the irreversible step (triggered by the photoactivity of the EDA complex **II**) on the concentration of enamine in solution. 1H NMR experiments were performed in CD_3CN at 298 K using a xenon lamp coupled with a monochromator and equipped with an optical fiber for the *in situ* illumination of the samples ($\lambda = 470 \pm 5$ nm, irradiance = 28.8 mW/cm²). The filled grey circle represents a bulky substituent on the chiral amine catalyst.

Moreover, when the mixture was irradiated *in situ* in the NMR spectrometer ($\lambda = 470 \pm 5$ nm, irradiance = 28.8 mW/cm²), after 60 seconds of irradiation, the signals of the free catalyst **A** could no longer be detected, meaning that the system dramatically shifted towards the enamine **I** (Scheme 5.22). This more pronounced shift towards the enamine formation, upon light irradiation, can be reconciled with the photochemical activity of the enamine-based EDA complex **II**. The excitation of **II** induces the irreversible formation of the electrophilic radical **IV** (upon fragmentation of the C-Br bond within the ion pair **III**) and the unstable α -iminyl radical cation **V**. These light-triggered events would therefore decrease both the concentration of the enamine **I** and the alkyl bromide **2a**, further shifting the enamine equilibrium forward.

Effect of the EDA complex formation with **5** on the enamine equilibrium

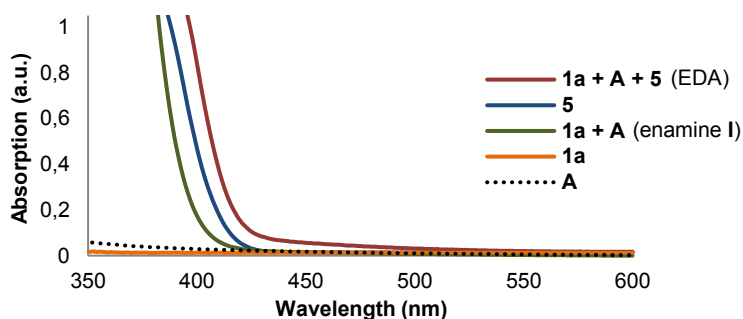
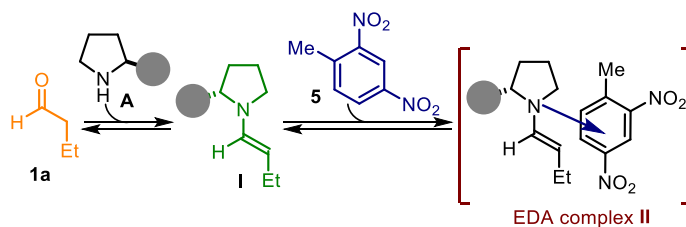
To test the importance of the irreversible events that follow the photo-induced SET, a similar experiment where **2a** was replaced by 2,4-dinitrotoluene (**5**) was conducted (Scheme 5.23). **5** lacks a suitable leaving group (e.g. the bromine within **2a**) thus it cannot undergo an irreversible fragmentation.



Scheme 5.23 Effect of the EDA complex formation with **5** on the enamine equilibrium.

The filled grey circle represents a bulky substituent on the chiral amine catalyst.

First we studied if **5** could act as an acceptor partner in EDA complex formation with the enamine **I**. As shown in Scheme 5.23, the absorption spectra recorded when mixing together the enamine, generated *in situ* upon condensation of catalyst **A** and **1a** (green line), with 2,4-dinitrotoluene **5**, showed a bathochromic displacement in the visible spectral region, where none of the substrates absorbs (red line). The new absorption band indicates the formation of an EDA complex.



Scheme 5.24 Optical absorption spectra, recorded in MTBE in 1 mm path quartz cuvettes using a Shimadzu 2401PC UV-visible spectrophotometer of the separate reaction components and of the colored EDA complex with 2,4-dinitrotoluene **5**; [**1a**] = 1.5 M; [**5**] = 0.5 M; [**A**] = 0.1 M. The filled grey circle represents a bulky substituent on the chiral amine catalyst.

Subsequently, the effect that 2,4-dinitrotoluene **5** had on the enamine equilibrium was investigated (Figure 5.5). In the dark, when 1 equivalent of **5** was added to a solution of

catalyst **A** and butanal a ratio of 1.6:1 **I**:**A** was observed (green spectrum). Upon illumination ($\lambda = 470 \pm 5$ nm, irradiance = 28.8 mW/cm^2), no change on the concentration of the enamine **I** was observed (blue spectrum).

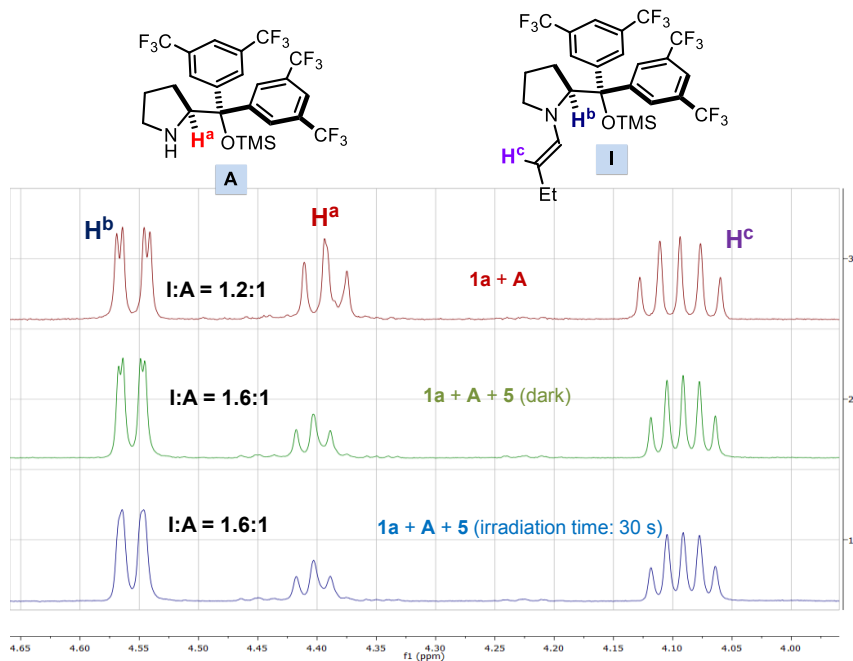
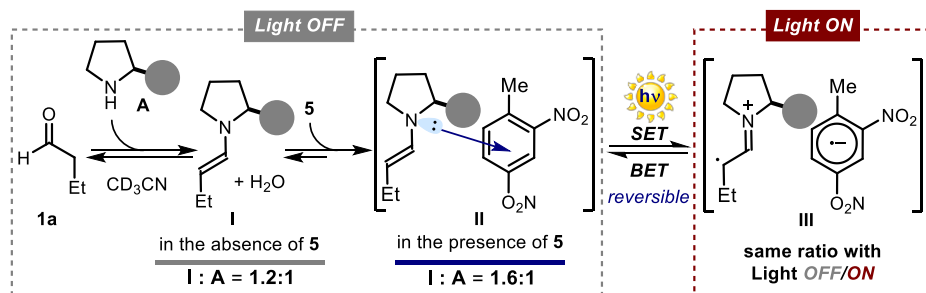


Figure 5.5 ^1H NMR spectra showing different ratios of enamine **I**:free catalyst **A** ratio.

Selected region of the ^1H NMR spectral window between 4.62 and 4.04 ppm showing diagnostic signals for the enamine **I** and the free catalyst **A**. Red spectrum: 0.02 mmol of **A**, 0.3 mmol of **1a** in 0.5 mL of CD_3CN ; green spectrum: 0.02 mmol of **A**, 0.3 mmol of **1a**, 0.1 mmol of 2,4-dinitrotoluene **5** in 0.5 mL of CD_3CN without illumination; blue spectrum: same mixture as green spectrum while *in situ* irradiating for 30 seconds ($\lambda = 470 \pm 5$ nm, irradiance = 28.8 mW/cm^2).

These spectra shows that employing 2,4-dinitrotoluene **5**, a non-reactive acceptor, as partner a displacement in the equilibrium is again detected, changing the **I**:**A** ratio from 1.2:1 to 1.6:1 (Scheme 5.25). These measurements corroborate the effect of the EDA formation on the enamine concentration in solution. However, in contrast with the previous experiment, when the mixture was irradiated no change was detected. This observation is in agreement with an unproductive photo-induced SET. As **5** lacks a suitable leaving group, the irradiation of the mixture leads to a fast back-electron transfer that, by restoring the ground-state EDA complex **II**, does not influence the overall equilibrium of the system.



Scheme 5.25 Influence of the EDA complex formation on the amount of enamine in solution. ^1H NMR experiments were performed in CD_3CN at 298 K using a xenon lamp coupled with a monochromator and equipped with an optical fiber for the *in situ* illumination of the samples ($\lambda = 470 \pm 5$ nm, irradiance = 28.8 mW/cm^2). The effect of an EDA complex, unable to undergo a photo-induced irreversible SET event, on the enamine concentration. BET: back-electron transfer. The filled grey circle represents a bulky substituent on the chiral amine catalyst.

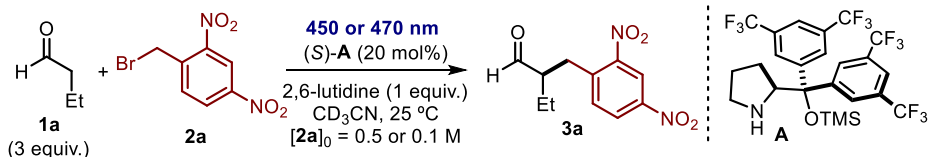
These experiments were then repeated with the bromomalonate **2c**. In this case, the equilibrium of the enamine formation ($K_{\text{enamine}} = 0.155$, Scheme 5.19) was not perturbed by the addition of **2c**. This is because the reaction between **2c** and **I** does not involve any pre-association, and the mechanism is based on the direct photo-excitation of the enamine **I**. As a result, the presence of **2c** does not influence the enamine formation equilibrium.

5.3.5 Kinetic studies

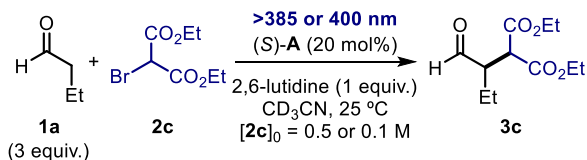
We then performed kinetic studies to gain a better understanding of the factors governing the photochemical enamine-based alkylations of butanal **1a**. In particular, we sought to assess whether the two different initiation methods would display distinct or analogous kinetic profiles. The reaction between **1a** and **2a** catalyzed by the secondary amine **A** was chosen as representative of the EDA-mediated methodology (Scheme 5.26a).³⁴ The results obtained for this transformation were in agreement with those obtained when **2b** was utilized as substrate (see Section 5.5.3 for details). For the alkylation of aldehydes based on the direct photoexcitation of the enamine, diethyl bromomalonate **2c** was chosen as model substrate (Scheme 5.26b).

³⁴ The reactions were performed in acetonitrile to avoid the precipitation of the lutidinium bromide.

a) EDA Complex Activation Strategy



b) Direct Photoexcitation of Enamines



Scheme 5.26 Model reactions used for initial-rate kinetics determined by ^1H NMR analysis and the observed rate orders. a) EDA complex-triggered photochemical alkylation of butanal **1a** with 2,4-dinitrobenzyl bromide **2a**. b) Alkylation of **1a** with diethyl bromomalonate **2c** driven by the direct photoexcitation of enamines. Reaction conditions: studies performed across a range of concentrations for each reaction component in CD_3CN (dried over 4 \AA molecular sieves), irradiation at 450 and >385 nm for **2a** and **2c**, respectively. The kinetic studies were repeated using *in situ* ^1H NMR spectroscopy ($\lambda = 470$ and 400 nm for **2a** and **2c**, respectively) to directly monitor the reaction progress.

Initial-rate kinetics were measured in these studies, keeping the conversion of the reactions below 15%. This allows us to approximate the concentration of the reactants, at this early stage of the reaction, to the initial concentration (Equation 5.2).³⁵ As a result, straight lines are obtained when the conversion is plotted vs. the time (Equation 5.3); and, in consequence, the order with respect to a reactant can be easily calculated from the slopes of these plots.

$$\text{For conversions} < 15\%; \quad [\text{reactant}] \approx [\text{reactant}]_0 \quad (\text{Eq. 5.2})$$

$$\text{rate} = k \cdot [\text{reactant}]^n \approx k \cdot [\text{reactant}]_0^n \quad (\text{Eq. 5.3})$$

The progress of the two reactions was monitored by ^1H NMR analysis using two different approaches (see Section 5.5.3 for details). In the first approach, we used a xenon lamp with a band-pass filter at 450 nm (irradiance = 4.7 mW/cm^2) to illuminate the EDA complex-mediated reaction with **2a** (Scheme 5.26a), while a cut-off filter at 385 nm (irradiation at $\lambda \geq 385$ nm; irradiance = 300 mW/cm^2) was employed for the process with **2c** (Scheme 5.26b). This set-up required an independent reaction to be performed for every data-point at different times.

³⁵ Anslyn, E. V.; Dougherty, D. A. "Modern physical organic chemistry" **2006**, Chapter 7, p. 389, University Science Books.

The initial-rate kinetic studies were repeated using *in situ* ^1H NMR spectroscopy to directly monitor the reaction progress. In this second case, we used a xenon lamp coupled with a monochromator which allowed for the *in situ* illumination of the samples. The EDA complex-based reaction with **2a** was irradiated at 470 nm (irradiance = 28.8 mW/cm²), while 400 nm (irradiance = 20.4 mW/cm²) was used for the alkylation chemistry with **2c**. Both approaches gave similar and reproducible kinetic profiles.

Table 5.1 Rate order assessment for the alkylation of **1a** with **2a** and **2c**.

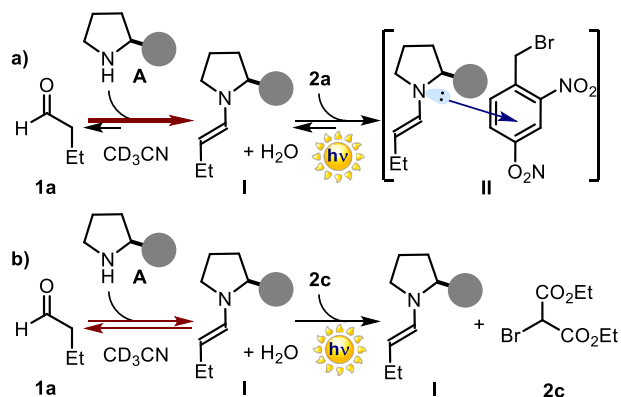
Component	EDA-mediated with 2a	Direct photoexcitation with 2c
catalyst A	first	first
aldehyde 1a	zeroth	fractional
H ₂ O	zeroth	zeroth
alkyl bromide 2	negative	fractional

Table 5.1 details the results of our initial-rate kinetic investigations, performed across a range of concentrations for each reaction component. A first-order dependence on the catalyst **A** was observed for both process; reactions with **2a** and with bromomalonate **2c**. However, we encounter the first discrepancy in the order with respect to the aldehyde. The EDA complex-mediated alkylation showed a zeroth-order dependence in [**1a**], whereas the rate of the reaction with bromomalonate was affected by the concentration of aldehyde, showing a fractional order. Furthermore, unexpected negative order in the alkyl halide was obtained for **2a**. In sharp contrast, a fractional order on [**2c**] was measured for the reaction driven by the direct photoexcitation of the enamine.

The effect of water on the reaction rate was also measured. No influence on the kinetic profiles was observed after the addition of either 1 or 2 equivalents of H₂O in both systems. These results indicate that the iminium ion hydrolysis, which leads to the alkylation product **3** and releases the catalyst **A**, is not turnover-limiting.

We then utilized our previous observations seeking to understand the different kinetic behaviors of the two systems. The zeroth-order dependence on butanal **1a** for the EDA complex-mediated alkylation with **2a** implies that the enamine **I**, generated *in situ* upon condensation of **A** and **1a**, is the resting state of catalyst **A** (Scheme 5.27a). This conclusion is consonant with the NMR spectroscopic studies reported in Scheme 5.22 indicating that, under the reaction conditions - that is, when the EDA complex between the enamine **I** and **2a** is formed and under illumination - the equilibrium position of the enamine formation is completely shifted toward the enamine **I**. This means that a negligible amount of catalyst **A** is available in its free state and, consequently, the concentration of **1a** does not affect the formation of the reactive enamine catalytic intermediate. In sharp contrast, our NMR studies established that the equilibrium of the

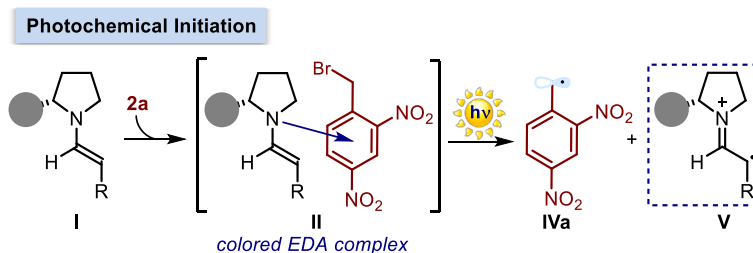
enamine formation is not perturbed by the addition of bromomalonate **2c**. In the direct photoexcitation of the enamine **I**, the amine catalyst **A** is partitioned between the free state and the enamine intermediate **I** (Scheme 5.27b). Thus, a definitive resting state cannot be identified, with the catalyst concentration shared between different intermediates. This situation is congruent with the observed positive fractional order in [**1a**] (Table 5.1).



Scheme 5.27 Order in the aldehyde **1a**. a) Influence of the EDA complex formation on the amount of enamine in solution. b) Equilibrium for the enamine formation not perturbed with bromomalonate **2c**. The filled grey circle represents a bulky substituent on the chiral amine catalyst.

Concerning the reaction rate's dependence on the alkyl halide **2**, the negative order in [**2a**] for the EDA complex-driven process (Table 5.1) deserves in-depth discussion. As previously mentioned, for any SET event taking place within the photoactive EDA complex (Scheme 5.28), a propagating radical **IV** is generated while a molecule of the chiral catalyst **A** is destroyed *via* decomposition of the unstable α -iminyl radical cation **V**.³⁶

³⁶ Monitoring [**A**] with an internal standard using both NMR spectroscopic and GC-FID analysis, we confirmed that the overall amount of the catalyst **A** decreased over time, further supporting the instability of the intermediate **V** generated upon photo-induced SET. Studies on the evolution of the catalyst concentration with time are reported in Section 5.5.2.



Scheme 5.28 Photochemical initiation of the α -alkylation of aldehydes with **2a** via EDA complex formation to afford the carbon-centered radical **IVa** and the α -iminyl radical cation **V**. The filled grey circle represents a bulky substituent on the chiral amine catalyst.

To verify whether the disappearance of the catalyst was related to the number of initiation events, we followed the evolution of $[A]$ ³⁷ over time across a range of concentrations of **2a**, which is the acceptor partner in the EDA complex formation.

The initial-rate measurements in Section 5.3.3 suggest that the decrease in $[A]$ correlates with the concentration of **2a**. If the rate of disappearance of $[A]$ is proportional to $[2a]^n$, then the data should fit Equation 5.4. As a result, the kinetic data can be plotted as indicated in Equation 5.5.

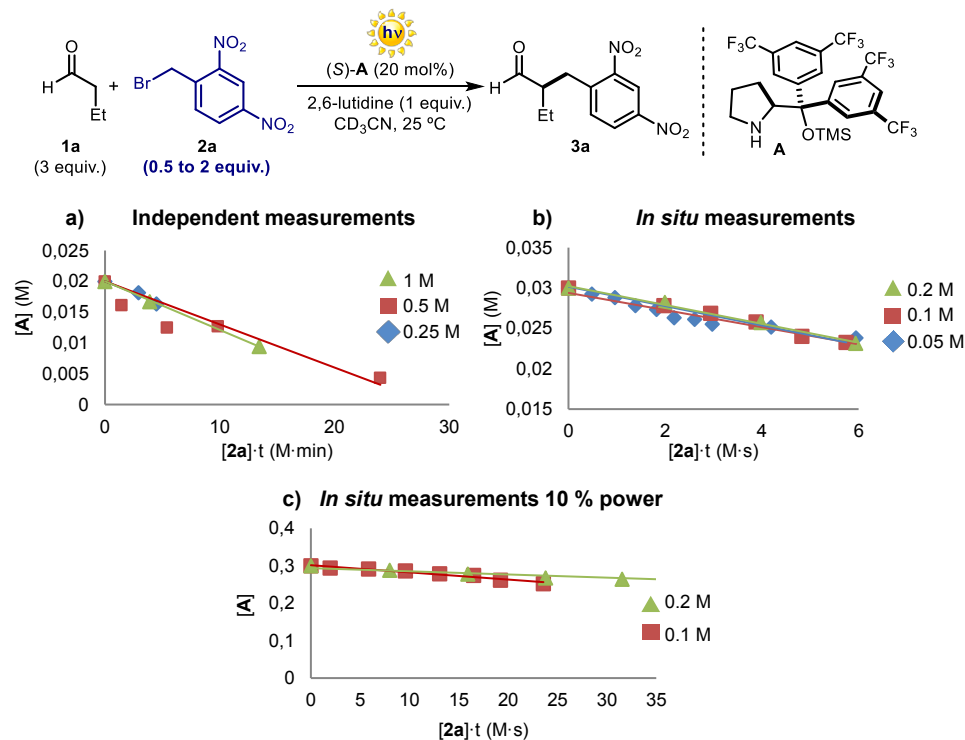
$$\text{disappearance of } A = -\frac{d[A]}{dt} \propto [2a]^n \quad (\text{Eq. 5.4})$$

$$[A] \propto [2a]^n \cdot t \quad (\text{Eq. 5.5})$$

Equation 5.5 indicates that, for reactions with the same initial concentrations of aminocatalyst **A**, plots of $[A]$ versus $[2a]^n \cdot t$ should be superimposable.³⁸ Scheme 5.29 shows such a superimposition for three reactions that have comparable initial concentrations of **A** but different concentrations of **2a**. In Scheme 5.29, the overlay found for plots of $[A]$ versus $[2a]^1 \cdot t$ ($n = 1$ in Equation 5.5) establishes a first-order dependence on $[2a]$ for the catalyst's disappearance. This behavior was observed when the reactions progress was monitored both *via* independent measurements and *in situ* NMR monitoring of the reaction progress. Such first order dependence with respect to **2a** suggests that one molecule of the acceptor is involved in the event that triggers the catalyst decomposition.

³⁷ Since there is zeroth-order dependence in $[1a]$ and due to the fact that we could not detect any trace of catalyst **A** in its free state by NMR analysis, we monitored the evolution of **A** in our experiments by determining the enamine concentration in solution.

³⁸ For a similar treatment of kinetic data for a reaction proceeding through a radical chain mechanism, see: Boisvert, L.; Denney, M. C.; Kloek Hanson, S.; Goldberg, K. I. "Insertion of molecular oxygen into a palladium (II) methyl bond: a radical chain mechanism involving palladium (III) intermediates" *J. Am. Chem. Soc.* **2009**, *131*, 15802.



Scheme 5.29 Overlay of plots for the kinetic data in Section 5.5.2 according to Equation 5.5 for $n=1$ for reactions containing different initial concentrations of **2a** performed at 298 K in CD_3CN . a) Progress of the reactions followed by ^1H NMR analysis; each point corresponds to an individual run. Illumination by a xenon lamp with a band-pass filter at 450 nm (irradiance = $4.7 \text{ mW}/\text{cm}^2$). $[\mathbf{2a}]_0 = 0.25 \text{ M}$ (blue line), $[\mathbf{2a}]_0 = 0.5 \text{ M}$ (red line) and $[\mathbf{2a}]_0 = 1 \text{ M}$ (green line). b) Experiments performed in NMR tubes using a monochromatic light ($\lambda = 470 \text{ nm}$, irradiance $28.8 \text{ mW}/\text{cm}^2$); $[\mathbf{2a}]_0 = 0.05 \text{ M}$ (blue line), $[\mathbf{2a}]_0 = 0.1 \text{ M}$ (red line) and $[\mathbf{2a}]_0 = 0.2 \text{ M}$ (green line). c) Experiments performed in NMR tubes using a monochromatic light ($\lambda = 470 \text{ nm}$, irradiance $3.0 \text{ mW}/\text{cm}^2$); $[\mathbf{2a}]_0 = 0.1 \text{ M}$ (red line) and $[\mathbf{2a}]_0 = 0.2 \text{ M}$ (green line).

Using the *in situ* monitoring approach, we performed two sets of experiments under the same conditions, but using a different intensity of irradiation ($\lambda = 470 \text{ nm}$ for both sets of experiments, but irradiance = 28.8 vs. $3.0 \text{ mW}/\text{cm}^2$, Scheme 5.29b and c). In the latter set of experiments, a lower absolute rate of catalyst degradation was determined, in consonance with a less effective initiation regime. This observation establishes a direct correlation between the disappearance of catalyst **A** and the number of photochemical initiation events, since both the concentration of **2a** and the intensity of light influence the rate of degradation for catalyst **A**.

We then wanted to measure the real effect of $[\mathbf{2a}]$ on the rate of alkylation leading to product **3a**, discounting the effects of catalyst **A** degradation in the initiation regime.

Considering the zeroth-order dependence on **1a**, the rate equation should read as Equation 5.6, with n being the rate order with respect to **2a**, overlooking its effect on $[A]$. Equation 5.7 is readily derived from Equation 5.6 and discounts the effect of the catalyst degradation on the product formation as $[3a]$ is normalized by $[A]$. Equation 5.8 is derived from Equation 5.7.

$$\text{rate} = \frac{d[3a]}{dt} \propto [A] \cdot [2a]^n \quad (\text{Eq. 5.6})$$

$$\frac{[3a]}{[A]} \propto [2a]^n \cdot t \quad (\text{Eq. 5.7})$$

$$\log\left(\frac{[3a]}{[A] \cdot t}\right) = n \cdot \log([2a]) + \log(c) \quad (\text{Eq. 5.8})$$

The order with respect to **2a** (n) was calculated by plotting the data according to Equation 5.8 (Figure 5.6a). The value of n is obtained from the slope of this logarithmic plot. It indicates a *positive* fractional-order dependence on **2a** ($n \approx 0.4$). Figure 5.6b displays the fitting of the kinetic data according to Equation 5.7 for $n=0.4$, showing a good overlay.

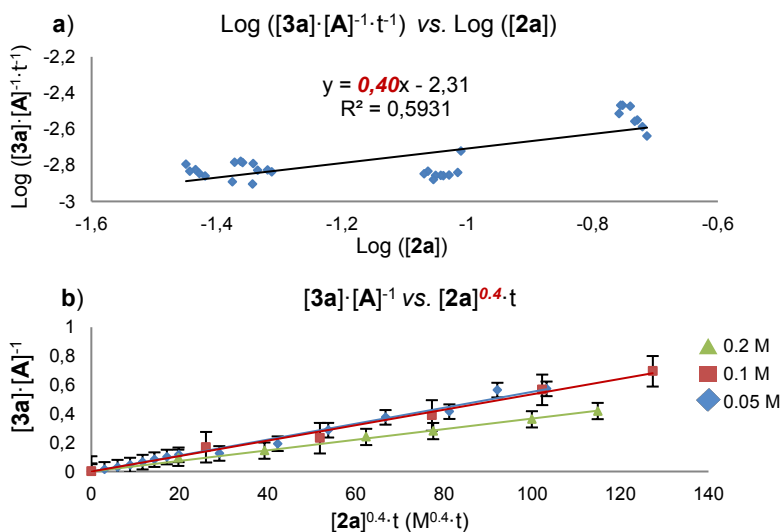
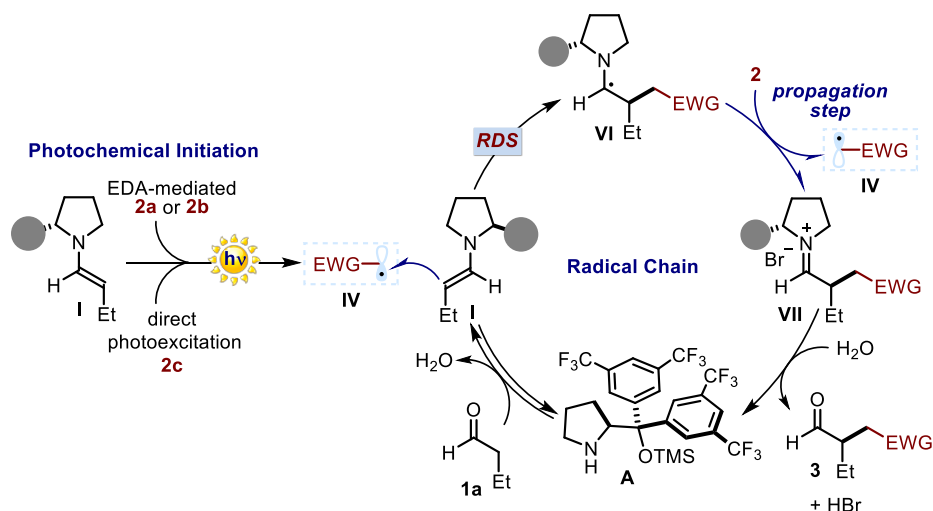


Figure 5.6 a) Logarithmic plot of the kinetic data according to Equation 5.8, slope shows $n = 0.4$. b) Plot of the kinetic data according to Equation 5.7 for $n = 0.4$. The plots should be superimposable for the value of n that better renders the reaction order with respect to **2a**. For this fitting, we have used the data obtained by *in situ* NMR monitoring of the reaction progress, which gives the same kinetic profiles as the other methodology (see Section 5.5.3). This approach has the advantage to provide a larger number of data, thus allowing for a more reliable fitting. Experiments performed in NMR tubes at 298 K in CD_3CN using a monochromatic light ($\lambda = 470$ nm, irradiance 28.8 mW/cm²); $[1a]_0 = 0.3$ M, $[A]_0 = 0.02$ M; initial concentrations of **2a**: 0.05 M (blue plot); 0.1 M (red plot) and 0.2 M (green plot). The error bars represent the standard deviation.

Overall, Equation 5.9 gives the empirical rate law for the EDA complex-mediated alkylation of butanal in Scheme 5.26a, discounting catalyst degradation related to the photochemical initiation:

$$\text{rate} = \frac{d[\mathbf{3a}]}{dt} = k \cdot [\mathbf{A}] \cdot [\mathbf{2a}]^{\approx 0.4} \quad (\text{Eq. 5.9})$$

The rate law indicates a turnover-limiting step within the radical chain propagation cycle (Scheme 5.30). If the initiation step was turnover-limiting, a first-order dependence with respect to both EDA partners **I** and **2a** would be expected instead. The first-order dependence on catalyst **A** (whose concentration is equal to the enamine **I** concentration) suggests that the turnover-limiting step is the trapping of the electrophilic carbon-centered radical **IV** from the ground-state chiral enamine **I** to form the new carbon-carbon bond. We would expect higher-order dependence in **[2a]** if the turnover-limiting step were the SET process, which regenerates the chain-propagating radical **IV** from the α -aminoalkyl radicals **VI**. Still, the feasibility for this step being rate-limiting cannot be completely excluded.



Scheme 5.30 General mechanism for the photochemical enantioselective α -alkylation of aldehydes. RDS: rate-determining step. The filled grey circle represents a bulky substituent on the chiral amine catalyst.

The alkylation of **1a** with bromomalonate, driven by the direct excitation of enamine, shows a fractional order in **[2c]**. The overall rate equation is then given by Equation 5.10:

$$\text{rate} = \frac{d[\mathbf{3c}]}{dt} = k \cdot [\mathbf{A}] \cdot [\mathbf{1a}]^{0.5} \cdot [\mathbf{2c}]^{0.5} \quad (\text{Eq. 5.10})$$

In analogy with the preceding discussion, the rate-order assessment indicates that the turnover-limiting step is the enamine trapping the electrophilic radical **IV**, derived from **2c**, to form the carbon-carbon bond (Scheme 5.30).

Notable, no significant degradation of catalyst **A** was observed during the alkylation with **2c** within the timeframe of interest for the initial-rate measurements using the method of independent experiments. When monitoring the progress of the alkylation with **2c** using *in situ* NMR methodology, we did observe catalyst degradation. This is presumably because of decomposition pathways triggered by the presence of oxygen in the system, as *in situ* monitoring did not allow for complete de-oxygenation of the reaction medium. When extending the time of irradiation of the photochemical alkylation with **2c**, the disappearance of catalyst **A** became significant. However, using the same 23 W CFL light source and considering the same time interval, the catalyst degradation was much higher in the alkylations of **2a** and **2b** than **2c** (details in Section 5.5.1). This observation, along with the measured quantum yields of photo-initiation ($\Phi_{\text{initiation}} = 0.77, 0.68, \text{ and } 0.11$ for **2a**, **2b**, and **2c**, respectively), suggests that the direct excitation of the enamine **I** is a less effective radical generation strategy than the enamine-based EDA complex approach. This scenario can be rationalized on the basis of the bimolecular nature of the initiation mechanism with **2c**, which requires the excited enamine to encounter **2c** for an effective SET. These conditions make an unproductive relaxation of the excited intermediate, which restores the ground-state enamine, more likely. In contrast, the photochemistry underlying the processes with **2a** and **2b** is dominated by EDA complexes. These aggregates form in the ground-state, holding together the two partners involved in the following photo-induced SET. In this case, the initiation mechanism is based on a more efficient unimolecular process.

5.4 Conclusions and remarks

A thorough investigation of the key mechanistic aspects of the previously reported asymmetric photochemical α -alkylation of aldehydes driven by both the formation of electron donor-acceptor complexes and the direct photochemical activity of enamines has been carried out. Measurements of the quantum yield provided evidence for a radical chain mechanism in both processes. Additionally, initial rate kinetic studies of the transformations contributed to confirm the radical chain process and pointed towards the trapping of the carbon centered radical **IV** by the enamine **I** as the turnover-limiting step. Furthermore, we presented evidence that the generation of EDA complexes can increase the reactivity of the system by influencing the enamine concentration in solution.

From a broader perspective, this study demonstrates that the synthetic potential of chiral enamines is not limited to the ground-state domain, but can be further expanded by

exploiting their photochemical activity, providing novel reactivity frameworks for conceiving light-driven enantioselective catalytic processes. The knowledge acquired during this study may serve for the development of new enamine-driven photochemical alkylations.

5.5 Experimental section

General information: The ^1H and ^{13}C NMR spectra were recorded at 400 MHz or 500 MHz for ^1H and at 100 MHz or 125 MHz for ^{13}C , respectively. The chemical shifts (δ) for ^1H and ^{13}C are given in ppm and are internally referenced to residual protio solvent signals (for CDCl_3 @ 7.26 ppm and 77.0 ppm, respectively; for CD_3CN @ 1.96 ppm ^1H NMR, 118.26 ppm and 1.79 ppm ^{13}C NMR). Coupling constants are given in Hz. When necessary, ^1H and ^{13}C signals were assigned by means of g-COSY 2D-NMR sequence. The following abbreviations are used to indicate the multiplicity: s, singlet; d, doublet; t, triplet; q, quartet; qn, quintet; m, multiplet; bs, broad signal. Optical rotations are reported as follows: $[\alpha]_D^{25}$ (c in g per 100 mL, solvent). Mass spectra (high and low resolution) were obtained from the ICIQ High Resolution Mass Spectrometry Unit on a Bruker Maxis Impact (QTOF) or Waters Micromass LCT-Premier (TOF) in Electrospray Ionization (ESI) by direct infusion. UV-vis measurements were carried out on a Shimadzu UV-2401PC spectrophotometer equipped with photomultiplier detector, double beam optics and D₂ and W light sources. Cyclic voltammetry studies was carried out on a Princeton Applied Research PARSTAT 2273 potentiostat offering compliance voltage up to ± 100 V (available at the counter electrode), ± 10 V scan range and ± 2 A current range.

The ^1H , ^{13}C NMR spectra and the HPLC traces are available in the literature^{1,2} and are not reported in the present thesis.

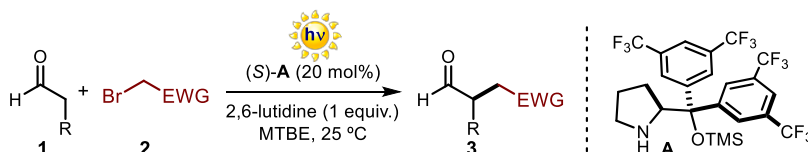
General procedures: All reactions were set up under an argon atmosphere in oven-dried glassware using standard Schlenk techniques, unless otherwise stated. Synthesis grade solvents were used as purchased and the reaction mixtures were deoxygenated by three cycles of freeze pump thaw. Chromatographic purification of products was accomplished using flash chromatography (FC) on silica gel (35-70 mesh). For thin layer chromatography (TLC) analysis throughout this work, Merck precoated TLC plates (silica gel 60 GF₂₅₄, 0.25 mm) were employed, using UV light as the visualizing agent and an acidic mixture of *para*-anisaldehyde or basic aqueous potassium permanganate (KMnO_4) stain solutions, and heat as developing agents. Organic solutions were concentrated under reduced pressure on a Büchi rotatory evaporator.

Determination of enantiomeric purity: HPLC analysis on chiral stationary phase was performed on an Agilent 1200-series instrument. Daicel Chiralpak IA or IC columns with hexane:*i*PrOH or hexane:*i*PrOH:DCM as the eluents were used. HPLC traces were compared to racemic samples of products **3a-c** prepared using a catalytic amount of morpholine (30 mol%).

Materials: Reagents were purchased at the highest commercial quality from Sigma Aldrich, Fluka, and Alfa Aesar and used as received, without further purification, unless otherwise stated.

The chiral secondary amine catalyst (*S*)-**A** is commercially available; catalyst (*S*)-**A** was purified by column chromatography (from pure hexane to hexane:Et₂O 1:1) prior to use and stored at 4 °C under argon to avoid desilylation of the tertiary alcohol. Both phenacyl bromide (**2b**) and diethyl bromomalonate (**2c**) are commercially available as well as butanal (**1a**). They were vacuum distilled prior to use. 2,4-Dinitrobenzyl bromide (**2a**) was prepared upon bromination of the commercially available 2,4-dinitrotoluene **5**, according to literature.³⁹ Enamine **4** was synthesized by condensation of the chiral amine **A** and the commercially available 2-phenylacetaldehyde according to literature.^{2b}

General procedure for the photochemical organocatalytic enantioselective alkylation



A 10 mL Schlenk tube was charged with the aminocatalyst (*S*)-**A** (20 mol%), MTBE (0.5 M referring to the alkyl bromide **2**), butanal **1a** (3 equiv.), 2,6-lutidine (1 equiv.) and the alkylating agents **2a-c** (1 equiv.). The reaction mixture was degassed *via* freeze pump thaw (x3), and the vessel back-filled with argon. The vial was then sealed and positioned approximately 5 cm away from a light source. After stirring for the indicated time, the crude mixture was purified by flash column chromatography to afford the title compounds **3a-c** in the stated yield and optical purity.

Purification by flash column chromatography on silica gel:

Compound **3a**: gradient eluent from pure hexane to 9:1 hexane:EtOAc.

Compound **3b**: gradient eluent from pure hexane to 95:5 hexane:EtOAc.

Compound **3c**: 10:1 hexane:EtOAc.

The enantiomeric excess was determined by HPLC analysis using the following conditions:

Compound **3a**: Daicel Chiralpak IC column, 70:30 hexane:*i*PrOH, flow rate 1.00 mL/min, $\lambda = 254$ nm: $\tau_{\text{minor}} = 16.7$ min, $\tau_{\text{major}} = 19.9$ min.

³⁹ Jan, T.; Dupas, B.; Floner, D.; Moinet, C. "Electrosynthesis of dibenzonaphthyridine derivatives from 2, 2-(2-nitrobenzyl)-2-substituted-acetonitriles" *Tetrahedron lett.* **2002**, *43*, 5949.

Compound **3b**: Daicel Chiralpak IA column, 98:2 hexane:*i*PrOH, flow rate 1.00 mL/min, $\lambda = 254$ nm: $\tau_{\text{minor}} = 12.0$ min, $\tau_{\text{major}} = 13.4$ min.

Compound **3c**: Daicel Chiralpak IA column, eluent 97:3 hexane:*i*PrOH, flow rate 1.00 mL/min, $\lambda = 215$ nm: $\tau_{\text{minor}} = 8.6$ min, $\tau_{\text{major}} = 9.3$ min.

Products **3a**, **3b**, and **3c** were fully characterized and the data corresponds with literature (2a, 2b).

Light Sources used in these studies:

- CFL light: A set of two household full spectrum 23 W compact fluorescent light (CFL) bulbs were used for irradiating the reaction mixture.

- Blue LED ($\lambda_{\text{max}} = 450$ nm): Commercialized under the name of blue LED Emitter LZ4-00B208. It was purchase from LED Engin. The LZ4-00B208 Blue LED emitter is a set of 4 single LEDs which provides 10W power centered at 450 nm. The irradiance at 2 cm of distance was 90.6 mW/cm².

- Cut off and band-pass photochemical experiments have been performed using a 300 W xenon lamp (commercialized under the name of Max-303, *Asashi Spectra Co., Ltd.*) to irradiate the reaction mixture.

- *In situ* irradiation inside the NMR spectrometer was performed using a 150 W xenon lamp coupled to a monochromator. Commercialized under the name of Polychrome V, it was purchased from Till Photonics. It is a monochromatizing device with an integrated light source. The wavelength (320-680 nm) delivered by the Polychrome V is controlled from a computer and the monochromatic light is conducted directly into the NMR tube by an optic fiber probe. The bandwidth and intensity of the light can be adjusted.

5.5.1 Quantum yield measurements

The procedure described in the Chapter IV (Section 4.6.1) was employed for the quantum yield measurements. Accordingly, the photon flux ($q_{n,p}^0$) was calculated utilizing Equation 5.11 and the quantum yield of our reaction ($\Phi_{\text{reac}}(\lambda)$) was determined employing Equation 5.12.⁴⁰

$$q_{n,p}^0 = \frac{\text{molecules generated}_{\text{acti}}/dt}{\Phi_{\text{acti}}(\lambda) \cdot (1 - 10^{-A_{\text{acti}}(\lambda)})} \quad (\text{Eq. 5.11})$$

$$\Phi_{\text{reac}}(\lambda) = \frac{\text{molecules generated}_{\text{reac}}/dt}{q_{n,p}^0 \cdot (1 - 10^{-A_{\text{reac}}(\lambda)})} \quad (\text{Eq. 5.12})$$

⁴⁰ a) Braslavsky, S. E. "Glossary of terms used in photochemistry, (IUPAC Recommendations 2006)" *Pure and App. Chem.* **2007**, 79, 293. b) Sun, L.; Bolton, J. R. "Determination of the quantum yield for the photochemical generation of hydroxyl radicals in TiO₂ suspensions" *J. Phys. Chem.* **1996**, 100, 4127.

A reproducible and stable irradiation is required for the quantum yield and kinetic measurements. As a result, the reactions were performed without stirring to prevent any splash of the solution, as well as maintaining the surface of irradiation constant. Furthermore, acetonitrile was used as solvent to avoid the precipitation of the lutidinium bromide salt generated during the reaction, which is insoluble in MTBE. The presence of a precipitate would scatter the irradiating light thus precluding reliable measurements. In addition, all the experiments herein described were performed at least twice each time utilizing a different photon flux to ensure the experiments were carried out under light-limiting conditions.

Quantum yield measurement for the EDA complex-mediated reactions

Solutions utilized for the measurements:

The solutions were prepared and stored in a dark laboratory (red light):

1. Potassium ferrioxalate solution: 589.5 mg of potassium ferrioxalate (commercially available from Alfa Aesar) and 278 μL of sulfuric acid (96%) added to a 100 mL volumetric flask and diluted to a total volume of 100 mL with water (HPLC grade).
2. Phenanthroline solution: 0.2% by weight of 1,10-phenanthroline in water (200 mg in 100 mL of water).
3. Buffer solution: 4.104 g of NaOAc and 1.0 mL of sulfuric acid (96%) were added to a 100 mL volumetric flask and diluted to a total volume of 100 mL with water (HPLC grade).
4. Model reaction solution: a stock solution containing 300 mg of the aminocatalyst **A** (0.5 mmol), and 300 μL of 2,6-lutidine (2.5 mmol) were added to a 5.0 mL volumetric flask and diluted to a total volume of 5.0 mL with acetonitrile (HPLC grade). To 1 mL of this solution, butyraldehyde **1a** (135 μL , 1.5 mmol, 3 equiv.) and 2,4-dinitrobenzyl bromide **2a** (130 mg, 0.5 mmol, 1 equiv.) were sequentially added. The mixture was kept in the dark for 20 minutes (1 hour in the case of the phenacyl bromide **2b**) in order to reach a constant amount of EDA in solution. Concomitantly, 1 mL of this mixture was degassed *via* freeze pump thaw and used to run the experiment.

Procedure for the sample irradiation:

1 mL of the actinometer solution and 1 mL of the degassed model reaction (alkylation of **1a** with **2a** or **2b**), whose quantum yield is being measured, were added to two identical quartz cuvettes ($l = 1$ cm). The cuvettes were placed 10 cm away from the light source. They were irradiated together with a 300 W xenon lamp operating at 50% of light

intensity with a bandpass filter of 450 ± 5 nm without stirring. This procedure was repeated 4 times, quenching the reactions after different time intervals: 10, 12.5, 15, and 17.5 minutes.

Photon flux calculation:

The moles of Fe^{2+} formed (calculated spectrophotometrically) are plotted as a function of time to obtain the numerator of Equation 5.11 as the slope of this line.

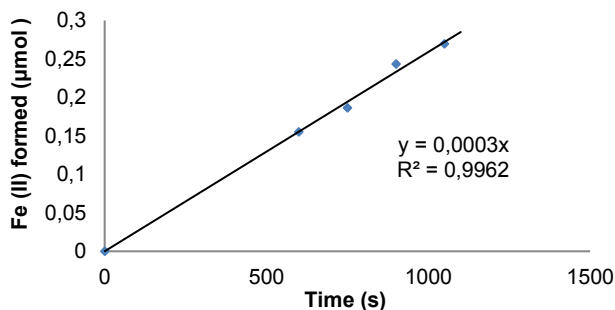


Figure 5.7 Relation between the moles of Fe (II) formed and the reaction time for the potassium ferrioxalate actinometer reaction.

Finally, the denominator of Equation 5.11 can be easily calculated from the quantum yield for the actinometer at 450 nm ($\Phi_{\text{acti}}(450 \text{ nm}) = 0.9$)⁴¹ and $A_{\text{acti}}(450)$, the absorbance of the actinometer solution at the excitation wavelength (450 nm). The absorbance was measured using a Shimadzu 2401PC UV-Vis spectrophotometer in 1 mm path quartz cuvettes in the presence of the bandpass filter of 450 nm employed to run the measurements. An absorbance of 0.156 was obtained. Therefore, the photon flux ($q_{\text{n,p}}^0$) was determined to be $9,58 \cdot 10^{-10}$ einstein s^{-1} .

Quantum yield calculation:

The quantum yield of the reaction under study was determined according to Equation 5.12. The moles of products formed (reaction performed by irradiating the sample alongside with the actinometer solution) were determined by GC measurement (FID detector) using 2,4-dinitrotoluene as internal standard when using **2a** as the substrate. 1,3,5-trimethoxybenzene was used instead when the alkylation was performed with phenacyl bromide **2b**. The number of moles of product was plotted as a function of time to obtain the numerator of Equation 5.12.

⁴¹ Hamai, S.; Hirayama, F. "Actinometric determination of absolute fluorescence quantum yields" *J. Phys. Chem.* **1983**, *87*, 83.

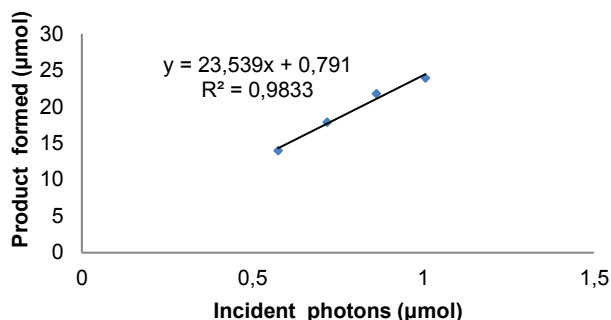


Figure 5.8 Relation between the moles of product formed and the moles of incident photons for the reaction between **1a** and **2a**.

The denominator of Equation 5.12 can be calculated from the previously obtained photon flux ($q_{n,p}^0$) and $A_{\text{reac}}(450)$, the absorbance of the reaction under study at the excitation wavelength (450 nm). The absorbance was measured using a Shimadzu 2401PC UV-Vis spectrophotometer in 1 mm path quartz cuvettes in the presence of the bandpass filter of 450 nm. An absorbance of 1.05 was determined for the reaction with **2a**.

The quantum yield (Φ_{measured}) of the photochemical alkylation of butanal **1a** with 2,4-dinitrobenzyl bromide **2a** catalyzed by **A** was calculated to be **26**. The procedure was repeated a second time to provide a similar value: quantum yield (Φ) at 450 nm of **24**. Using the same procedure, we calculated the quantum yield of the photochemical alkylation of butanal **1a** with phenacyl bromide **2b**. In this case, quantum yields of **19** and **20** were obtained in two independent experiments.

Quantum yield measurement for the alkylation with bromomalonate (**2c**)

The quantum yield measurement was performed following the procedure described in the previous section. Instead of using cuvettes, two identical Schlenk tubes were employed to run the experiments under complete absence of oxygen. The reaction mixtures, containing the actinometer and the model reaction, were placed alongside 10 cm away from a 300 W xenon lamp operating at 100% of light intensity with a bandpass filter of 400 ± 5 nm. The reaction mixtures were not stirred. The model reaction was prepared as follows: a stock solution was prepared adding 75 mg of the aminocatalyst **A** (0.125 mmol) and 146 μL of 2,6-lutidine (1.25 mmol) to a 5 mL volumetric flask while filling to the mark with acetonitrile (HPLC grade). To 1 mL of this solution, butyraldehyde **1a** (70 μL , 0.75 mmol, 3 equiv.) and ethyl bromomalonate **2c** (43 μL , 0.25 mmol, 1 equiv.) were added. Subsequently, 1 mL of this reaction mixture was degassed and used to run the experiment.

Photon flux calculation:

The moles of Fe (II) generated per second were measured. At 400 nm, the quantum yield (Φ) for Fe^{2+} is 1.13.⁴² The absorbance of the actinometer solution at 400 nm was measured using a Shimadzu 2401PC UV-Vis spectrophotometer in 1 mm path quartz cuvettes in the presence of the bandpass filter of 400 nm employed to carry out the measurements. An absorbance of 0.288 was obtained. And therefore, the photon flux $q_{n,p}^0$ was determined to be $2,73 \cdot 10^{-9}$ einstein s^{-1} .

Quantum yield calculation:

The quantum yield of the reaction under study was determined according to Equation 5.12. The moles of products formed (reaction performed by irradiating the sample alongside with the actinometer solution) were determined by ^1H NMR spectroscopy. The number of moles of product was plotted as a function of time to obtain the numerator of Equation 5.12.

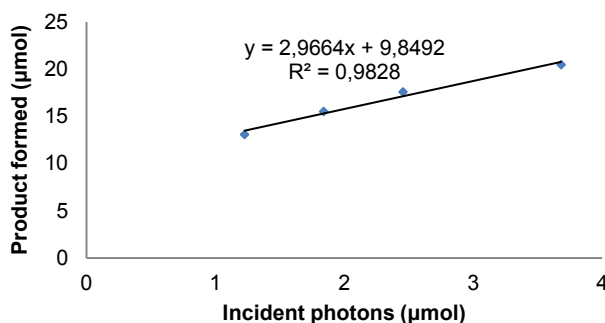


Figure 5.9 Relation between the moles of product formed and the moles of incident photons for the reaction between **1a** and **2c**.

The denominator of Equation 5.12 was calculated from the previously obtained photon flux ($q_{n,p}^0$) and $A_{\text{reac}}(400)$, the absorbance of the reaction under study at the excitation wavelength (400 nm). The absorbance was measured using a Shimadzu 2401PC UV-Vis spectrophotometer in 1 mm path quartz cuvettes in the presence of the bandpass filter of 400 nm. An absorbance of 0.069 was determined.

The quantum yield determined for the photochemical reaction of **1a** with **2c** was **20**.

Initiation step quantum yield and chain length estimations

The measured quantum yields (Φ_{measured}) are referred to the overall reactions. As such, these values do not take into account any possible non-productive processes which can

⁴² Murov, S. L. "Handbook of photochemistry" 1973 Marcel Dekker.

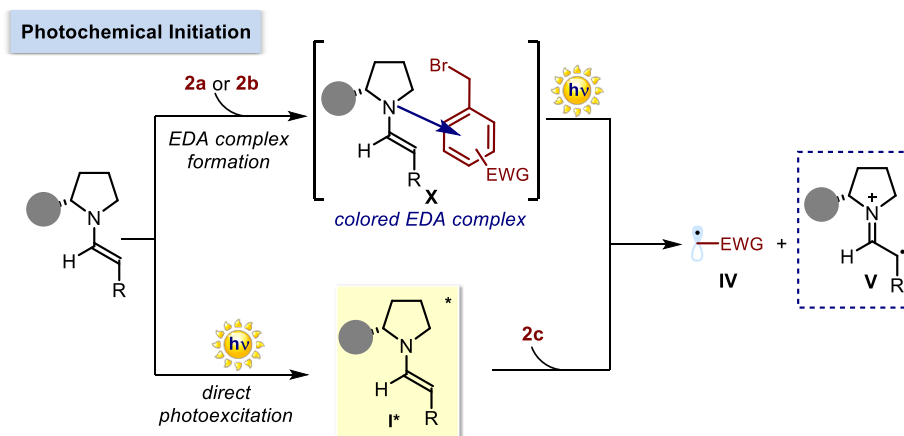
reduce the efficiency of the photo-initiation, directly affecting the overall quantum yield (Φ_{measured}). For example, the photoexcited enamine could relax to the ground-state *via* either radiative or vibrational pathways without undergoing electron-transfer processes, while a back-electron transfer from the chiral ion-pair **III** (Scheme 5.9) would unproductively restore the ground-state enamine-based EDA complex **II**.

To better estimate the actual chain length of the reactions, we measured the quantum yield of the initiation step ($\Phi_{\text{initiation}}$). These measurements will allow us to calculate a more accurate chain length ($\Phi_{\text{estimated}}$) as given by the following equation.

$$\text{Chain length} = \Phi_{\text{estimated}} = \frac{\Phi_{\text{measured}}}{\Phi_{\text{initiation}}} \quad (\text{Eq. 5.13})$$

Using the procedure described in the previous sections, the quantum yield of the initiation step was measured to better estimate the effective chain length. This has been done by monitoring the decomposition of the catalyst **A**.

According to the proposed mechanism, each initiation step affords an equivalent of the carbon-centered radical **IV**, which propagates the chain, together with an equivalent of the α -iminyl radical cation **V**, which degrades (Scheme 5.31). In consequence, the enamine **I**, generated upon condensation of catalyst **A** and butanal **1a**, serves as a sacrificial initiator of the chain mechanism and every initiation event destroys an equivalent of catalyst **A** *via* decomposition of the intermediate **V** (see Section 5.5.2 for a detailed discussion). Thus, any photo-induced initiation consumes a molecule of the catalyst **A**, and the rate of decomposition correlates with the efficiency of the chain initiation.



Scheme 5.31 Photochemical initiation of the α -alkylation of aldehydes *via* either EDA complex formation or direct enamine photoexcitation to render carbon-centered radical **IV** and the α -iminyl radical cation **V**. The filled grey circle represents a bulky substituent on the chiral amine catalyst.

Quantum yield of the initiation step for the EDA complex-mediated reactions

Our analysis requires that the decomposition of the catalyst **A** is triggered by a productive photochemical initiation only and not by other secondary reactions. To avoid any side reaction with oxygen which would degrade the catalyst, the experiments were carried out in identical Schlenk tubes, as they allow a thorough degassing process.

The photon flux was calculated utilizing potassium ferrioxalate as actinometer. Two identical Schlenk tubes, containing the actinometer solution and the degassed model reaction (alkylation of **1a** with **2a** catalyzed by **A**), were placed 10 cm away from the light source. They were irradiated together with a 300 W xenon lamp operating at 50% of light intensity with a bandpass filter of 450 ± 5 nm.

The moles of Fe (II) generated per second were measured and a photon flux ($q_{n,p}^0$) of $5.50 \cdot 10^{-9}$ einstein s^{-1} was determined using Equation 5.11.

The quantum yield of the reaction under study was calculated according to Equation 5.12. The moles of remaining catalyst **A** were determined by GC measurement (FID detector) using 1,3,5-trimethoxybenzene as internal standard (see Section 5.5.2 for details). The number of moles of catalyst degraded was plotted as a function of time to obtain the numerator of Equation 5.12.

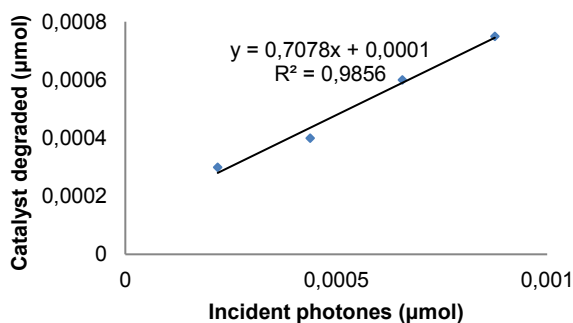


Figure 5.10 Relation between the moles of catalyst (**A**) formed and the moles of incident photons for the reaction between **1a** and **2a**.

The denominator of Equation 5.12 was calculated from the previously obtained photon flux ($q_{n,p}^0$) and $A_{\text{reac}}(450)$, the absorbance of the reaction under study at the excitation wavelength (450 nm). The absorbance was measured using a Shimadzu 2401PC UV-Vis spectrophotometer in 1 mm path quartz cuvettes in the presence of the bandpass filter of 450 nm. An absorbance of 1.05 was determined for the reaction with **2a**.

The quantum yield of initiation ($\Phi_{\text{initiation}}$) for the photochemical alkylation of butanal **1a** with 2,4-dinitrobenzyl bromide **2a** catalyzed by **A** was calculated to be **0.77**, meaning that the actual chain length of the model reaction ($\Phi_{\text{estimated}}$, see Equation 5.13) would

have a lower limit of **32**. The same procedure was repeated for the photochemical alkylation of **1a** with phenacyl bromide **2b**, affording a quantum yield of initiation ($\Phi_{\text{initiation}}$) of **0.68**. As a result, the actual chain length can be approximated to **29**.

Quantum yield of the initiation step for the for the alkylation with bromomalonate

The quantum yield of the initiation step was measured to better estimate the effective chain length for the reaction of **1a** and diethyl bromomalonate **2c**. The same procedure described for the estimation of the quantum yield of the initiation step for EDA mediated was repeated to monitor the decomposition of catalyst **A**. The photon flux $q_{n,p}^0$ was determined to be $2,45 \cdot 10^{-9}$ einstein s^{-1} .

The quantum yield of the reaction under study was determined according to Equation 5.12. The moles of remaining catalyst **A** were determined by GC measurement (FID detector) using 1,3,5-trimethoxybenzene as internal standard (see Section 5.5.2 for details). The number of moles of catalyst degraded was plotted as a function of time to obtain the numerator of Equation 5.12.

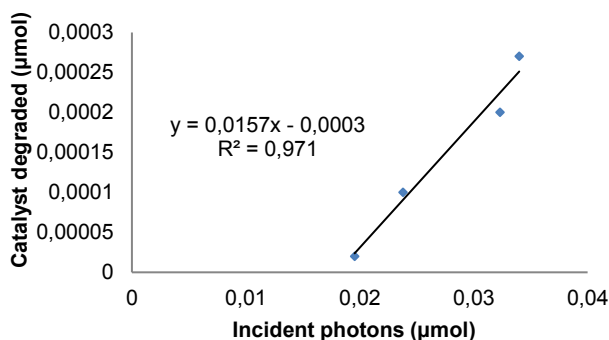


Figure 5.11 Relation between the moles of catalyst (**A**) formed and the moles of incident photons for the reaction between **1a** and **2c**.

The denominator of Equation 5.12 was calculated from the previously obtained photon flux ($q_{n,p}^0$) and $A_{\text{reac}}(400)$, the absorbance of the reaction under study at the excitation wavelength (400 nm). The absorbance was measured using a Shimadzu 2401PC UV-Vis spectrophotometer in 1 mm path quartz cuvettes in the presence of the bandpass filter of 400 nm. An absorbance of 0.069 was determined.

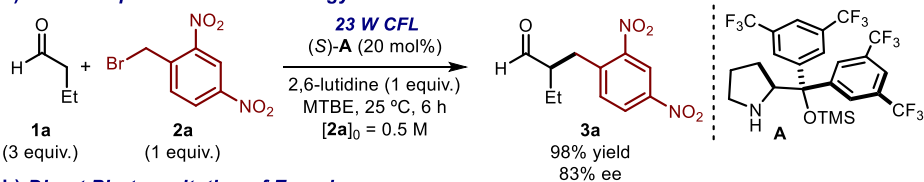
The quantum yield of initiation ($\Phi_{\text{initiation}}$) for the photochemical alkylation of butanal **1a** with diethyl bromomalonate **2c** catalyzed by **A** was calculated to be **0.11**. As a result, the actual chain length ($\Phi_{\text{estimated}}$, see Equation 5.13) can be approximated to **182**.

5.5.2 Evolution of the catalyst concentration over time

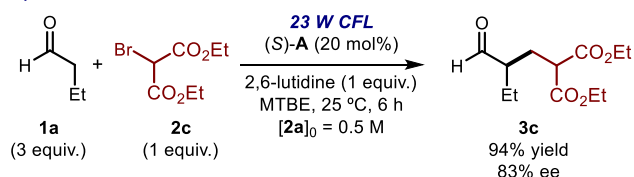
Experiments conducted irradiating with a CFL 23 W

The evolution of the catalyst **A** concentration under the optimal reaction conditions, depicted in Scheme 5.32, has been studied.

a) EDA Complex Activation Strategy



b) Direct Photoexcitation of Enamines



Scheme 5.32 Model reactions employed for the study of the catalyst concentration evolution over time.

A GC-FID was calibrated to correlate the signal of the catalyst **A** with the signal obtained for 1,3,5-trimethoxybenzene, which was used as the internal standard (**IS**). The calibration line is depicted in Figure 5.12.

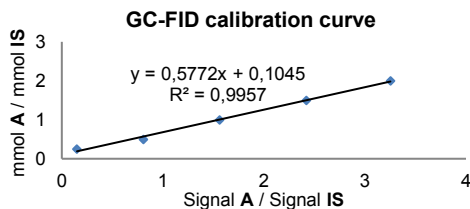


Figure 5.12 GC-FID calibration curve for different catalyst (**A**) to 1,3,5-trimethoxybenzene (**IS**) ratios.

For each one of the two-different photochemical alkylations in Scheme 5.32, three identical reactions were set up in Schlenk tubes according to the general procedure described in Section 5.5. The reactions were subsequently quenched after 2, 4, and 6 hours.

For the EDA-based system (Scheme 5.32a), a stock solution containing 47.6 mg of **A** (0.08 mmol) and 13.6 mg of 1,3,5-trimethoxybenzene (0.08 mmol) in 800 μL of MTBE was prepared. Each Schlenk tube was filled with 200 μL of the stock solution, 27 μL of **1a** (0.3 mmol, 3 equiv.), 12 μL of 2,6-lutidine (0.1 mmol, 1 equiv.) and 26 mg of **2a** (0.1

mmol, 1 equiv.). The solutions were thoroughly degassed with three cycles of freeze-pump-thaw and then placed 4 cm away from a 23 W CFL bulb.

For the alkylation with bromomalonate **2c** (Scheme 5.32b), the same procedure was carried out. An equivalent stock solution was prepared, each Schlenk tube was filled with 200 μL of the stock solution, 27 μL of **1a** (0.3 mmol, 3 equiv.), 12 μL of 2,6-lutidine (0.1 mmol, 1 equiv.) and 17 μL of **2c** (0.1 mmol, 1 equiv.). The solutions were thoroughly degassed with three cycles of freeze-pump-thaw and then placed 4 cm away from a 23 W CFL bulb.

The reactions were stopped after irradiating for 2, 4 or 6 hours and the amount of catalyst present was monitored by GC-FID. As shown in Table 5.2, the catalyst **A** degradation is more pronounced in the EDA complex-mediated alkylation with **2a**. For the α -alkylation of aldehydes with bromomalonate **2c**, a much slower degradation is observed.

Table 5.2 Evolution of the [**A**] and the product **3** formation over time.

Entry	Alkyl halide	time (h)	Yield of 3 ^a	Catalyst A remaining ^b
1	2a	2	3a , 36%	76%
2	2a	4	3a , 75%	40%
3	2a	6	3a , >95%	31%
4	2c	2	3c , 45%	85%
5	2c	4	3c , >95%	79%
6	2c	6	3c , >95%	78%

^a Determined by ¹H NMR analysis of the crude reaction mixture. ^b Yield of the remaining catalyst **A** measured by GC-FID.

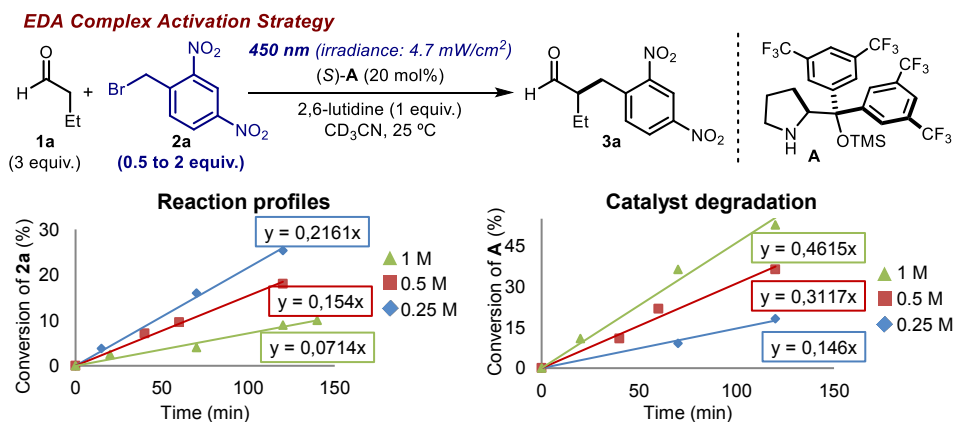
Experiments conducted irradiating with monochromatic light

A more thorough investigation of the change of the catalyst **A** concentration over time was carried out measuring the catalyst degradation irradiating with a more stable light source. We used a 300 W xenon lamp coupled with a band pass filter at 450 nm for the reaction with **2a** and a cut-off filter at 385 nm for the transformation driven by the direct photoexcitation of the enamine with **2c**. A series of experiments were performed in identical Schlenk tubes quenched at different conversions (all below 20% of conversion). These experiments were carried out with different initial concentrations of **2a** or **2c** and using NMR analysis to monitor the amount of catalyst in solution.

For the EDA-based system, sets of three reactions with equivalent concentrations of every reactant except for **2a** were carried out in three identical Schlenk tubes. The Schlenk tubes containing the degassed reaction mixtures were positioned 10 cm away from the light source. They were irradiated with 300 W xenon lamp operating at 100% of light intensity with a bandpass filter of 450 ± 5 nm without stirring (irradiance: 4.7 mW/cm^2). This procedure was repeated 4 times, quenching the reactions after different time intervals.

The model reaction was set up utilizing a stock solution containing 360 mg of the aminocatalyst **A** (0.6 mmol) and 15 mg of 1,3,5-trimethoxybenzene (employed as internal standard to measure the conversion of the enamine in solution) dissolved in 6 mL of CD_3CN . Butyraldehyde **1a** (54 μL , 0.6 mmol, 3 equiv.) was added to 400 μL of this solution, followed by the addition of 24 μL of 2,6-lutidine (0.2 mmol, 1 equiv.) and 54 mg of 2,4-dinitrobenzyl bromide **2a** (0.2 mmol, 1 equiv.). The reaction mixtures were degassed *via* freeze-pump-thaw (x 3 cycles), and the vessel refilled with argon. After irradiating for the indicated time, the conversion of 2,4-dinitrobenzyl bromide **2a** was checked by ^1H NMR and the remaining catalyst in solution was calculated employing 1,3,5-trimethoxybenzene as internal standard by integration of the enamine peaks (under the reaction conditions, no free catalyst **A** could be detected). For this reaction, the concentrations are: $[\text{A}] = 0.1 \text{ M}$, $[\mathbf{1a}] = 1.5 \text{ M}$, $[\mathbf{2a}] = [\text{2,6-lutidine}] = 0.5 \text{ M}$. Alongside with this reaction, other two identical solutions were prepared varying the concentration of the reagent **2a**: $[\mathbf{2a}]_0 = 0.25 \text{ M}$ and 1 M .

The experiments, performed irradiating with a xenon lamp with a band-pass filter at 450 nm, confirmed that the catalyst concentration in solution decreases as the reaction proceeds. Furthermore, a more rapid decrease in $[\text{A}]$ is observed when a higher concentration of **2a** is used (Scheme 5.33).



Scheme 5.33 Reaction profiles for different $[\mathbf{2a}]$ (*left* panel) irradiating at 450 nm (irradiance 4.7 mW/cm^2): $[\mathbf{2a}]_0 = 0.25 \text{ M}$ (blue line), $[\mathbf{2a}]_0 = 0.5 \text{ M}$ (red line) and $[\mathbf{2a}]_0 = 1 \text{ M}$ (green line). Evolution of the catalyst concentration in solution for the same reactions (*right* panel). Since there is zero-order dependence in $[\mathbf{1a}]$ and due to the fact that we could not detect any trace of catalyst **A** in its free state by NMR analysis, we monitored the change of the concentration of **A** in our experiments by determining the enamine concentration in solution.

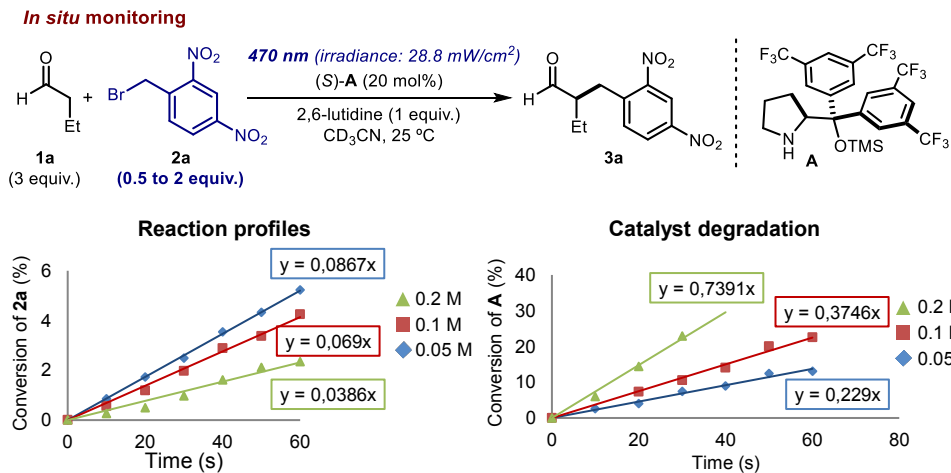
Equivalent experiments were carried out to study the change of catalyst **A** concentration over time in the alkylation of **1a** with **2c**. A 300 W xenon lamp operating at 100% of light intensity and equipped with a cut-off filter at 385 nm ($\lambda \geq 385$ nm; irradiance = 300 mW/cm²) was used to irradiate the reactions. In these experiments, conducted upon thorough de-oxygenation of the reaction medium, *no significant* degradation of catalyst **A** was observed below 20 % conversion.

Experiments conducted using *in situ* NMR monitoring

The reaction progress and the catalyst degradation were also followed using *in situ* monitoring by direct irradiation of non-degassed solutions. The reactions were run directly in the NMR tube, which precluded a thorough de-oxygenation of the reaction medium. For these experiments, we used a xenon lamp coupled with a monochromator that, by bringing the light in close contact with the NMR tube through an optical fiber, allowed for the *in situ* illumination of the samples. A larger rate of catalyst degradation was observed when the reaction was conducted in the presence of oxygen (degassing the reaction mixtures *via* freeze-pump-thaw was unviable).

The reactions were carried out employing a regular NMR tube as the reaction vessel. They were irradiated at 470 nm with a 150 W xenon high stability light lamp Tilluxe P45 coupled to a monochromator for exact wavelength definition. This polychromator is connected to an optical fiber that can be directly introduced into the NMR tube. This allowed us to monitor the reactions in real time with *in situ* irradiation inside the NMR spectrometer. The conversion of **2a** was checked by ¹H NMR and the concentration of the remaining catalyst **A** in solution was calculated employing 1,3,5-trimethoxybenzene as internal standard. We monitored the evolution of **A** in our experiments by determining the enamine concentration as the catalyst **A** in its free state could not be detected by NMR analysis.

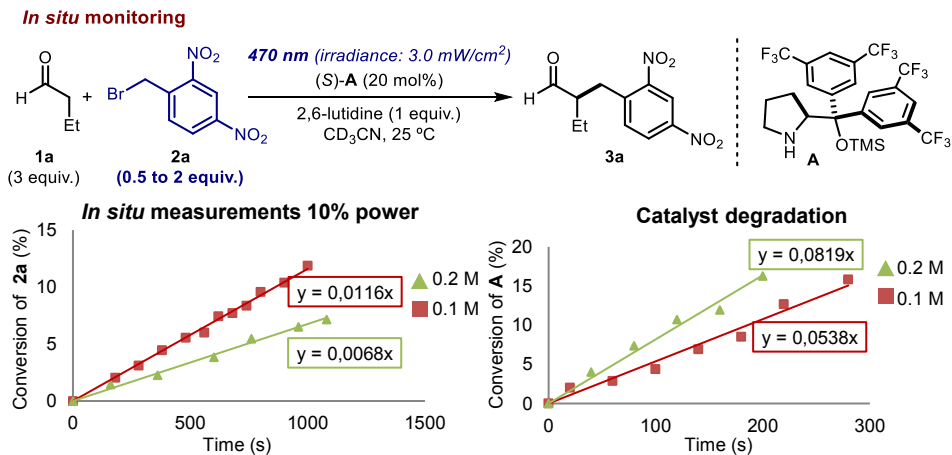
The model reaction (Scheme 5.34) was set up utilizing a stock solution containing 72 mg of the aminocatalyst **A** (0.12 mmol) and 3 mg of 1,3,5-trimethoxybenzene (employed as internal standard to measure the concentration of the enamine in solution) dissolved in 6 mL of CD₃CN. Butyraldehyde **1a** (13.5 μ L, 0.15 mmol, 3 equiv.) was added to 500 μ L of this solution, followed by the addition of 2,6-lutidine (6 μ L, 0.05 mmol, 1 equiv.), and 2,4-dinitrobenzyl bromide **2a** (13 mg, 0.05 mmol, 1 equiv.). Resultantly, the concentrations utilized for the model reaction were: $[\mathbf{A}] = 0.02$ M, $[\mathbf{1a}] = 0.3$ M and $[\mathbf{2a}] = [\text{2,6-lutidine}] = 0.1$ M. Alongside with this reaction, other two identical solutions were prepared with a different concentration of **2a**: $[\mathbf{2a}]_0 = 0.05$ M and 0.2 M.



Scheme 5.34 Reaction profiles for different [**2a**] (*left* panel) irradiating *in situ* at 470 nm (irradiance 28.8 mW/cm²): [**2a**]₀ = 0.05 M (blue line), [**2a**]₀ = 0.1 M (red line) and [**2a**]₀ = 0.2 M (green line). Evolution of the catalyst concentration in solution for the same reactions (*right* panel). Since there is zero-order dependence in [**1a**] and due to the fact that we could not detect any trace of catalyst **A** in its free state by NMR analysis, we monitored the change of the concentration of **A** in our experiments by determining the enamine concentration in solution.

Using the *in situ* monitoring of the processes, we confirmed that the catalyst concentration in solution decreases as the reaction proceeds. Furthermore, the decrease in [**A**] was again faster when the reaction was conducted in the presence of a higher concentration of **2a**. The same experiments as in Scheme 5.34 were repeated using a different intensity of irradiation ($\lambda = 470$ nm, but irradiance = 3.0 instead of 28.8 mW/cm²). In the latter set of experiments, detailed in Scheme 5.35, a lower absolute rate of catalyst disappearance was determined, in consonance with a less effective initiation regime.

This observation establishes a *direct correlation between the disappearance of catalyst A and the number of photochemical initiation events*, since both the concentration of **2a** and the intensity of light influence the rate of degradation for catalyst **A**.



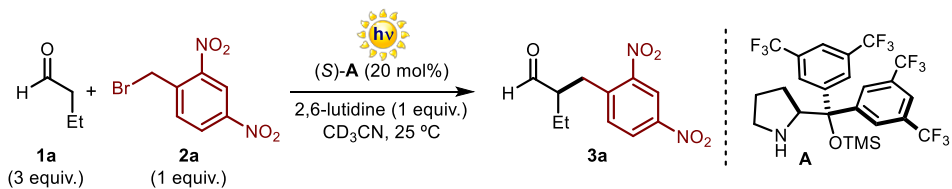
Scheme 5.35 Reaction profiles for different [2a] (*left panel*) irradiating *in situ* at 470 nm (irradiance 3.0 mW/cm²): [2a]₀ = 0.1 M (red line) and [2a]₀ = 0.2 M (green line). Change on the catalyst concentration in solution for the same reactions (*right panel*).

Equivalent experiments, using *in situ* irradiation, were carried out to study the evolution of the concentration of catalyst **A** in the reaction with **2c**. When irradiating at $\lambda = 400$ nm (irradiance = 20.4 mW/cm²), we *did observe catalyst degradation* (after 150 seconds of reaction, 5% yield of product **3c** and 97% of catalyst **A** remaining; after 350 seconds of reaction, 10% yield of product **3c** and 45% of catalyst **A** remaining).

This is presumably because of the decomposition pathways triggered by the presence of oxygen in the system, as *in situ* monitoring did not allow for complete de-oxygenation of the reaction medium.

5.5.3 Kinetic studies

Kinetic studies for the EDA complex-mediated alkylation of butanal with **2a**



Scheme 5.36 The EDA complex-mediated alkylation of butanal **1a** with 2,4-dinitrobenzyl bromide **2a**.

Two different procedures, detailed below as Methods A and B, have been used for the initial-rate kinetic measurements.

Method A - Independent experiments:

Three sets of reactions with identical concentrations of each reactant, except for the reagent whose order is being measured, were carried out in three identical Schlenk tubes. The Schlenk tubes containing the reaction mixtures were positioned laterally, 10 cm away from the light source. They were irradiated with 300 W xenon lamp operating at 100% of light intensity (irradiance: 4.7 mW/cm²) with a bandpass filter at 450 \pm 5 nm without stirring. This procedure was repeated 4 times quenching the reactions at different time intervals (this set-up required an independent reaction to be performed for every data-point at different times).

The model reaction was set up utilizing a stock solution containing 360 mg of the aminocatalyst **A** (0.6 mmol) and 15 mg of 1,3,5-trimethoxybenzene (employed as internal standard to measure the conversion of the enamine in solution) dissolved in 6 mL of CD₃CN. To 400 μ L of this solution (0.1 M in **A**), 54 μ L of butyraldehyde **1a** (0.6 mmol, 3 equiv.), 24 μ L of 2,6-lutidine (0.2 mmol, 1 equiv.) and 52 mg of 2,4-dinitrobenzyl bromide **2a** (0.2 mmol, 1 equiv.) were sequentially added. The reaction mixture was thoroughly degassed *via* freeze pump thaw (x 3 cycles), and the vessel refilled with argon. After irradiating for the indicated time, the conversion of 2,4-dinitrobenzyl bromide **2a** into the final product **3a** was determined by ¹H NMR analysis.

These conditions account for the following concentrations: [**A**] = 0.1 M, [**1a**] = 1.5 M and [**2a**] = 0.5 M and [2,6-lutidine] = 0.5 M.

Range of concentrations employed:

To measure the order with respect to each reactant, we varied the concentration of the reagent under study in the following ranges:

- [**A**] from 0.05 M to 0.2 M.
- [**1a**] from 0.75 M to 3 M.
- [**2a**] from 0.25 M to 1 M.
- H₂O from anhydrous to 1 M.

Method B - In situ monitoring of the reaction progress:

The reactions were carried out utilizing the same stoichiometry as described in Method A. However, no degassing process was carried out and the reaction vessel was a regular NMR tube. The reactions were irradiated at 470 nm with a 150 W high-stability light xenon lamp Tilluxe P45 coupled to a monochromator for exact wavelength definition (irradiance: 28.8 mW/cm² at 2 mm). The monochromator was connected to an optical fiber which was directly introduced into the NMR tube inside the instrument (Bruker, 500 MHz). The conversion of 2,4-dinitrobenzyl bromide **2a** into the final product **3a** was

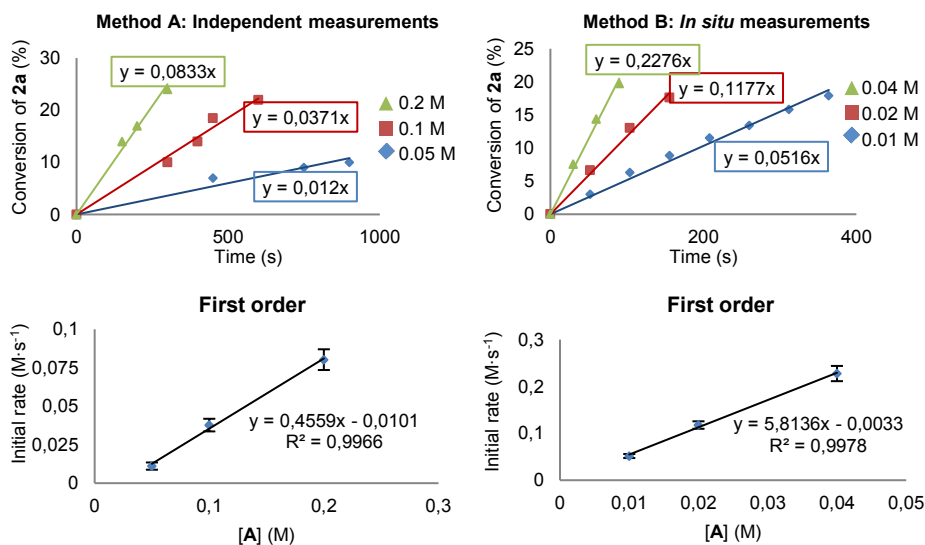
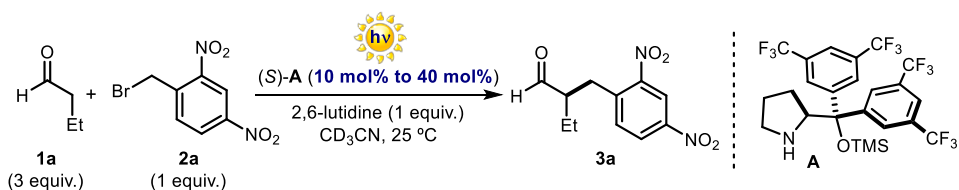
determined by ^1H NMR spectroscopy. This process was repeated changing the stoichiometry of the reactants as explained above.

The model reaction was set up utilizing a stock solution containing 72 mg of the aminocatalyst **A** (0.12 mmol) and 3 mg of 1,3,5-trimethoxybenzene (employed as internal standard to measure the conversion of the enamine in solution) dissolved in 6 mL of deuterated acetonitrile. To 500 μL of this solution (0.02 M in **A**), butyraldehyde **1a** (13.5 μL , 0.15 mmol, 3 equiv.), 2,6-lutidine (6 μL , 0.05 mmol, 1 equiv.) and 2,4-dinitrobenzyl bromide **2a** (13 mg, 0.05 mmol, 1 equiv.) were sequentially added. These conditions account for the following concentrations: $[\text{A}] = 0.02$ M, $[\mathbf{1a}] = 0.3$ M, $[\mathbf{2a}] = 0.1$ M and $[\text{2,6-lutidine}] = 0.1$ M.

Range of concentrations employed:

To measure the order with respect to each reactant, we used the conditions described above while varying the concentration of the reagent under study in the following ranges:

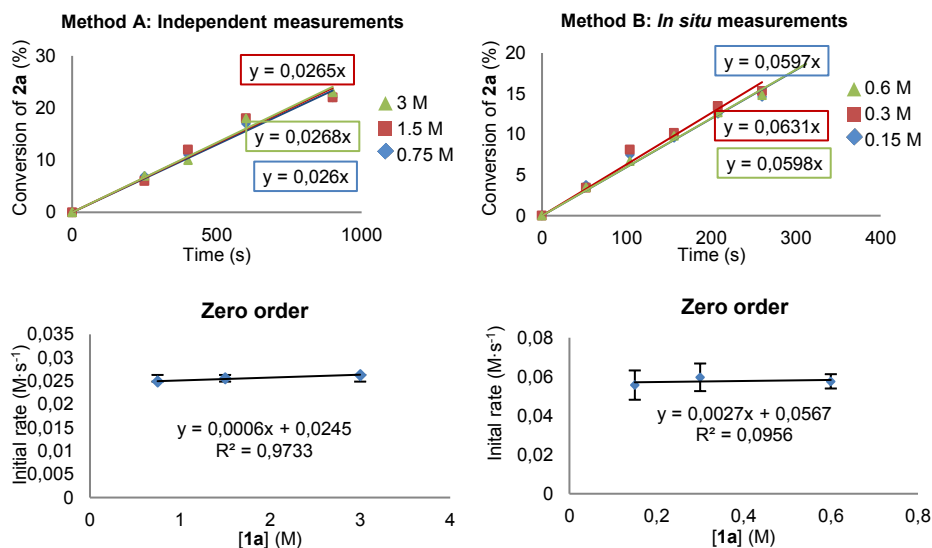
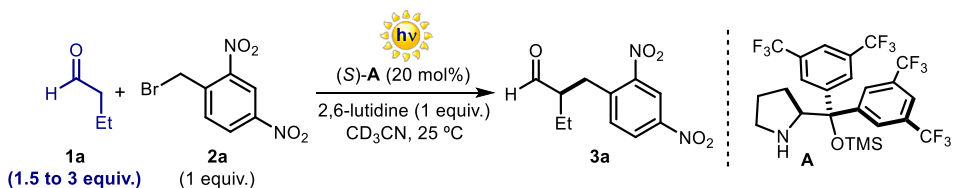
- $[\text{A}]$ from 0.01 M to 0.04 M.
- $[\mathbf{1a}]$ from 0.15 M to 0.6 M.
- $[\mathbf{2a}]$ from 0.05 M to 0.2 M.
- H_2O form anhydrous to 0.2 M.

Order dependence in catalyst **A**

Scheme 5.37 Reaction profiles at different initial concentrations of **A** showing a first-order dependence in **[A]**. Rate constants calculated from the slope of the plots. Reaction profiles using independent measurements (Method A, *left* panel, $\lambda = 450$ nm, irradiance = 4.7 mW/cm^2): $[\mathbf{1a}] = 1.5$ M; $[\mathbf{2a}] = 0.5$ M; [2,6-lutidine] = 0.5 M and $[\mathbf{A}]_0 = 0.05$ M (blue line), $[\mathbf{A}]_0 = 0.1$ M (red line) and $[\mathbf{A}]_0 = 0.2$ M (green line). Reaction profiles using *in situ* measurements (Method B, *right* panel, $\lambda = 470$ nm, irradiance = 28.8 mW/cm^2): $[\mathbf{1a}] = 0.3$ M; $[\mathbf{2a}] = 0.1$ M; [2,6-lutidine] = 0.1 M and $[\mathbf{A}]_0 = 0.01$ M (blue line), $[\mathbf{A}]_0 = 0.02$ M (red line) and $[\mathbf{A}]_0 = 0.04$ M (green line). The error bars represent the standard deviation.

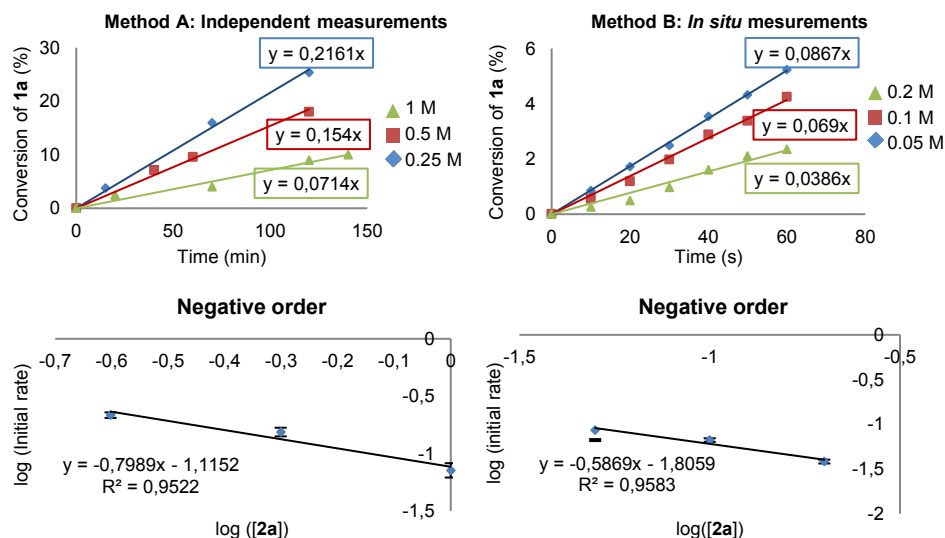
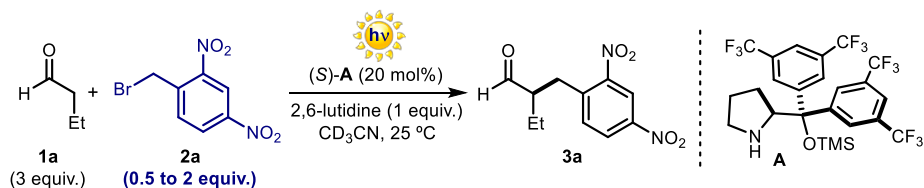
As shown in Scheme 5.37, a first-order dependence in **[A]** was determined.

Order dependence in **1a**



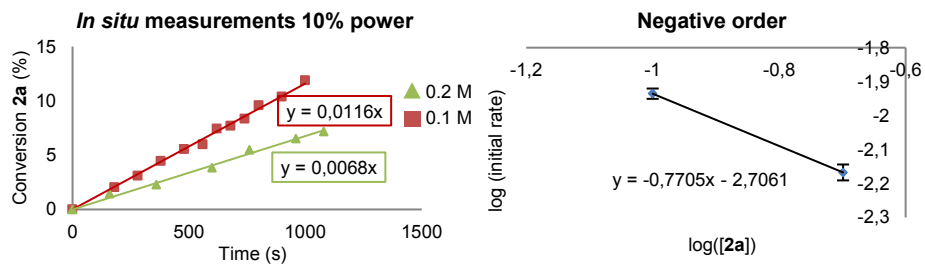
Scheme 5.38 Reaction profiles of initial-rate measurements at different initial concentrations of **1a** showing a zero-order dependence. Rate constants calculated from the slope of the plots. Reaction profiles using independent measurements (Method A, *left* panel, $\lambda = 450$ nm, irradiance = 4.7 mW/cm²): $[\mathbf{A}] = 0.1$ M; $[\mathbf{2a}] = 0.5$ M; $[\mathbf{2,6-lutidine}] = 0.5$ M and $[\mathbf{1a}]_0 = 0.75$ M (blue line), $[\mathbf{1a}]_0 = 1.5$ M (red line) and $[\mathbf{1a}]_0 = 3$ M (green line). Reaction profiles using *in situ* measurements (Method B, *right* panel, $\lambda = 470$ nm, irradiance = 28.8 mW/cm²): $[\mathbf{A}] = 0.02$ M; $[\mathbf{2a}] = 0.1$ M; $[\mathbf{2,6-lutidine}] = 0.1$ M and $[\mathbf{1a}]_0 = 0.15$ M (blue line), $[\mathbf{1a}]_0 = 0.3$ M (red line) and $[\mathbf{1a}]_0 = 0.6$ M (green line). The error bars represent the standard deviation.

As shown in Scheme 5.38, a zeroth-order dependence in **1a** was determined.

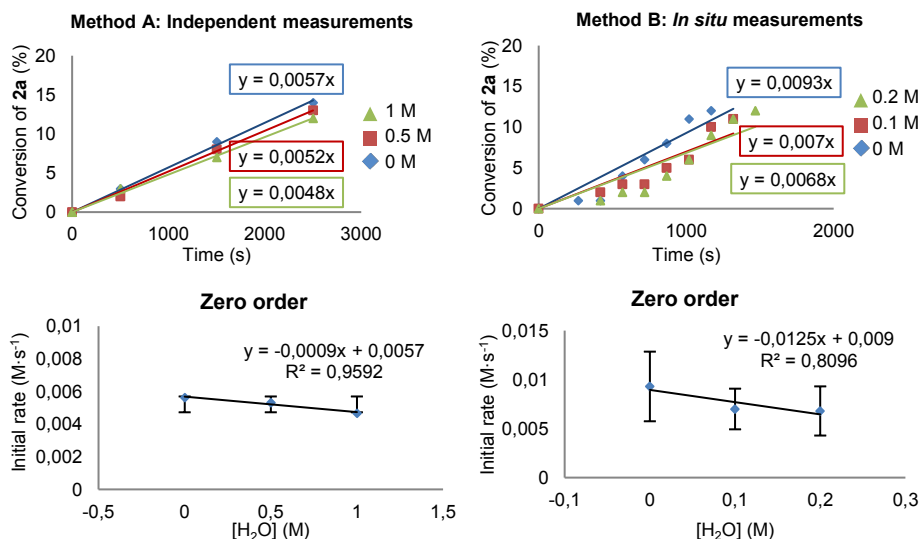
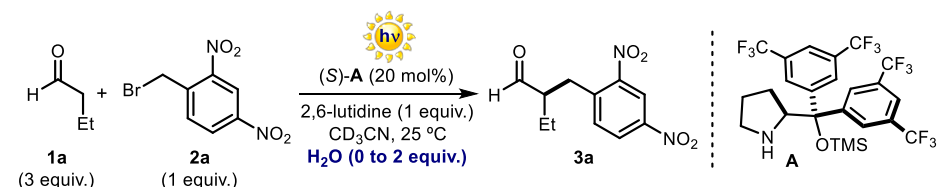
Order dependence in **2a**

Scheme 5.39 Reaction profiles of initial-rate measurements at different initial concentrations of **2a** showing a negative-order dependence. Rate constants calculated from the slope of the plots. Reaction profiles using independent measurements (Method A, *left* panel, $\lambda = 450$ nm, irradiance = 4.7 mW/cm^2): $[\mathbf{A}] = 0.1$ M; $[\mathbf{1a}] = 1.5$ M; $[\mathbf{2,6-lutidine}] = 0.5$ M and $[\mathbf{2a}]_0 = 0.25$ M (blue line), $[\mathbf{2a}]_0 = 0.5$ M (red line) and $[\mathbf{2a}]_0 = 1$ M (green line). Reaction profiles using *in situ* measurements (Method B, *right* panel, $\lambda = 470$ nm, irradiance = 28.8 mW/cm^2): $[\mathbf{A}] = 0.02$ M; $[\mathbf{1a}] = 0.3$ M; $[\mathbf{2,6-lutidine}] = 0.1$ M and $[\mathbf{2a}]_0 = 0.05$ M (blue line), $[\mathbf{2a}]_0 = 0.1$ M (red line) and $[\mathbf{2a}]_0 = 0.2$ M. The error bars represent the standard deviation.

As shown in Scheme 5.39, a negative fractional order dependence in $[\mathbf{2a}]$ was determined. The negative dependence was also observed when performing the same *in situ* NMR monitoring of the reaction progress as in Scheme 5.39, right panel, but using a different intensity of irradiation ($\lambda = 470$ nm, but irradiance = 3.0 vs. 28.8 mW/cm^2), see Scheme 5.40.



Scheme 5.40 Reaction profiles of initial-rate measurements at different initial concentrations of **2a** showing a fractional negative-order dependence. Rate constants calculated from the slope of the plots. Reaction profiles using *in situ* measurements ($\lambda = 470$ nm, irradiance = 3.0 mW/cm^2): [**A**] = 0.02 M ; [**1a**] = 0.3 M ; [2,6-lutidine] = 0.1 M ; [**2a**] $_0$ = 0.1 M (red line) and [**2a**] $_0$ = 0.2 M (green line). The error bars represent the standard deviation.

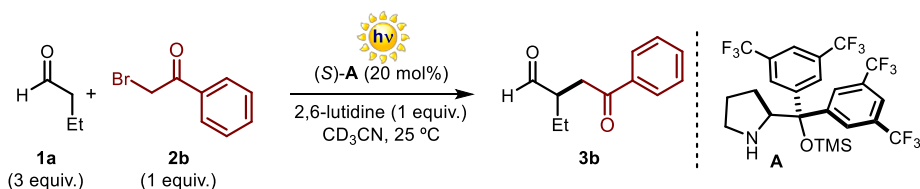
Order dependence in H_2O 

Scheme 5.41 Reaction profiles of initial-rate measurements at different initial concentrations of H_2O showing a zero-order dependence. Rate constants calculated from the slope of the plots. Reaction profiles using independent measurements (Method A, left panel, $\lambda = 450$ nm, irradiance = 4.7 mW/cm^2): $[\text{A}] = 0.1$ M; $[\mathbf{1a}] = 1.5$ M; $[\text{2,6-lutidine}] = 0.5$ M; $[\mathbf{2a}]_0 = 0.5$ M and $[\text{H}_2\text{O}]_0 \approx 0$ M (blue line), $[\text{H}_2\text{O}]_0 = 0.5$ M (red line) and $[\text{H}_2\text{O}]_0 = 1.0$ M (green line). Reaction profiles using *in situ* measurements (Method B, right panel, $\lambda = 470$ nm, irradiance = 28.8 mW/cm^2): $[\text{A}] = 0.02$ M; $[\mathbf{1a}] = 0.3$ M; $[\text{2,6-lutidine}] = 0.1$ M; $[\mathbf{2b}]_0 = 0.1$ M and $[\text{H}_2\text{O}]_0 \approx 0$ M (blue line), $[\text{H}_2\text{O}]_0 = 0.1$ M (red line) and $[\text{H}_2\text{O}]_0 = 0.2$ M (green line). d [benzoic acid] = 0.1 M. The error bars represent the standard deviation.

The effect of water on the reaction rate was measured with both the independent measurement approach and *in situ* ^1H NMR spectroscopy without adding any water (blue line in Scheme 5.41) and by adding one (red line in Scheme 5.41), or two (green line in Scheme 5.41) equivalents of water. The reactions were performed using dried CD_3CN (stored over 4 \AA molecular sieves).

As shown in Scheme 5.41, a zeroth-order dependence with respect to **water** was observed.

Kinetic studies for the EDA complex-mediated alkylation of butanal with **2b**



Scheme 5.42 EDA complex-mediated alkylation of butanal **1a** with phenacyl bromide **2b**.

In order to measure the initial-rates of the reaction with **2b**, a series of experiments were carried out in a regular NMR tubes without degassing. The reactions were irradiated at 450 nm with a 150 W high-stability light xenon lamp Tilluxe P45 coupled to a monochromator for exact wavelength definition (irradiance: 23.5 mW/cm²). This polychromator is connected to an optical fiber which was directly introduced into the NMR tube. This allowed us to monitor the conversion of phenacyl bromide **2b** into the final product **3b** in real time as we can irradiate *in situ* inside an NMR spectrometer (Bruker, 500 MHz). This process was repeated changing the stoichiometry of the reactants.

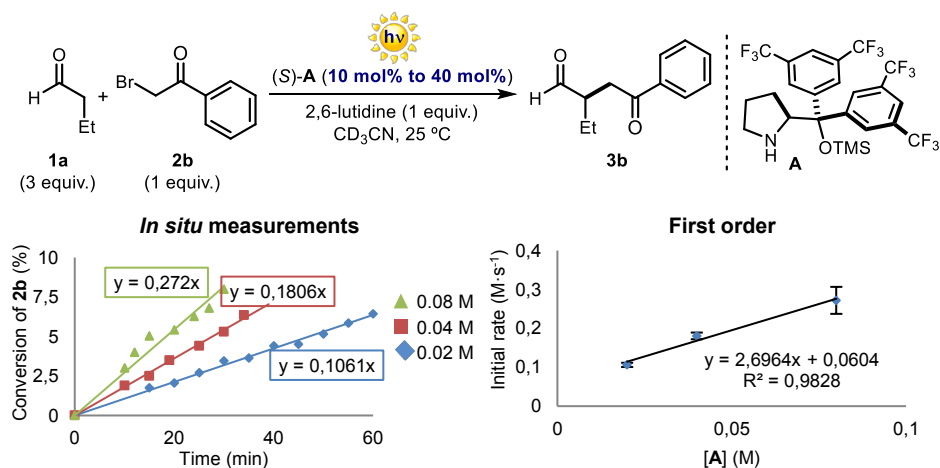
The model reaction was set up utilizing a stock solution containing 144 mg of the aminocatalyst **A** (0.24 mmol) and 6 mg of 1,3,5-trimethoxybenzene (employed as internal standard to measure the conversion of the enamine in solution) dissolved in 6 mL of CD₃CN. To 500 μL of this solution (0.04 M in **A**), butyraldehyde **1a** (27 μL, 0.3 mmol, 3 equiv.), 2,6-lutidine (12 μL, 0.1 mmol, 1 equiv.) and phenacyl bromide **2b** (20 mg, 0.1 mmol, 1 equiv.) were sequentially added. These conditions account for the following concentrations: [**A**] = 0.04 M, [**1a**] = 0.6 M and [**2b**] = 0.2 M and [2,6-lutidine] = 0.2 M.

Range of concentrations employed:

To measure the order with respect to each reactant, we varied the concentration of the reagent under study in the following ranges:

- [**A**] from 0.02 M to 0.08 M.
- [**1a**] from 0.3 M to 1.2 M.
- [**2b**] from 0.1 M to 0.4 M.

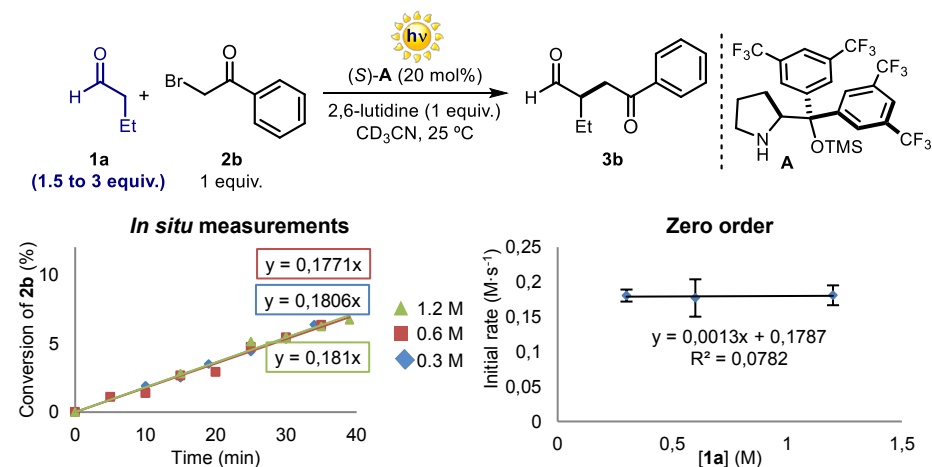
Order dependence in catalyst A



Scheme 5.43 Reaction profiles of initial-rate measurements at different initial concentrations of **A** showing a first-order dependence: $[A]_0 = 0.02$ M (blue line), $[A]_0 = 0.04$ M (red line) and $[A]_0 = 0.08$ M (green line) (*left*). Rates determined while varying $[A]_0$ (*right*). The error bars represent the standard deviation.

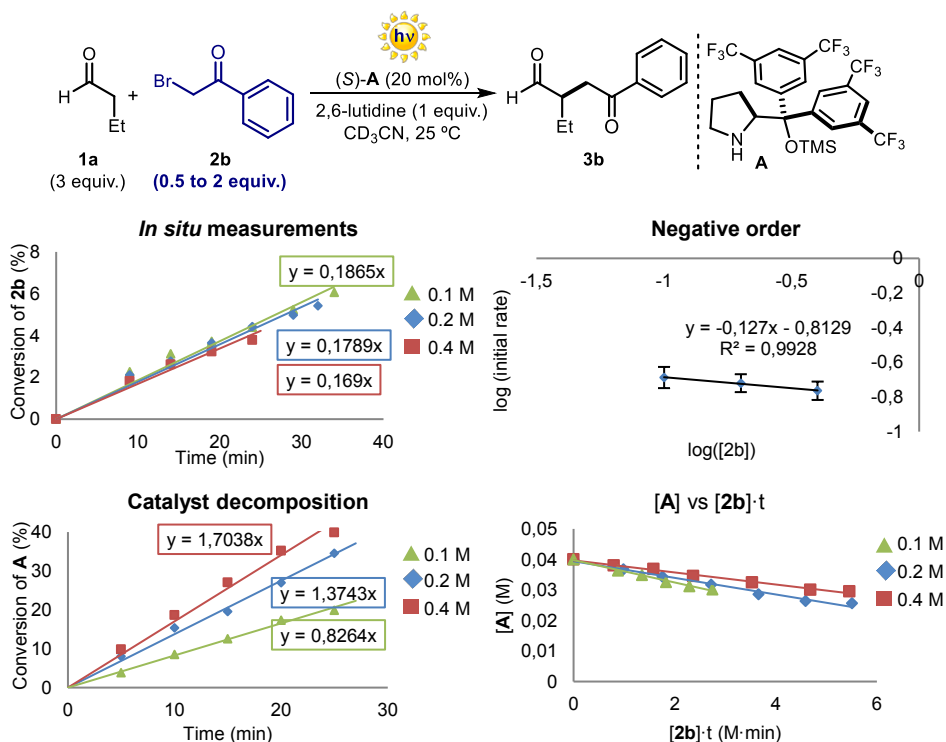
As shown in Scheme 5.43, a first-order dependence in $[A]$ was determined.

Order dependence in 1a



Scheme 5.44 Reaction profiles at different initial concentrations of **1a**: $[1a]_0 = 0.3$ M (blue line), $[1a]_0 = 0.6$ M (red line) and $[1a]_0 = 1.2$ M (green line) (*left*). Rates determined while varying $[1a]_0$ (*right*). The error bars represent the standard deviation.

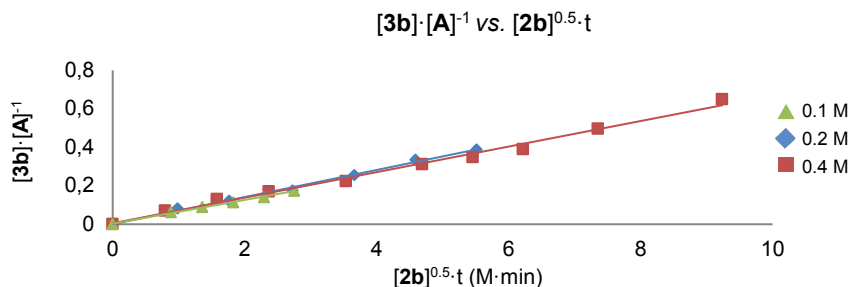
As shown in Scheme 5.44, a zeroth-order dependence in $[1a]$ was determined.

Order dependence in catalyst **2b**

Scheme 5.45 Experiments performed at different initial concentrations of **2b**: [**2b**]₀ = 0.4 M (red line), [**2b**]₀ = 0.2 M (blue line) and [**2b**]₀ = 0.1 M (green line). Reaction profiles used for initial-rate calculations (*up left*). Logarithmic plot of the rates determined while varying [**2b**]₀ (*up right*). Evolution of the catalyst **A** concentration for the same reactions (*down left*), measured from the concentration of enamine **I** in solution. Overlay of plots according to Equation 5.5 in Section 5.3.5 for $n=1$ for reactions containing different initial concentrations of **2b**. The error bars represent the standard deviation.

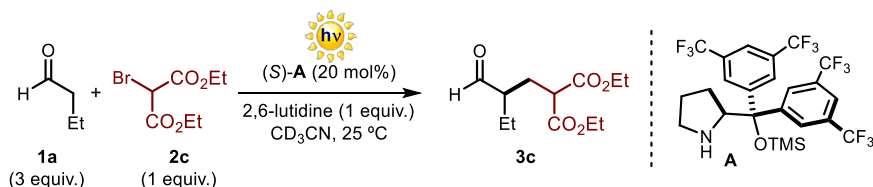
As shown in Scheme 5.45, a negative order in **2b** was determined. Furthermore, catalyst degradation was observed over time. The overlay found for plots of [**A**] versus [**2b**]¹·*t* ($n = 1$ in Equation 5.5) establishes a first-order dependence on [**2b**] for the catalyst's disappearance (Scheme 5.45, right bottom panel).

We then wanted to measure the real effect of [**2b**] on the rate of alkylation leading to product **3b**, discounting the effects of catalyst **A** degradation in the initiation regime. The plotting of the kinetic data (Scheme 5.46) according to Equation 5.7 Section 5.3.5 shows a good fit for [**3b**]·[**A**]⁻¹ vs. [**2b**]^{0.5}·*t* ($n = 0.5$ in Equation 5.8). This indicates a *positive* half-order dependence on [**2b**].



Scheme 5.46 Overlay of plots, according to Equation 5.8 in Section 5.3.5, for $n=0.5$ ($[3b] \cdot [A]^{-1}$ vs. $[2b]^{n \cdot t}$) for reactions containing different initial concentrations of **2b**: $[2b]_0 = 0.4$ M (red line), 0.2 M (blue line) and $[2b]_0 = 0.1$ M (green line).

Kinetic studies for the alkylation of butanal with bromomalonate **2c**



Scheme 5.47 alkylation of butanal **1a** with bromomalonate **2c**.

Two different procedures, detailed below as Methods A and B, have been used for the initial-rate kinetic measurements.

Method A - Independent experiments:

Sets of three reactions with identical concentrations of every reactant except for the specie whose order is being measured were carried out in three identical Schlenk tubes. The Schlenk tubes containing the reaction mixtures were positioned alongside, 10 cm away from the light source. They were irradiated with a 300 W xenon lamp operating at 100% of light intensity (irradiance: 300 mW/cm²; 150 mW/cm² when 50% power was applied) with a cut-off filter at 385 nm ($\lambda \geq 385$ nm) without stirring. This procedure was repeated 4 times quenching the reactions at different time intervals (this set-up required an independent reaction to be performed for every data-point at different times).

The reaction was set up utilizing a stock solution containing 360 mg of the aminocatalyst **A** (0.6 mmol) and 15 mg of 1,3,5-trimethoxybenzene (employed as internal standard to measure the conversion of the enamine in solution), dissolved in 6 mL of CD₃CN. To 100 μ L of this solution (0.1 M in **A**), butyraldehyde **1a** (13.5 μ L, 0.15 mmol, 3 equiv.), 2,6-lutidine (6 μ L, 0.05 mmol, 1 equiv.) and ethyl bromomalonate **2c** (8.5 μ L, 0.05 mmol, 1 equiv.) were sequentially added. The reaction mixture was thoroughly degassed *via* freeze

pump thaw (x 3 cycles), and the vessel refilled with argon. After irradiating for the indicated time, the conversion of ethyl bromomalonate **2c** was measured by ^1H NMR analysis. These conditions account for the following concentrations: $[\text{A}] = 0.1 \text{ M}$, $[\mathbf{1a}] = 1.5 \text{ M}$, $[\mathbf{2c}] = 0.5 \text{ M}$ and $[\text{2,6-lutidine}] = 0.5 \text{ M}$.

Range of concentrations employed:

To measure the order with respect to each reactant, we used the conditions described above while varying the concentration of the reagent under study in the following ranges:

- $[\text{A}]$ from 0.05 M to 0.15 M.
- $[\mathbf{1a}]$ from 0.75 M to 3 M.
- $[\mathbf{2c}]$ from 0.25 M to 1 M.
- H_2O form anhydrous to 1 M.

Method B - In situ monitoring of the reaction progress:

The reactions were carried out using the same stoichiometry as described in Method A. However, no degassing process was carried out and the reaction vessel was a regular NMR tube. The reactions were irradiated at 400 nm with a 150 W high-stability light xenon lamp Tilluxe P45 coupled to a monochromator for exact wavelength definition (irradiance: 20.4 mW/cm^2 at 2 mm). The monochromator was connected to an optical fiber which was directly introduced into the NMR tube inside the instrument (Bruker, 500 MHz). The conversion of bromomalonate **2c** into the final product **3c** was determined by ^1H NMR spectroscopy. This process was repeated changing the stoichiometry of the reactants.

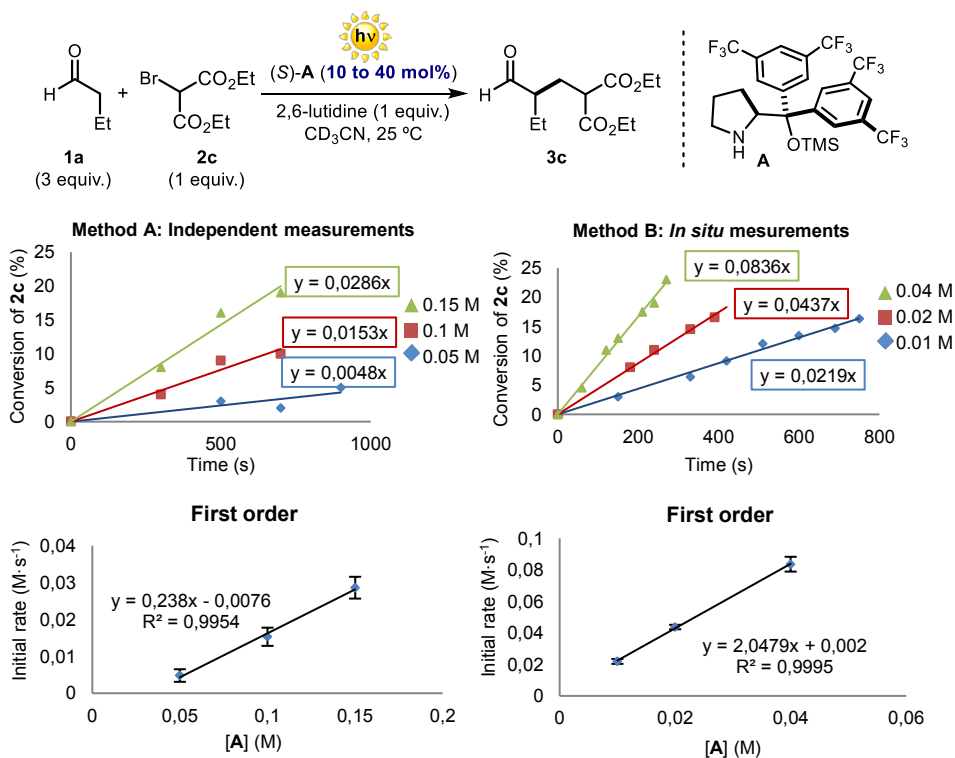
The model reaction was set up utilizing a stock solution containing 72 mg of the aminocatalyst **A** (0.12 mmol) and 3 mg of 1,3,5-trimethoxybenzene (employed as internal standard to measure the conversion of the enamine in solution) dissolved in 6 mL of CD_3CN . To 500 μL of this solution (0.02 M in **A**), butyraldehyde **1a** (13.5 μL , 0.15 mmol, 3 equiv.), 2,6-lutidine (6 μL , 0.05 mmol, 1 equiv.) and ethyl bromomalonate **2c** (8.5 μL , 0.05 mmol, 1 equiv.) were sequentially added. These conditions account for the following concentrations: $[\text{A}] = 0.02 \text{ M}$, $[\mathbf{1a}] = 0.3 \text{ M}$, $[\mathbf{2c}] = 0.1 \text{ M}$ and $[\text{2,6-lutidine}] = 0.1 \text{ M}$.

Range of concentrations employed:

To measure the order with respect to each reactant, we used the conditions described above while varying the concentration of the reagent under study in the following ranges:

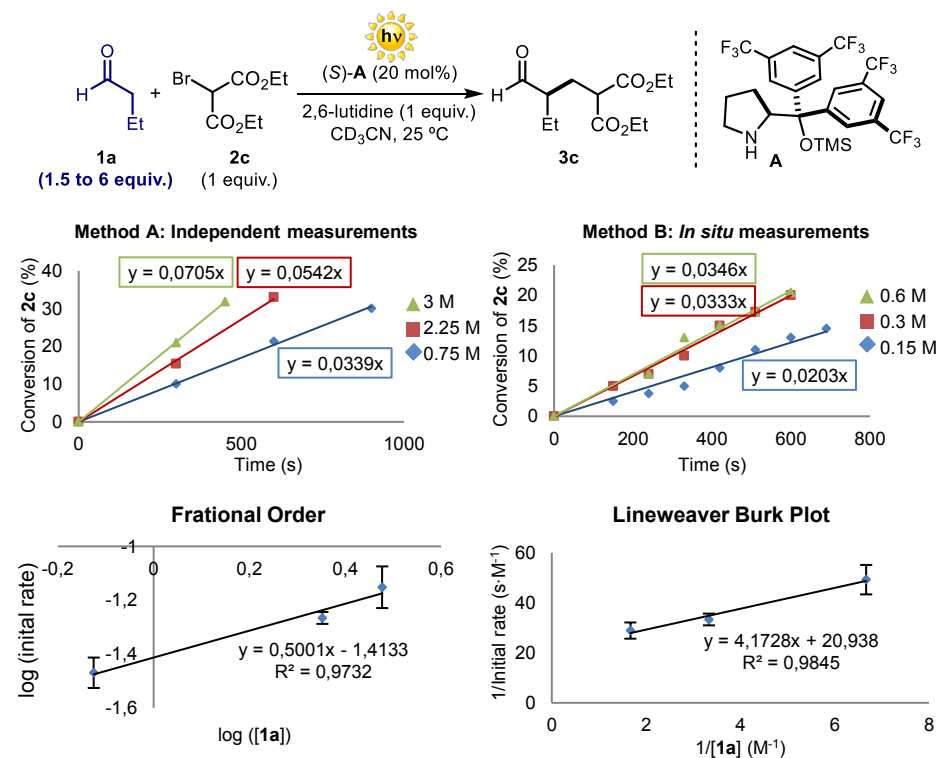
- [A] from 0.01 M to 0.04 M.
- [1a] from 0.15 M to 0.6 M.
- [2c] from 0.05 M to 0.2 M.
- H₂O from 0 to 0.2 M.

Order dependence in catalyst A



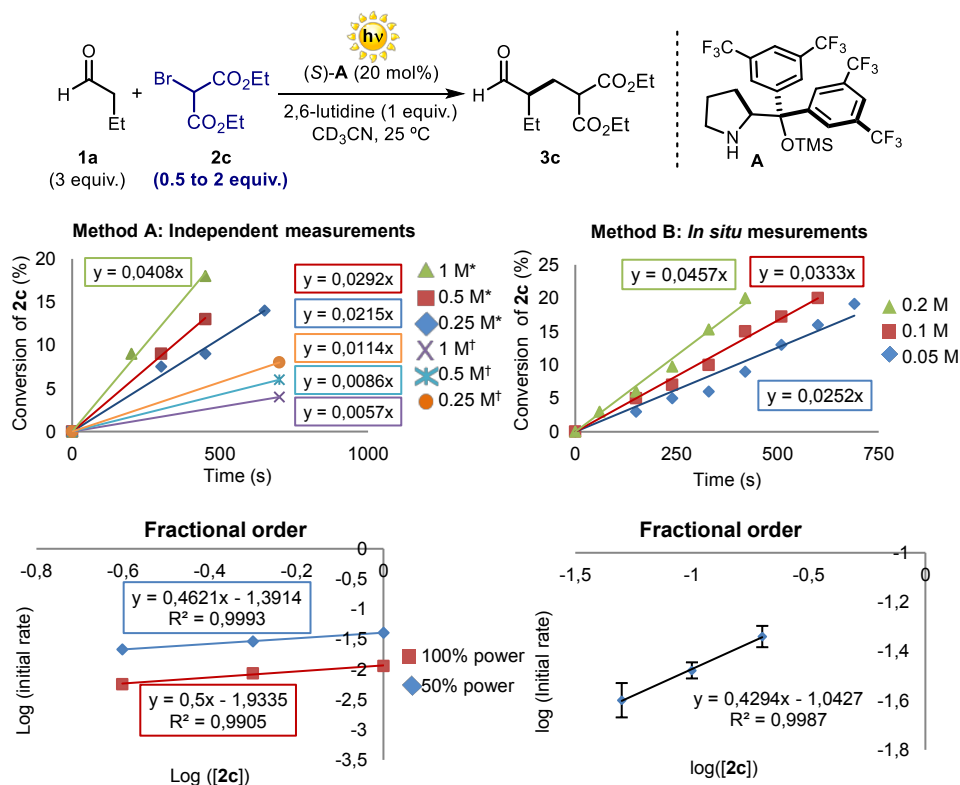
Scheme 5.48 Reaction profiles at different initial concentrations of **A** showing a first-order dependence in [A]. Rate constants calculated from the slope of the plots. Reaction profiles using independent measurements (Method A, *left* panel, $\lambda \geq 385$ nm (*cut-off*), irradiance = 300 mW/cm²): [1a] = 1.5 M; [2c] = 0.5 M; [2,6-lutidine] = 0.5 M and [A]₀ = 0.05 M (blue line), [A]₀ = 0.1 M (red line) and [A]₀ = 0.15 M (green line). Reaction profiles using *in situ* measurements (Method B, *right* panel, $\lambda = 400$ nm, irradiance = 20.4 mW/cm²): [1a] = 0.3 M; [2c] = 0.1 M; [2,6-lutidine] = 0.1 M and [A]₀ = 0.01 M (blue line), [A]₀ = 0.02 M (red line) and [A]₀ = 0.04 M (green line). The error bars represent the standard deviation.

As shown in Scheme 5.48, a first-order dependence in [A] was determined.

Order dependence in **1a**

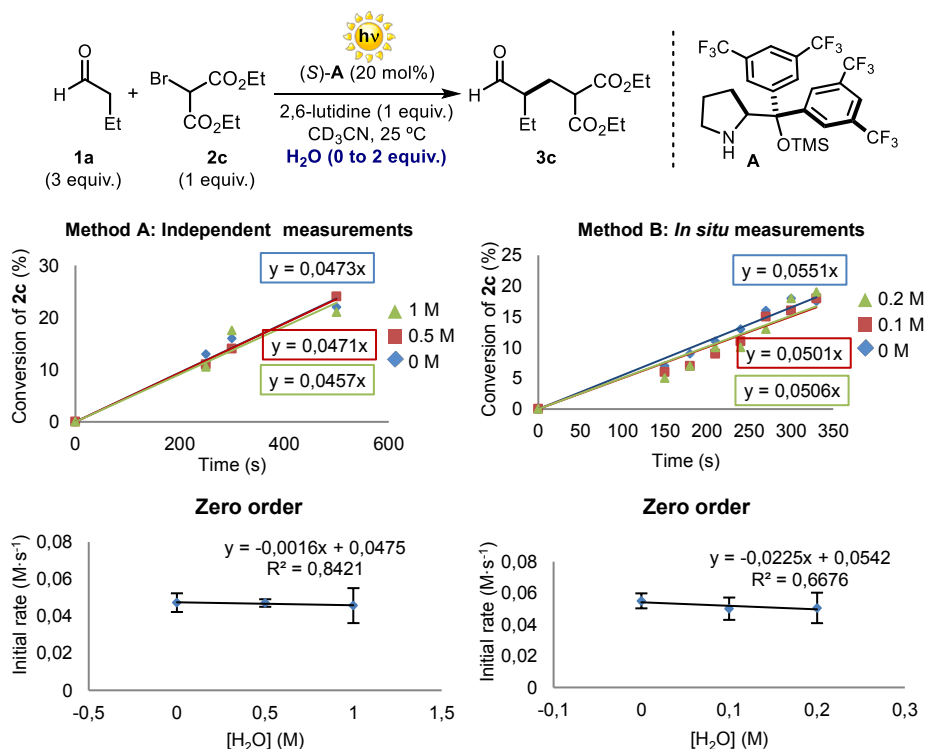
Scheme 5.49 Reaction profiles at different initial concentrations of **1a**. Rate constants calculated from the slope of the plots. Reaction profiles using independent measurements (Method A, *left* panel, $\lambda \geq 385$ nm (*cut-off*), irradiance = 300 mW/cm²): [**A**] = 0.1 M; [**2c**] = 0.5 M; [2,6-lutidine] = 0.5 M and [**1a**]₀ = 0.75 M (blue line), [**1a**]₀ = 2.25 M (red line) and [**1a**]₀ = 3.0 M (green line). Reaction profiles using *in situ* measurements (Method B, *right* panel, $\lambda = 400$ nm, irradiance = 20.4 mW/cm²): [**A**] = 0.02 M; [**2c**] = 0.1 M; [2,6-lutidine] = 0.1 M and [**1a**]₀ = 0.15 M (blue line), [**1a**]₀ = 0.3 M (red line) and [**1a**]₀ = 0.6 M (green line). Logarithmic plot of the rates determined while varying [**1a**]₀ using independent measurements (*down left*). Lineweaver Burk plot for the rates determined while varying [**1a**]₀ using *in situ* measurements (*down right*). The error bars represent the standard deviation.

As shown in Scheme 5.49, a fractional order dependence in [**1a**] was determined using the method of independent measurements. A saturation kinetic profile was observed instead when using the *in situ* monitoring. This is presumably because of catalyst decomposition pathways triggered by the presence of oxygen in the system, as *in situ* monitoring did not allow for complete de-oxygenation of the reaction medium (see Section 5.5.2 for further details on the catalyst decomposition). When using the independent measurement approach, instead, we *did not observe any catalyst degradation* before than 20% conversion.

Order dependence in **2c**

Scheme 5.50 Reaction profiles at different initial concentrations of **2c**. Rate constants calculated from the slope of the plots. Reaction profiles using independent measurements (Method A, *left panel*, $\lambda \geq 385$ nm (*cut-off*)): we performed two sets of experiments under the same conditions, but using a different intensity of irradiation: *reaction irradiated with **100% power**, irradiance = 300 mW/cm²: [**A**] = 0.1 M; [**1a**] = 1.5 M; [2,6-lutidine] = 0.5 M and [**2c**]₀ = 0.25 M (blue line), [**2c**]₀ = 0.5 M (red line) and [**2c**]₀ = 1.0 M (green line). †Reaction irradiated with **50% power**, irradiance = 150 mW/cm²: [**A**] = 0.1 M; [**1a**] = 1.5 M; [2,6-lutidine] = 0.5 M and [**2c**]₀ = 0.25 M (orange line), [**2c**]₀ = 0.5 M (light blue line) and [**2c**]₀ = 1.0 M (purple line). Reaction profiles using *in situ* measurements (Method B, *right panel*, $\lambda = 400$ nm, irradiance = 20.4 mW/cm²): [**A**] = 0.02 M; [**1a**] = 0.3 M; [2,6-lutidine] = 0.1 M and [**2c**]₀ = 0.05 M (blue line), [**2c**]₀ = 0.1 M (red line) and [**2c**]₀ = 0.2 M (green line). Logarithmic plot of the rates determined while varying [**2c**]₀ using independent measurements at two different irradiation intensities (*down left*) and using *in situ* measurements (*down right*). The error bars represent the standard deviation.

As shown in Scheme 5.50, a fractional order dependence with respect to **2c** was observed.

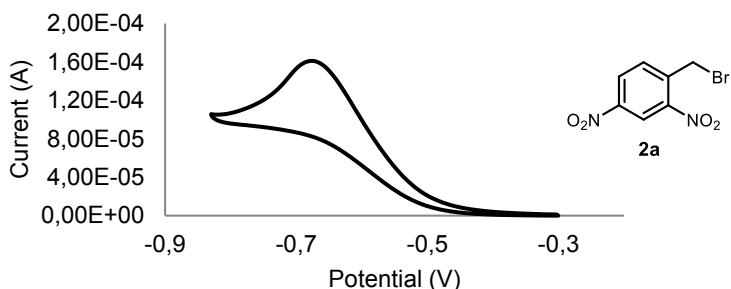
Order dependence in H₂O

Scheme 5.51 Reaction profiles of initial-rate measurements at different initial concentrations of H₂O showing a zero-order dependence. Rate constants calculated from the slope of the plots. Reaction profiles using independent measurements (Method A, *left* panel, $\lambda \geq 385$ nm (*cut-off*), irradiance = 300 mW/cm²): [A] = 0.1 M; [1a] = 1.5 M; [2,6-lutidine] = 0.5 M; [2c]₀ = 0.5 M and [H₂O]₀ \approx 0 M (blue line), [H₂O]₀ = 0.5 M (red line) and [H₂O]₀ = 1.0 M (green line). Reaction profiles using *in situ* measurements (Method B, *right* panel, $\lambda = 400$ nm, irradiance = 20.4 mW/cm²): [A] = 0.02 M; [1a] = 0.3 M; [2,6-lutidine] = 0.1 M; [2c]₀ = 0.1 M and [H₂O]₀ \approx 0 M (blue line), [H₂O]₀ = 0.1 M (red line) and [H₂O]₀ = 0.2 M (green line). The error bars represent the standard deviation.

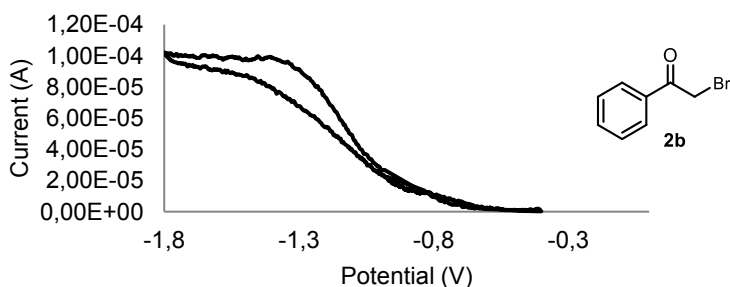
The effect of water on the reaction rate was measured with both methods without adding any water (blue line in Scheme 5.51) and by adding one (red line in Scheme 5.51) or two (green line in Scheme 5.51) equivalents of water to the reaction.

As shown in Scheme 5.51, a zeroth-order dependence with respect to **water** was observed.

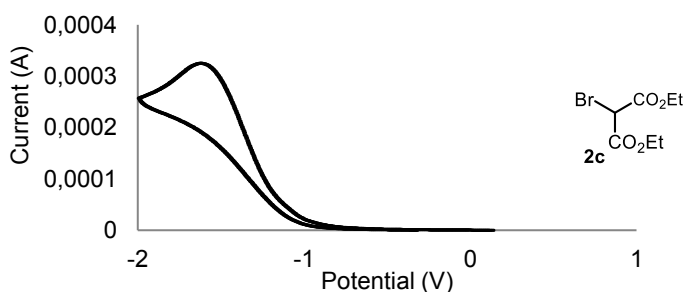
5.5.4 Cyclic voltammetry



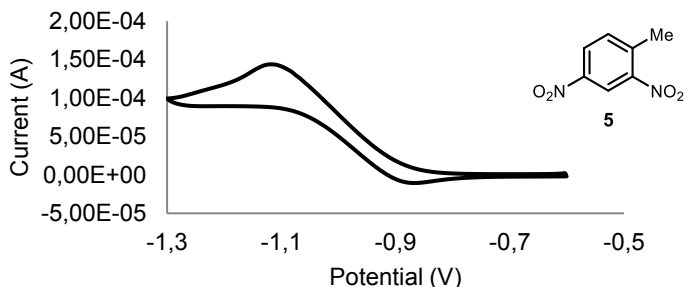
Scheme 5.52 Cyclic voltammogram of 2,4-dinitrobenzyl bromide **2a** [0.02 M] in [0.1 M] TBAPF₆ in CH₃CN. Sweep rate: 50 mV/s. Pt electrode working electrode, Ag/AgCl (NaCl saturated) reference electrode, Pt wire auxiliary electrode. $E_{p}^{red} = -0.66$ V.



Scheme 5.53 Cyclic voltammogram of phenacyl bromide **2b** [0.02 M] in [0.2 M] TBAPF₆ in CH₃CN. Sweep rate: 10 mV/s. Pt electrode working electrode, Ag/AgCl (NaCl saturated) reference electrode, Pt wire auxiliary electrode. Irreversible reduction. $E_{p}^{red} = -1.35$ V.

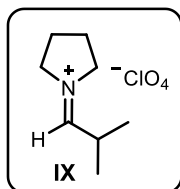


Scheme 5.54 Cyclic voltammogram of diethyl bromomalonate **2c** [0.05 M] in [0.1 M] TBAPF₆ in CH₃CN. Sweep rate: 50 mV/s. Pt electrode working electrode, Ag/AgCl (NaCl saturated) reference electrode, Pt wire auxiliary electrode. Irreversible reduction. $E_{p}^{red} = -1.69$ V.



Scheme 5.55 Cyclic voltammogram of 2,4-dinitrotoluene **5** [0.02 M] in [0.1 M] TBAPF₆ in CH₃CN. Sweep rate: 20 mV/s. Pt electrode working electrode, Ag/AgCl (NaCl saturated) reference electrode, Pt wire auxiliary electrode. $E_{p}^{\text{red}} = -1.10$ V, quasi-reversible reduction potential.

5.5.5 Synthesis and characterization of iminium ion IX



1-(2-methylpropylidene)pyrrolidin-1-ium perchlorate (**IX**) was synthesized from pyrrolidine, perchloric acid and isobutyraldehyde according to the literature.⁴³ The pyrrolidine perchlorate salt was prepared by adding 3 mmol of pyrrolidine (0.025 mL) to a solution of 3 mmol of perchloric acid (0.026 mL of a 70% solution) in 1 mL of ether. A slightly yellow precipitate formed, which was filtered and

washed with dry ether. The pyrrolidinium perchlorate salt was used for the following step without further purification. Pyrrolidinium perchlorate (0.23 mmol, 40 mg) was suspended in 2 mL of dry ether and freshly distilled *isobutyraldehyde* (1 mmol, 0.91 mL) was added. After the addition, the precipitate dissolved while the slow precipitation of a white solid was observed. The reaction was stirred overnight at room temperature. The precipitate was washed with dry hexane (10 mL) under argon and then dried using high vacuum pump. The iminium ion **IX** was obtained in a 23% yield (12 mg) as a white solid.

¹H NMR (400 MHz, CD₃CN): δ 8.16 (d, $J = 9.2$ Hz, 1H), 4.07 (t, $J = 7.0$ Hz, 2H), 3.94 (t, $J = 7.0$ Hz, 2H), 2.93 (dh, $J = 9.2, 6.6$ Hz, 1H), 2.13 (m, 4H), 1.24 (d, $J = 6.6$ Hz, 6H).

¹³C NMR (101 MHz, CD₃CN): δ 180.9, 58.6, 52.2, 32.3, 23.8, 23.6, 17.1.

⁴³ Leonard, N. J.; Paukstelis, J. V. "Direct synthesis of ternary iminium salts by combination of aldehydes or ketones with secondary amine salts" *J. Org. Chem.* **1963**, *28*, 3021.

Chapter VI

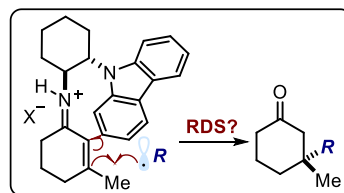
Studies on the iminium ion trapping of radicals triggered by an electron-relay mechanism

Target

Mechanistic studies to elucidate the key mechanistic aspects of the enantioselective iminium ion trapping of photochemically generated carbon-centered radicals.

Tools

A combination of electrochemical, spectroscopic, and kinetic studies.¹



6.1 Introduction

Over the last decades, it has been shown that the formation of iminium ions is a powerful strategy for the asymmetric β -functionalization of enals and enones *via* conjugate additions of soft nucleophiles (Scheme 6.1a).² However, chiral iminium ions **I** have never been used to stereoselectively trap nucleophilic radicals. This is surprising given the strong tendency of open-shell species to react with electron-deficient olefins.³

Recently, our research group showed that the iminium ion activation is not limited to two-electron reaction manifolds (Scheme 6.1b).⁴ It can also be employed to trap nucleophilic radicals. Synthetically, the chemistry provided a catalytic method to forge quaternary

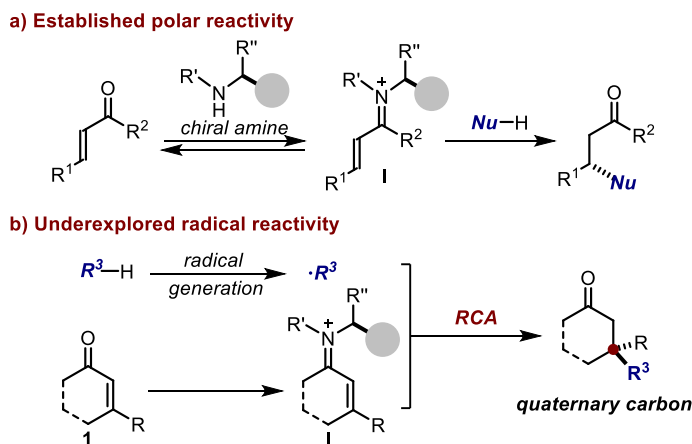
¹ The work discussed in this chapter has been published: Bahamonde, A.; Murphy, J. J.; Savarese, M.; Brémond, E.; Cavalli, A.; Melchiorre, P. "Studies on the enantioselective iminium ion trapping of radicals triggered by an electron-relay mechanism" *J. Am. Chem. Soc.* **2017**, *139*, 4559.

² a) Lelais, G.; MacMillan, D. W. C. "Modern strategies in organic catalysis: the advent and development of iminium activation" *Aldrichim. Acta* **2006**, *39*, 79. b) Erkkilä, A.; Majander, I.; Pihko, P. M. "Iminium catalysis" *Chem. Rev.* **2007**, *107*, 5416.

³ a) Giese, B. "The stereoselectivity of intermolecular free radical reactions [new synthetic methods (78)]" *Angew. Chem. Int. Ed.* **1989**, *28*, 969. b) Srikanth, G. S. C.; Castle, S. L. "Advances in radical conjugate additions" *Tetrahedron* **2005**, *61*, 10377.

⁴ Murphy, J. J.; Bastida, D.; Paria, S.; Fagnoni, M.; Melchiorre, P. "Asymmetric catalytic formation of quaternary carbons by iminium ion trapping of radicals" *Nature* **2016**, *532*, 218.

carbon stereocenters⁵ with high fidelity by means of an enantioselective radical conjugate addition (RCA)⁶ to β -disubstituted cyclic enones **1**.



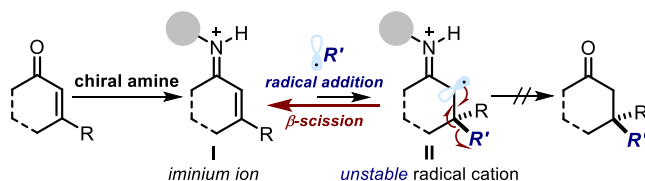
Scheme 6.1 Iminium-ion-mediated catalysis: a) Established polar reactivity of chiral iminium ions **I** in enantioselective conjugate additions of soft nucleophiles. b) Radical conjugate addition (RCA) to chiral iminium ions **I** catalytically generated from β -disubstituted enones **1** to forge quaternary stereocenters. Filled gray circle represents a bulky substituent on the chiral amine catalyst.

Extensive studies and optimization concluded that the presence of a carbazole, which acts as a redox-active moiety, tethered to the aminocatalyst was crucial for the stereocontrolled iminium ion trapping of radicals. Indeed, the main problem for the

⁵ In general, radical conjugate additions to electron-deficient olefins are rather insensitive to steric hindrance because of the long incipient carbon-carbon forming bond in the early transition state, see: a) Damm, W.; Giese, B.; Hartung, J.; Hasskerl, T.; Houk, K. N.; Hüter, O.; Zipse, H. "Diastereofacial selectivity in reactions of substituted cyclohexyl radicals. An experimental and theoretical study" *J. Am. Chem. Soc.* **1992**, *114*, 4067. b) Fischer, H.; Radom, L. "Factors controlling the addition of carbon-centered radicals to alkenes - an experimental and theoretical perspective" *Angew. Chem. Int. Ed.* **2001**, *40*, 1340.

⁶ Previous examples of metal-catalyzed enantioselective radical conjugate additions to electron-deficient olefins did not provide for the formation of sterically demanding quaternary carbons, see: a) Sibi, M. P.; Ji, J.; Wu, J. H.; Gürtler, S.; Porter, N. "Chiral Lewis acid catalysis in radical reactions: enantioselective conjugate radical additions" *J. Am. Chem. Soc.* **1996**, *118*, 9200. b) Sibi, M. P.; Ji, J.; Sausker, J. B.; Jasperse, C. P. "Free radical-mediated intermolecular conjugate additions. Effect of the Lewis acid, chiral auxiliary, and additives on diastereoselectivity" *J. Am. Chem. Soc.* **1999**, *121*, 7517. c) Gansäuer, A.; Lauterbach, T.; Bluhm, H.; Noltemeyer, M. "A catalytic enantioselective electron transfer reaction: titanocene-catalyzed enantioselective formation of radicals from *meso*-epoxides" *Angew. Chem. Int. Ed.* **1999**, *38*, 2909. d) Ruiz Espelt, L.; McPherson, I. S.; Wiensch, E. M.; Yoon, T. P. "Enantioselective conjugate additions of α -amino radicals *via* cooperative photoredox and Lewis acid catalysis" *J. Am. Chem. Soc.* **2015**, *137*, 2452. e) Huo, H.; Harms, K.; Meggers, E. "Asymmetric photoredox transition-metal catalysis activated by visible light" *J. Am. Chem. Soc.* **2016**, *138*, 6936.

successful realization of the RCA was the formation of a highly unstable intermediate, the α -iminyl radical cation⁷ **II**, which is generated upon radical trap from the positively charged iminium ion **I** (Scheme 6.2). In consonance with the classical behavior of radical ions,⁸ intermediate **II** has a high tendency to undergo radical elimination (β -scission), thus reforming the more stable conjugated iminium ion **I**.⁹ We recognized that the main obstacle to reaction development was the high reactivity and fleeting nature of the distonic radical **II**.



Scheme 6.2 Challenges associated with implementing the iminium-ion-catalyzed conjugate additions of radicals ($\cdot R$). The filled grey circle represents a bulky substituent on the chiral amine catalyst.

Our strategy to overcome the difficulties derived from the formation of this troublesome intermediate was to tether an electron-rich carbazole moiety (*electron pool* unit in Scheme 6.3) at a strategic position on the organocatalyst so that it would be poised to undergo a very rapid intramolecular single-electron transfer (SET) reduction of the unstable species **II**, preventing it from breaking down. A possible back-electron transfer (BET) would be prevented by the tautomerization of the enamine **III** to form the more stable imine **IV**.¹⁰ Finally, the carbazole radical cation (*electron hole* unit within **IV**), arising from the intramolecular SET event, undergoes single-electron reduction from the photoredox catalyst (PC_{red} in Scheme 6.3). As a result, the neutral carbazole is regenerated, and the final quaternary product **3**, bearing a quaternary stereocenter, and the original organocatalyst are released upon hydrolysis of **V**.

Notably, the photocatalyst (PC in Scheme 6.3) both creates the nucleophilic radical and promotes the final SET event (full mechanistic details in Scheme 6.6). Overall, in this catalytic system, the carbazole unit serves as an electron-relay center, since it behaves

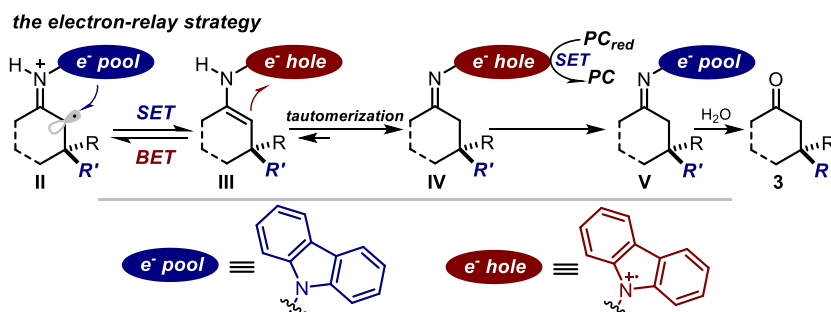
⁷ The instability of α -iminyl radical cations has been extensively discussed during the previous chapter.

⁸ Forbes, M. D. "Carbon-centered free radicals and radical cations: structure, reactivity, and dynamics" **2010**, John Wiley & Sons.

⁹ Jakobsen, H. J.; Lawesson, S. O.; Marshall, J. T. B.; Schroll, G.; Williams, D. H. "Studies in mass spectrometry. Part XII. Mass spectra of enamines" *J. Chem. Soc. B.* **1966**, 940.

¹⁰ b) Clark, R. A.; Parker, D. C. "Imine-enamine tautomerism. I. 2-(*N*-Cyclohexylimino)-1,3-diphenylpropane" *J. Am. Chem. Soc.* **1971**, 93, 7257. See Section 3.1.2 in Chapter III for full discussion.

alternately as an acceptor and a donor to shuttle electrons.¹¹ First, the excellent electron-donating capabilities of the carbazole trigger a fast proximity-driven intramolecular reduction of **II**.¹² Then, the kinetic stability of the long-lived carbazole radical cation¹³ in **IV** facilitates a productive intermolecular SET reduction from the reduced photocatalyst (PC_{red} in Scheme 6.3).



Scheme 6.3 The electron-relay strategy to bypass the short-lived α -iminyl radical cation **II** by intramolecular reduction, and the role of tautomerization to prevent back-electron transfer. **PC** = photocatalyst; **PC_{red}** = reduced form of the photocatalyst. The blue ellipse represents the electron-rich reducing carbazole moiety, while the magenta ellipse represents the persistent carbazole radical cation.

The effectiveness of this *electron-relay mechanism* was initially demonstrated in the reaction between the commercially available β -methyl cyclohexenone **1a** and benzodioxole **2a** (Scheme 6.4a).⁴ Tetrabutylammonium decatungstate¹⁴ (TBADT, 5 mol%), an inorganic photocatalyst, was employed for the radical generation (full

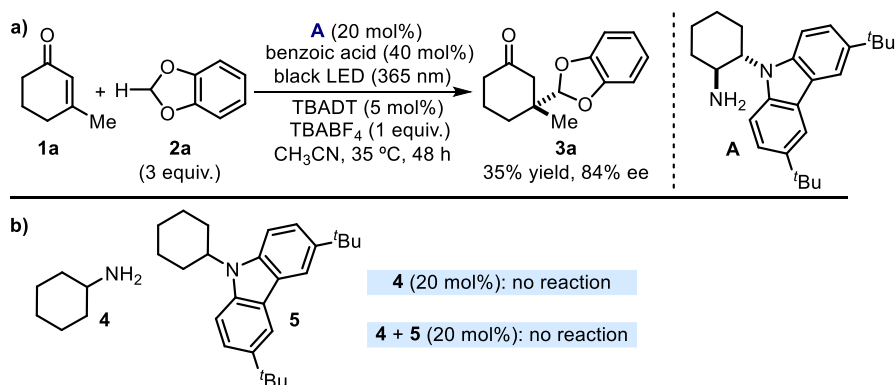
¹¹ Bollinger, J. M., Jr. “Electron relay in proteins” *Science* **2008**, *320*, 1730. b) Okada, Y.; Nishimoto, A.; Akaba, R.; Chiba, K. “Electron-transfer-induced intermolecular [2+2] cycloaddition reactions based on the aromatic “redox tag” strategy” *J. Org. Chem.* **2011**, *76*, 3470.

¹² The idea of proximity-driven redox processes finds support in the mechanism of electron-transfer within biological systems, where even endergonic SET events can be achieved *via* electron tunneling if the redox centers are in close proximity, see: Page, C. C.; Moser, C. C.; Chen, X.; Dutton, P. L. “Natural engineering principles of electron tunnelling in biological oxidation-reduction” *Nature* **1999**, *402*, 47.

¹³ Carbazole derivatives are also utilized in hole-transport materials for light-emitting diodes and photovoltaic cells, due to the unique redox properties, see: a) Uoyama, H.; Goushi, K.; Shizu, K.; Nomura, H.; Adachi, C. “Highly efficient organic light-emitting diodes from delayed fluorescence” *Nature* **2012**, *492*, 234. b) Blouin, N.; Leclerc, M. “Poly(2,7-carbazole)s: structure-property relationships” *Acc. Chem. Res.* **2008**, *41*, 1110.

¹⁴ a) Tzirakis, M. D.; Lykakis, I. N.; Orfanopoulos, M. “Decatungstate as an efficient photocatalyst in organic chemistry” *Chem. Soc. Rev.* **2009**, *38*, 2609. b) Ravelli, D.; Protti, S.; Fagnoni, M. “Decatungstate anion for photocatalyzed “window ledge” reactions” *Acc. Chem. Res.* **2016**, *49*, 2232. c) De Waele, V.; Poizat, O.; Fagnoni, M.; Bagno, A.; Ravelli, D. “Unraveling the key features of the reactive state of decatungstate anion in hydrogen atom transfer (HAT) photocatalysis” *ACS Catal.* **2016**, *6*, 7174.

mechanistic details in Scheme 6.6). The experiments were conducted at 35 °C in acetonitrile (CH₃CN) and under irradiation by a single black-light-emitting diode (black LED, $\lambda_{\text{max}} = 365 \text{ nm}$). Under these conditions, the aminocatalyst **A**, adorned with the carbazole moiety, provided the final product **3a** with a 35% yield and moderate enantioselectivity (84% ee). In sharp contrast, when the simple cyclohexylamine **4** (20 mol%), which mimics the catalyst's **A** scaffold while lacking the redox-active moiety, was utilized as aminocatalyst, no product formation was observed (Scheme 6.4b). Moreover, an equimolar combination of cyclohexylamine **4** and exogenous *N*-cyclohexyl 3,6-di-*tert*-butyl-carbazole **5** (20 mol%) was tested for the catalysis of this transformation. However, again no alkylation product was detected, indicating the importance of a proximity-driven intramolecular SET process to reduce the unstable α -iminyl radical cation **II** (see Scheme 6.3).



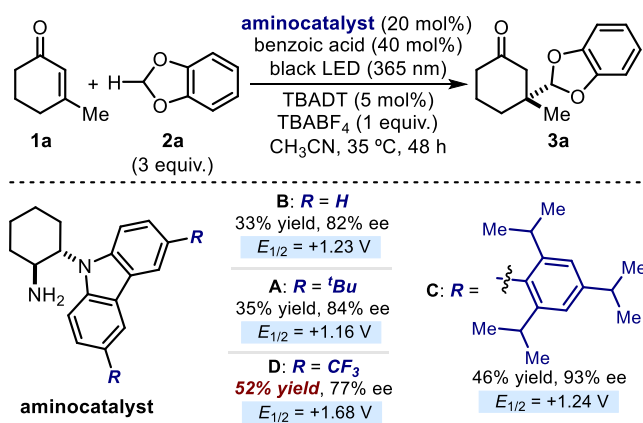
Scheme 6.4 a) The model reaction to test the feasibility of the electron-relay strategy. b) Experiments suggesting that, to make the electron-relay mechanism operative, there needs to be close spatial proximity between the iminium ion handle and the redox active carbazole moiety. TBABF₄: tetrabutylammonium tetrafluoroborate.

6.1.1 The unexpected result

During our optimization studies, we came across a surprising effect of the electronic properties of the carbazole moiety within the amine catalysts on the reaction rate (Scheme 6.5). We expected that, by introducing electron-donating groups at the 3- and 6-positions,¹⁵ the reactivity would increase. This is because the SET reduction of

¹⁵ In addition to modulating the redox properties of the carbazole scaffold, introducing substituents at the 3- and 6-positions can further stabilize the carbazole radical cation, see: Prudhomme, D. R.; Wang, Z.; Rizzo, C. J. *J. Org. Chem.* **1997**, *62*, 8257. Concurrently, the increased steric hindrance carries the additional benefit of inferring a higher stereocontrol, as evinced when using the highly encumbered primary amine catalyst **C**.

intermediate **II** would be favoured by a more electron-rich carbazole, a step which we envisioned would be crucial for reactivity. However, a considerably higher reactivity was observed when the catalyst **D**, bearing a CF₃ electron-withdrawing group at the 3,6-positions of the carbazole, which depletes the electron pool, was used instead of the more reducing catalysts **A** and **C**. The redox potentials of catalysts **A-D** were measured by cyclic voltammetry *vs.* Ag/Ag⁺ in CH₃CN ($E_{1/2}$ (**A**) = +1.16 V; $E_{1/2}$ (**C**) = +1.24 V; and $E_{1/2}$ (**D**) = +1.68 V, where $E_{1/2}$ is the reduction potential of the carbazole unit undergoing a reversible oxidation to produce the corresponding carbazoliumyl radical cation). These experiments further indicated that the catalyst **D**, bearing the less reducing carbazole, displayed the highest catalytic activity.



Scheme 6.5 The unanticipated effect that the redox properties of the carbazole-based primary amine catalysts have on the reactivity. $E_{1/2}$ is the reduction potential of the carbazole-based catalysts **A-D** as measured by cyclic voltammetry *vs.* Ag/Ag⁺ in CH₃CN; the carbazole within the aminocatalyst undergoes a reversible oxidation to produce the corresponding carbazoliumyl radical cation.

This unexpected result¹⁶ challenged our understanding of the reaction mechanism and prompted us to undertake extensive mechanistic investigations.

¹⁶ For an overview of the relevance of apparent outliers in the mechanistic interrogation of asymmetric catalytic processes, see: Sigman, M. S.; Harper, K. C.; Bess, E. N.; Milo, A. "The development of multidimensional analysis tools for asymmetric catalysis and beyond" *Acc. Chem. Res.* **2016**, *49*, 1292.

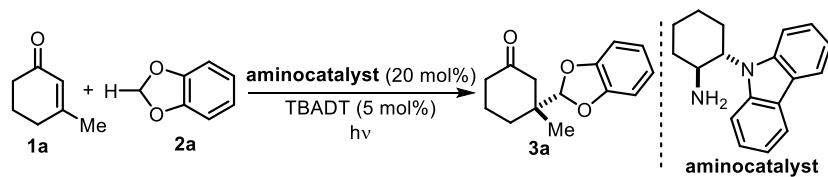
6.2 Target of the project

We wanted to rationalize the effects the electronic properties of the redox-active carbazole unit have on the reaction rate. Additionally, we intended to elucidate which was the turnover-limiting step of the transformation. Accordingly, a combination of physical organic techniques, including electrochemical and kinetic studies were used to achieve this goal.

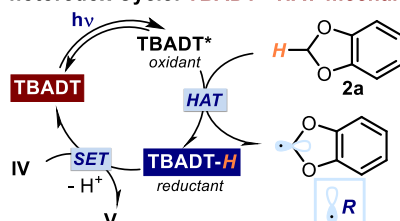
6.3 Results and discussion

Scheme 6.6 presents a detailed description of the proposed mechanism for the iminium ion-mediated RCA, which is characterized by the synergistic activities of two intertwined manifolds: the iminium ion (Scheme 6.6b) and the photoredox (Scheme 6.6a) catalytic cycles. It is important to note that a radical chain mechanism is not possible in this system. This is because generating a radical from substrate **2a** requires a HAT mechanism, while the feasibility of a chain propagation sequence could only rely on the oxidation ability of the carbazole radical cation within intermediate **D-1**, which could manifest itself only through an outer-sphere SET manifold.

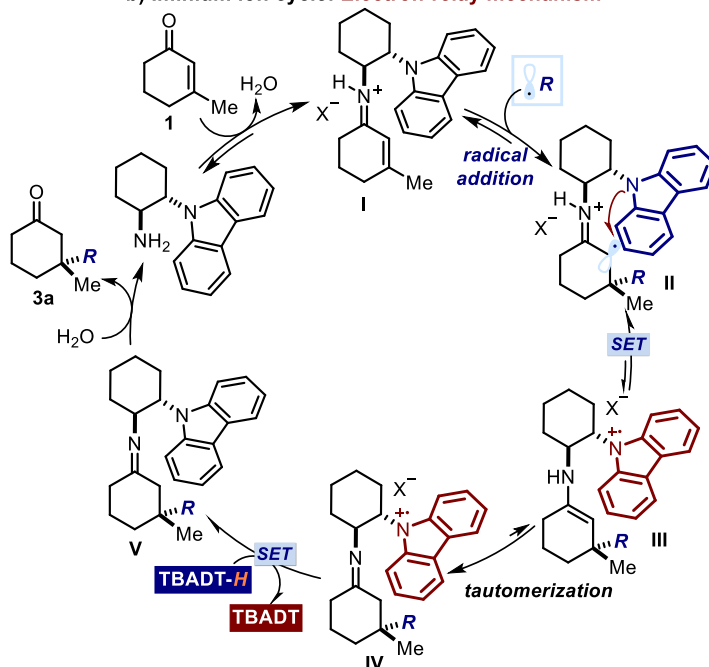
We initially hypothesized that an easier reduction of the short-lived α -iminyl radical cation **II** would facilitate the reaction. However, this idea was dissonant with the reactivity trend depicted in Scheme 6.5, where CF₃-containing catalyst **D** offered an improved reactivity. Indeed, this step should be hampered by an electron-poor carbazole unit. Nevertheless, the intramolecular SET reduction of **II** to give the enamine intermediate **III** is not the only electron-relay step in which the redox-active carbazole unit is involved. The carbazole radical cation in the imine **IV**, arising from the tautomerization of the secondary enamine **III**, acts as an oxidant of the reduced photocatalyst (TBADT-H). This bimolecular SET event is essential to restore the neutral carbazole moiety within **V** while closing the photoredox cycle, returning the TBADT catalyst in the original state. This step could be facilitated by an electron-poor substituent which magnifies the oxidizing power of the carbazole radical cation in **IV**.



a) Photoredox Cycle: **TBADT - HAT mechanism**



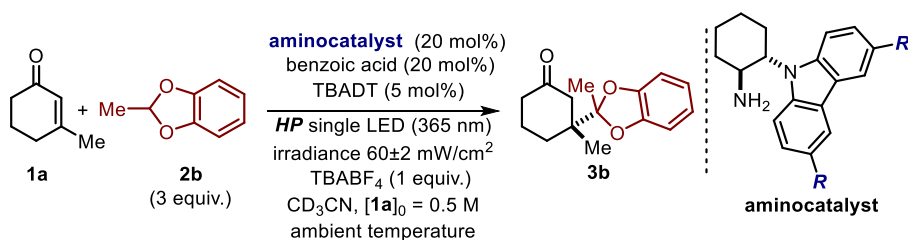
b) Iminium ion cycle: **Electron-relay mechanism**



Scheme 6.6 Mechanism for the enantioselective catalytic radical conjugated addition to enones. a) TBADT-mediated photoredox cycle, which affords the carbon-centered radical from benzodioxole precursors **2** by means of a HAT mechanism. b) The electron-relay mechanism underlying the iminium ion-mediated enantioselective radical conjugate addition to enone **1**.

We performed detailed kinetic studies to assess the relative importance of the two SET steps of the electron-relay mechanism (intramolecular reduction of **II** to afford the carbazole radical cation and regeneration of the neutral carbazole unit in **V** by intermolecular SET) and their influence on the overall reactivity.

As the model for the kinetic studies, we chose the reaction between the commercially available β -methyl cyclohexenone **1a** and 2-methyl benzodioxole **2b** to afford the radical conjugate addition product **3b** (Scheme 6.7). This decision was based on the complete lack of reactivity observed in the absence of the chiral carbazole-containing aminocatalyst,¹⁷ which precluded any background process from altering the kinetic analysis.



Scheme 6.7 The model reaction for the kinetic investigations. Reactions conducted under irradiation from a high-power (HP) single black-light-emitting diode (black LED, λ_{max} = 365 nm). [aminocatalyst] = 0.1 M, [**1a**] = 0.5 M, [**2b**] = 1.5 M, [TBADT] = 0.025 M, [TBABF₄] = 0.5 M and [benzoic acid] = 0.1 M.

The experiments were conducted at ambient temperature in the presence of a carbazole-based aminocatalyst (20 mol%), TBADT (5 mol%), benzoic acid (20 mol%, to facilitate iminium ion formation),¹⁸ and an excess of radical precursor **2b** (3 equiv.). Deuterated acetonitrile (CD₃CN) was used as the solvent for it ensured full substrate solubility and homogeneity of the system. We applied the method of initial-rate kinetics, monitoring the progress of the reactions by ¹H NMR analysis and following the conversion until 15%. The initial rates were plotted against concentration to obtain straight lines (see Section 6.5.2 for details). Our initial-rate kinetic studies required an independent reaction to be performed for every data-point at different times.

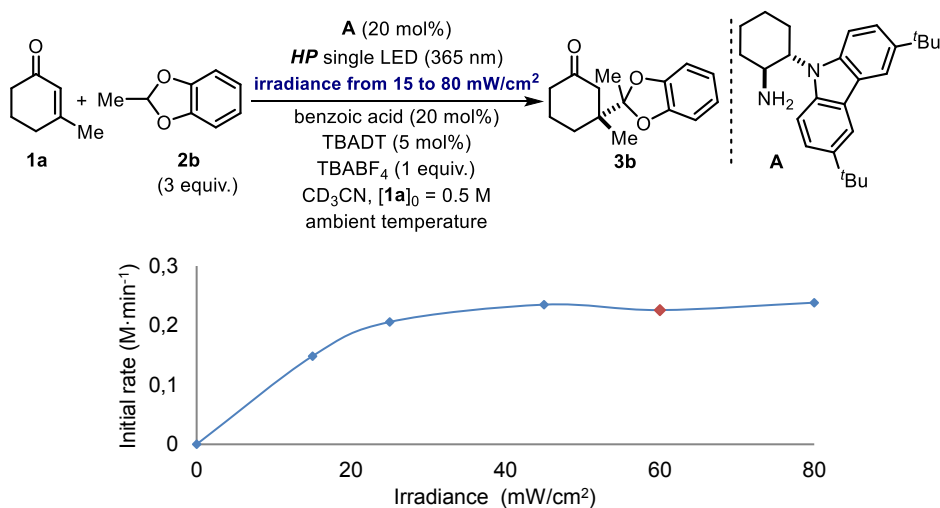
6.3.1 Light intensity/reactivity correlation studies

First, we evaluated the influence of the light intensity on the rate of the model reaction detailed in Scheme 6.7 catalyzed by the chiral amine **A** (Scheme 6.8). For the illumination system, we used a single high-power (HP) black-light-emitting diode (black LED, λ_{max} =

¹⁷ The use of benzodioxole **2a** as the radical precursor (chemistry detailed in Scheme 6.4a) resulted in a slow but detectable background process, with the product **3a** being obtained in ≈10% yield after 15 hours in the absence of any aminocatalyst.

¹⁸ In the original study (Ref. 4), 40 mol% of benzoic acid were used to accelerate the formation of iminium ion (the reaction does not proceed at all without the acid). A careful analysis conducted before the kinetic investigations revealed that the amount of acid could be halved without significantly affecting the reaction rate (see Scheme 6.22, Section 6.5.2).

365 nm) connected to an external power supply, which allowed us to finely tune and control the intensity of light emission. The irradiance was carefully measured with a photodiode light detector at the start of each reaction. To secure a reliable and consistent irradiation throughout the kinetic investigation, we used an apparatus that maintained a constant distance of 1.5 cm between the reaction vessel and the light source (full details in Section 6.5, Figure 6.6).



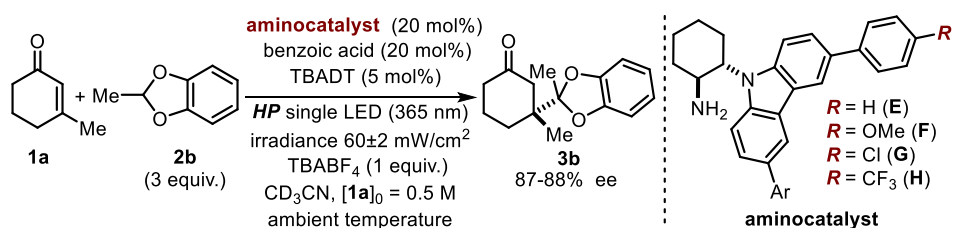
Scheme 6.8 Light intensity/reactivity correlation studies. Model reactions conducted as specified in Scheme 6.7 and catalyzed by **A**.

The rate of the model reaction catalyzed by **A** showed a saturation kinetic profile, since no effect of the light intensity on the reactivity was observed for irradiance greater than 40 mW/cm². Under this regime, the reaction is not light-limited and the excitation of the TBADT photocatalyst would not be the turnover-limiting step. Considering the light intensity/reactivity correlation depicted in Scheme 6.8, all the following kinetic studies were performed using the reaction set-up discussed above and an illumination system (HP black LED, $\lambda_{\text{max}} = 365$ nm) with an irradiance of 60 ± 2 mW/cm²; this ensured the reactions were not light-limited and that the overwhelming majority of the TBADT photocatalyst could be opportunely excited.

6.3.2 Rate dependence on the electronic properties of different aminocatalysts

A family of catalysts containing 3,6-diaryl-substituted carbazoles was synthesized to rationalize the unexpected effect of the electronic properties of the carbazole moiety contained within the catalyst (Scheme 6.5). The aryl groups were adorned with an array of *para*-substituents having different electronic properties. The *para*-substitution pattern

was carefully chosen to provide the redox-active carbazole unit with a wide range of electronic properties but a comparable steric shielding ability. *Para*-substituted aryl moieties were specifically selected to avoid possible contributions on the reaction rate from the different steric environment around the β -carbon of the iminium ion.¹⁹ In consonance with this design plan, catalysts **E** to **H** (Scheme 6.9) all provided the β -adduct **3b** with comparable stereocontrol (87-88% ee), thus demonstrating that a comparable chiral environment and shielding effect was created at the remote β -carbon of the reactive iminium ion intermediate. These results suggested that the *para*-substituted 3,6-aryl carbazole catalysts **E-H** are characterized by a similar steric profile, and that possible differences in reaction rate should arise from electronic factors exclusively.



Scheme 6.9 Family of *para*-substituted carbazole-based aminocatalyst displaying comparable steric shielding properties in the enantioselective radical conjugate addition to enone **1a**.

With this family of catalysts in hand (**E-H**), we explored how the electronic properties of the chiral carbazole catalysts affected the rate of the model reaction depicted in Scheme 6.9. Applying the method of initial-rate kinetics, we confirmed that catalysts bearing more electron-withdrawing groups within the carbazole unit imparted a higher rate, with catalyst **H** (R = CF₃) providing the faster reaction Figure 6.1.

¹⁹ The data in Scheme 6.5 indicated how the steric profile of the carbazole substituents in catalysts **A-D** was strongly connected with the level of stereo-induction in the RCA process.

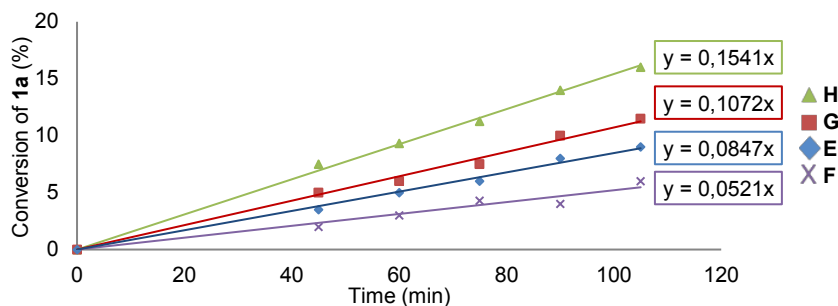


Figure 6.1 Initial-rate measurements using different aminocatalysts. Reactions performed in CD_3CN under illumination by a high power LED centered at 365 nm (irradiance = $60 \pm 2 \text{ mW/cm}^2$). $[\text{aminocatalyst}] = 0.1 \text{ M}$, $[\mathbf{1a}] = 0.5 \text{ M}$, $[\mathbf{2b}] = 1.5 \text{ M}$, $[\text{TBADT}] = 0.025 \text{ M}$, $[\text{TBABF}_4] = 0.5 \text{ M}$ and $[\text{benzoic acid}] = 0.1 \text{ M}$.

Furthermore, a positive linear correlation was obtained when the measured rate constants were plotted against their Hammett σ_{para} value. Figure 6.2 shows the linear free-energy relationship (LFER)²⁰ between the electronics of the carbazole unit of the aminocatalysts and the rate constant of the catalyzed reaction.

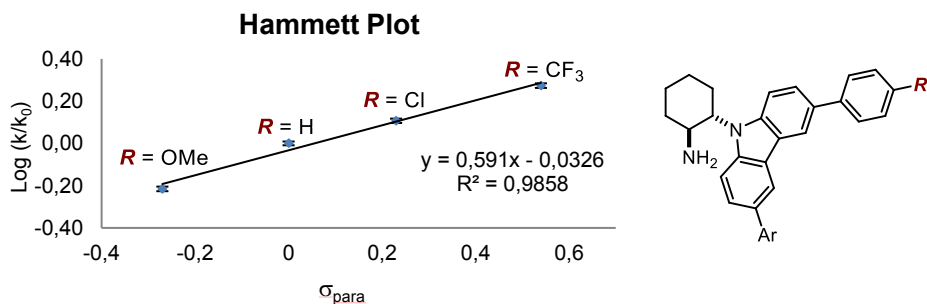


Figure 6.2 LFER correlating the Hammett σ value of the *para*-substituted aryl carbazole moiety with the initial rates, calculated from the plots depicted in Figure 6.1. The error bars represent the standard deviation.

Since the electronic properties directly influence the redox power of the carbazole unit, it is not surprising that the observed initial rates also correlated linearly with the redox potentials of aminocatalysts **E–H**, measured electrochemically by cyclic voltammetry *vs.* Ag/Ag^+ in CH_3CN (Figure 6.3a). A linear relationship was also observed between the catalyst redox potentials and the σ_{para} value of the *para*-substituted aryl substituents

²⁰ a) Schreck, J. O. “Nonlinear Hammett relationships” *J. Chem. Educ.* **1971**, *48*, 103. b) For the seminal report of a Linear Free Energy Relationships (LFER) in asymmetric catalysis, see: Jacobsen, E. N.; Zhang, W.; Güler, M. L. “Electronic tuning of asymmetric catalysts” *J. Am. Chem. Soc.* **1991**, *113*, 6703.

(Figure 6.3b). This correlation provides a way to predict²¹ both the electrochemical potential and the catalytic activity of new members of the *para*-substituted 3,6-aryl carbazole catalyst family.

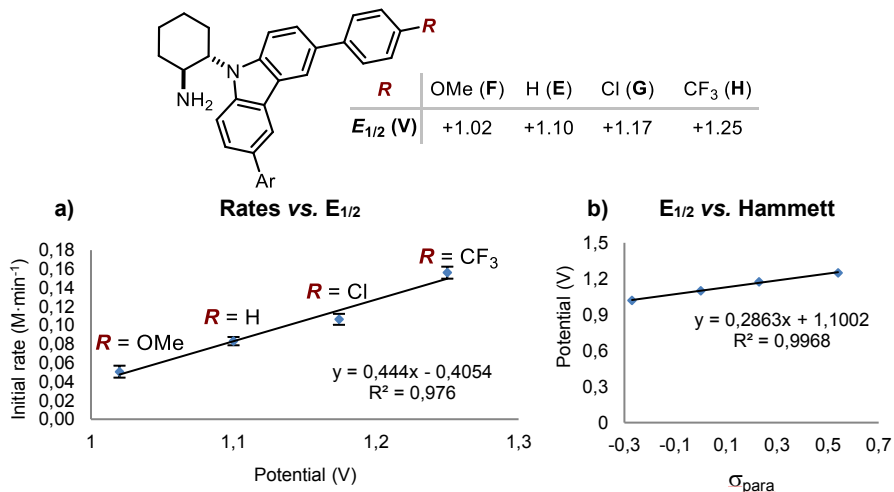


Figure 6.3 a) Correlation between the initial rates, calculated from the plots depicted in Figure 6.1, and the redox potentials. b) Linear relationship between the redox potentials for the different aminocatalysts and the corresponding Hammett σ value of their aryl moiety. The error bars represent the standard deviation.

Collectively, these results indicate that the electronic properties of the catalyst carbazole unit, which are strictly correlated with their redox abilities, strongly influence the rate of the model reaction. Specifically, the larger the reduction potential of the carbazole tethered to the aminocatalyst, the faster the reaction proceeds.

6.3.3 Rate order assessment

To fully rationalize this redox properties/reactivity relationship, we undertook a reaction-profile analysis and rate-order assessment to establish the turnover-limiting step. Initial-rate kinetic investigations of the model reaction depicted in Scheme 6.7 were performed across a range of concentrations for each reaction component (see Section 6.5.2 for details). In these studies, we used an illumination system (HP black LED, $\lambda_{max} = 365$ nm) with an irradiance of 60 ± 2 mW/cm² to ensure that the processes were not light-limited. Two independent series of kinetic investigations were performed using carbazole-based aminocatalysts **A** and **E**, which provided similar and reproducible kinetic profiles. This

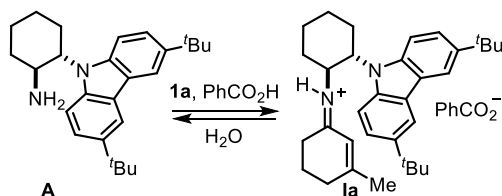
²¹ Hickey, D. P.; Schiedler, D. A.; Matanovic, I.; Doan, P. V.; Atanassov, P.; Minter, S. D.; Sigman, M. S. "Predicting electrocatalytic properties: modeling structure-activity relationships of nitroxyl radicals" *J. Am. Chem. Soc.* **2015**, *137*, 16179.

was done to ensure that similar trends could be observed when using catalysts with different architectures and steric profiles on the redox-active carbazole unit.

Table 6.1 Rate order assessment for the alkylation of **1a** with **2b**.

Component	rate order
aminocatalyst	first
enone 1a	saturation
H ₂ O	zeroth
benzodioxole 2b	zeroth
TBADT	saturation

Table 6.1 details the results of our initial-rate kinetic investigations. The reaction was found to be first order in the catalyst (both amines **A** and **E**). In addition, a saturation kinetic profile was observed for the β -methyl cyclohexenone **1a**. This observation suggests that the amine catalyst is partitioned between the free-state and the iminium ion intermediate **I**, not opting for a particular resting state (Scheme 6.10).



Scheme 6.10 Condensation equilibrium for the formation of the iminium **1a**.

¹H NMR spectroscopy studies on the equilibrium of iminium ion formation

To test this hypothesis, the equilibrium of iminium ion formation under the conditions used in the kinetic experiments was studied by ¹H NMR spectroscopy. The ¹H NMR spectrum of a solution containing the aminocatalyst **A** (18.8 mg, 0.05 mmol, 20 mol%), benzoic acid (6 mg, 0.05 mmol, 20 mol%), 3-methyl-2-cyclohexen-1-one **1a** (28 μ L, 0.25 mmol, 1 equiv.), benzodioxole **2b** (86 μ L, 0.75 mmol, 3 equiv.), TBADT (41.3 mg, 0.0125 mmol, 5 mol%), and tetrabutylammonium tetrafluoroborate (82.2 mg, 0.25 mmol, 1 equiv.) in 0.5 mL of CD₃CN was recorded (Figure 6.4).

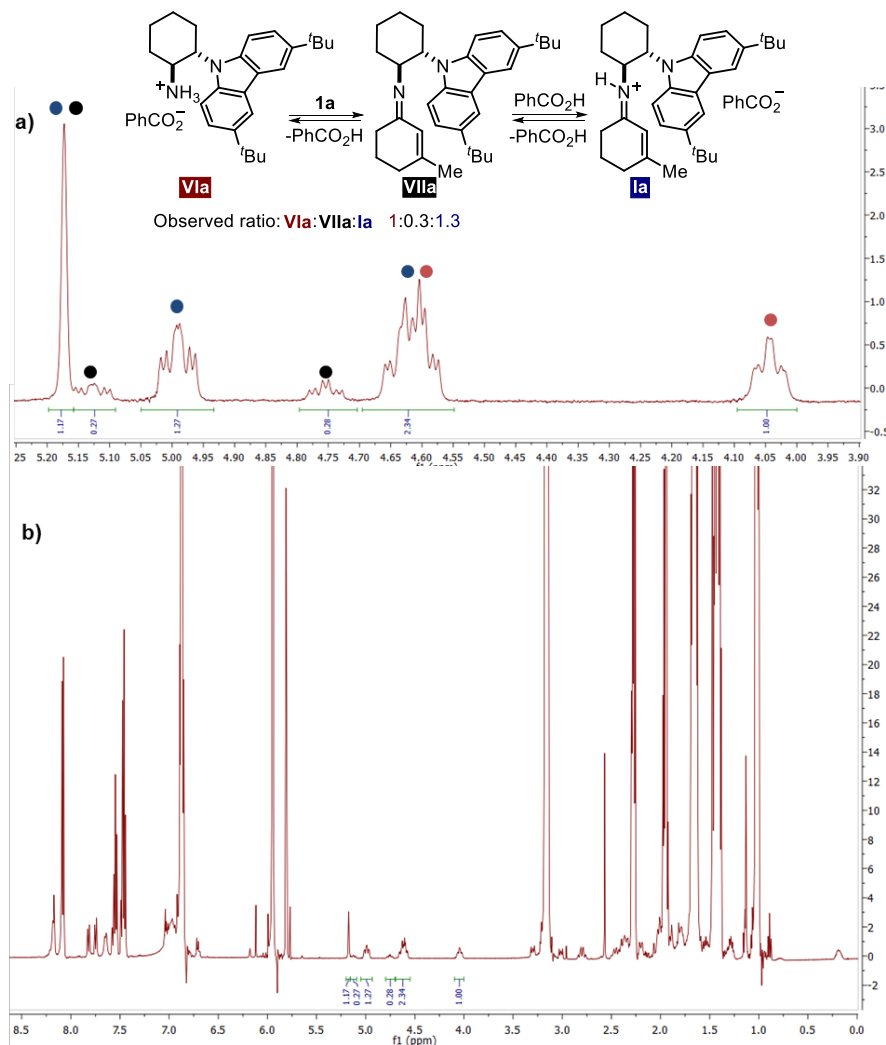


Figure 6.4 ^1H NMR spectrum of the crude reaction mixture showing the 1:0.3:1.3 ratio between the protonated catalyst **A** (**VIa**), the imine **VIIa**, and the iminium ion **Ia**. ^1H NMR experiments performed in 0.5 mL of anhydrous CD_3CN at 298 K with $[\mathbf{A}] = 0.1$ M, $[\mathbf{1a}] = 0.5$ M, $[\mathbf{2b}] = 1.5$ M, $[\text{TBADT}] = 0.025$ M, $[\text{TBABF}_4] = 0.5$ M and $[\text{benzoic acid}] = 0.1$ M.

The experiment was conducted in the dark. a) Selected region of the ^1H NMR spectral window between 5.25 and 3.9 ppm. b) ^1H NMR spectra between 11.0 and -1.0 ppm. The large peaks observed at 5.8, 2.3, 2.0 and 1.5 ppm correspond to the enone **1a**. The peaks observed at 6.9 and 6.0 correspond to the benzodioxole **2b**. The peaks observed at 3.1, 1.6, 1.4 and 1.0 ppm correspond to the tetrabutylammonium tetrafluoroborate.

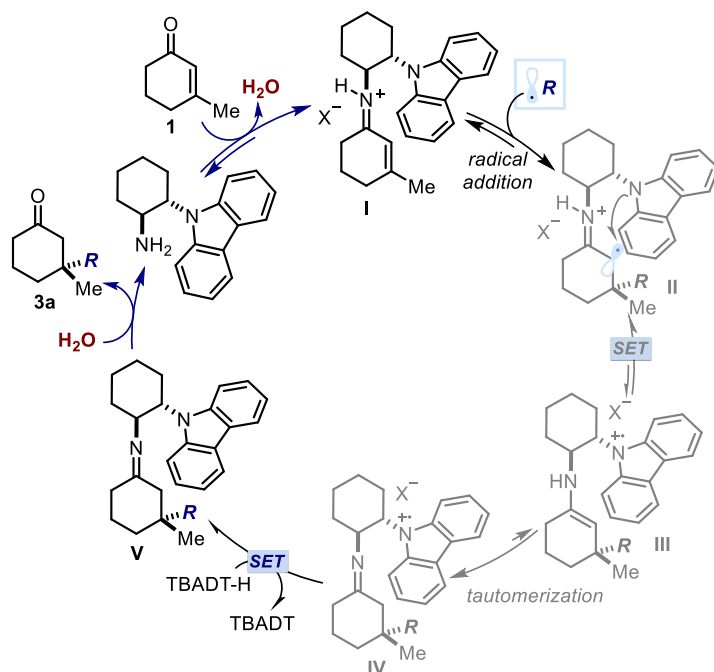
The protonated catalyst **A** (**VIa**), the imine **VIIa**, and the iminium ion **Ia** were detected in a ratio of 1:0.3:1.3, respectively (Figure 6.4). These spectroscopic studies are consonant with the notion that a definitive resting state for catalyst **A** cannot be identified,

with the catalyst concentration shared between different closed-shell intermediates. Notably, the non-protonated free catalyst **A** was not detected.

The assignment of the different species was made on the basis of diagnostic NMR peaks extrapolated by the characterization data of authentic samples (see Section 6.5.3), as discussed below:

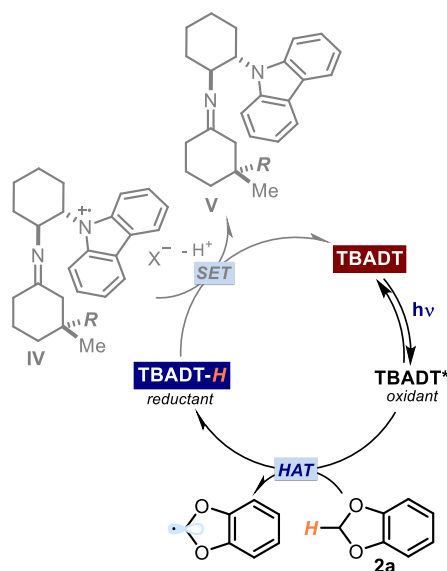
- Protonated aminocatalyst **VIa**: one of the protons contained in the multiplet 4.81 – 4.55 (2H) and triplet of doublets at 4.04 ppm ($J = 10.5, 3.2$ Hz, 1H).
- Imine **VIIa**: triplet of doublets at 5.12 ppm ($J = 10.5, 4.7$ Hz, 1H) and triplet of doublets at 4.75 ppm ($J = 10.5, 4.8$ Hz, 1H).
- Iminium **Ia**: singlet at 5.17 ppm (1H), triplet of doublets at 4.99 ppm ($J = 11.8, 4.5$ Hz, 1H), one of the protons contained in the multiplet 4.81 – 4.55 (2H).

The concentration of water in solution may play a role on the equilibrium formation of the iminium ion **I** (Scheme 6.11). We thus explored the effect of water on the rate of the model reaction. No alteration of the kinetic profile was observed after the addition of either 1 or 5 equivalents of H₂O.



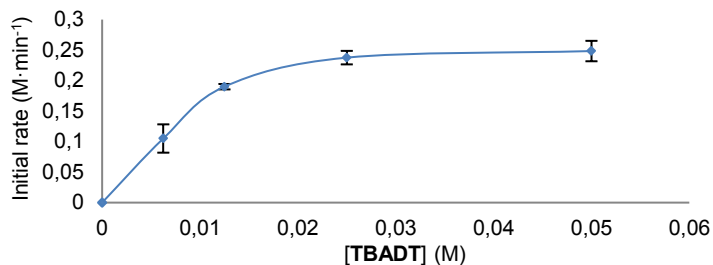
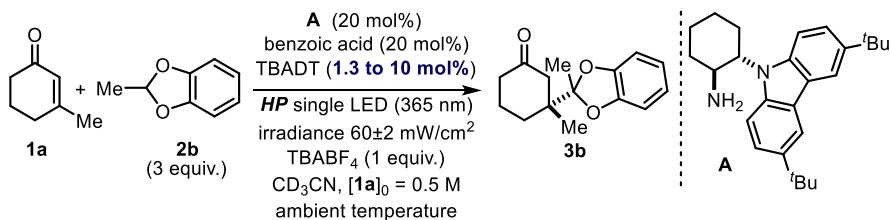
Scheme 6.11 Highlighted are the water-mediated steps in the mechanism for the enantioselective catalytic radical conjugated addition to enones.

The saturation kinetic profile of **1a**, the observable levels of both imine **VII** and iminium **I** in solution, and the zeroth order in water allows us to discard the catalyst condensation as being turnover-limiting step. A negative effect on the reaction rate should be observed when water is added to the system if this was the turnover-limiting step of the transformation. Furthermore, the zeroth order observed with respect to water also suggests that the hydrolysis of the imine intermediate **V**, which leads to the alkylation product **3b** while liberating the aminocatalyst, is not the turnover-limiting step either. The zeroth-order dependence on radical precursor **2b** is not surprising, given that the amount of radicals in solution is dictated by the amount of TBADT photocatalyst, which is present in low concentration (generally 5 mol%).



Scheme 6.12 Highlighted is the TBADT-mediated photoredox cycle, which affords the carbon-centered radical from benzodioxole precursors **2** by means of a HAT mechanism.

We thus focused on the dependence of the reaction rate on TBADT, which could give useful information for extrapolating the reaction mechanism. When doubling the amount of photocatalyst (10 mol%), no change was observed in the reaction rate (Scheme 6.13). However, lowering the amount of TBADT to 2.5 or 1.25 mol%, the rate of the model reaction decreased, indicating saturation kinetic in the concentration of TBADT.

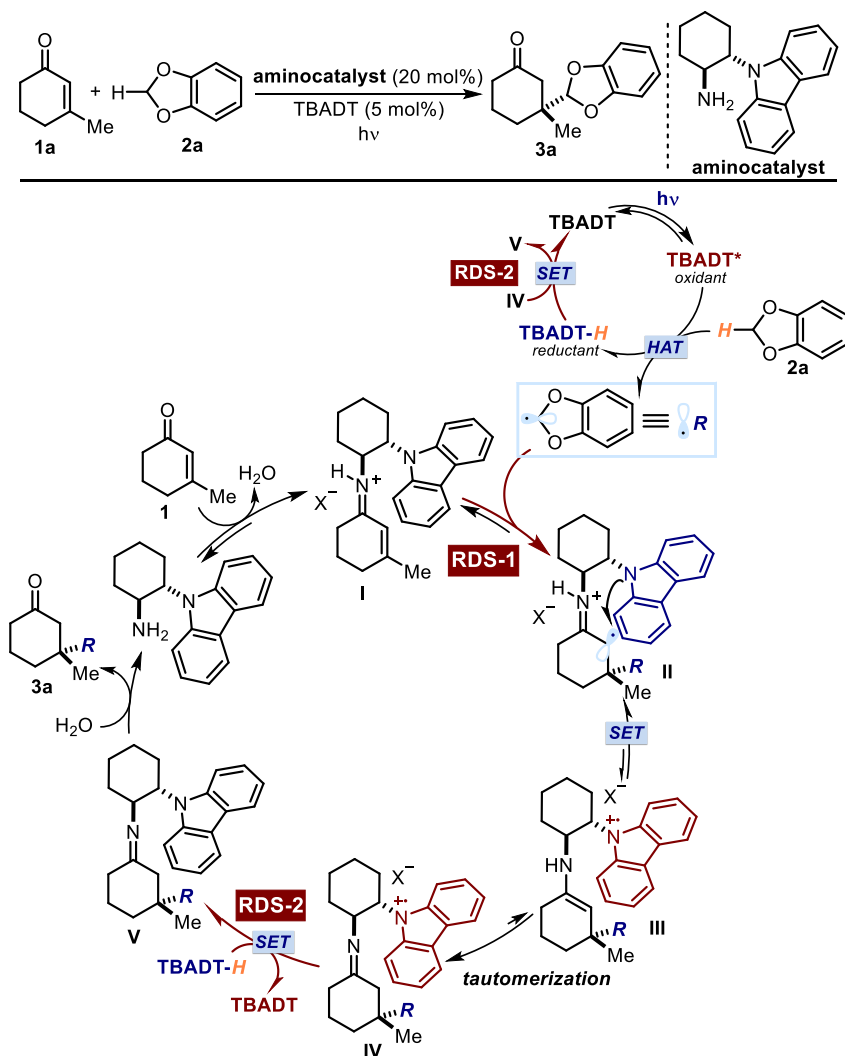


Scheme 6.13 Reaction profile for different initial concentrations of TBADT showing saturation kinetics. [A] = 0.1 M, [1a] = 0.5 M, [2b] = 1.5 M, [TBABF₄] = 0.5 M and [benzoic acid] = 0.1 M and [TBADT] = 0.006 M, 0.0125 M, 0.025 M, and 0.05 M. The error bars represent the standard deviation.

Mechanistically, the kinetic order assessment (particularly the effect of TBADT concentration on the reaction rate) can be reconciled with two possible scenarios, characterized by different turnover-limiting steps (RDS-1 and 2 in Scheme 6.14).

- On the one hand, the concentration of reactive open-shell intermediates is related to the amount of photocatalyst employed. This is because they are generated from substrate **2b** through a HAT mechanism triggered by the photoexcited TBADT. As a result, the effect of the concentration of TBADT on the reaction rate could be explained with the turnover-limiting step being the trapping of these radical intermediates by the iminium ion **I** (RDS-1, Scheme 6.14). In this scenario, the strong influence of the electronic properties of the catalyst on the reaction rate could be rationalized in terms of the inductive effect of the carbazole moiety influencing the electrophilicity (the LUMO energy) of the iminium ion intermediate **I**.²²

²² Since the transmission of polar effects through σ -bonds dies out over short distances (the iminium ion nitrogen in **I** is three σ -bonds away from the nitrogen carbazole), a more plausible explanation for why the carbazole electronic properties influence the reaction rate can be as follows: we have already shown that the electron-rich carbazole unit is engaged in a charge-transfer interaction with the LUMO of **I** (see Ref 4). The observed reaction behavior may then be explained by a drop in donation of electron density from the carbazole-bearing electron-withdrawing substituents into the LUMO of the iminium ion. This would increase the electrophilicity of **I** accelerating the radical trap and the carbon-carbon bond formation.



Scheme 6.14 Mechanism for the enantioselective catalytic radical conjugated addition to enones showing the two possible turnover-limiting steps: RDS-1 and RDS-2. RDS: rate-determining step.

- On the other hand, if the concentration of TBADT in solution is reduced, a lower amount of the reduced photocatalyst (TBADT-H in Scheme 6.14) would be generated upon radical formation (HAT from substrate **2**). TBADT-H is directly involved in the intermolecular SET event that reduces the long-lived carbazoliumyl radical cation in **IV** to return both the neutral organic catalyst (intermediate **V**) and the photoredox catalyst in the original state. This bimolecular SET event, which is essential to close both the iminium ion and the photoredox cycles, could also be the turnover-limiting

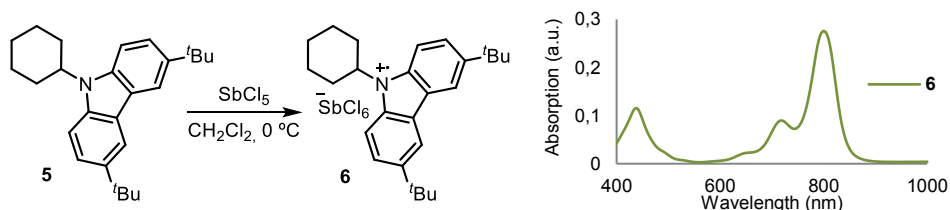
step of the overall process (RDS-2, Scheme 6.14). This could easily explain the striking correlation (Figure 6.3a) between the reaction rate and the reduction potential of the carbazole unit tethered to the aminocatalyst. Since the TBADT⁴/TBADT⁵-H redox couple is reported at -0.96 V vs. Ag/Ag⁺,²³ a greater oxidizing power of the carbazoliumyl radical cation should greatly facilitate the oxidation of TBADT-H by the intermediate **IV**. This is because the exergonic character of the SET from TBADT-H to **IV** increases when the electron density on the carbazole unit is reduced (**F** < **E** < **G** < **H**). This was the exact reactivity trend observed in the kinetic studies: for example, the reaction catalyzed by amine **H** ($E_{1/2} = +1.25$ V) is faster than the amine **F**-mediated process ($E_{1/2} = +1.02$ V).

Our goal was to unambiguously discriminate between these two possibilities and to eventually identify the overall turnover-limiting event. The second mechanistic scenario required the bimolecular SET reduction of intermediate **IV** from the reduced photocatalyst TBADT-H to be turnover-limiting step (RDS-2 in Scheme 6.14). If this mechanistic hypothesis were to hold true, the intermediate **IV** would accumulate in solution. In sharp contrast, if the radical trapping from the iminium ion were turnover-limiting, it would not be possible to detect any carbazoliumyl radical cation intermediate during the process. We therefore performed further experimental studies to detect the presence of mechanistically relevant transient intermediates in the reaction medium.

6.3.4 Photophysical studies

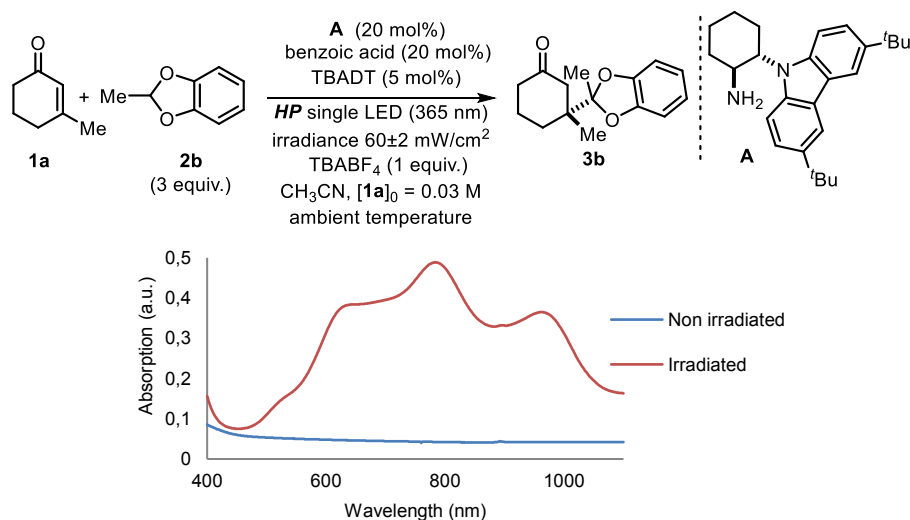
In our previous studies⁴ it was shown that we could isolate the bench-stable hexachloroantimonate carbazoliumyl radical cation salt **6** from *N*-cyclohexyl-3,6-di-*tert*-butyl-carbazole **5**. This species was found to have a characteristic green coloration and the visible absorption spectrum recorded for **6** showed a maximum value at 800 nm (see green spectrum in Scheme 6.15). The striking green coloration of the *N*-cyclohexyl carbazoliumyl radical cation offered an ideal opportunity to check whether a similar intermediate accumulated during the reaction.

²³ Yamase, T.; Takabayashi, N.; Kaji, M. "Solution photochemistry of tetrakis (tetrabutylammonium) decatungstate (VI) and catalytic hydrogen evolution from alcohols" *J. Chem. Soc. Dalton Trans.* **1984**, 793.



Scheme 6.15 Synthesis and optical absorption spectra recorded in CH_3CN in 1 mm path quartz cuvettes of *N*-cyclohexyl carbazoliumyl radical cation **6**. $[\mathbf{6}] = 0.4\text{ mM}$ in CH_3CN .

For this purpose, we recorded the optical absorption spectrum of the reaction mixture. A series of model reactions were performed in CH_3CN under the standard conditions (Scheme 6.7), but in quartz cuvettes. Their absorption spectra were acquired at different irradiation times (a high-power black LED, $\lambda_{\text{max}} = 365\text{ nm}$, with an irradiance of $60 \pm 2\text{ mW/cm}^2$ was used as light source).

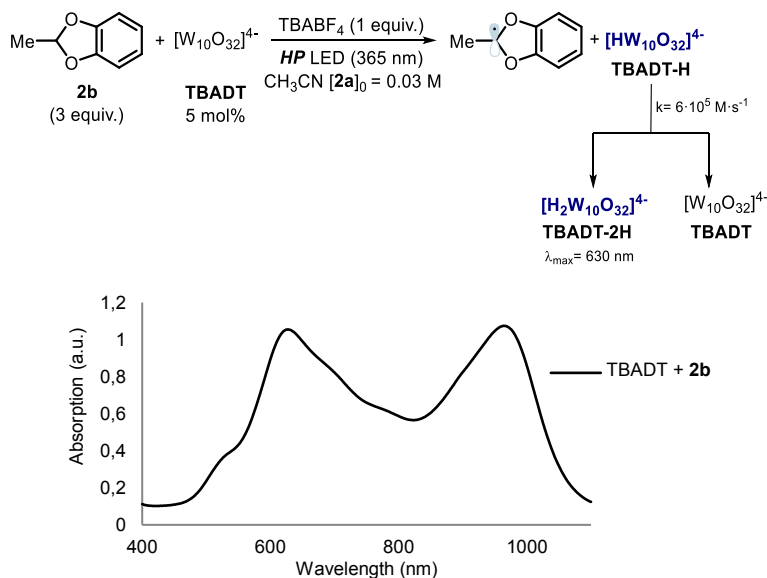


Scheme 6.16 Optical absorption spectra, recorded in CH_3CN . Blue spectrum: mixture containing $[\mathbf{1a}] = 0.03\text{ M}$ ($3.4\text{ }\mu\text{L}$, 0.03 mmol , 1 equiv.), $[\mathbf{A}] = 0.006\text{ M}$ (2.3 mg , 0.006 mmol , 20 mol%), [benzoic acid] = 0.006 M (0.7 mg , 0.006 mmol , 20 mol%), $[\mathbf{2b}] = 0.09\text{ M}$ ($12.5\text{ }\mu\text{L}$, 0.09 mmol , 3 equiv.), $[\text{TBABF}_4] = 0.03\text{ M}$ (9.9 mg , 0.03 mmol , 1 equiv.) and $[\text{TBADT}] = 0.0015\text{ M}$ (5 mg , 0.0015 mmol , 5 mol%) dissolved in 1 mL of CH_3CN , recorded after mixing the reagents *but without illumination*. Red spectrum: same mixture as for the blue spectrum but recorded after *irradiating* for 30 minutes with a high power LED centred at 365 nm (irradiance = $60 \pm 2\text{ mW/cm}^2$).

The mixture containing all the reaction components did not absorb in the visible region if it was kept in dark (blue spectrum in Scheme 6.16). However, upon irradiation, also after as little as 10 minutes of irradiation time, the absorption spectrum of the overall reaction

displayed three maxima in the visible region at 630, 800, and 900 nm (red spectrum in Scheme 6.16).

As a parallel control experiment, the spectra of identically irradiated solutions containing the same mixture but excluding the enone **1a** and the aminocatalyst **A** were recorded (Scheme 6.17). It is known that the reduced photocatalyst TBADT-H and its disproportionated byproduct²⁴ are blue in solution. Accordingly, characteristic peaks were clearly observable in the absorption spectrum of the control experiment, with maxima at 630 nm and 980 nm. However, this spectrum lacks the characteristic band at ≈ 800 nm.



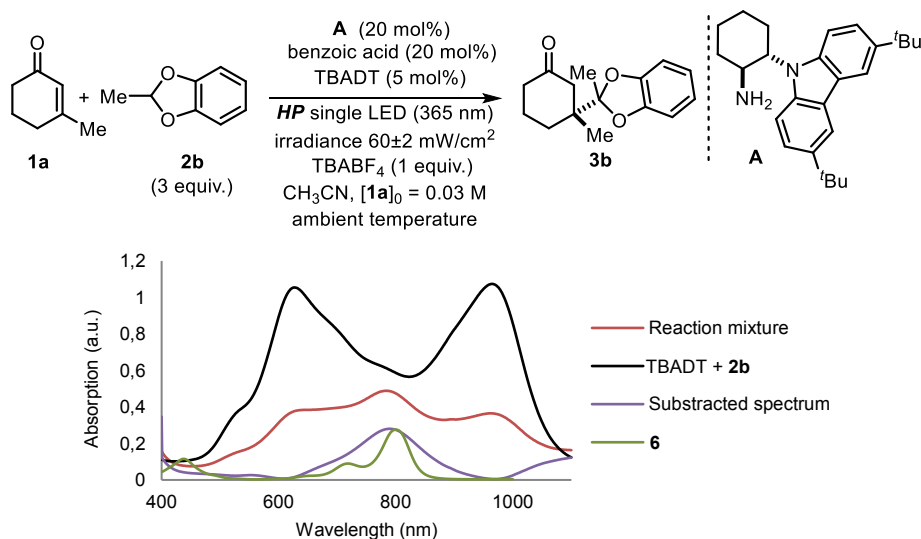
Scheme 6.17 Optical absorption spectra, recorded in CH_3CN after irradiating for 30 minutes with a high power LED centred at 365 nm (irradiance = $60 \pm 2 \text{ mW/cm}^2$). Mixture containing $[\text{benzoic acid}] = 0.006 \text{ M}$ (0.7 mg, 0.006 mmol, 20 mol%), $[2b] = 0.09 \text{ M}$ (12.5 μL , 0.09 mmol, 3 equiv.), $[\text{TBABF}_4] = 0.03 \text{ M}$ (9.9 mg, 0.03 mmol, 1 equiv.) and $[\text{TBADT}] = 0.0015 \text{ M}$ (5 mg, 0.0015 mmol, 5 mol%) dissolved in 1 mL of CH_3CN .

Scheme 6.18 provides a direct comparison of the absorption spectra of the reaction mixture and the TBADT absorption (red and black lines, respectively), showing an

²⁴ a) Renneke, R.F.; Pasquali, M.; Hill, C. L. "Polyoxometalate systems for the catalytic selective production of non-thermodynamics alkenes from alkanes. Nature of excited-state deactivation processes and control of subsequent thermal processes in polyoxometalate photoredox chemistry" *J. Am. Chem. Soc.* **1990**, *112*, 6585.

The nature of the active species generated after the excitation of TBADT is a matter of current debate, see: b) Ravelli, D.; Dondi, D.; Fagnoni, M.; Albini, A.; Bagno, A. "Electronic and EPR spectra of the species involved in $[\text{W}_{10}\text{O}_{32}]^{4-}$ photocatalysis. A relativistic DFT investigation" *Phys. Chem. Chem. Phys.* **2013**, *15*, 2890.

obvious discrepancy in the form of a new band which is only present when all the reaction components are irradiated together. The purple spectrum in Scheme 6.18 is obtained by subtracting the normalized spectrum recorded after irradiation of TBADT and **2b** (black line) from the spectrum recorded for the irradiated reaction mixture (red line). This new spectrum shows an absorption maximum at 800 nm, which is reminiscent of the characteristic line shape of the *N*-cyclohexyl-3,6-di-*tert*-butyl-carbazoliumyl radical cation **6** (green spectrum).



Scheme 6.18 Optical absorption spectra, recorded in CH₃CN. Red spectrum: mixture containing [**1a**] = 0.03 M (3.4 μ L, 0.03 mmol, 1 equiv.), [**A**] = 0.006 M (2.3 mg, 0.006 mmol, 20 mol%), [benzoic acid] = 0.006 M (0.7 mg, 0.006 mmol, 20 mol%), [**2b**] = 0.09 M (12.5 μ L, 0.09 mmol, 3 equiv.), [TBABF₄] = 0.03 M (9.9 mg, 0.03 mmol, 1 equiv.) and [TBADT] = 0.0015 M (5 mg, 0.0015 mmol, 5 mol%) dissolved in 1 mL of CH₃CN.

Black spectrum: mixture containing [**2b**] = 0.09 M (12.5 μ L, 0.09 mmol, 3 equiv.), [TBABF₄] = 0.03 M (9.9 mg, 0.03 mmol, 1 equiv.) and [TBADT] = 0.0015 M dissolved in 1 mL of CH₃CN. Both spectra were recorded after *irradiating* for for 30 minutes with a high power LED centred at 365 nm (irradiance = 60 \pm 2 mW/cm²). Purple spectrum: subtraction of the normalized red spectrum from black spectrum. Green spectra: [**6**] = 0.4 mM in CH₃CN.

The carbazoliumyl radical cation **IVa** could also be generated during the reaction if an off-cycle direct oxidation of the aminocatalyst **A** by the excited-state of TBADT was taking place. This SET event would be highly exergonic²⁵ despite the molar excess of **2b**.

²⁵ Excited photocatalyst/TBADT^S-H redox couple has been estimated to have a value of around > +2.0 V vs. SCE. See: Texier, I.; Delaire, J. A.; Giannotti, C. "Reactivity of the charge transfer

The absorption spectra of a mixture, irradiated in the same manner as the previous samples, containing all the reaction components except for the enone **1a** was recorded. As shown in Figure 6.5, the absorption spectrum of this mixture (orange line) overlaps with the spectra obtained for an identical solution but excluding the aminocatalyst **A** (black line). This experiments exclude the direct oxidation of the catalyst **A** by the excited-state of TBADT under the reaction conditions.

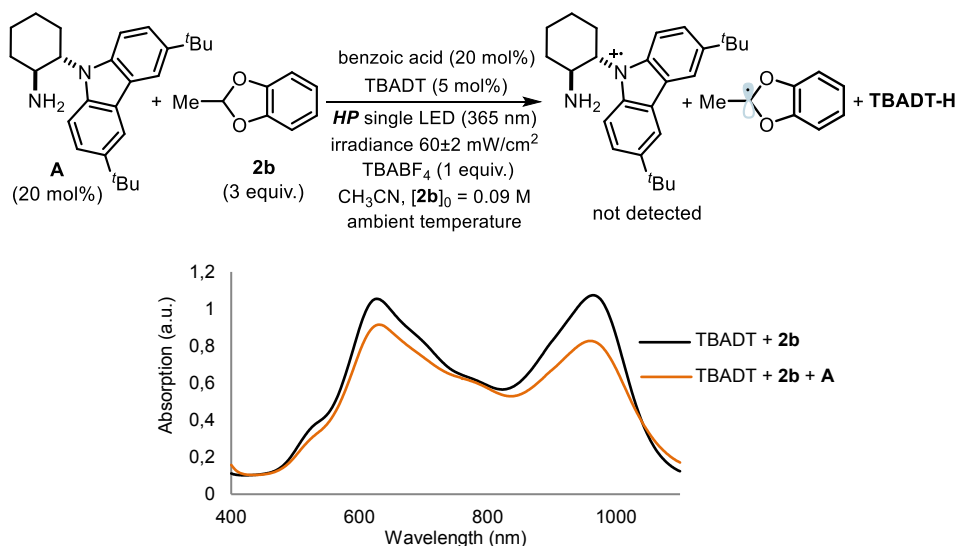


Figure 6.5 Optical absorption spectra, recorded in CH_3CN after irradiating for 30 minutes with a high power LED centred at 365 nm (irradiance = $60 \pm 2 \text{ mW/cm}^2$). Black spectrum: mixture containing [benzoic acid] = 0.006 M (0.7 mg, 0.006 mmol, 20 mol%), **[2b]** = 0.09 M (12.5 μL , 0.09 mmol, 3 equiv.), [TBABF₄] = 0.03 M (9.9 mg, 0.03 mmol, 1 equiv.) and [TBADT] = 0.0015 M (5 mg, 0.0015 mmol, 5 mol%) dissolved in 1 mL of CH_3CN . Orange spectrum: mixture containing [**A**] = 0.006 M (2.3 mg, 0.006 mmol, 20 mol%), [benzoic acid] = 0.006 M (0.7 mg, 0.006 mmol, 20 mol%), **[2b]** = 0.09 M (12.5 μL , 0.09 mmol, 3 equiv.), [TBABF₄] = 0.03 M (9.9 mg, 0.03 mmol, 1 equiv.) and [TBADT] = 0.0015 M (5 mg, 0.0015 mmol, 5 mol%) dissolved in 1 mL of CH_3CN .

The fact that, in the absence of **1a**, the spectrum does not show the characteristic new band at $\approx 800 \text{ nm}$ (observable in the red spectrum instead) further corroborates that the carbazoliumyl radical cation (which can be generated only in the presence of enone **1a** upon radical conjugate addition to the iminium ion) is responsible for the appearance of this peak.

Collectively, the spectroscopic studies indicate that the intermediate **IV** accumulates during the radical conjugate addition process. This behavior is consistent with the overall turnover-limiting step being the reduction of the long-lived carbazoliumyl radical cation in **IV** to return both the neutral organic catalyst and the TBADT photoredox catalyst in the original state (RDS-2, Scheme 6.14).

6.4 Conclusions and remarks

In summary, we have carried out studies aimed at elucidating the key mechanistic aspects of the enantioselective photochemical radical conjugated addition to enones, previously reported by the group.⁴ The experiments herein described point towards the reduction of **IV** as being the turnover-limiting step. In line with this proposal, the carbazoliumyl radical cation **IV** was detected by visible absorption spectrophotometry in the reaction medium, which suggests it is generated before of the turnover-limiting step of the reaction.

The insight that the radical trapping and the enantioselective carbon-carbon bond forming step is not turnover-limiting may pave the way for the mechanistically driven design of the next generation of electron-relay catalysts. In this regard, we have found a strong and predictable correlation between the reaction rate and the reduction potential of the carbazole unit tethered to the aminocatalyst. The knowledge that the redox properties can be rationally tuned for improving catalytic activity may enable the development of new iminium ion-mediated asymmetric RCA of other open-shell intermediates.

6.5 Experimental section

General information: The ^1H and ^{13}C NMR spectra were recorded at 400 MHz or 500 MHz for ^1H and at 100 MHz or 125 MHz for ^{13}C , respectively. The chemical shifts (δ) for ^1H and ^{13}C are given in ppm and are internally referenced to residual protio solvent signals (for CDCl_3 @ 7.26 ppm and 77.0 ppm, respectively; for CD_3CN @ 1.96 ppm ^1H NMR, 118.26 ppm and 1.79 ppm ^{13}C NMR). Coupling constants are given in Hz. When necessary, ^1H and ^{13}C signals were assigned by means of g-COSY 2D-NMR sequence. The following abbreviations are used to indicate the multiplicity: s, singlet; d, doublet; t, triplet; q, quartet; qn, quintet; m, multiplet; bs, broad signal. Optical rotations are reported as follows: $[\alpha]_D^{25}$ (c in g per 100 mL, solvent). Mass spectra (high and low resolution) were obtained from the ICIQ High Resolution Mass Spectrometry Unit on a MicroTOF Focus and Maxis Impact (Bruker Daltonics) with electrospray ionization. UV-vis measurements were carried out on a Shimadzu UV-2401PC spectrophotometer equipped with photomultiplier detector, double beam optics and D₂ and W light sources. Cyclic voltammetry studies was carried out on a Princeton Applied Research PARSTAT 2273 potentiostat offering compliance voltage up to ± 100 V (available at the counter electrode), ± 10 V scan range and ± 2 A current range.

The ^1H , ^{13}C NMR spectra, and the HPLC traces are available in the literature^{1,4} and are not reported in the present thesis.

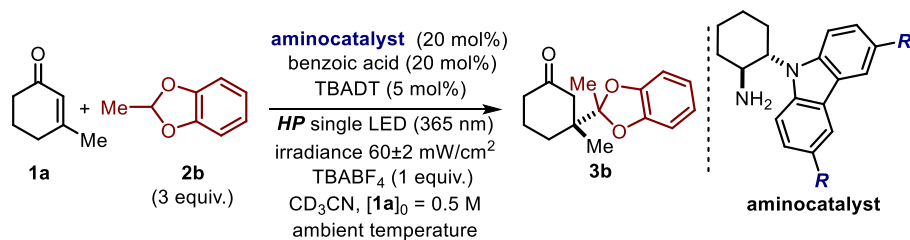
General procedures: All reactions were set up under an argon atmosphere in oven-dried glassware using standard Schlenk techniques, unless otherwise stated. Synthesis grade solvents were used as purchased, anhydrous solvents were taken from a commercial SPS solvent dispenser. Chromatographic purification of products was accomplished using force-flow chromatography (FC) on silica gel (35-70 mesh). Deactivated silica was prepared by adding triethylamine (12.5 g, 2.5 w/w%) to silica gel (35-70 mesh, 500 g) in a 2 L round-bottomed flask and spinning on a rotary evaporator for 12 hours to homogenize the mixture. For thin layer chromatography (TLC) analysis throughout this work, Merck pre-coated TLC plates (silica gel 60 GF254, 0.25 mm) were employed, using UV light as the visualizing agent and an acidic mixture of *para*-anisaldehyde or basic aqueous potassium permanganate (KMnO_4) stain solutions, and heat as developing agents. Organic solutions were concentrated under reduced pressure on a Büchi rotary evaporator.

Determination of enantiomeric purity: HPLC analysis on chiral stationary phase was performed on a Waters ACQUITY® UPC² instrument, using Trefoil AMY1, CEL1, and

CEL2 and Daicel Chiralpak IC-3 as the chiral columns. The exact conditions for the analyses are specified within the characterization section. HPLC traces were compared to racemic samples prepared performing the reaction in the presence of racemic carbazole-derived primary amine catalyst **A**.

Materials: Reagents were purchased at the highest commercial quality from Sigma Aldrich, Fluka, and Alfa Aesar and used as received, without further purification, unless otherwise stated. The inorganic photocatalyst tetrabutylammonium decatungstate (TBADT) was prepared following a literature procedure.²⁶ 2-methylbenzo[d][1,3]dioxole **2b** was prepared following a literature procedure.²⁷ β -Methyl cyclohexenone **1a** and benzodioxole **2a** are commercially available. Catalysts **B**, **C**, and **D** were prepared according to literature procedure.⁴ Full details for the synthesis of other aminocatalysts **A**, **E**, **F**, **G** and **H** used within this study are provided in the following Section 6.5.1; the 1-nitrocyclohexene employed for catalyst preparation is commercially available.

General procedure for the enantioselective iminium ion trapping of radicals

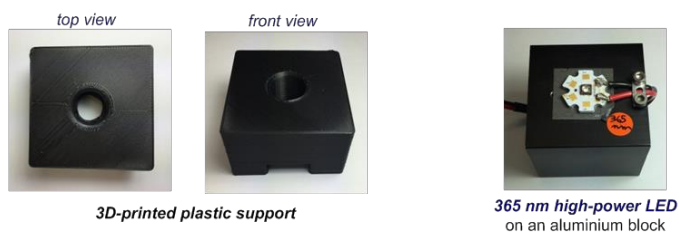


A 5 mL argon-purged glass vial was charged with the tetrabutylammonium decatungstate photocatalyst (TBADT, 0.01 mmol, 5 mol%), the chiral carbazole-derived (*S,S*)-primary amine catalyst (0.04 mmol, 20 mol%), benzoic acid (0.04 mmol, 20 mol%), and tetrabutylammonium tetrafluoroborate (0.2 mmol, 100 mol%). To the vial was then added anhydrous acetonitrile (400 μ L), β -methyl cyclohexenone **1a** (0.2 mmol, 1 equiv.) and 2-methyl benzodioxole **2b** (0.6 mmol, 3 equiv.). The vial was further flushed with argon, closed with a Teflon-coated cap, and sealed with Parafilm, and then placed into a 3D-printed plastic support mounted on an aluminium block fitted with a 365 nm high-power single LED ($\lambda = 365$ nm, irradiance = 60±2 mW/cm², as controlled by an external power supply and measured using a photodiode light detector at the start of each reaction; the

²⁶ Yamase, T.; Usami, T. "Photocatalytic dimerization of olefins by decatungstate (VI) [W₁₀O₃₂]⁴⁻ in acetonitrile and magnetic resonance studies of photoreduced species" *J. Chem. Soc., Dalton Trans.* **1988**, 1, 183.

²⁷ Nichols, D. E.; Kostuba, L. J. "Steric effects of substituents on phenethylamine hallucinogens. 3,4-(Methylenedioxy)amphetamine analogues alkylated on the dioxole ring" *J. Med. Chem.* **1979**, 22, 1264.

set-up is detailed in Figure 6.6). This set-up secured a reliable irradiation while keeping a constant distance of 1.5 cm between the reaction vessel and the light source. No stirring was applied and the irradiation was maintained for the indicated time. The reaction was then diluted with methylene chloride (5 mL) and passed through a pad of silica. The volatiles were removed in vacuum and the residue was purified by column chromatography to give product **3b** in the stated yield and optical purity.



Controlling the light intensity



Photodiode
(measures light intensity)

Power supply
(controls the light intensity)

Reaction set up



aluminium block holding the LED

Figure 6.6 Reaction set-up and the illumination system. The light source for illuminating the reaction vessel consisted in a 365 nm high-power single black LED ($\lambda_{\text{max}} = 365 \text{ nm}$) commercialized under the name of 365nm UV LED Gen 2 Emitter LZ1-00UV00. It was purchase from LED Engin. The LZ1-00UV00 365nm UV LED Gen 2 Emitter is a single LED which provides 2.7 W power centered at 365 nm.

Purification of compound **3b** by flash column chromatography on silica gel: gradient eluent from pure hexane to 9:1 hexane: diethyl ether.

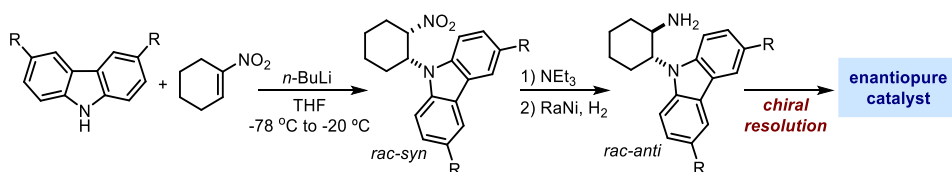
The enantiomeric excess of **3b** was determined by UPC² analysis using the following conditions: Daicel Chiralpak IC-3 column with a gradient (100% CO₂ to 60/40 CO₂/EtOH over 4 minutes, curve 6), flow rate 3 mL/min, $\lambda = 283$ nm: $\tau_{Major} = 2.21$ min, $\tau_{Minor} = 2.27$ min.

Catalyst **A** and **E** afforded the compound with an enantiomeric excess of 88%. Catalyst **F**, **G** and **H** afforded the compound with an enantiomeric excess of 87%.

Products **3a** and **3b** were fully characterized and the data are in agreement with literature.⁴

6.5.1 Synthesis of the aminocatalysts

All the enantiopure chiral aminocatalysts **A**, **E**, **F**, **G** and **H** were synthesized according to the general scheme below.



Scheme 6.19 Preparation of the enantiopure chiral carbazole-based primary amine catalysts.

General procedure for the aza-Michael addition

To an oven dried, argon purged 2-neck round bottomed flask fitted with an argon inlet and septum was added the requisite carbazole (1 equiv.) and anhydrous THF (0.05 M). The reaction mixture was brought to 0 °C and *n*-butyllithium (1.05 equiv.) was added dropwise. The reaction was stirred at 0 °C for 30 minutes. The mixture was cooled to -78 °C. 1-Nitrocyclohex-1-ene (1.1 equiv.) was added to the cold solution. The solution was allowed to reach -20 °C and stirred until full consumption of the carbazole, as inferred by TLC analysis (hexane:ethyl acetate 20:1). The reaction was subsequently quenched with saturated aqueous NH₄Cl solution and extracted with EtOAc. The organic phase was washed with water and brine, dried over magnesium sulphate and concentrated. The crude material (*syn* nitroalkane) was continued to the next step without further purification.

General procedure for the *syn* to *anti* epimerization of the aza-Michael addition adducts

To the crude *syn* nitroalkane (1 equiv.) in a round bottomed flask was added ethyl acetate (0.1 M), methanol (2 equiv.) and triethylamine (2 equiv.). The reaction mixture was

stirred at 40 °C until epimerization was complete as determined by ¹H NMR analysis of the epimeric protons. The reaction mixture was then concentrated to dryness. The crude material containing the *anti* nitroalkane was continued to the next step immediately.

General procedure for the reduction of the nitroalkane.

To the crude *anti* nitroalkane (1 equiv.) suspended in a solution of EtOAc/*n*BuOH (1:3) in a Parr hydrogenation flask was added Raney nickel (commercial slurry in water, 2 tsps per mmol of nitroalkane). The flask was then charged with a hydrogen atmosphere (3-3.5 bar) and shook for 12-24 hours. The reaction mixture was filtered through celite and rinsed with ethyl acetate (*CAUTION*: Raney nickel oxidizes exothermically, the filter cake must not be allowed to become dry) and concentrated. The residue was purified by flash chromatography (1-3% MeOH in DCM, deactivated silica) to obtain the racemic aminocatalyst as a white-yellow solid (70-89% yield over 3 steps).

General procedure for the resolution of the racemic catalyst.

To an oven dried, argon purged, round-bottomed flask was added *rac*-aminocatalyst (3.56 mmol, 1 equiv.) and anhydrous tetrahydrofuran (40 mL). The solution was cooled to 0 °C and anhydrous pyridine (401 μL, 4.98 mmol, 1.4 equiv.) was added followed by dropwise addition of (1*R*)-(-)-menthyl chloroformate (0.916 mL, 4.27 mmol). The reaction was then stirred for 12 hours at room temperature. The reaction was diluted with methylene chloride and washed with 2 M HCl solution, water and then brine solution. The organic phase was then dried over MgSO₄, and concentrated to an off-white solid. The residue containing both menthyl carbamates of (*S,S*)-enantiomer and (*R,R*)-enantiomer was separated by flash chromatography (pentane:DCM 1:1) to afford both of the enantiopure menthyl carbamates of (*R,R*)- enantiomer (first fraction) and (*S,S*)- enantiomer (second fraction).

General procedure for the hydrolysis of enantiopure (-)-menthyl carbamate to give enantiopure aminocatalysts

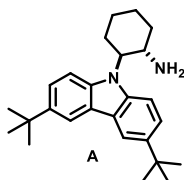
To an oven dried, argon purged, two neck flask fitted with a condenser/argon inlet and septum was added the enantiopure (-)-menthyl carbamate (1 equiv.) and it was diluted with anhydrous methylene chloride (0.1 M). To this mixture was sequentially added trifluoroacetic acid (10 equiv.) and trifluoromethanesulfonic acid (3 equiv.). The green reaction mixture was heated to reflux for exactly 2 hours, then cautiously quenched with a saturated solution of NaHCO₃, and extracted with methylene chloride (2 x 20 mL). The organic phases were combined, washed with water, brine and dried over MgSO₄ before being concentrated. The enantiopure catalyst was obtained after flash chromatography (1-

2% MeOH in DCM, deactivated silica) as a white solid: 50-60% yields for (*R,R*)-enantiomer and 55-70% yields for (*S,S*)-enantiomer over 2 steps.

General procedure for the determination of enantiomeric excess of the aminocatalysts

The aminocatalyst (2 mg) was added to a small sample vial and dissolved in methylene chloride (200 μ L), followed by the addition of one drop of triethylamine and one drop of 1-fluoro-2,4-dinitrobenzene (Sanger's reagent). The crude material was then filtered through a pipette filled with silica gel using a solution of hexane:EtOAc (9:1). Only the brightly colored portion of the filtrate was collected, and diluted for injection in the HPLC or UPC² equipped with a chiral stationary phase column.

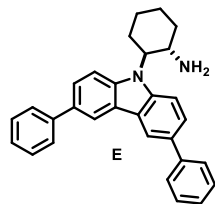
(1*S*,2*S*)-2-(3,6-di-*tert*-butyl-9*H*-carbazol-9-yl)cyclohexan-1-amine (A)



The enantiomeric excess of the catalyst, derived with Sanger's reagent, was determined to be 99% by HPLC analysis on a Daicel Chiralpak IC-3 column: 70/30 hexane/isopropanol, flow rate 0.8 mL/min, $\lambda = 350$ nm: $\tau_{\text{Major}} = 12.34$ min, $\tau_{\text{Minor}} = 8.33$. $[\alpha]_{\text{D}}^{26} = -65.4$ ($c = 0.06$, CHCl_3). **¹H NMR:** (500 MHz, CDCl_3) δ 8.12 (d, $J = 8.9$ Hz, 2H), 7.60-7.37 (m, 4H), 4.14 (ddd, $J = 12.4$ Hz, 10.2 Hz, 3.9 Hz, 1H), 3.72 (td, $J = 10.6$ Hz, 4.1 Hz, 1H), 2.39 (qd, $J = 12.6$ Hz, 3.7 Hz, 1H), 2.25-2.12 (m, 1H), 1.94 (t, $J = 13.3$ Hz, 3H), 1.67-1.52 (m, 2H), 1.48 (s, 18H), 1.45-1.34 (m, 1H). **¹³C NMR:** (126 MHz, CDCl_3) δ 141.6, 140.2, 137.0, 124.0, 123.5, 122.9, 122.5, 116.4, 116.0, 111.0, 108.4, 63.2, 52.1, 35.4, 34.6, 32.01, 29.5, 26.2, 25.2.

Characterization data in agreement with the literature.⁴

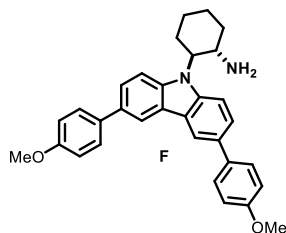
(1*S*,2*S*)-2-(3,6-diphenyl-9*H*-carbazol-9-yl)cyclohexan-1-amine (E)



The enantiomeric excess of the catalyst, derived with Sanger's reagent, was determined to be 99% by UPC² analysis using the following conditions: Daicel Chiralpak IC-3 column with a gradient (100% CO_2 to 60/40 CO_2/MeOH over 4 minutes, curve 6), flow rate 3 mL/min, $\lambda = 260$ nm: $\tau_{\text{Major}} = 7.72$ min, $\tau_{\text{Minor}} = 6.70$ min. $[\alpha]_{\text{D}}^{25} = -25 \pm 2$ ($c = 0.10$, CHCl_3). **HRMS:** calculated for $\text{C}_{30}\text{H}_{29}\text{N}_2$ 417.2325, found 417.2343. **¹H NMR:** (400 MHz, CDCl_3) δ 8.47 (d, $J = 10.7$ Hz, 2H), 7.85 – 7.78 (d, $J = 7.6$ Hz, 4H), 7.70 (d, $J = 8.4$ Hz, 2H), 7.64 (bs, $J = 8.8$ Hz, 2H), 7.55 (bs, $J = 7.7$ Hz, 4H), 7.46 – 7.38 (m, 2H), 4.29 (ddd, $J = 12.6, 10.5, 3.7$ Hz, 1H), 3.82 (bs, $J = 10.5, 4.1$ Hz, 1H), 2.48 (tq, $J = 11.4, 3.7$ Hz, 1H), 2.32 – 2.18 (bs, 1H), 2.09 – 1.95 (m, 3H), 1.67 – 1.34 (m, 3H). **¹³C NMR:** (101 MHz, CDCl_3) δ 141.9, 141.8,

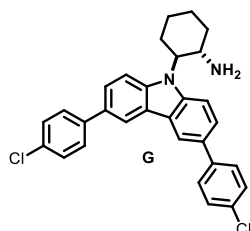
141.62, 138.40, 132.74, 132.63, 128.87, 127.31, 126.62, 125.65, 125.04, 124.87, 123.40, 119.07, 118.70, 111.96, 109.63, 62.92, 52.09, 34.9, 29.5, 26.1, 25.1.

(1*S*,2*S*)-2-(3,6-bis(4-methoxyphenyl)-9*H*-carbazol-9-yl)cyclohexan-1-amine (F)



The enantiomeric excess of the catalyst, derived with Sanger's reagent, was determined to be 99% by UPC² analysis using the following conditions: Daicel Chiralpak IC-3 column with a gradient (100% CO₂ to 60/40 CO₂/MeOH over 4 minutes, curve 6), flow rate 3 mL/min, $\lambda = 260$ nm: $\tau_{Major} = 7.43$ min, $\tau_{Minor} = 6.57$ min. $[\alpha]_D^{25} = -19 \pm 2$ ($c = 0.06$, CHCl₃). **HRMS**: calculated for C₃₂H₃₃N₂O₂ 477.2537, found 477.2554. **¹H NMR**: (400 MHz, CDCl₃) δ 8.29 (d, $J = 8.8$ Hz, 2H), 7.77 – 7.58 (m, 6H), 7.58 – 7.41 (m, 2H), 7.02 (d, $J = 8.3$ Hz, 4H), 4.42 – 4.24 (m, 1H), 3.88 (s, 6H), 3.69 (td, $J = 10.8$, 10.0, 4.0 Hz, 1H), 2.45 – 2.25 (m, 1H), 2.22 – 2.08 (m, 1H), 2.02 – 1.75 (m, 3H), 1.65 – 1.42 (m, 3H). **¹³C NMR**: (101 MHz, CDCl₃) δ 158.6, 141.1, 137.9, 134.4, 134.2, 132.3, 132.2, 128.9, 128.1, 125.2, 124.6, 123.3, 118.4, 118.0, 114.2, 111.7, 109.6, 62.0, 55.3, 52.0, 34.1, 29.3, 25.8, 24.9.

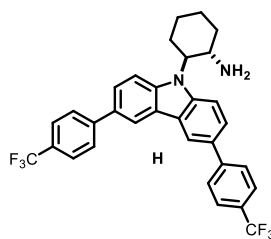
(1*S*,2*S*)-2-(3,6-bis(4-chlorophenyl)-9*H*-carbazol-9-yl)cyclohexan-1-amine (G)



The enantiomeric excess of the catalyst, derived with Sanger's reagent, was determined to be 99% by UPC² analysis using the following conditions: Daicel Chiralpak IC-3 column with a gradient (100% CO₂ to 60/40 CO₂/EtOH over 4 minutes, curve 6), flow rate 3 mL/min, $\lambda = 260$ nm: $\tau_{Major} = 6.89$ min, $\tau_{Minor} = 6.22$ min. $[\alpha]_D^{25} = -33 \pm 2$ ($c = 0.09$, CHCl₃). **HRMS**: calculated for C₃₀H₂₇Cl₂N₂ 485.1546, found 485.1563. **¹H NMR**: (400 MHz, CDCl₃) δ 8.32 (d, $J = 7.5$ Hz, 2H), 7.78 – 7.56 (m, 8H), 7.54 – 7.35 (m, 4H), 4.32 (ddd, $J = 12.5$, 10.4, 3.9 Hz, 1H), 3.74 (td, $J = 9.6$, 4.2 Hz, 1H), 2.38 (td, $J = 12.8$, 9.0 Hz, 1H), 2.26 – 2.12 (m, 1H), 2.04 – 1.81 (m, 3H), 1.65 – 1.39 (m, 3H). **¹³C NMR**: (101 MHz, CDCl₃) δ 141.8, 140.3, 138.6, 132.6, 131.4, 128.9, 128.4, 127.3, 125.5, 124.8, 123.3, 118.9, 118.5, 112.1, 109.7, 63.4, 52.1, 35.3, 29.6, 26.2, 25.2.

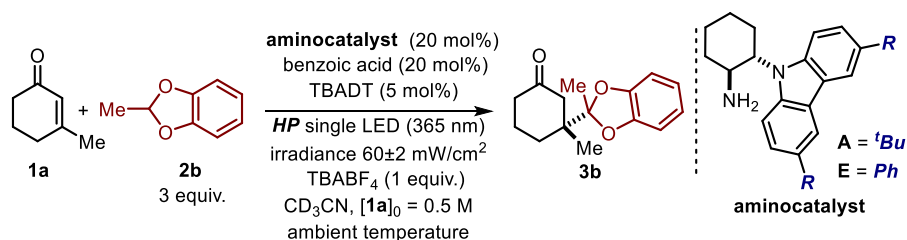
(1*S*,2*S*)-2-(3,6-bis(4-(trifluoromethyl)phenyl)-9*H*-carbazol-9-yl)cyclohexan-1-amine (H)

The enantiomeric excess of the catalyst, derived with Sanger's reagent, was determined to be 99% by UPC² analysis using the following conditions: Daicel Chiralpak IC-3 column with a gradient (100% CO₂ to 60/40 CO₂/MeOH over 4 minutes, curve 6), flow rate 3 mL/min, $\lambda = 260$ nm: $\tau_{Major} = 4.58$ min, $\tau_{Minor} = 4.26$ min. $[\alpha]_D^{25} = -19 \pm 2$ ($c = 0.12$,



CHCl₃). **HRMS**: calculated for C₃₂H₂₇F₆N₂ 553.2073, found 553.2100. **¹H NMR**: (400 MHz, CDCl₃) δ 8.43 (d, *J* = 8.0 Hz, 2H), 7.85 (d, *J* = 8.2 Hz, 4H), 7.81 – 7.69 (m, 8H), 4.38 – 4.23 (m, 1H), 3.82 (s, 1H), 2.45 (tt, *J* = 12.3, 6.5 Hz, 1H), 2.24 (d, *J* = 12.3 Hz, 1H), 2.07 – 1.86 (m, 2H), 1.71 – 1.44 (m, 3H), 1.41 – 1.22 (m, 1H). **¹³C NMR**: (101 MHz, CDCl₃) δ 145.3, 145.2, 142.1, 138.9, 131.3, 131.2, 128.5, 127.4, 125.8, 125.8, 125.8, 125.7, 125.2, 124.8, 123.3, 123.1, 119.3, 118.9, 112.3, 109.9, 63.2, 52.0, 35.1, 29.6, 26.0, 25.1. **¹⁹F NMR**: (376 MHz, CDCl₃) δ -61.9.

6.5.2 Kinetic studies



Scheme 6.20 The model reaction for the kinetic studies.

All kinetic experiments were conducted using the set-up depicted in Figure 6.6, and an illumination system (HP black LED, $\lambda_{\text{max}} = 365 \text{ nm}$) with an irradiance of $60 \pm 2 \text{ mW/cm}^2$. This ensured the reactions not to be light-limited.

The reaction between β -methyl cyclohexenone (**1a**) and 2-methyl benzodioxole (**2b**) to afford the radical conjugate addition product **3b** was chosen as the model for the kinetic studies (Scheme 6.20). We applied the method of initial-rate kinetics, monitoring the progress of the reactions by ¹H NMR analysis and following the conversion until 15%. The initial rates were plotted against concentration to obtain straight lines. Our initial-rate kinetic studies required an independent reaction to be performed for every data-point at different times.

Two independent series of kinetic investigations were performed using both carbazole-based aminocatalysts **A** and **E**, which provided similar and reproducible kinetic profiles.

Procedure for the initial-rate kinetics:

Three sets of reactions with equivalent concentrations of each reactant, except for the component whose order is being measured, were carried out in three identical 5 mL glass vials. The vials containing the reaction mixtures were positioned 1.5 cm away from the light source. Each one was irradiated from the bottom with a HP LED centered at 365 nm

irradiating with 450 μA (irradiance of $60\pm 2 \text{ mW/cm}^2$) without stirring. This procedure was repeated 4 times quenching the reactions at different time intervals and the whole experiment was repeated twice.

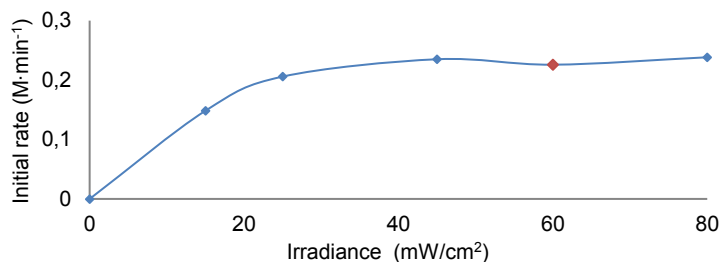
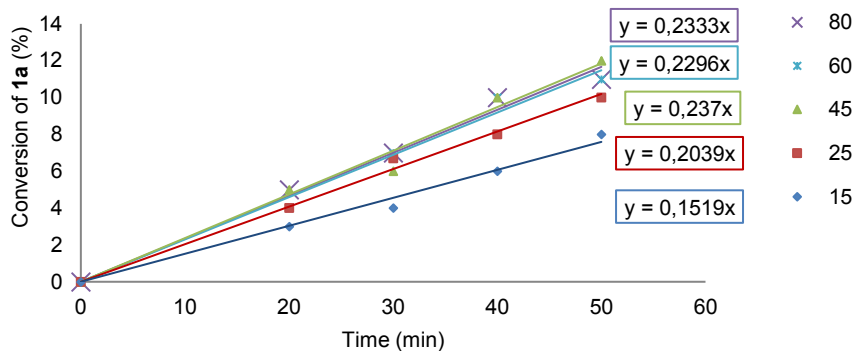
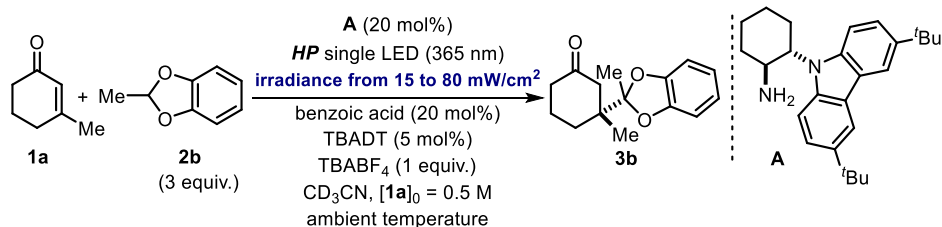
The model reaction was set up utilizing a stock solution containing 105 mg of the aminocatalyst (**A** or **E**) (0.28 mmol, 20 mol%), 34 mg of benzoic acid (0.28 mmol, 20 mol%), 464 mg of TBABF₄ (1.4 mmol, 1 equiv.), 231 mg of TBADT (0.07 mmol, 5 mol%) dissolved in 2.8 mL of anhydrous acetonitrile. To this solution (0.1 M in aminocatalyst), 158 μL of 3-methyl-2-cyclohexenone **1a** (1.4 mmol, 1 equiv.) and 560 μL of 3-methylbenzodioxole **2b** (4.2 mmol, 3 equiv.) were sequentially added. After irradiating for the indicated time, the conversion of both substrates (3-methyl-2-cyclohexenone **1a** and 3-methylbenzodioxole **2b**) into the final product **3b** was determined by ¹H NMR analysis of the crude reaction mixture. The reaction is clean and nor byproducts or substrate decomposition has been observed.

These conditions account for the following concentrations: [aminocatalyst] = 0.1 M, [**1a**] = 0.5 M, [**2b**] = 1.5 M, [TBADT] = 0.025 M, [TBABF₄] = 0.5 M and [benzoic acid] = 0.1 M.

Range of concentrations employed

To measure the order with respect to each component, we varied the concentration of the reagent under study in the following ranges:

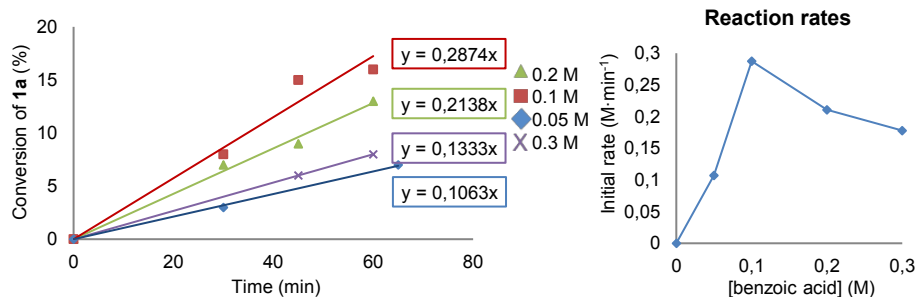
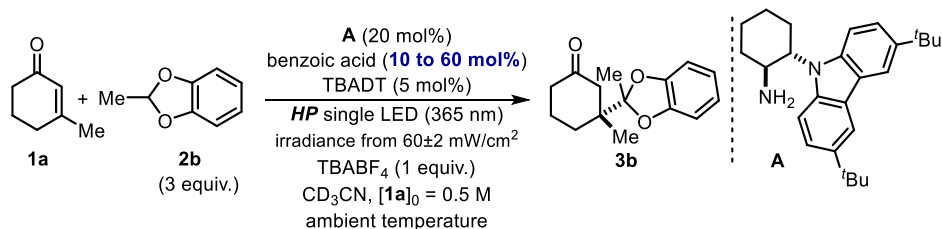
- [benzoic acid] from 0.05 M to 0.3 M.
- [aminocatalyst] from 0.05 M to 0.2 M.
- [**1a**] from 0.25 M to 1 M.
- [**2b**] from 0.75 M to 3 M.
- [TBADT] from 0.006 to 0.05 M.
- [H₂O] from anhydrous to 2.5 M.

Rate dependence on the light intensity:

Scheme 6.21 Reaction profiles at different light intensities: 15 mW/cm² (dark blue line); 25 mW/cm² (red line); 45 mW/cm² (green line); 60 mW/cm² (light blue line); 80 mW/cm² (purple line) (*up*). Rate constants calculated from the slope of the plots.

As shown in Scheme 6.21, the rate of the model reaction catalyzed by **A** was found to linearly correlate with the light intensity to then reach a standstill for irradiances higher than 40 mW/cm². All the following kinetic studies were performed using the set-up discussed in Figure 6.6 and an illumination system (HP black LED, $\lambda_{\text{max}} = 365 \text{ nm}$) with an irradiance of $60 \pm 2 \text{ mW/cm}^2$. This ensured the reactions not to be light-limited.

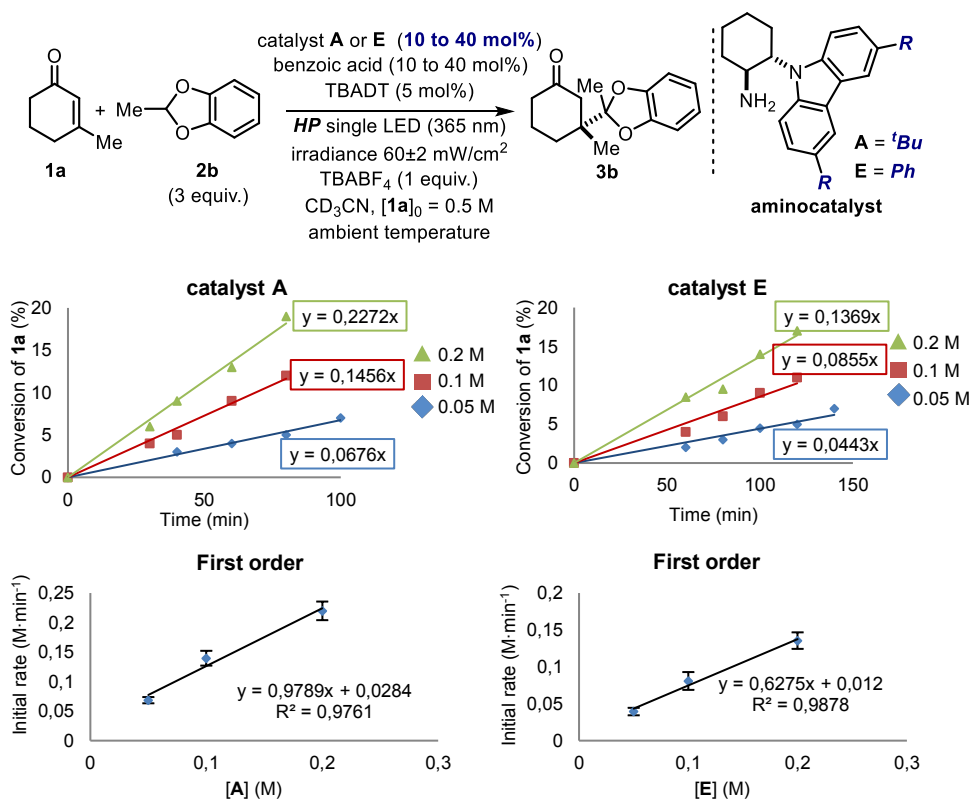
Rate dependence on [benzoic acid]



Scheme 6.22 Reaction profiles of initial-rate measurements at different initial concentrations of benzoic acid: [benzoic acid]₀ = 0.05 M (blue line); [benzoic acid]₀ = 0.1 M (red line); [benzoic acid]₀ = 0.2 M (green line); [benzoic acid]₀ = 0.3 M (purple line). Rate constants calculated from the slope of the plots.

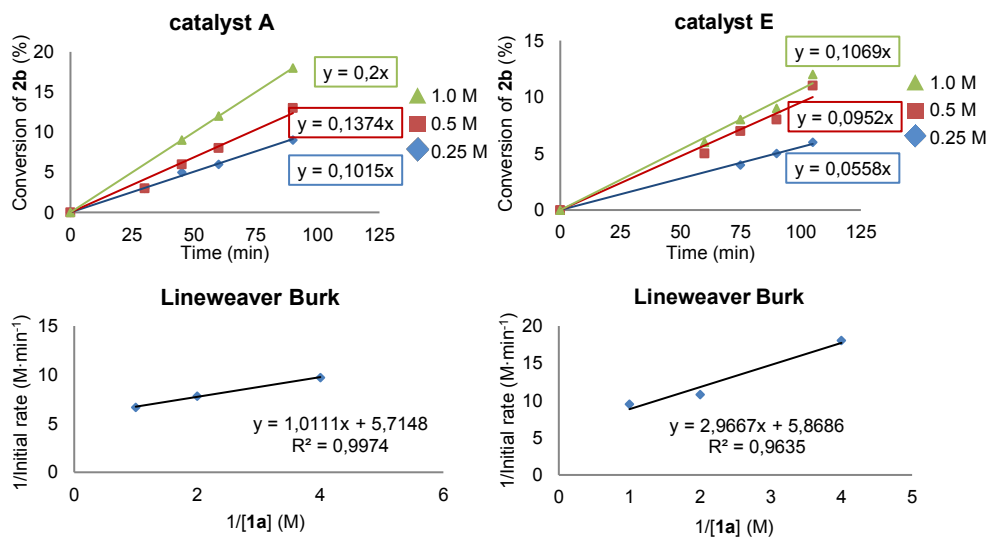
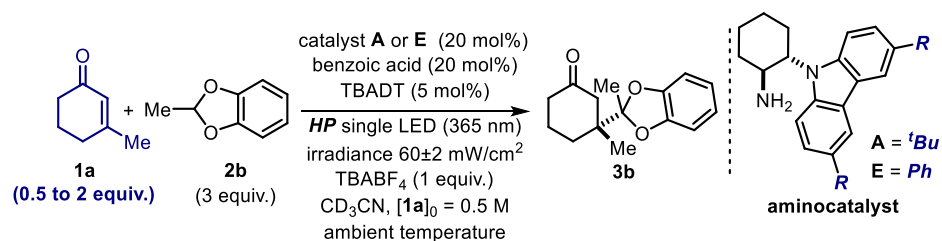
As shown in Scheme 6.22, a 0.1 M (20 mol%) concentration of benzoic acid provided for the highest reaction rate. All other kinetic experiments were conducted using a 1:1 aminocatalyst:benzoic acid ratio (20 mol%).

Order dependence in aminocatalyst



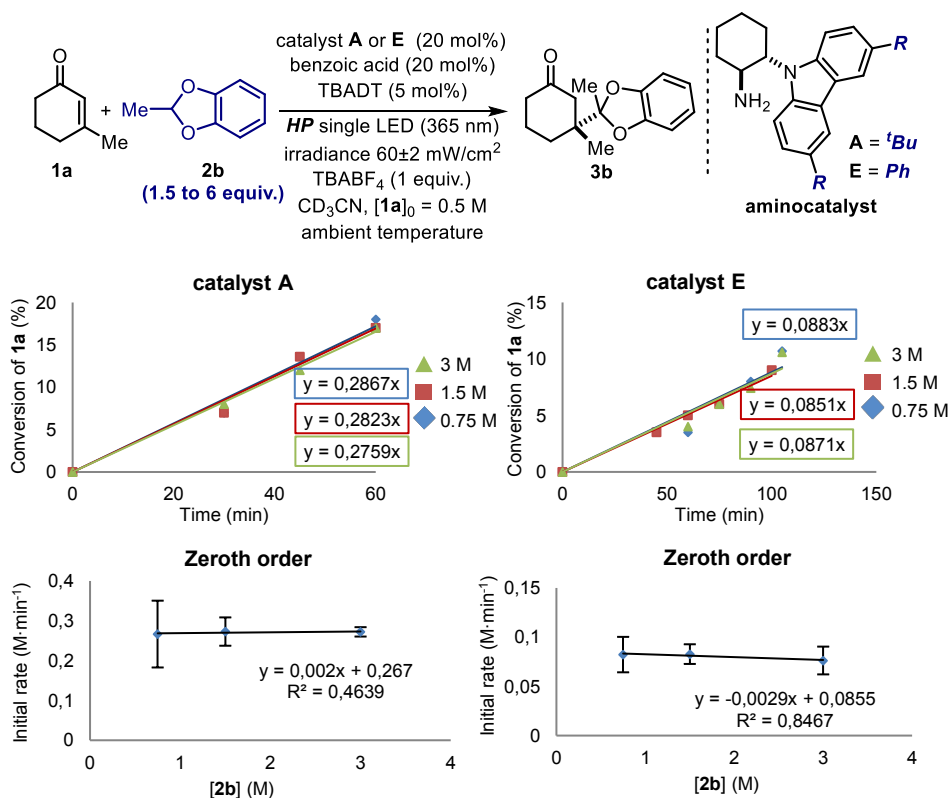
Scheme 6.23 Reaction profiles at different initial concentrations of catalyst **A/E** showing a first-order dependence in [aminocatalyst]. Rate constants calculated from the slope of the plots. [A]₀ = [BA]₀ = 0.05 M (blue line); [A]₀ = [BA]₀ = 0.1 M (red line); [A]₀ = [BA]₀ = 0.2 M (green line) (*up left*); [E]₀ = [BA]₀ = 0.05 M (blue line); [E]₀ = [BA]₀ = 0.1 M (red line); [E]₀ = [BA]₀ = 0.2 M (green line) (*up right*). Rates determined while varying: [A]₀ (*down left*) and [E]₀ (*down right*). The error bars represent the standard deviation.

As shown in Scheme 6.23, a first-order dependence in [aminocatalyst] was determined.

Order dependence in enone **1a**

Scheme 6.24 Reaction profiles of initial-rate measurements at different initial concentrations of **1a** showing a saturation kinetic profile. Rate constants calculated from the slope of the plots. [1a]₀ = 1.0 M (green line), [1a]₀ = 0.5 M (red line) and [1a]₀ = 0.25 M (blue line) (*up*). Lineweaver-Burk plot for the rates determined while varying [1a]₀ (*down* panels). Both data obtained employing catalyst **A** (*plots in the left panel*), and catalyst **E** (*plots in the right panel*) show saturation kinetics.

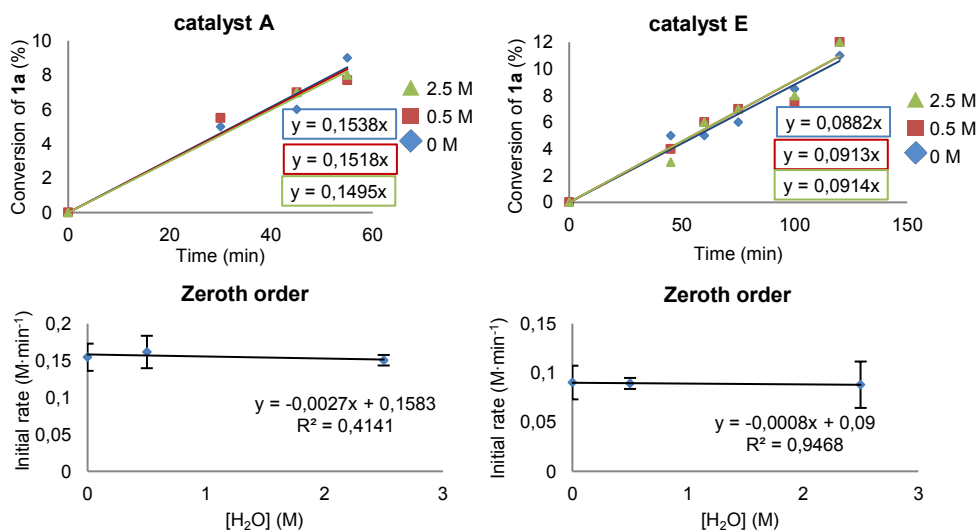
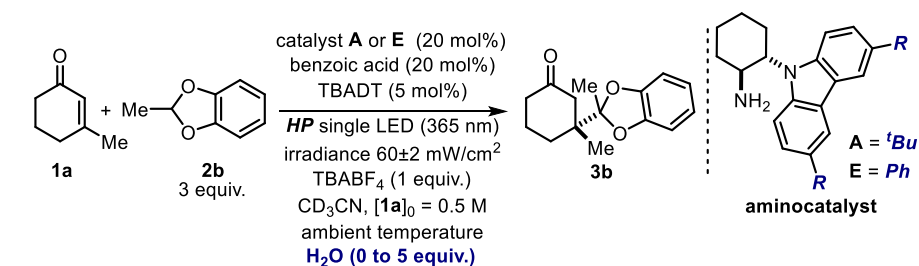
As shown in Scheme 6.24, a saturation kinetics profile with respect to [1a] was observed for both catalysts **A** and **E**. It was confirmed by Lineweaver-Burk plot.

Order dependence in benzodioxole **2b**

Scheme 6.25 Reaction profiles of initial-rate measurements at different initial concentrations of **2b** showing a zeroth-order dependence. Rate constants calculated from the slope of the plots. [2b]₀ = 0.75 M (blue line); [2b]₀ = 1.5 M (red line); [2b]₀ = 3 M (green line) (*upper panel*). Rates determined while varying [2b]₀ (*down panels*). Both data obtained employing catalyst **A** (*plots in the left panel*), and catalyst **E** (*plots in the right panel*) show zeroth-order kinetics. The error bars represent the standard deviation.

As shown in Scheme 6.25, a zeroth-order dependence in [2b] was determined.

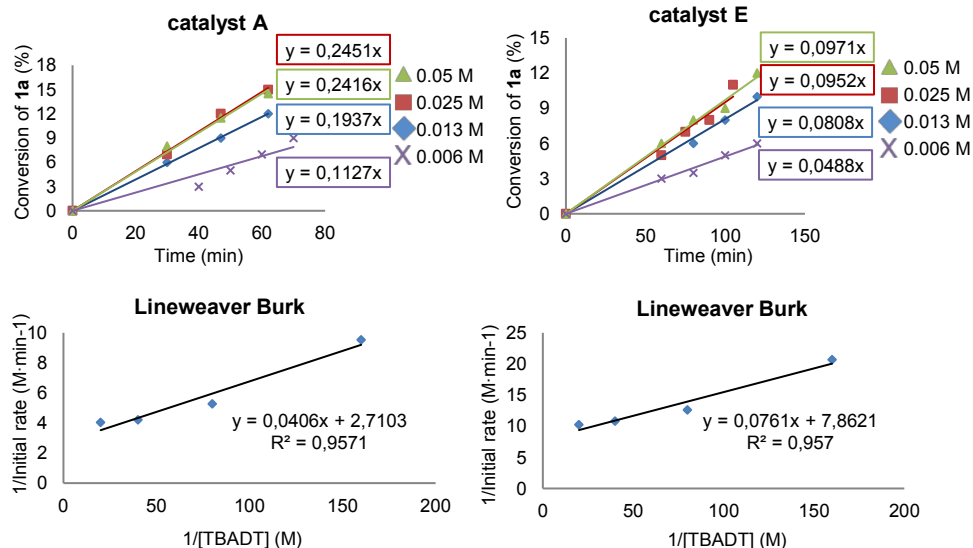
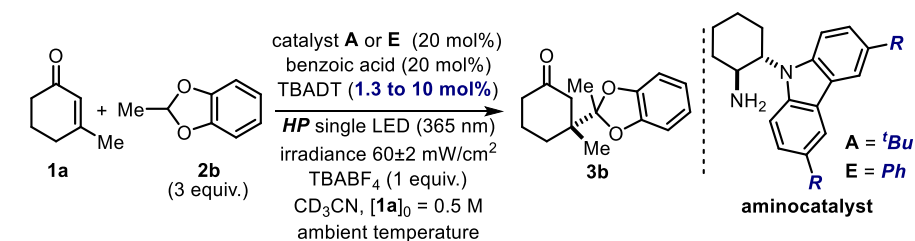
Order dependence in water



Scheme 6.26 Reaction profiles of initial-rate measurements at different initial concentrations of water showing a zeroth-order dependence. Rate constants calculated from the slope of the plots. [H₂O]₀ ≈ 0 (blue line); [H₂O]₀ = 0.5 M (red line); [H₂O]₀ = 2.5 M (green line) (*upper panels*). Rates determined while varying [H₂O]₀ (*down panels*). Both data obtained employing catalyst **A** (*plots in the left panel*), and catalyst **E** (*plots in the right panel*) show zeroth order kinetics. The error bars represent the standard deviation.

As shown in Scheme 6.26, a zeroth-order dependence in [water] was determined.

Order dependence in the photocatalyst (TBADT)

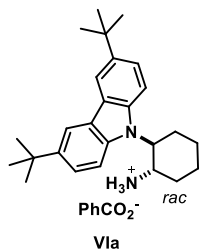


Scheme 6.27 Reaction profiles of initial-rate measurements at different initial concentrations of **TBADT** showing a saturation kinetic profile. Rate constants calculated from the slope of the plots. [TBADT]₀ = 0.006 M (purple line); [TBADT]₀ = 0.0125 M (blue line); [TBADT]₀ = 0.025 M (red line); [TBADT]₀ = 0.05 M (green line) (*upper panels*). Lineweaver-Burk plot for the rates determined while varying [TBADT]₀ (*down panels*). Both data obtained employing catalyst **A** (*plots in the left panel*), and catalyst **E** (*plots in the right panel*) show a saturation kinetics profiles. The error bars represent the standard deviation.

As shown in Scheme 6.27, when doubling the amount of photocatalyst (from 5 to 10 mol%), no change in the reaction rate was observed. However, lowering the amount of TBADT to 2.5 or 1.25 mol% decreased the rate of the model reaction, indicating a saturation kinetic profile in [TBADT]. This profile was confirmed by the Lineweaver-Burk plot.

6.5.3 Characterization of the intermediates involved in iminium ion formation

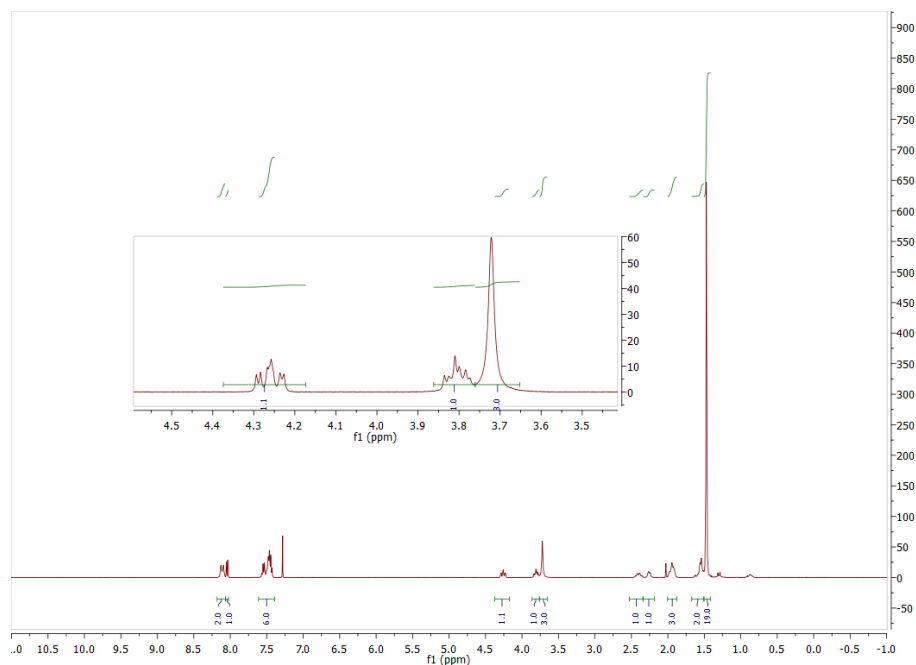
2-(3,6-di-tert-butyl-9H-carbazol-9-yl)cyclohexan-1-aminium benzoate (VIa):



An authentic sample of the protonated catalyst **A** was synthesized as follows: to an oven-dried, argon purged 5 mL glass vial sealed with a Teflon septum was added (*rac*)-2-(3,6-di-tert-butyl-9H-carbazol-9-yl)cyclohexan-1-amine **A** (15.2 mg, 0.04 mmol, 1 equiv.) and benzoic acid (4.9 mg, 0.04 mmol, 1 equiv.). The vial was then charged with anhydrous acetonitrile (0.5 mL). The mixture was heated to 70 °C until the precipitate was dissolved. The mixture was

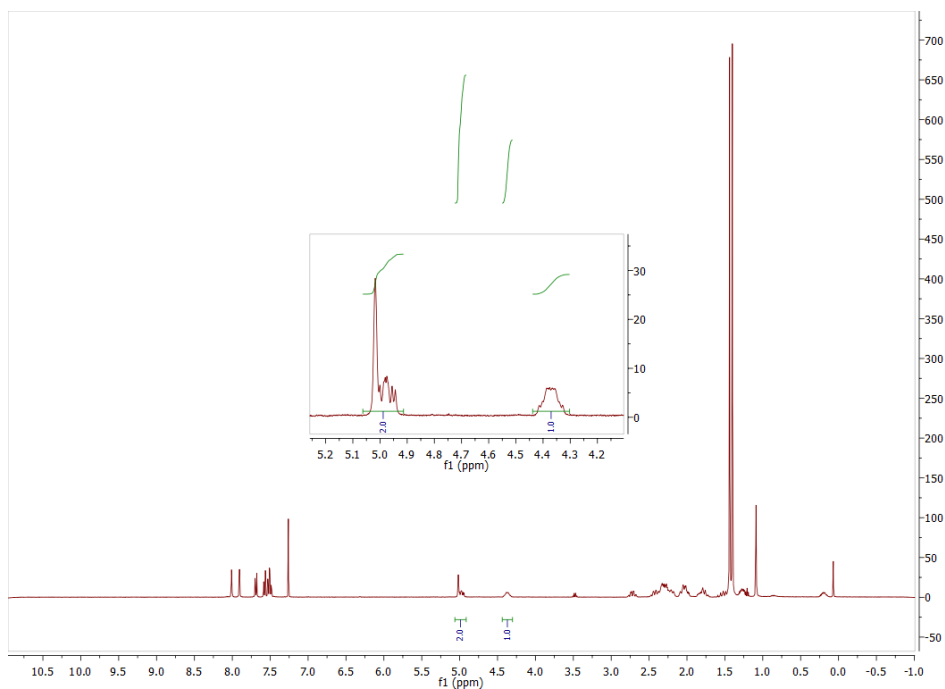
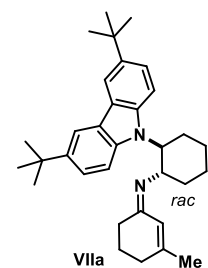
allowed to cool; a white crystalline solid formed. The solid was collected by filtration and washed with cold anhydrous acetonitrile to give white crystalline solid, 10.1 mg (51%).

HRMS: Calculated for C₂₆H₃₇N₂ 377.2951, found 377.2958. **¹H NMR:** (400 MHz, CDCl₃) δ 8.11 (d, *J* = 13.9 Hz, 2H), 8.07 – 8.02 (m, 1H), 7.61 – 7.39 (m, 6H), 4.26 (ddd, *J* = 12.3, 10.3, 3.9 Hz, 1H), 3.80 (td, *J* = 10.4, 4.5 Hz, 1H), 3.72 (s, 3H), 2.40 (qd, *J* = 13.4, 12.6, 4.8 Hz, 1H), 2.34 – 2.18 (m, 1H), 2.00 – 1.87 (m, 3H), 1.67 – 1.50 (m, 2H), 1.47 (s, 19H). **¹³C NMR:** (101 MHz, CDCl₃) δ 170.5, 141.8, 140.00, 136.9, 132.4, 132.2, 129.8, 128.1, 124.1, 123.6, 122.9, 122.6, 116.5, 115.99, 111.0, 108.4, 62.2, 52.0, 34.6, 34.4, 32.0, 29.4, 26.0, 25.1.

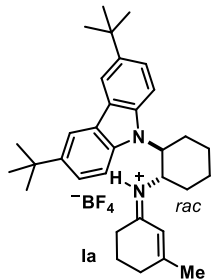


(Z)-N-(2-(3,6-di-tert-butyl-9H-carbazol-9-yl)cyclohexyl)-3-methylcyclohex-2-en-1-imine (VIIa):

An authentic sample of the imine intermediate **VIIa** was synthesized according to the literature.⁴ **HRMS**: Calculated for C₃₃H₄₅N₂ 469.3577, found 469.3575. **¹H NMR**: (400 MHz, CDCl₃) δ 8.00 (d, *J* = 1.7 Hz, 1 H), 7.91 (d, *J* = 1.7 Hz, 1 H), 7.69 (d, *J* = 8.8 Hz, 1 H), 7.58 (d, *J* = 8.6 Hz, 1 H), 7.51 (td, *J* = 8.7 Hz, 1.8 Hz, 2 H), 4.92-5.07 (m, 2 H), 4.30-4.34 (m, 1 H), 2.72 (qd, *J* = 12.8 Hz, 3.7 Hz, 1 H), 2.14-2.50 (m, 6 H), 1.95-2.13 (m, 3 H), 1.69-1.88 (m, 2 H), 1.35-1.60 (m, 19 H), 1.23-1.33 (m, 1 H), 1.09 (s, 3 H). **¹³C NMR**: (101 MHz, CDCl₃) δ 175.8, 171.7, 142.7, 142.0, 139.6, 137.2, 124.6, 124.5, 123.2, 121.8, 116.6, 115.0, 114.8, 110.5, 109.3, 57.2, 57.1, 34.6, 34.6, 32.0, 32.0, 30.9, 29.6, 29.3, 29.2, 25.2, 24.8, 24.2, 19.7.

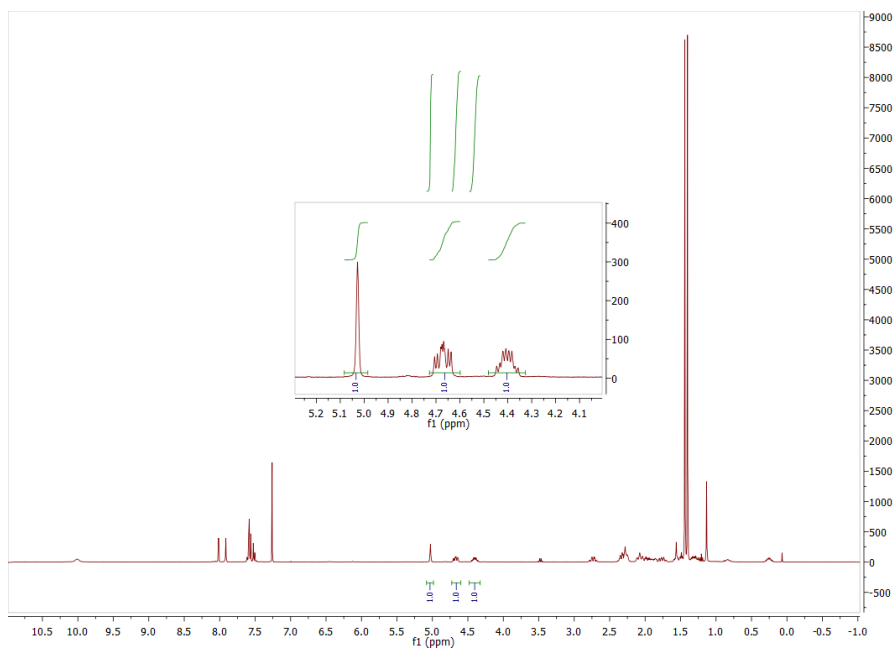


(Z)-2-(3,6-di-tert-butyl-9H-carbazol-9-yl)-N-(3-methylcyclohex-2-en-1-ylidene)cyclohexan-1-aminium tetrafluoroborate (Ia):



An authentic sample of the iminium ion **Ia** was synthesized according to the literature.⁴ **HRMS** Calculated for C₃₃H₄₅N₂ 469.3577, found 469.3573. **¹H NMR**: (400 MHz, CDCl₃) δ 10.01 (bs, 1 H), 8.02 (d, *J* = 1.8 Hz, 1 H), 7.91 (d, *J* = 0.9 Hz), 7.49 - 7.62 (m, 4 H), 5.03 (s, 1 H), 4.61-4.72 (m, 1 H), 4.34-4.46 (m, 1 H), 2.74 (qd, *J* = 13.1 Hz, 3.7 Hz, 1 H), 2.21-2.40 (m, 4 H), 2.02-2.15 (m, 2 H), 1.83-2.01 (m, 2 H), 1.68-1.83 (m, 1 H), 1.53-1.61 (m, 2 H), 1.47-1.53 (m, 1 H), 1.38-1.47 (m, 18 H), 1.27-1.37 (m, 1 H), 1.14 (m, 3 H). **¹³C NMR**: (101 MHz, CDCl₃) δ 177.2, 175.2, 143.4, 142.4, 139.3, 137.0, 125.0, 124.5, 123.4, 121.9, 116.7, 115.1, 114.7, 110.4, 108.8, 57.3, 57.2, 34.7, 34.6, 32.0, 32.0, 31.1, 30.4, 29.5, 29.3, 25.5, 24.7, 24.1, 19.7.

The structure of the carbazole-based iminium ion **Ia** was confirmed by X-ray analysis: **CCDC1437991**.



6.5.4 Cyclic voltammetry

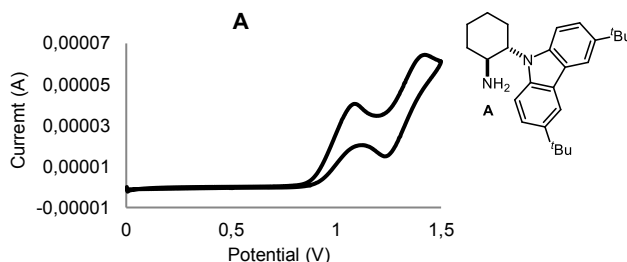


Figure 6.7 Cyclic voltammogram of aminocatalyst **A** [0.02 M] in [0.1 M] TBAPF₆ in CH₃CN. Sweep rate: 50 mV/s. Pt electrode working electrode, Ag/AgCl (KCl 3.0 M) reference electrode, Pt wire auxiliary electrode. **A**: $E_{1/2} = 1.16$ V.

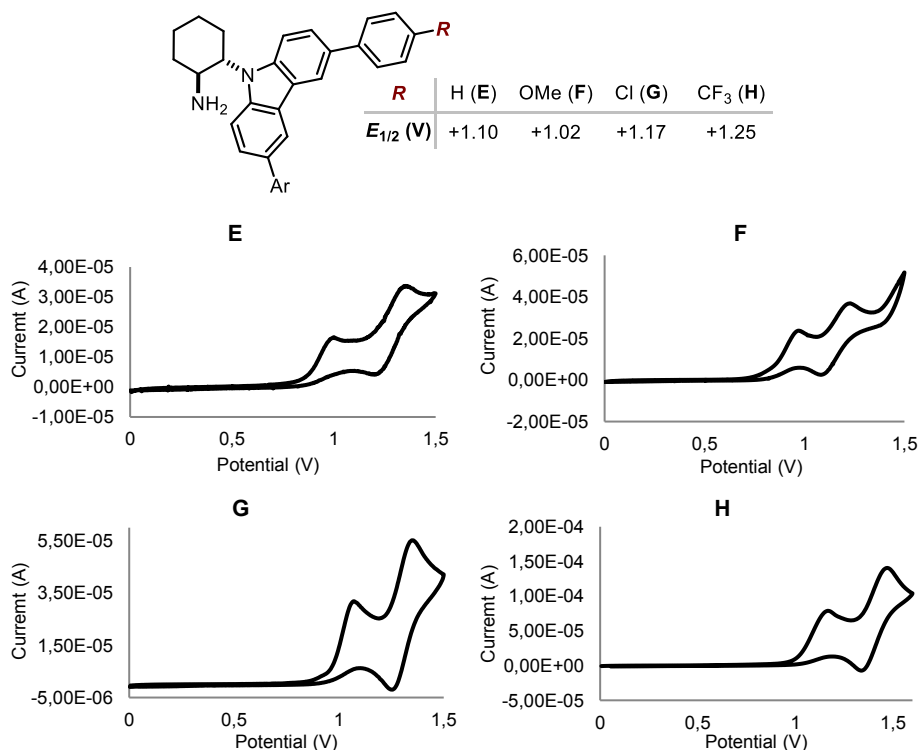


Figure 6.8 Cyclic voltammograms of the aminocatalysts [0.02 M] in [0.1 M] TBAPF₆ in CH₃CN. Sweep rate: 50 mV/s. Pt electrode working electrode, Ag/AgCl (KCl 3.0 M) reference electrode, Pt wire auxiliary electrode. **E**: $E_{1/2} = 1.10$ V (*top left*), **F**: $E_{1/2} = 1.02$ V (*top right*), **G**: $E_{1/2} = 1.17$ V (*bottom left*) and **H**: $E_{1/2} = 1.25$ V (*bottom right*).

In all voltammograms, a first reversible oxidation, corresponding to the oxidation of the carbazole moiety to give the carbazole radical cation, is followed by an additional

irreversible oxidation at about +1.4 V, which is due to the oxidation of the primary amine moiety within the aminocatalyst, are observed. In addition, in the voltammogram of **F** an extra oxidation, corresponding to further oxidation of the carbazole radical cation, is observed.

The electrochemical characterization of catalysts **B**, **C**, and **D** is detailed in our original report.⁴

UNIVERSITAT ROVIRA I VIRGILI

Development and Mechanistic Understanding of Photochemical Reactions

Ana Bahamonde Jiménez

UNIVERSITAT ROVIRA I VIRGILI

Development and Mechanistic Understanding of Photochemical Reactions

Ana Bahamonde Jiménez